Preparation, characterization, and application of the flexible fluid in the composite antenna

By

Abdelrahman Ameen Shehata Taha

Prof. Fouad Erchiqui

Directeur du doctorat en ingénierie Coresponsable

du Laboratoire de biomatériaux Directeur du Laboratoire de bioplasturgie

Prof. Mourad Nedil   Prof. Mohamed Siaj

Thèse présentée à l'Université du Québec à Abitibi-Témiscamingue en vue de l'obtention du grade de [Docteur en philosophie (Ph.D)] en ingénierie – concentration [Génie des matériaux]) offert en extension en vertu d'un protocole d'entente avec l'Université du Québec à Chicoutimi

Soutenue le 12 Sep.2023

Jury :

Hamidi Kaddami, Professor, Cadi Ayyad University (Morocco), external member

Abdellah Cheri, Professor, Royal Military College of Canada, external member

Fouad Erchiqui, Professor, Université du Québec en Abitibi-Témiscamingue, research director

Mourad Nedil, Professor, Université du Québec en Abitibi-Témiscamingue, co-director of research

Mohamed Siaj, Professor, Université du Québec à Montréal, co-supervisor

Québec, Canada [Abdelrahman Ameen Shehata Taha], [2023]

SUMMARY

Innovation is generally the main driver of most technological developments. This work deals with a typical example in the communication sector, through the development of some flexible composite-based antennas. The efficiency of ordinary fluidic antenna was increased by using ionic liquid assembled with nano metals composites. They possess unique advantages like their conductivity, flexibility, non-toxicity and profitability. Moreover, they are highly efficient with a radio wave frequency of 2GH applicable in the underground mining sector.

An ideal solution is to realise the EM components on flexible/stretchable materials encapsulation using a micro in polydimethylsiloxane (PDMS) substrates. This thesis contains various innovative and creative aspects divided into different sections.

Chapter one gives the general introduction and the literature review

Chapter two explores the fabrication, characterization, and applications of polydimethylsiloxane and bentonite clay nanocomposites impregnated with silver, copper, and graphene nanoparticles for the fabrication of a stretchable and robust micro-strip antenna. The nanocomposites' physical, mechanical, and thermal properties were evaluated based on their respective reinforcements' proportions. The applied techniques included the tensile and flexural tests for the mechanical characterization as well as the rheological and the thermogravimetric analysis. In addition, the surface morphology was evaluated by different techniques such as the X-ray diffraction, the scanning and transmission electron microscopy, and the UV-Vis spectroscopy. Moreover, the conductivity was characterized by electrochemical impedance spectroscopy, the dynamic viscosity analysis, and the ion coupled plasma measurements. The fabricated nanocomposites were shown to be excellent candidates for microstrip antenna applications due to both their electrical conductivity and their mechanical flexibility. These findings pave the way for the fabrication of flexible RF devices for advanced applications in the military, sensor, and space industries.

Chapter three deals with Fabricated Wearable and Flexible Chip made of Gallium and Silver Metals composites assembled on Graphene inside a PDMS Matrix.

Chapter four deals with the topic entitled "Perparation and evaluation of Conductive polymeric composites from Metal and Alloys and Graphene to be future flexible Antenna Device".

Chapter five presents the Studying and Evaluting The Physical characteristics of the Composite Substrate Chip and its Applications

Chapter six presents the topic entitled "Preparation and Estimation of the physical characterization of Nanofluidic Solution and its application".

Chapter Seven discusses the topic entitled "Specific Integrated Imidazole Solution Incorporating with Metallic Copper-Silver alloys in Nanoscales assembled on Graphene to be applicable FOR Future Antenna Devices ".

TABLE OF CONTENTS

CONTENTS

LIST OF TABLES

X

LIST OF FIGURES

ABBREVIATIONSTIONS AND SYMBOLS

σi.. .... ionic conductivity of the material

E........... .... Electrochemical cell

E_o............... .... Standard reduction potential of a specimen.

$m A$ .... Milliampere

(η)............. .... Coefficient of viscosity

Ea .... Apparent activation energy

F............... .... Faraday constant

η .... Absolute or Dynamic viscosity ($N\ s/m^2$).

dp/dt............... .... Pressure and Temperature changes

α.. Coefficient of thermal expansion 1/K

ρ .... Density kg/m^3

v .... kinematic viscosity (m^2/s)

Tc .... : Crystallization temperature

Tm .... : Melting temperature

ΔH.. : Enthalpy of fusion

Xc .... : Crystallinity rate

ε .... …….... : Dynamic deformation

εo .... ………... : Maximum dynamic deformation

ω .... : Angular velocity

Tc .... ……….. : Crystallization temperature

Tm .... : Melting temperature

ΔH.. : Enthalpy of fusion

Xc .... : Crystallinity rate

ε .... : Dynamic deformation

εo .... : Maximum dynamic deformation

ω .... : Angular velocity

t .... : Time

E' .... : Elastic modulus

E'' .... : Loss module

$\tan \delta$ .... : Tangent of the phase shift angle between E' and E''

$K\alpha$ .... : Wavelength of the Kα line

$Si-O_4$ .... ,,,,................ : Silica cyclic unit

δ .... : Chemical shift

$wt. \%$ .... : Mass percentage

$Zave$ .... : Mid sized

A

Ag NPs..: *Silver Nano Particles*

AG AC… ....…………………………………………..: *Silver Acetate*

ATR...: *Attenuated Total Reflectance*

AFM ....: *Microscope à Force Atomique*

Al2O3 ....: *Alumine*

APS ....: *Aerodynamic Particle Sizer*

ASTM ....: *American Society for Testing and Materials*

ATR-FTIR...: *Attenuated Total Reflection - Fourier Transform Ifrared*

B

BE ....: *Binding Energy*

C

Cv…………………………………………………………………… ……………..: *Cyclic voltammetry*

CENETE ....: *Centre National en Électrochimie et en Technologies Environnementales*

CERMAV...: *Centre de Recherche sur les Macromolécules Végétales*

Cl ………………………………………………..……………………………………………: *Chlore*

CNC ....: *Nanocristaux de cellulose*

CNF ....: *Cellulose Nanofibrille*

Co ....: *Cobalt*

CPMAS ....: *Cross Polarization Magic Angle Spinning*

CRMAA ....: *Self-Assembled Materials Research Center*

CRSNG ....: *Natural Sciences and Engineering Research Council*

CTMP ....: *Center for Mineral Technology and Plastics Technology*

CuO ....: *Copper oxide*

Cu NWs...: *Copper Nano wires*

D

DLS ....: *Dynamic Light Scattering*

DMA ....: *Mechanical dynamic analysis*

DMAc ....: *Dimethylacetamide*

E

EIS... : Electrochemical Impedance Spectroscopy

EDS .... : Energy Dispersive Spectroscopy

F

Fe O…………...………...: Iron Oxide

FEG-SEM..: Field Emission Gun- Scanning Electron Microscopy

FRQNT... …………….... : Quebec Research Fund - Nature and Technology

---

H

H2O2 .... : Oxygen peroxide

H2SO4 .... : Sulfuric acid

HCl .... : Hydrochloric acid

HDPE .... : High density polyethylene

HNO3 .... : Nitric acid

I

ICP .... …………..   Ion coupled plasma
.

J

JEOL .... : Japan Electron Optics Laboratory

M

MEB ....: Electronique scanning microscope

MnO .... : magnesium oxide

MTMS .... : Methyltrimethoxysilane

Mw .... : Molecular mass by weight

N

NMR…………..…................... Nuclear Magnetic Resonance

N2 ....……………………………:Nitrogen

NaOH .... Sodium hydroxide

O

OCV.. : Open circuit potential

OH .... : Alcohol function

OR .... : Alkoxy

Ox .... : Oxidation

P

PA .... : Polyamide

PC .... : Polycarbonate

Pd .... : Paladium

PET .... ………: Polyethylene terephthalate.

PPSQ .... : Polyphénylesilsesquioxane

PS .... : Polystyrene

PVA .... : Polyvenyl alcohol

R

Red .... : Reduction

RMN/NMR .... ………. …. : Nuclear Magnetic Resonance

S

SE ....………: Secondary Electron

SiO_2..Silicon Oxide

T

TEM .... : Transmission Electron Microscopy

TEOS .... : Tetraethoxysilane

TGA .... : Thermogravimetric Analysis

THF .... : Tetrahydrofuran

TiO_2 .... : Titanium dioxide

T .... : Temperature

U

UQAC ....: University of Quebec at Chicoutimi

UQAT .... : University of Quebec in Abitibi-Témiscamingue

X

XPS .... X-ray Spectroscopy.

XRD .... : X-ray Diffraction

V

DEDICATION

To the family Ameen Abdelrahan

ACKNOWLEDGEMENT

FOREWORD

With my supervisors, professors Fouad Erchiqui, Mourad Nedil, and Mohamed Siaj, the scientific project was discussed. The preparation and performing of tests on the synthesis of fluidic and micro-strip composite antenna and their application were done at the mineral technology center (CTMP) and Nano-Qam, chemistry department at the University of Quebec in Montreal.

In most cases, innovation is the primary force behind technical advancements. This work focuses on a common communication industry example through the creation of a few flexible composite-based antennas. By combining ionic liquid with nano metal composites, the effectiveness of regular fluidic antenna was improved. Their conductivity, flexibility, non-toxicity, and profitability are just a few of their special characteristics. Additionally, they have a radio wave frequency of 2GH that may be used in the underground mining industry and are quite effective. Realizing the EM components on flexible/stretchable materials and encapsulating them utilizing a micro in polydimethylsiloxane (PDMS) substrates is the optimal method. The numerous portions of this thesis each incorporate a variety of inventive and unique elements. Chapter 1 provides an overview of the subject and a survey of the literature. The creation of a flexible and durable micro-strip antenna is the focus of Chapter 2's investigation into the production, characterisation, and applications of polydimethylsiloxane and bentonite clay nanocomposites.In Chapter 3, a wearable and flexible chip comprised of composite gallium and silver metals is constructed on graphene inside a PDMS matrix. "Perparation and evaluation of Conductive polymeric composites from Metal and Alloys and Graphene to be future flexible Antenna Device" is the theme of Chapter 4. Studying and Evaluating is covered in Chapter 5.The Composite Substrate Chip's physical properties and applications."Preparation and Estimation of the physical characterization of

Nanofluidic Solution and its application" is the topic covered in Chapter 6. In Chapter 7, the subject of "Specific Integrated Imidazole Solution Incorporating with Metallic Copper-Silver Alloys in Nanoscales Assembled on Graphene to be applicable FOR Future Antenna Devices" is covered.

GENERAL INTRODUCTION

BACKGROUND

This work demonstrates the method of fabrication of a stretchable and robust micro-strip for future antennas of the mining industry, using polydimethylsiloxane and bentonite clay nanocomposites, loaded with silver, copper, and graphene nanoparticles. The fabrication process was carried out with a deep characterization of the composites, and the results were discussed with respect to the loads of the nano additives, their corresponding electrical conductivity, and their mechanical flexibility.

The underground mining activities which are characterized by tough working conditions in hazardous environments, require fool-proof communication systems to ensure smooth and safe operations. In fact, proper and reliable communication systems significantly reduce the machine breakdown time, and ensure instant messages tranfer from the vicinity of underground working area to the surface. This is both valid for normal daily mining operations and for speedy rescue operations in case of a disaster. Therefore, a reliable and effective communication system is an essential asset for the productivity and safety of the underground mines. Most of the actual communication systems operating in the underground mines are line-based thus their inability to withstand the disasters coupled with the challenge of their deployment in inaccessible areas. Therefore, the wireless communication appears as an alternative which is indispensable, reliable, and a convenient system for handling both the normal daily activities and the disasters. However, the actual literature regarding the wireless communication systems in both the underground mines and the hazardous area are rather poor. Therefore, a publication of a comprehensive textbook on wireless communication for underground mines which provides both a deeper understanding of the subject and the design of an intrinsic safe system is vital for both the mining and the electronics engineers. While taking into consideration the above-mentioned facts, this thesis is written by incorporating various communication devices designed and fabricated by the authors, for an application of wireless communication in different areas of the underground mines. The wireless communication systems used on the surface are not applicable to the underground mines without modifications. This is due to the high attenuation of the radio waves in underground strata, the presence of inflammable gases and the hazardous nature of the environments. Furthermore, asymmetric mine topologies, uneven mine structures,

1

complex geological features, and extensive labyrinths are additional challenges faced by such communication systems. The wireless communication in the underground mines is a complex technique involving multiple disciplines.

The most reliable and user-friendly devices used in the communication field are a product of an active and continuous research and development (R&D) process. This is particularly important for the underground mines which are very harsh working environments. . Underground mines are usually a few meters wide and a few kilometers long. The risk levels of the activities in underground mines are generally very high compared to other industries. An underground mining environment is known as dynamic because of the mobile operations required for the ore extraction. Inside such mine, ore is embedded in the ground and found in variable chunks over a long distance; thus, the distribution of its activities over its entire surface area.

CHAPTER-1

BACKGROUND

The past decades had witnessed a growing interest in the development of flexible antennas due to an increasing demand for wearable electronics, Internet of Things (IoT), point of care devices, personalized medicine platforms, 5G technology, wireless sensor networks, and smaller communication devices. The choice of a flexible antenna is specific for each application and it depends on numerous parameters such as the type of the substrate used, the conductive materials involved, the fabrication techniques, the targeted performance, and the surroundding environment. A plethora of novel materials, innovative fabrication methods, and specific applications are gradually being introduced to improve various features of those antenas [1] – [4]. A schematic representation of the interconnection between IoT and the 5G network is shown in Figure 1-1.
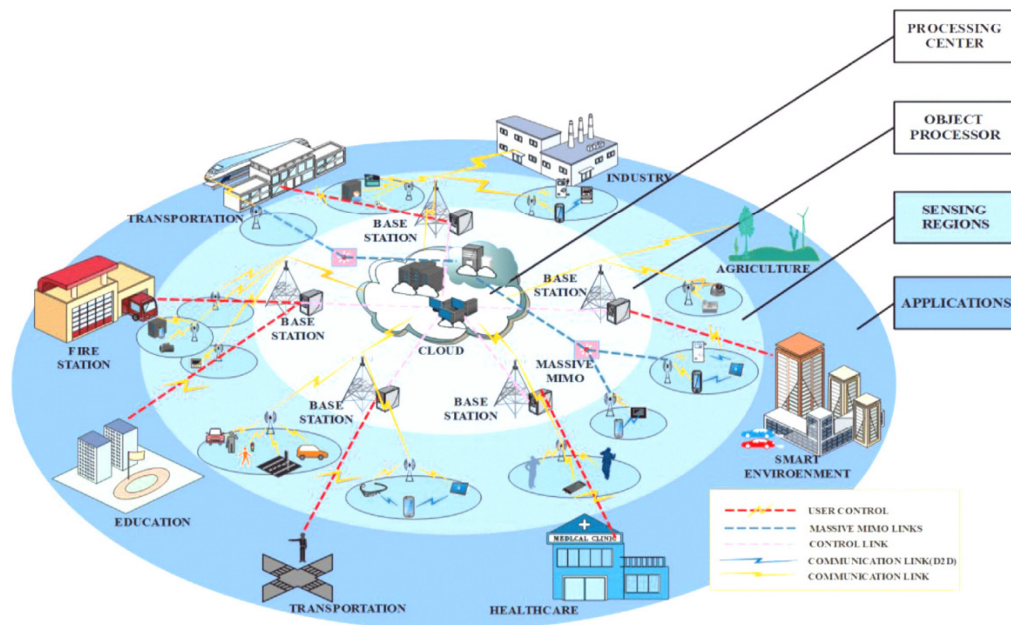
Figure 1-1: An overview of the architectural connection between the 5G network and the Internet of Things (IoT). Adapted with permission from Wang et al. [5].

1.1 ORIGINALITY

This work is original as it addresses some of the communication challenges faced by the mining industry. Those challenges stem from a number of factors, including the environment's inherent harshness and the damages caused to the network's infrastructure by some unwanted events such as fires, explosions, as well as the falling and hauling of roofs. In fact, this work is significantly important since the industries involved with the underground mining are in constant search of dependable and efficient communication systems which could both handle their daily operations and any arising emergency event. When the following circumstances are met and disater strikes in the mining industry, the rescue team can accurately communicate the information required to speed up the rescue operations. In this regard, the originality of this work is partitioned into the following three components:

• Ensuring the communication safety in the mining industry, based on the design of an effective wireless system.

• Desiging the mining communication system while taking into consideration the tense and hostile work environment, the possible damages to its wires, and the possibility to switch to a wireless truck electronic system which is both effective inside and outside the mine.

• Ensuring an improvement of the wireless communication and networking techniques in and outside the mine using portable and wearable chips.

1.2 PROBLEM FORMULATION

In order to address the safety issues related to the communication systems of both the underground mines and the related mining camp in the example of the lack of connectivity and the low reliability of the network, the main challenges which need to be tackled can be partitioned into the following two groups:

• The fabrication of the appropriete materials with specific properties required for setting up the mines communication system. These properties include the flexibility, stiffness, wearability, and conductivity.

• Lowering the associated cost in order to guarantee the profitability of the process

1.3 OBJECTIVES AND SCOPE OF THE THESIS

The objectives of this research are the development of the methods to improve the radiation performance of the fluidic and composite transparent antennas using highly conductive, flexible, and robust materials. It can be further subdivided into the following sub-objectives:

- The verification of the developed method by the fabrication of a flexible antenna for conformal applications, including its applications in the underground mining sector

- The selection and evaluation of the ideal composite materials for the most efficient antennas application

- An evaluation of the flexible composite materials and its application to the design of an antenna for the underground mining

- The use of different mechanical and chemical compatibility methods, as well as the resulting materials characterization and application at a broadband of 2.4 KHz.

This research will particularly impact the mining industry by improving the mining communication and reducing the surface miscommunication. In fact, the development and application of those antennas would result into the fatality reduction as improved communication would result into an efficient accidents mitigation and subsequent evacuations.

This study is limited to developing a method to integrate a highly conductive flexible material onto flexible dielectric materials to produce a flexible antenna that can efficiently perform when used in the mining sector and in future wireless networks. It covers the flexible fluidic antenna technology, the flexible clay composite matrix, the electrolyte solution, and the graphene /Elgin Composite. Moreover, the study investigates the use of a low-cost metal like silver and iron in the case of conformal antennas case where the antenna is bent to a certain curved surface.

CHAPTER-2

2. Literature Review

2.1 Mine Communication Techniques

During the past decades, the workplace occupational safety and health (OSH) has gained much importance across the industries. The OSH which is crucial for the prevention of the work-related deaths and injuries, is particularly suited for the dynamic and dangerous working environment of the mines [1-10]. In fact, the actual statistical data across the industries show a worldwide higher incidence of fatalities and injuries in the mining sector [12-14]. Australia for example which is one of the greatest producers of minerals in the world, showed the fourth-highest mortality rate of any business in 2019 with an average of seven fatalities per year (Safe Work Australia, 2020).

The daily monitoring and management of safety and rescue operations in the mining industry has proven to be exceedingly difficult due to the high complexity and hazardous nature of their underground activities [15-18]. The literature shows that the poor visibility, the unsafe behavior of the miners, the jobsite circumstances and environmental conditions such as the poor lighting, poor ventilation, gas emission, wet conditions, confined space, falling rocks, as well as the structural failures, and the communication restrictions, are some of the main risk factors that contribute to the fatal and non-fatal accidents involved in the mining operations [19-22].

It is critical for safety managers to continuously monitor both the physiological status of the employees and the environmental factors associated to their workplace in order to safeguard the health and safety of the subterranean workforce [24]. In this regard, an appreciable amount of real-time data must be gathered and analyzed using advanced technological methods in order to improve the OSH in the underground mines [25-31]. In fact, the dynamic and complex working environment of the underground

mines causes the insufficiency of their traditional safety system [32]. In recent years, the use of wireless sensor network (WSN) technologies has been adopted for tracking down the whereabouts and the physical health of the miners, while monitoring the environmental parameters of the deep mines. According to Ranjan et al., a WSN consists of a collection of tightly packed sensor nodes that can sense, process, and communicate the relevant data [33].

Apart from the WSN, the IoT is another technique used in improving the communication in the mining industry. However, the design and deployment of the IoT devices is limited by both their weight restrictons, and their rigidy.

Although significant steps have been achieved in the size reduction of these devices, their mechanical flexibility remains a challenging aspect to tackle. Due to their importance, several approaches have been proposed to deal with flexible electronic devices as they are meant to be lightweight, portable, cost-effective, and environmentally friendly [34]. The projection from the available data shows that the flexible electronic device industry is expected to exceed $40 billion by 2023 [35-36]. Figure 2-1 shows some applications of the flexible electronic devices. The flexible electronic systems require the implementation of flexible antennas which operate in a specific frequency range to supply the most-needed wireless connectivity..
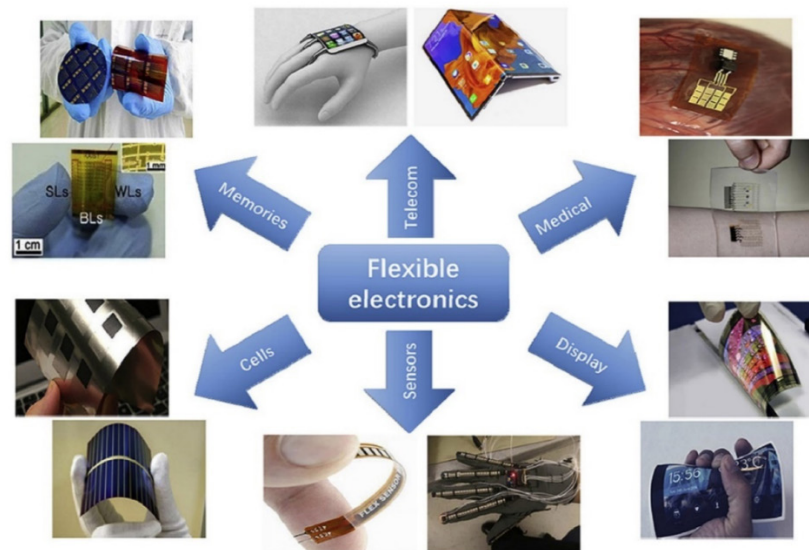
Figure 2.1 : Areas of application of flexible electronic devices. Adapted with permission from Hall et al. [9].

2.2 The Wireless communications systems

The actual literature does not indicate any single technology or system that can provide the full spectrum of the communications system with the capacity for operating, managing and supporting every type and size of mine. In general, the mines can either be classified as short life for very small operations with a dozen miners, or large scale fully mechanized systems with thousands of daily miners. Moreover, they may either include open cut or underground operations [37]. LT and Communications Technologies play a critical role for ensuring a smooth running of the mining operations: This includes keeping the maximum operational efficiencies, achieving an effective management of both the workforce and the equipments, and finally maintaining the minimization of both the downtime and the equipment failures. Consequently, mines are required to deploy a collection of communications systems, networks and technologies for the voice communications the equipment monitoring and control, the ventilation systems, the video remote blasting, the vehicle management, the personnel, equipments and vehicles tracking, and the emergency evacuation systems [37].

2.3 The Types of WBAN systems of communications

The wireless sensor networks (WSN) have attracted much attention during the last few years [38]. They offer several advantages over the traditional sensor networks: These include an elimination of costly wires, the security provided, and a larger coverage area [39,40].

An overview of the wireless networks classification is given in Figure 2.2. Their main differences lie in the area covered
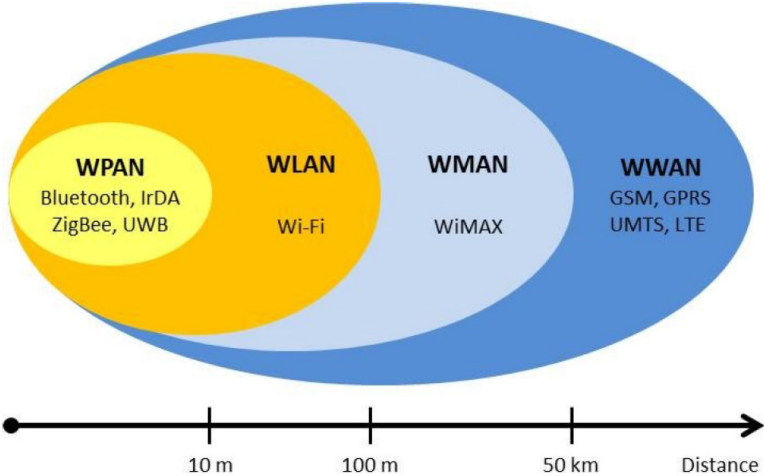
Figure 1.2 : An overview of the Wireless networks classification

2.4 The advantages   and disadvantages of the existing wireless antennas

The wireless networks are those that use radio waves instead of cables for devices connection.

$$E = mC^2 \qquad (2\text{-}1)$$

These devices commonly used for wireless networking include portable computers, desktop computers, hand-held computers, personal digital assistants (PDAs), cellular phones, pen-based computers, and pagers. Wireless networks work similarly with wired networks; however, wireless networks must convert information signals into a form that is suitable for transmission through the air. Wireless networks serve many purposes: In some cases, they are used as

cable replacements, while in others, they are used to provide access to corporate data from remote locations.

There is a number of advantages that wireless networks show over wired ones. They include their mobility, cost-effectiveness, adaptability, and security. All improved data communications lead to faster information transfer within the businesses, and between partners and customers. Sales agents for example can make a beter use of such advantage by remotely checking the stock levels and prices while they are on a sales call.

The advantages of the wireless networks are further discussed in the specific paragraphs that follow.

2.4.1 Better coverge and mobility

Wireless communication systems provide the most desired freedom for changing locations without loosing connection. In fact, wires tend to restrict the activities down to one location. Moreover, the wireless system can be deployed without the need of extra cables and adaptors to access the office networks

2.4.2 Flexiblity

The communication system is quite flexible since office-based workers can be networked without sitting at dedicated computers; Moreover, they can continue to be productive away from the office. Such flexibility results in new working habits, such as working from home, or directly accessing corporate data from customer sites

2.4.3 Cost savings

Wireless networks can be easier and cheaper to install, especially in listed buildings or in those where installation of cables is forbidden. The absence of wires and cables significantly lowers the overall installation cost. Such low-cost results from a combination of many factors such as the savings associated with the purchase of the cables, their installations (trenching, drilling) and their maintenance, and the relatively low cost of the wireless routers.

2.4.4 Their Adaptablity

The wireless communication system is highly adaptable as it provides a fast and easy integration of the devices into the network, coupled with the flexibility associated with potential installations modification.

2.4.5 New opportunites and applications

The wireless networking is an opportunity to offer new products or services. This is the case of many airports' departure lounges, train stations, hotels, cafes and restaurants, where the newly installed wireless hot spots allow mobile users to connect their equipment to their home offices while travelling. Unfortunately, there are many drawbacks associated to those new opportunities. In fact, the wireless transmission is more vulnerable to hacking and access by unauthorised user; consequently, a particular attention has to be paid to security.

2.4.6 The Coverage

Although the wireless communication systems provide an appreciable coverage, it is sometimes plagued by the existence of black spots where no signal is available. In some buildings in the example the structures built using steel reinforcing materials, getting a consistent coverage can be difficult; it is quite difficult to pick up the radio frequencies used.

2.4.7 The Transmission speeds

The wireless transmission can be slower, which results in wireless networks being less efficient than wired ones. That is why the backbone in larger wireless networks is usually wired.

2.5 The Electronic Packaging

Multifunctional materials offer a lot of potential for such applications as they perform better at the aforementioned functions. This method provides a single material that performs several tasks in a synergistic manner, outperforming the capabilities of the constituent components as a whole [42]. Multifunctional materials offer a way to improve on the efficiency and adaptability; however this may result in a decrease in some parameters such as size, weight, cost, and complexity [43]. Multifunctional materials are necessary for electronic packaging as they provide the structural support, the mechanical and chemical protection, and finally the thermal management. Despites the advances made in the communication field, a degradation of some electronic elements is possible due to the presence of moisture, pollutants, mobile ions,

radiation (including alpha particles, gamma photons, and x-rays), and harsh environmental conditions such corrosion and oxidation [43]. In this regard, electronic gadgets need to be packaged in a way that ensures long-term dependability and environmental protection. Multifunctional materials frequently have competing properties, thus the necessity to further work on the optimization of their properties.

Polymers have been generally adopted for the packaging of many electronic packaging components. These materials can be used as die adhesives, encapsulants, conformal coatings, passivation layers, and as the body of the package of an integrated circuit (IC) [44, 45]. Recently, an interest in the formulation of polymer based composite materials for electronic packaging has substantially increased. More information about the use of polymer based composite materials to replace the standard materials is further given in Section 2.3

(a)   (b)   (c)
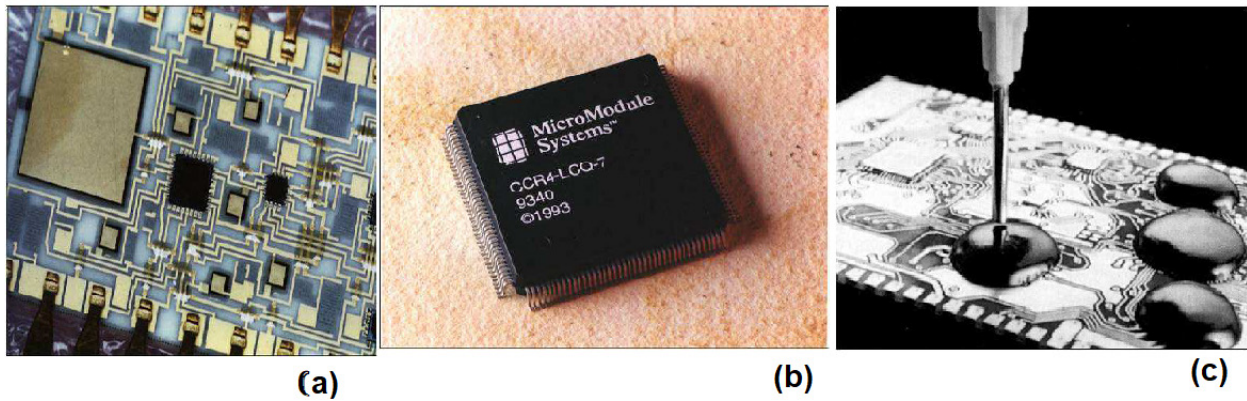
Figure 2.3: : An overview of some examples of types of electronic packaging, (a) Integrated circuits, (b) Electronic chips, (c) Liquid epoxy encapsulation [45].

2.5.1 The composite materials used for the antenna's fabrication.

The flexible/stretchable EM components are receiving significant attention from different research groups, due to their tremendous potential to enhance the emerging field of flexible

electronics. In conventional electromagnetic component design, rigid materials like solid metals are used as conductors, while rigid dielectric materials are used for mechanical support.

2.5.2 The Flexiable materials in electromagnetic components

2.5.3   The Flexibility and low loss dielectric loss properties

A large amount of research has focused on using flexible materials on diverse electromagnetic components which operate from the microwave to the optical frequencies. The key features of an ideal flexible microwave material are appreciable flexibility and excellent mechanical strength. Those flexible materials play a very important role in the resonant frequency tunability of electromagnetic components especially through their natural ability for mechanical deformations. The low loss of dielectric properties is essential for either providing a maximum signal transmission through the materials, or propagating it along electromagnetic structures. The different groups of flexible materials used in the design of electromagnetic components are further discussed in the following sections.

2.5.4   The flexible substrates

Over the past decades, the core advancements made in the field of electronics devices relied on the use of semiconducting materials, especially those using a silicon wafer, which is both a brittle and rigid material. However, other forms of silicon such as nanoscale ribbons, wires, or membranes are flexible. Generally, any material which is presented in a sufficiently thin form is flexible, and its flexibility decreases linearly with the thickness. Unfortunately, its use is restricted by its important cost. Consequently, other polymeric materials such as silicone rubber, butyl rubber and fluoro-polymer are the preferred substrate material used for many microwaves and many electronic applications, as they offer the needed flexibility at a lower cost. A wide range of flexible polymers with varying mechanical and electrical properties have been investigated for the fabrication of flexible devices; they include Kapton polyimide, polyethylene naphthalate (PEN) and polydimenthylsiloxane (PDMS).

2.5.5   The polymer-based composite materials

It is quite difficult to identify a homogeneous material which is flexible and which offers a low loss of electromagnetic properties. Generally, polymer-ceramic composites are the proposed

solution, as most polymers offer excellent flexibility at low cost, while several ceramics have a low loss of dielectric properties. Some micro/nano-composite materials can be formulated with those elements to yield similar mechanical properties with the intrinsic form of its matrix. Ceramics are inorganic, non-metallic, often crystalline oxide, nitride or carbide materials. Many researchers have studied the effects of ceramic fillers such as $SiO2$ [MgO], and $TiO2$ on the composites surface [46].

2.5.6 The conductive materials

Thin metal films of gold or silver have been associated with flexible substrates used for the fabrication of microwave components such as antennas metamaterials and switches. However, the integration of thin metalllic films with flexible materials leads to the formation of micro-cracks during the bending and stretching cycles, and eventually to creation of electrical open circuits. Such has been the example of thin films of gold deposited on a PDMS substrate which have exhibited micro-cracks.

2.5.7 The carbon nantubes

The Interest in the carbon nanotubes was sparked by the observations of tubular shaped carbon nanometer by Iljima [47], and by the reports showing the possibility for their synthesis in large quantities [48]. Carbon nanotubes exist in the form of cylinder made of graphene sheets. Due to their remarkable mechanical qualities, carbon nanotubes, which have a diameter of a few nanometers and a length of a few microns, are regarded as some of the best reinforcements for thermoplastic matrices. In fact, their exhibited excellent mechanical properties are well-known characteristics of carbon nanotubes. These mechanical properties can be attributed to their C-C covalent bonds. Carbon nanotubes have been shown to have an elastic modulus of 1.2 TPa and a tensile strength of roughly 50-200 GPa [49]. However, this does not ensure the generation of the nanocomposites with superior structural properties.

The following key elements directly affect the mechanical strength of the thermoplastic nanocomposites reinforced with carbon nanotubes:

- The homogeneous dispersion and the distribution of the carbon nanotubes in the matrix
- The alignment and orientation of the nanotubes in the matrix
- The quality of the interface between the matrix and the carbon nanotube reinforcements.

2.5.8 The modified organo clays

Organo clays such as smectites are a special class of clay-based minerals which are highly prized in the field of nanocomposi . Their importance is justified by their abundance, their physicochemical characteristics, and their structural characteristics when compared to other materials. The organo clay structures consist of sheets that are stacked on top of one another to create smectites with the layers' thickness of a few nanometers and lateral diameters ranging from 200 to 600 nm..

2.6 The Properties of composite materials

2.6.1 The thermally conductive materials

The phenomena of heat transmission from the higher to the lower temperature portions of a material is known as thermal conduction [50]. Consequently, the parameter that describes a material's capacity to transfer heat is called thermal conductivity..

There are two primary heat flow mechnisms through a solid material: The first is via free electrons and the second is via photons, which are lattice vibration waves. The free or conducting electrons take part in the electronic thermal conduction, while the movement of phonons photons is linked to a certain amount of thermal energy [51]. Photons or lattice vibrations account for the majority of the heat transfer within a non-metallic material [52].

In the case of metals, the free electron heat transfer mechanism is more efficient than the photon movement since electrons which are more resistant to scattering also move at higher velocities. The large number of electrons present within the metallic structure is an added advantage for the thermal conduction process. Apart from promoting heat conduction, this mechanism also increases the electrical conductivity in accordance to the Wiedemann Franz law [53]. Ceramics are generally known as electrical insulators which means that contrary to metals, they do not possess important amounts of free electrons. Consequently, the heat transfer is in ceramics occurs predominantly through photons Eventhough free electrons are much more efficient for heat conduction, some ceramics exhibit relatively high thermal conductivities..

Table 2.1 Examples of electronic packaging: (a) integrated circuits, (b) electronic chips, and (c) liquid epoxy encapsulation [52].

Material	Thermal Conductivity (W/m-K)
Metals	
Aluminum (Al)	234
Copper (Cu)	400
Stainless Steel	15
Ceramics	
Silica (SiO_2)	1.5
Aluminum Nitride (AlN)	80 – 200
Silicon Carbide (SiC)	70 – 490
Alumina (Al_2O_3)	18 – 36
Boron Nitride (BN)	300+
Diamond	1000
Polymers	
Linear Low Density Polyethylene (LLDPE)	0.31
Polyether Ether Ketone (PEEK)	0.29
Polyphenylene Sulfide (PPS)	0.22
Liquid Crystal Polymer (LCP)	0.20

2.6.2   The electrically insulating materials

The electrical resistivity (ρ), which is the opposite of the electrical conductivity, describes a material's capacity to resist the conduction of electrical current. Based on the electrical conduction, the materials can be classified in three major groups which are the conductors, semiconductors, and insulators. By definition, conductive materials must exhibit an electrical conductivity of at least 103 (S/cm). In the same manner, an electrical conductivity which is less than 108 (S/cm) indicates an insulator; and finally, those materials found between the conductors and the insulators are known as semiconductors. An overview of this general classification is given in Figure 2.4.

When insulators are required in some applications, polymers are frequently used because of their strong electrical resistivities [54]. Such is the case for the polymers used in flexible

coatings of electrical wires and cables [55]. These materials can also be found in printed circuit boards, transformers, end-fittings, and capacitors [56, 57].
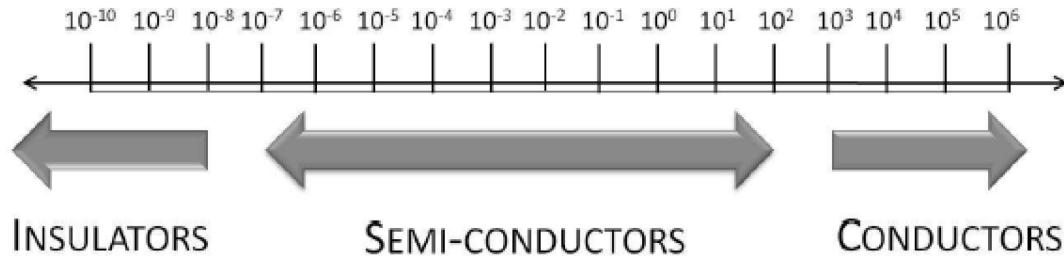
Figure 2.4: : Scope of the electrical conductivities (S/cm) of different classes of materials.

2.6.3 The stretchable component of the materials

Various flexible/stretchable EM components like resonators, antennas, switches, filters and oscillators have been reported in diverse applications, especially in the electronics, communications, biomedical and industrial fields. The flexible/stretchable EM components can be produced by integrating flexible substrates with fluidic liquid metal as conductor. Normally, the liquid metals are encapsulated in flexible substrates with a resulting tolerance change caused by external bending/stretching forces. In the case of stretchable devices, liquid metals are suitable materials due to both their ability of not forming micro-cracks when stretched repeatedly, and their exhibited self-healing properties.

2.7 The fabrication methods

Some studies have been conducted about the best methods of combining a polymer with the filler particles to achieve the desirable properties. Agari et al. [54] tested four methods of fabricating test specimen that were in the form of powder, solution, roll-milled, and melt mixed materials [58]. It appears that powder mixed referred to a dry-blend method where the materials are combined at room temperature and then melted into the appropriate shape. Solution mixing however, refers to the cases where the filler was dispersed into the matrix with the help of toluene used as solvent until it evaporated and the solute was removed and then melted. In the case of roll-milled samples, the fillers were mechanically kneaded into the melted polymer

followed by melt mixing using a twin-screw compounder to combine the filler and matrix while the polymer was in a molten state. The thermal conductivity of the prepared specimen increased in the following order: melt mixture < roll milled = solution mixture < powder mixing [59]. These results suggest a non-uniform composite morphology, which facilitates the formation of conductive networks through the material.

2.8 The nanocomposites manufacturing process based on thermoplastic matrices

The successful formulation of nanocomposite materials based on thermoplastic matrices primarily depends on the polymer matrix's chemical, physical, and thermal properties, but also on the following conditions:

      a. polymer-filler interaction

      b. interaction between the charges

      c. Nanocomposites based on thermoplastic matrices can be created using three different techniques

      d. Clay, carbon dioxide, or organic fibers can be used in the formulation of nanocomposites based on thermoplastic matrices.

The first, and the most common method is the elaboration by solution. In this case, nanoparticles are first dispersed in an organic solvent in which the polymer serving as matrix has previously been dissolved. The nanocomposite is obtained by evaporating the solvent. This method is less advantageous because of its high cost driven by the slow process and its consumption of important solvent volumes.

The second method is known as the "in-situ polymerization". During this process, the nanoparticles are dispersed in the monomers, with or without solvent, then the polymerization reaction is initiated to obtain the nanocomposite. The presence of nanoparticles in the prepolymerization state makes it possible to establish the chemical interactions with the polymer matrix. This method was applied for the processing of polyamide-based nanocomposites loaded with CNC, with an interesting improvement of the mechanical properties of the polyamide

The third method consists in mixing the melt. This method derives from the difficulty in dissolving some polymers in organic solvents. Generally, any molten polymer can be blended with nanoparticles as long as the polymer's temperature is high enough. However, the implementation must be carried out at a temperature lower than the load's degrading temperature, and the frequent issues of dispersion, and compatibilization must be addressed.

Normally, the distribution across the polymer melt is caused by the shear forces applied in this method. This method is the favorite of industrial promotors because it is both cost efficient with respect to other methods, and environmentally friendly.

The literature reports numerous attempts to create nanocomposites using thermoplastics loaded with clay, natural fibers, or carbon-based nanoparticles using extrusion by Hasegawa et al. [60].

The case of clay minerals reinforcing polyamide 6 matrices have also been reported. It indicates that minerals from clay were distributed into the polymeric matrix by extrusion. The fillers and the polymer were combined at the polyamide-6 processing temperature. the ocean Vacuum is used to expel evaporated . Mack et al. [61] have reported the use of this technique while reinforcing polycarbonate with carbon nanotubes. In fact, 1 to 5% of polycarbonate was melted before an addition of the carbon nanotubes.

2.9 The economic potential of nanocomposites

The commercialization of polymer-based nanocomposites began in 1991 with the Toyota Motor Co.'s introduction of nylon-6/clay nanocomposites into the market [62].

Ube Sectors and Toyota created a timing belt covers for the Toyota Camry's engine. The polymer matrix nanocomposites have taken over the market with their peculiar properties such as high modulus, low weight, excellent mechanical properties, and dimensional stability. They have a higher shock resistance, they are not flammable, they show a better scratch resistance, and better thermal resistance. All these qualities are the reason why nanocomposite materials are replacing specific components in different industries; such is the case for some metallic components of the automotive industry.

2.10 Conclusion

In order to enhance the rigidity, fire resistance, and in some circumstances the electrical conductivity of the polymer material, some traditional composite materials are formulated by using organic, inorganic, and hybrid fillers. Typically, these fillers take the shape of the fibers; that is larger than one micrometer in diameter. The anticipated performance is improved from the addition of these fillers; however, such performance depends on the quality of the filler and the matrix interface, and in some cases, on the filler's capacity to create a three-dimensional network within the matrix. Moreover, the microscopic additions lead to a high fillers (fibers) concentration.

The reason for the actual appearance of nanoscopic fillers is their ability to maintain the same levels of efficacy at lower filler compositions. The quality and extend of the polymer-filler interfaces can be improved due to their compact size. This work has shown that an ideal anticipated improvement of the nanocomposites for the intended applications can be achieved by an even dispersion of the nano-reinforcements in the matrix. This kind of dispersion is still a challenge for researchers, whose major achievements have been the chemical alteration of the surfaces of both the nanofillers and the matrix in order to boost the compatibilization process.

This chapter is based on a number of published findings that address the connected concerns that, in the context of our research, appear to be the most intriguing. We were able to locate the resources we used in our study thanks to the analytical bibliographies. In the chapters that follow, the findings are reported. Before that, the next chapter develops the experimental methodology that was applied in this work.

CHAPTER 3

ELECTRICALLY CONDUCTIVE PDMS/CLAY NANOCOMPOSITES ASSEMBLED WITH GRAPHENE, COPPER AND SILVER NANOPARTICLES FOR FLEXIBLE ELECTRONIC APPLICATIONS

Ameen Abdelrahmana[a], Fouad. Erchiqui[b], Mourad. Nedil,[c] Brahim. Aïssa[c] , and Mohemed. Siaj[d]

[a]Material science department / School of Engineering, Université du Québec en Abitibi-Témiscamingue (UQAT),445 Boulevard de l'Université Rouyn-Noranda (QC) J9X 5E4,

[b]Professeure- d'université | UQAT - Université du Québec en Abitibi-Témiscamingue 445 boul. de l'Université Rouyn-Noranda J9X 5E4 819 762-0971 |

[c]Professeur Titulaire / Professor Directeur du programme de la maîtrise en ingénierie École de génie / School of Engineering, Université du Québec en Abitibi-Témiscamingue (UQAT), Campus de Val d'Or , :- 675, 1ère Avenue, Val d'Or, Québec, Canada, J9P 1Y3

[d]Département of Chemistry, Université du Québec àMontréal (UQÀM) / NanoQÀM-CQMF, 2101 Jeanne-Mance street, Montreal, QC H2X 2J6, Canada.

Abstract

We describe the development and characterization of a stretchy and resilient micro-strip antenna made from a nanocomposite of polydimethylsiloxane (PDMS) and bentonite clay loaded with silver, copper, and graphene nanoparticles. The physical, mechanical, and thermal characteristics of the nanocomposite were extensively evaluated in relation to the different nanomaterial loading into the PDMS. This has included UV-Vis spectroscopy, X-ray diffraction, and other techniques in addition to tensile and flexural tests, rheological analysis, thermogravimetric analysis, scanning and transmission electron microscopy, dynamic viscosity study, and ion coupled plasma. The conductivity of the fabricated micro-strip antennas was assessed using electrochemical impedance spectroscopy, and the antenna pattern was suitable for usage in RF equipment for cutting-edge applications like military, sensing, and space.

Keywords: composite; nanoparticles; polydimethylsiloxane; patch antenna, electrochemical impedance.

3.1 Introduction

There is a growing interest in applying flexible antennas in critical areas such as healthcare monitoring, search and rescue, and public safety [61]. A highly desired characteristic of such applications is the robustness of the antenna to withstand dynamic operating conditions. Etching metal patterns usually fabricate rigid antennas on rigid substrates [62]. However, they are susceptible to either permanent deformation or fracture from bending or twisting stress. To deal with such rigidity issues, some flexible antennas have been created with copper tape [64] and conductive ink [63,64] on flexible substrates. However, copper-based designs were still found to be rigid, while those based on conductive inks are not suited for long-term use due to peeling. Consequently, other designs have been tried using embroidered antennas and wearable sensors using conductive fibers on textiles and polymer composite substrates [63], [65,66] and embroidered wearable RFID tags on textile and polymer composites [67], [68].

Morris et al. reported using a 2.45 GHz dipole antenna on a PDMS substrate with copper mesh arms whose performance was compared to a copper wire dipole [69]. Similarly, a dual-band textile antenna on PDMS substrate was reported by the group of Simorangkir [68] and its performance compared to those of its rigid version [70]. Lanlin and coworkers reported a textile antenna used in body-worn communications and medical sensors with comparable performance to their copper counterparts [71]. However, only a narrow bandwidth has been considered in all these designs.

In general, flexible antennas are fabricated using various conductive materials and substrates. The substrate is selected based on its dielectric properties, tolerance to mechanical deformations (bending, twisting, and wrapping), susceptibility to miniaturization, and durability in the external environment. On the contrary, the selection of conductive materials dictates the antenna's performance features, such as its radiation efficiency. Conductivity is essential for ensuring high gain, efficiency, and appropriate bandwidth. Additionally, resistance to the degradation induced by mechanical deformation is another desired feature for the conductive material. For this reason, nanoparticle (NP) inks such as silver and copper are often preferred for the fabrication of flexible antennas due to their high electrical conductivity; however, silver-nanoparticle ink edges are preferred over copper nanoparticles due to their low oxidation rate [72]. At the time of writing, very few investigations into flexible antennas made of copper-based nanoparticles have been reported [73].

Besides nanoparticles, electro-textile materials like Ni/Ag-plated, metalized conductive nylon fabrics in the example of Flectron™ and nonwoven conductive fabrics (NWCFs) are generally used in flexible antennas. Various types of textile and non-textile conductive materials such as adhesive copper [74], copper tapes [75], and copper cladding [76] have been reviewed in previous works for the development of flexible antennas ,
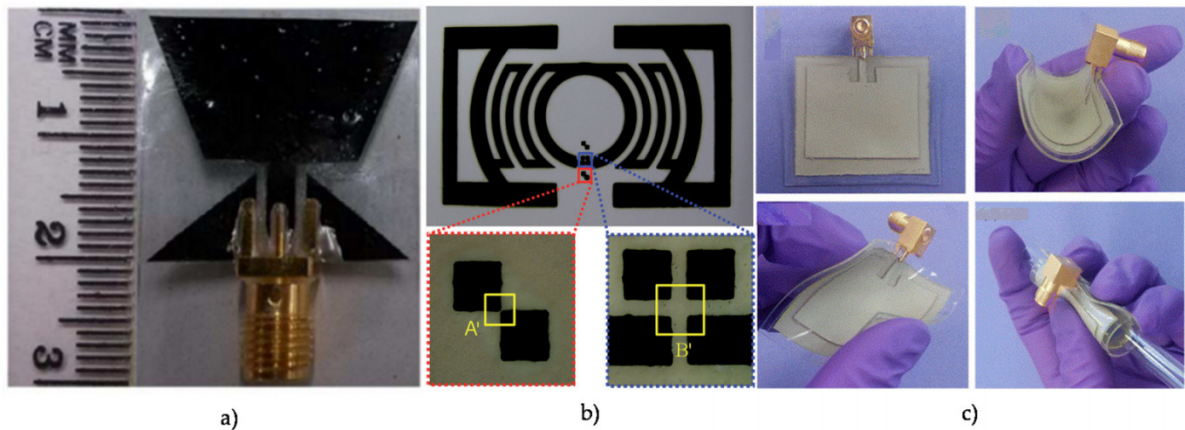
Figure 3-1: Schematic representation of various antennas with different conducting materials. (a) Polymer ultra-wideband antenna using poly (3,4-ethylenedioxythiophene) and polystyrene sulfonate (PEDOT: PSS) [77]; (b) Platinum-decorated carbon nanoparticle/polyaniline hybrid paste for flexible wideband dipole tag-antenna [78]; and (c) A stretchable microstrip patch antenna with a flexible conductor made of silver nanowire (AgNW) and polydimethylsiloxane (PDMS) [79].

Figure 3-1 shows different antennas designed with various conducting materials. Conductive polymers like polyaniline (PANI) [80], polypyrrole (PPy) [81], and poly (3,4-ethylenedioxythiophene) polystyrene sulfonate (PEDOT: PSS) [32] seem promising for flexible and wearable antennas. The addition of different conducting materials improved the low conductivity of these polymers in carbon nanotubes [83], graphene [84], and carbon nanoparticles [85]. The future of flexible antennas made with graphene is promising as they combine both decent electrical conductivity and excellent mechanical properties. In fact, the performance of flexible antennas relies on their conducting traces; meanwhile, a combination of high deformation and good electrical conductivity is desired [36]. In this regard, graphene paper [78], graphene nanoflake ink [88], graphene oxide ink [89], and graphene nanoparticle ink [90] have been used in previous studies to fabricate flexible antennas.

Table 3-1 : Conductive materials and their conductivity values

Material types	Conductive materials	Conductivity, σ (S/m)
Metal nanoparticles	Ag nanoparticle [91]	2.173×10^7
	Cu nanoparticle [92]	1×10^6
Conductive polymers	PEDOT:PSS [93]	100-1500
	Polyaniline (Pani) [93]	5
	Polypyrrole (PPy) [94]	40-200
Conductive polymers with additives	C nanotube [95]	4000-7000
	PANI/CCo Composite	7.3×10^3
	AgNW/PDMS [96]	8130
	Ag flakes + Fluorine Rubber [96]	8.5×10^4
Graphene-based materials Liquid Metal	Nanoflakes [97]	6×10^5
	Paper [93]	4.2×10^5
	Meshed Fabric [98]	2×10^5
	Eutectic GaIn [80]	3.4×10^6

Table 3-2: **Commonly** used flexible substrates with dielectric constant, loss, and thickness**.**

Substrates	Dielectric constant (εr)	Dielectric loss (tan δ)	Thickness (mm)
PET [49]	3	0.008	0.140
PEN [50]	2.9	0.025	0.125
Polyimide [51]	2.91	0.005	0.2
PDMS-MCT [52]	3.8	0.015	-

Material		Dielectric constant	Dielectric loss	Thickness
PDMS [53]		2.65	0.02	-
		1.85	0.014	-
PDMS/phenolic microspheres [54]		2.24	0.022	-
PDMS/silicate microspheres [55]		2.45	0.02	-
Paper (Kodak photo paper) [56]		2.85	0.05	0.254
Liquid crystal polymer [57]		2.9	0.0025	0.1
Wearable antenna substrate	Fleece Fabric [58]	1.25	-	2.56
	Cordura [59]	1.1-1.7	0.0098	0.5
	Woolen felt [60]	1.16	0.02	3.5
	Felt [61]	1.3	0.02	1.1
	Cotton/polyester [62]	1.6	0.02	2.808

In order to accommodate the mechanical strain and deformation while preserving the performance of the antennas, the conductivity of different stretchable materials used is often improved by the doping process. Some of the examples found in the literature include silver nanowire embedded silicone [98], silver loaded fluorine rubber [99], carbon nanotubes (CNT)-based conductive polymers [100], liquid metals in the stretchable substrate [101], and astretchable fabric itself [102]. Table 3-1 lists the different conductive materials used to fabricate a flexible antenna and their conductivity values. Table 3-2 shows some substrates commonly used to fabricate flexible antennas and their dielectric constant, dielectric loss, and thickness values.

In 2018, Romano et al. applied the integral convolution between elastic strain and a nonlocal kernel, adapted for the simulation of nonlocal long-range interactions [103]. Moreover, they worked on Eringen's strain-driven nonlocal integral model to collude against significant

obstructions, which is a significant structural application. Although the stress field is associated with the nonlocal constitutive law, it does not meet the requirements for equilibrium. In contrast, another study on EDM, widely recorded in previous literature, interprets the nano-beam mechanical conduct .The difference between EIM and SDM leads to excellent structural-like technically significant SDM flexural and torsional analysis [104], nonisothermal structural problems . linear and nonlinear analysis of transverse free vibrations , and longitudinal free vibrations of Bernoulli-Euler nano-beams [105].

3. 2 MATERIALS AND METHODS

3.2.1 Materials

The chemicals reagents, copper (II) sulfate ($CuSO_4 \cdot 5H_2O$), silver nitrate ($AgNO_3$) with 99% purity, and graphene powder used in the preparation of the composite were purchased from Sigma Aldrich (Montréal, Canada). Meanwhile, the organic solvents, polymers, and bentonite clay (B-clay) were supplied by Fisher Scientific Canada (Montréal, Canada). Finally, the Dow Corning®Sylgard 184 PDMS elastomer and the curing agent (silicone elastomer) were supplied by Dow Chemical (Toronto, Canada).

3.2.1 Fabrication of clay-graphene composites.

Graphene and the right amount of B-clay were mixed with distilled water and ultra-sonicated for 24 hours. The precipitate was separated by centrifugation and dried under a vacuum. The solution was further treated with 3ml of a 0.5 M electrolyte solution, stirred by centrifugation for 5 hours, and dried.

3.2.2 Fabrication of the clay assembled nanoparticles.

B-clay nanopowder was crushed using a planetary ball mill type PM 400 from RETSCH (Montréal, Canada) at 150 rpm for 5 hours, followed by the modification preparation methods [64]. In details, 5g of graphene nanopowder and 2.5g of $NaNO_3$,10ml of the electrolyte solution 0.5 M ($CuSO_4$ and $AgNO_3$) were mixed with 5 drops of concentrated H_2SO_4, 5ml of H_3PO_4 and stirred in an ice bath to keep the temperature below 5°C. The suspension solution was

centrifuged and washed repeatedly with deionized water and 5% HCl. Finally, the product was dried at 60°C [106].

3.2.3 Fabrication of the clay graphene – PDMS copolymer.

Using the stoichiometry ratio (1:1) wt/wt dried graphene and B-clay composite, then dissolved in 10ml of PDMS solution and stirred for 45 minutes, then a suspension of the curing agent was added at a ratio of (1:10 w/w). The mixture was further cast with a thickness of roughly 1.5 mm, cut into 2.5 cm by 2.5 cm squares, and transferred into a degasser vacuum for 10 minutes to remove bubbles. The samples were finally molded by compression with the plates heated at 75 °C for 45 minutes, followed by cooling to room temperature.

3.2.4   Fabrication of the PDMS substrate.

The PDMS substrates were prepared using the conventional method; mixing the PDMS elastomer and its curing agent at a ratio of (10:1) wt/wt, stirring for 15 minutes, and transferring into a degasser vacuum for 10 minutes to remove the bubbles. The mixture was finally molded onto a hotplate at 75 °C for 45 min, cooled down to room temperature, and put inside the O_2 plasma reactor.

3.3 Characterization methods.

3.3.1 *X-ray diffraction (XRD) analysis.*

X-ray diffraction (XRD) analysis was carried out to survey the crystalline structure and the phase composition of the investigated materials. This was done using a D8 Advance X-ray diffractometer from Bruker (Montréal, Canada) equipped with a copper (Cu) source. It allows the qualitative and quantitative characterization of the samples depending on their crystallographic evaluation, grain size, and thickness of their layers. The device consists of a standard sample holder, several analyzer stations, a 9-position auto-sampler (FLIP-STICK), a control software, and a high-temperature furnace (HTK, 1200N). The measurements were executed in a 2θ range of 10°C to 70°C.

3.3.2 The scanning electron microscopy (SEM).

A scanning electron microscope (SEM) model Oxford instrument INCA/Sight 40 kV, consisting of a Vega3SB connected with a Bruker Energy Dispersive Spectroscopy (EDS), was used to study the morphology of the investigated samples.

3.3.3 Transmission electron microscopy (TEM).

A TEM model JEM-1230 from JEOL operating at 120 kV with an integrated CCD camera was further used for the samples' characterization. TEM is an appropriate way to investigate the surface morphology of the prepared samples using copper grids pre-wrapped on a thin amorphous carbon film. Each sample was placed on the carbon-coated grid and tested at ambient temperature.

3.3.4 Electrochemical characterization.

The electrochemical behavior of the samples was investigated through electrochemical impedance spectroscopy (EIS), in which measurements are related to both their resistance and conductivity. The tests were conducted on a potentiostat-galvanostat instrument containing eight channels using batteries (10V and 4Amp). Based on its association with Corrware/Corrview, the operating software, it can be applied for most electrochemical analyses. In addition, by coupling with the 1255B frequency analyzers, the equipment is used to measure the electrochemical impedance. This equipment detects the physicochemical properties such as the resistivity, the electron transfer rates, and the charge transfer kinetics associated with different frequency ranges based on the samples' impedance. Such analysis is the classical method of studying the variations of different parameters, such as impedance and capacitance, and bio-sensors applications. The prepared material's conductivity was investigated at frequencies ranging from 1.5 kHz to 2 MHz with an open circuit potential (OCV) of 0.44 V using specific electrodes with 15 mm diameter at room temperature. These measurements are based on the following material ionic conductivity equation:

$$\sigma = \frac{L}{R} \cdot S \qquad\qquad (3\text{-}1)$$

where σ is the ionic conductivity, L is the working electrode thickness, and S is the electroactive surface area of the electrode.

3.3.5 Dielectric measurements of the PDMS substrate.

The dielectric constant of the PDMS substrate was measured with a dielectric analyzer (Novocontrol BDS 20 GmbH). The samples holder was in a vacuum chamber to avoid any measurement errors. Further analysis of the PDMS substrate was conducted using the Inductively Coupled Plasma Atomic Emission Spectroscopy (ICP-AES). It is a qualitative and quantitative technique used to determine the chemical composition of the investigated substance, especially traces of the major elements found in the periodic table. It was carried out using an ICP-AES spectrometer model 5100 from Agilent Technologies. The methods consisted in dissolving the samples into a solution of 2-5% nitric acid followed by their injection into an argon plasma gas of around 6000 K.

3.3.6 UV analysis.

A comparative qualitative analysis was performed between the samples of clay assembled with graphene, copper, and silver nanoparticles and the samples of PDMS composite using a combination of the UV-visible and near-infrared techniques. The measurements were made using a Lambda 750 double-beam spectrometer from Perkin Elmer (Montréal, Canada) over a wavelength range between 175 and 3000 nm.

3.3.7 Measuring the dynamic viscosity and the particle size analysis of the fluidic solution.

The samples' viscosity was analyzed using a vibrating viscometer model SV-10 from A&D (Montréal, Canada). The measurements were performed at room temperature with a 1% reading accuracy based on Equation 2 -2, where α_ρ, T, ρ and P are the apparent viscosity, temperature, density, and atmospheric pressure, respectively.

$$\alpha_P = -\frac{1}{\rho}\left(\frac{d\rho}{dT}\right)_p \qquad (3\text{-}2)$$

Similarly, the characterization of the particle size distribution in the mixing phases was done using the Zetasizer Nano analyzer model S90 from Malvern (Montreal, Canada), in combination with a red laser whose wavelength and power are respectively 632.8nm and 4mW. The Zetasizer instrument could detect particles with diameters between 1nm and 5 microns.

3.3.8 Thermal characterization of PDMS and its composites.

The thermal behavior of PDMS and its composites was evaluated based on both the thermo-gravimetric analysis (TGA) carried out with a TGA model Q500 from TA Instruments (Montéal, Canada) and the differential scanning calorimetry (DSC) with a DSC model Mettler Toledo from (Montréal, Canada). The TGA samples weighing between 0 and 200 mg were heated at 10°C/min in an N_2 atmosphere while the variations and thermal events were recorded with a sensitivity of 0.01%; meanwhile, the DSC samples weighing an average of 0.2 mg were sealed in aluminum pans and heated in comparison with decomposition based on its stability. The thermal events were recorded following a three stages protocol between -60 and +600°C

The fabricated antenna analysis was done using a vector network analyzer (Model #5071 B) from Agilent Technologies, Polytechnique in Montreal, Canada. Initially, the network analyzer was slandered using the two-port Ecal module posture model #85092C using frequency applied ranges from 300 kHz to 10GHz, which supplied an excellent accuracy.

3.4 RESULTS AND DISCUSSION.

3.4.1 XRD analysis.

The XRD analysis of the structures of clay, NPS-metals assembled on clay, and the composite are presented in Figures 2-2(a), 2-2(b), and 2-2(c), respectively. The 2-theta of the particle size for crystallography structure of pure metals and composite scattered X-rays interference is calculated using the Debye Scherrer Equation:

$$D = \frac{0.9\,\lambda}{\beta\,Cos\theta} \qquad (3\text{-}3)$$

Where D is the mean size of crystallites (nm), K is a crystallite shape factor, and a good approximation is 0.9, λ is the X-ray wavelength, B is the full width at half the maximum (FWHM) in radians of the X-ray diffraction peak, and θ is the Braggs' angle (degré.). The spectra are given in terms of the peak intensity versus the angle 2θ. It shows an increase of the peak intensities in the following order: clay, clay nanoparticle composites, and nanoparticles. NP and graphene clay composites show the same group of peaks with different intensities, while clay

shows some differences, notably an extra peak around 2θ value of 5° and the absence of others after 40°. Some of the representative peaks include a peak at the middle 2θ value of 29.9° matching the (110) plane, as well as slightly weak triple peaks at 2θ value of 46.4°, 63.8°, and 78.9°, respectively, parallel to the (200), (220) and (310) planes.
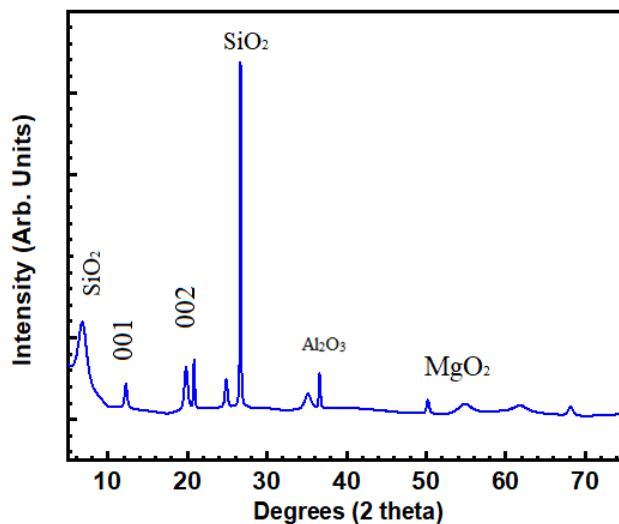
Figure 3-2: An XRD analysis of the bentonite clay used: Chemical structure:

$Al_2H_2Na_2O_{13}Si_4$.
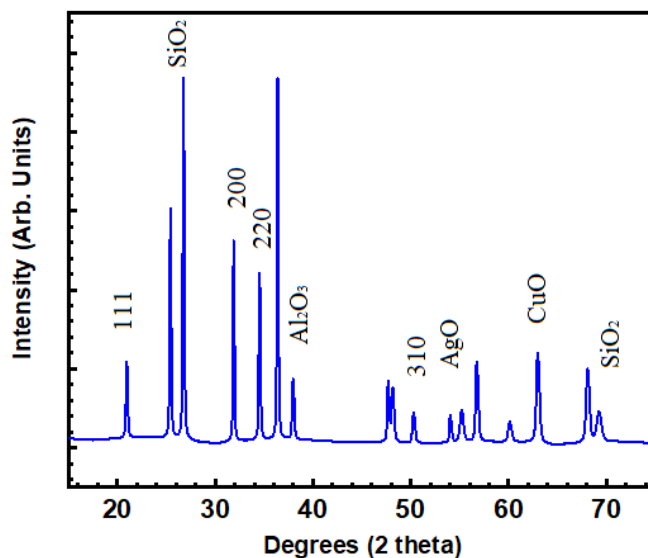
Figure 3-3: XRD analysis of the NPs—metals assembled on clay.
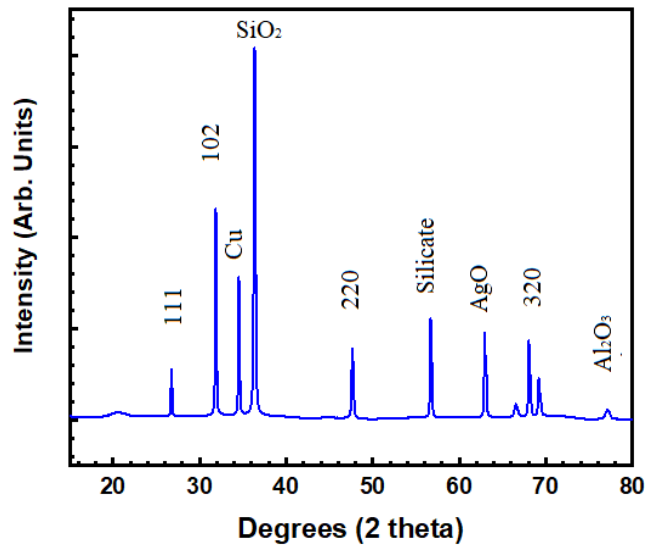
Figure 3-4: XRD analysis of the composite.

3.4.2 Scanning electron microscopy.

Figure 3-5 illustrates the morphology of the various samples, partitioned into Figure 3-5(a), Figure 3-5(b), and Figure 3-5(c) for clay, nanopowder, and graphene clay composites, respectively. Figure 3-5(a) shows a uniform shape of bentonite crystal. Its diameter and width are 20 and 2 μm as compared to Figures 3-5(b, c). This can be associated with the treatments with graphene and PDMS, which increase the surface area of clay that can bind nanoparticles like silver, copper, and graphene. Furthermore, Figure 3-5(c) shows some layers of flocculated clay resulting from the impregnation process by nano-metals. These observations are comparable and shown in Figures 3-5(a) and 3-5(b).
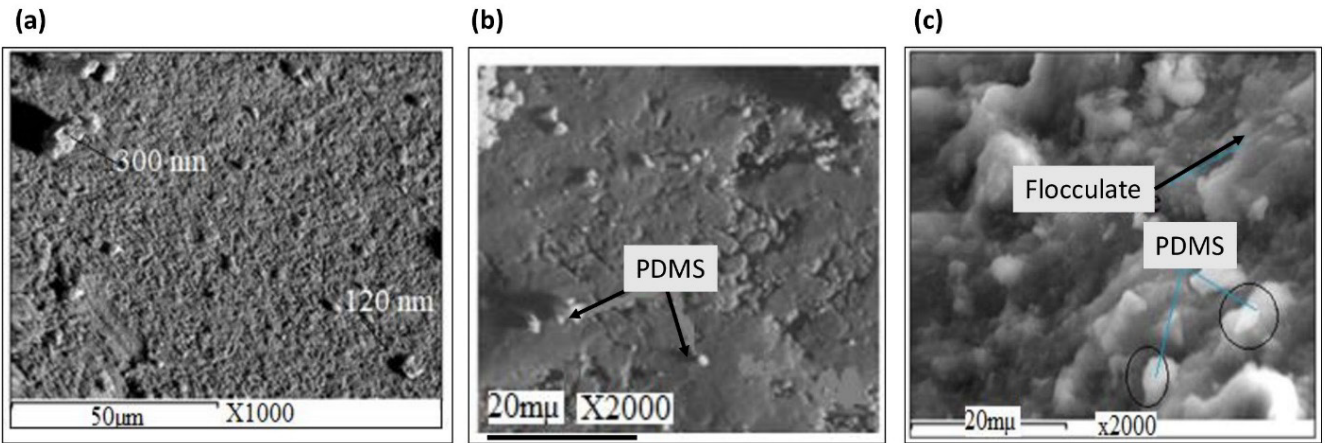
Figure 3-5: SEM micrographs of different materials: a) Pure clay; b) Nano-powder; c) Graphene- clay-composite.

3.4.3 Transmission electron microscopy (TEM).

Figure 3-6 shows the TEM micrographs of the investigated samples. Moreover, Figure 3-6(a), Figure 3-6(b), and Figure 3-6(c) show the structures for the samples for clay, nanopowder, and graphene clay composites, respectively.
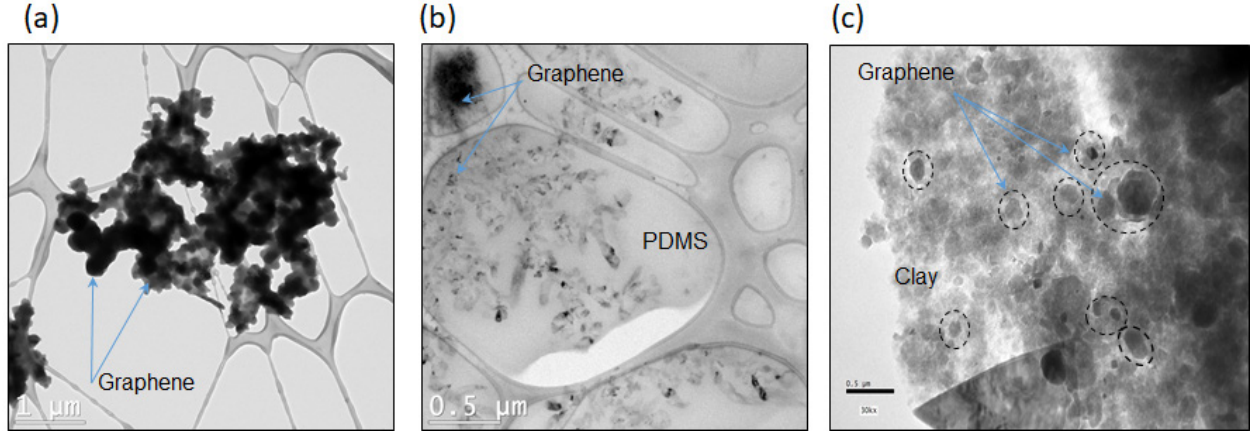
Figure 3-6: Representative TEM images of (a) and (b) graphene dispersed into PDMS solution, (c) composite of clay PDMS polymeric assembling graphene.

Figure 3-6(c) points out the typical structure of sodium montmorillonite clay, which describes a homogeneous distribution of clay flakes carrying out nanoparticles inside the clay sheets due to the size of the arranged nanoparticles≈ 20 - 28 nm.

The surface morphologies of the clay-PDMS composites indicate an immense layered structure and huge flakes coupled with some spaces between the layers. Important changes can be observed between Figures 3-6(a) and 2-6(c). They include a reduction of the interlayer of the clay composites, indicating a distribution of the nanoparticles (graphene, silver, and copper) between the clay layers. Furthermore, the smooth surface morphology of graphene-PDMS shown in Figure 3-6(b) is completely transformed in Figure 3-6(c). It shows an aggregation of the nanoparticles on the surface of PDMS, resulting in a decrease in the structure's surface area.

Moreover, the images' differences are evidence of the grafting of the nanoparticles on clay and PDMS matrix to form novel composite materials. Furthermore, The TEM image of Figure 3-6(a) displays tiny spaces between individual silver particles and copper nanoparticles, which self-aggregate and relate to the surrounding negative charges. Consequently, there is a possibility for forced interactions between the cations of clay and the anions resulting from the reduction of the Cu/Cu^{+2} // Ag^-/Ag cell.

Figure 3-6(c) shows that PDMS is tied to the outer shell of both copper and silver nanoparticles. In addition, mitigation of free ions charge (Ag and Cu) which are suspended with Graphene Nanoparticles inside the colloidal solution is, made the boundary of output a negative charge (cloud) on the graphene surface, forming dual characterization resonating of electrons (π-π) on a layer and the other layer is an electrochemical reaction of Cu/Ag cations in conclude. Both Figure 3-5 and Figure 3-6 confirm the complete distribution of nanostructure of nanoparticles assembled interlayer spaces clay and PDMS matrix.

3.4.4 Electrochemical characterization.

Figure3-7 shows a comparative variation of the electrochemical resistivity of the various investigated samples. They all show the same pattern; moreover, they increase as a function of their composition, starting from clay, then the composites and PDMS. This behavior is probably

related to the motion of free ions, the viscosity, and the disturbance of the ions inside the solution. It is then suspected that the graphene bond types, such as the (π-π) and the metallic, have a large impact on the conductivity of these substances and the facility of ions transfer inside the solution.
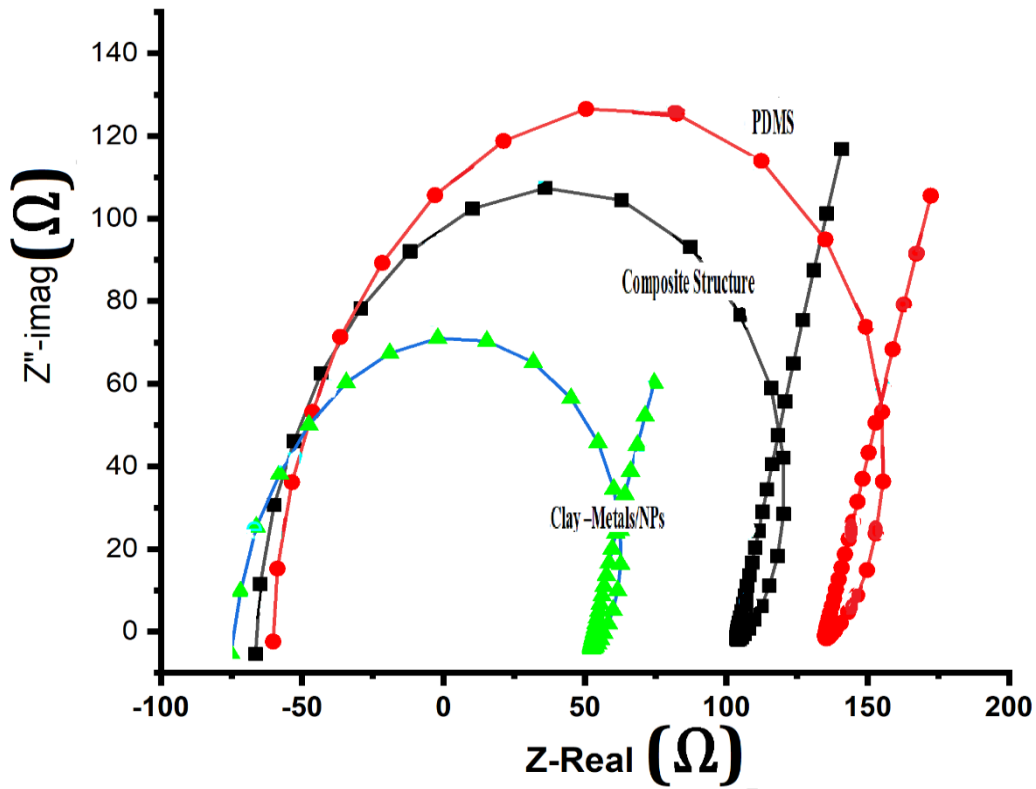
Figure 3-7: Variations of the EIS measurements for pure PDMS, clay-NPs, and

graphene-clay-composites.

3.4.5 Dielectric measurements of the PDMS substrate.

Figure 3-8 shows the variations in the dielectric constant of pure PDMS with the frequency. It shows a constant value of 2.67 throughout the observed frequencies. This can be related to both the chemical structure and the intermolecular interactions. Apart from the

polarization of the Si-O-Si bonds, the system appears to be internally stable and under the influence of no external force which could enhance the conductivity of the dielectric material.
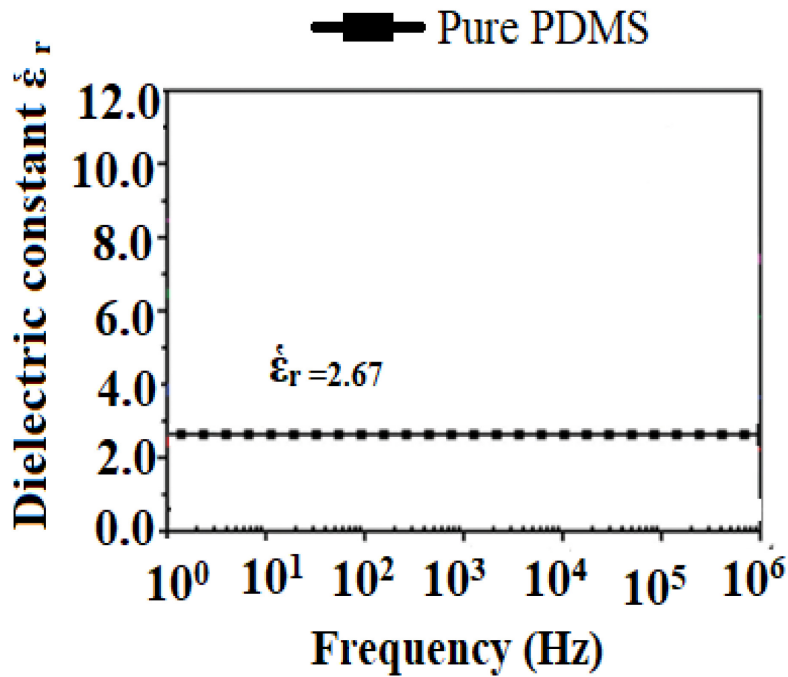
Figure 3-8. Variations in thedielectric constant of the PDMS substrate.

Figure 3-9 shows the ICP composition of the nanoparticles while validating the presence of silver, copper, nickel, and the elements related to the graphene composition.
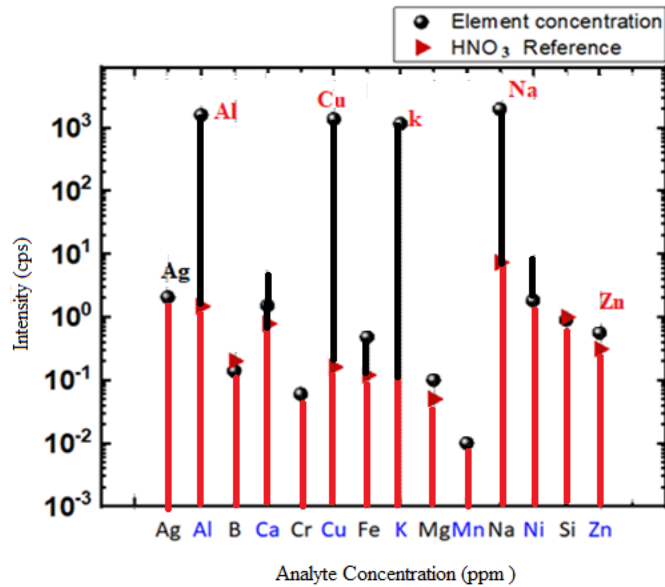
Figure 3-9: ICP in the composite structure.

3.4.6 UV analysis.

Figure 2-10 shows the variations in the absorbance of the samples of the composite geo polymeric of clay PDMS assembling graphene as a function of the wavelength. It shows that the equivalent of some peaks found on the composite spectra is nonexistent on the clay nanopowder spectra. This is a good indication of the presence of silver, copper, and graphene NPs in the interspace of the PDMS substrate. In addition, there is a slight shift for copper and silver in the first structure (clay-NPS), which indicates the formation of a chelating complex from the cation exchange between clay arrangements and the nanoparticles. Overall, the UV analysis confirms the clay-NPS-PDMS composite composition as a matrix block.
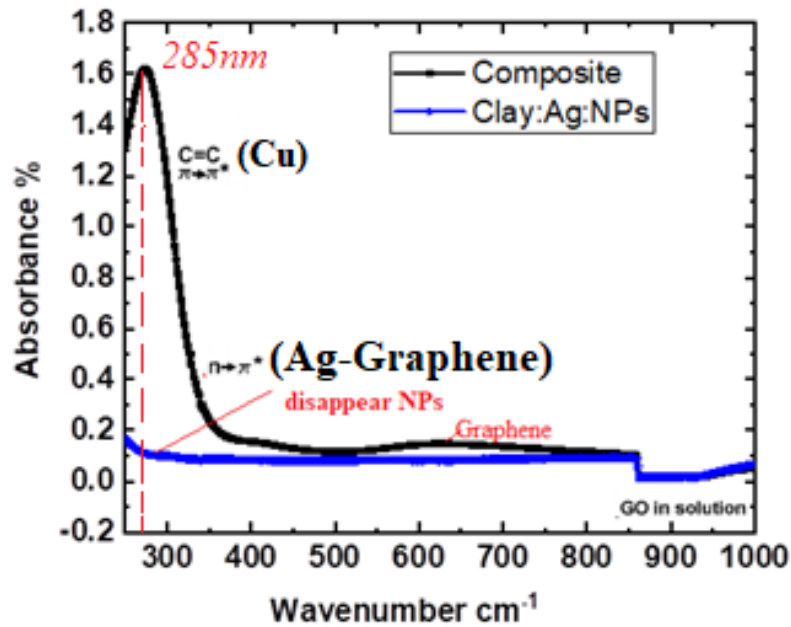
Figure 3-10: Comparative UV-Vis-NIR analysis of graphene assembled clay composite and metals/clay nanopowder.

3.4.7 Measurement of the dynamic viscosity and the particle size analysis of the fluidic solution.

Figure 3-11 shows the variations in the apparent viscosity with both the investigated materials and the temperature. It indicates an increase in the nanoparticles that it contains, resulting from the co-aggregation and conjugation of the particles. Such observation is also related to the interactions between the outer sphere charges of the particles suspended in the solution and the various solutions containing cations such as bentonite, the anions of the dissolved nanoparticles, and the PDMS matrix. The resulting increase in the dynamic viscosity occurs in the following order: clay, clay-NPs, graphene, graphene-NPs, and finally clay-PDMS. Moreover, the lowest and highest values attributed to clay and clay-PDMS are 7.02 and 13.98 m.ps.

η PDMS-Clay /Graphene/NPs>> η Graphene >>ηClay-NPs>> η Clay
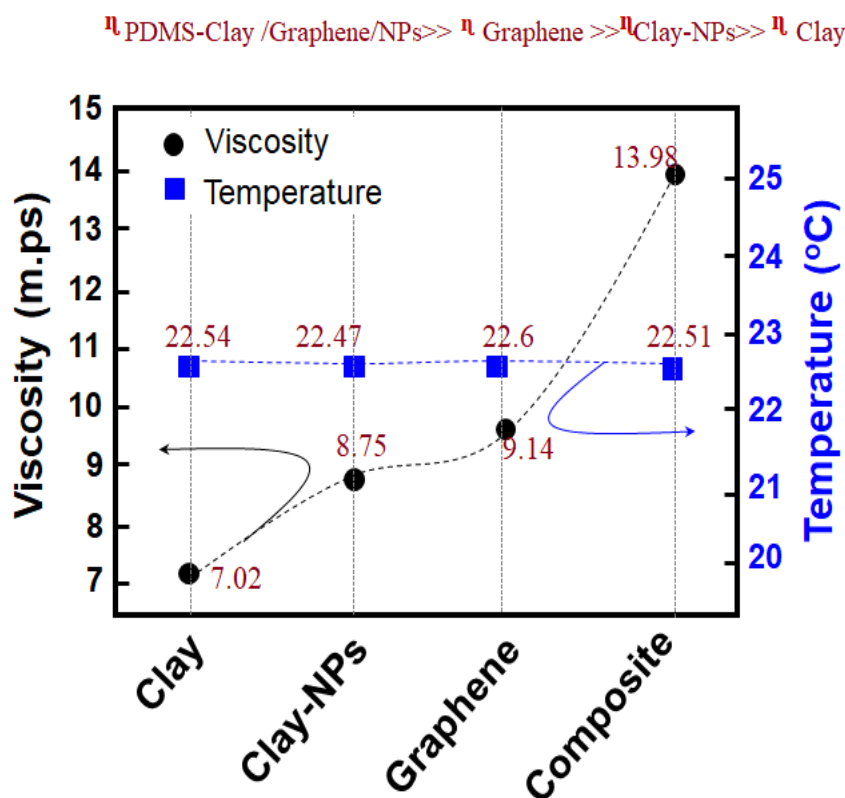
Figure 3-11: Variations in the dynamic viscosity of the samples with their composition and temperature.

The particle size analysis is given in Figure 3-12. The results are shown as frequency variations with the size for graphene-PDMS in Figure 2-12 graphene/nanoparticles in Figure 3-13 and clay/PDMS-NPs in Figure 3-14

In Figure 3 -12 graphene nanoparticles are mainly found suspended and uniformly distributed inside the PDMS solution. As large as 118.6 nm, the resulting particle size could be caused by either a combination or an aggregation of small particles. However, in Figure 3-12(b), the particle size analyzer recorded two significantly different particle sizes of 640 and 5565 nm. This may be attributed to the adhesion of metal nanoparticles of different sizes on the graphene surface. Finally, Figure 3- 10 shows the presence of medium-sized particles with an average of 540nm. It probably results from various causes, such as the process where metal nanoparticles

fill the voids between clay interlayers while graphene nanoparticles are distributed inside PDMS solution and the shielding of huge particles. It is also important for the charge transfer through the fluidic solution. In the overall, no massive flocculation is formed during the process, indicating a solution that can transfer charge without restriction.
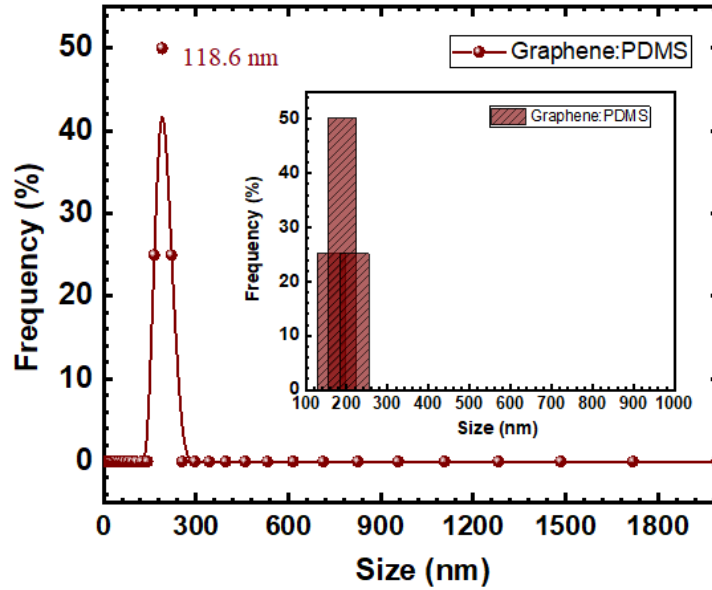
Figure 3-12: Particle size analysis of graphene-PDMS.
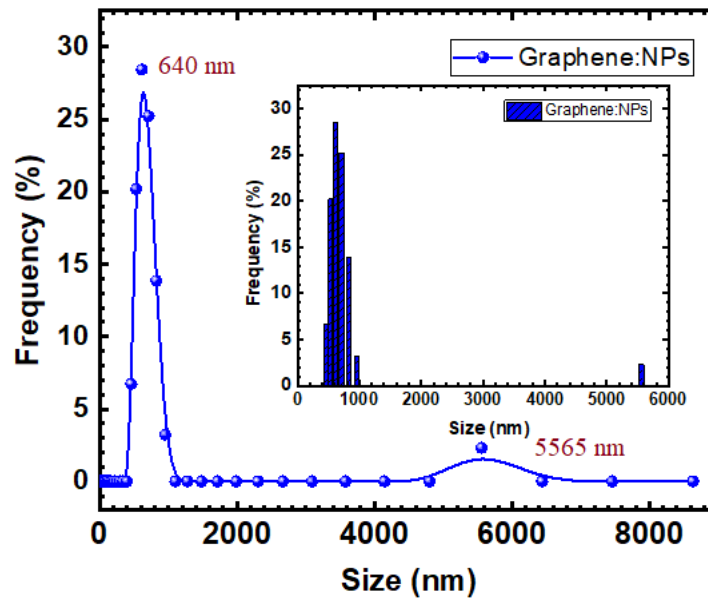
Figure 3-13: Particle size analysis of graphene/nanoparticles.
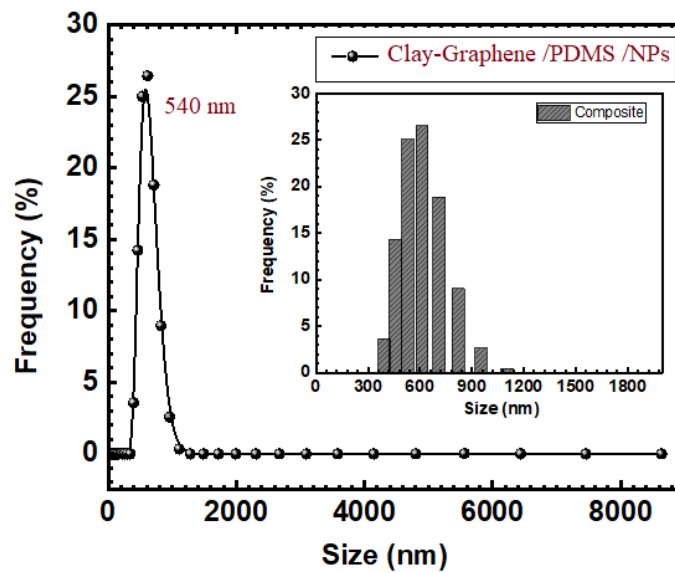
Figure 3-14: Particle size analysis of clay/NP/PDMS Composites.

3.4.8 Thermal characterization of PDMS and its composites.

The DSC and TGA measurements are respectively found in the thermograms of Figures 3-15(a) and 3-15(b). They indicate different thermal behavior for the pure PDMS, PDMS-graphene, and PDMS-NPS-clay.

a) DSC
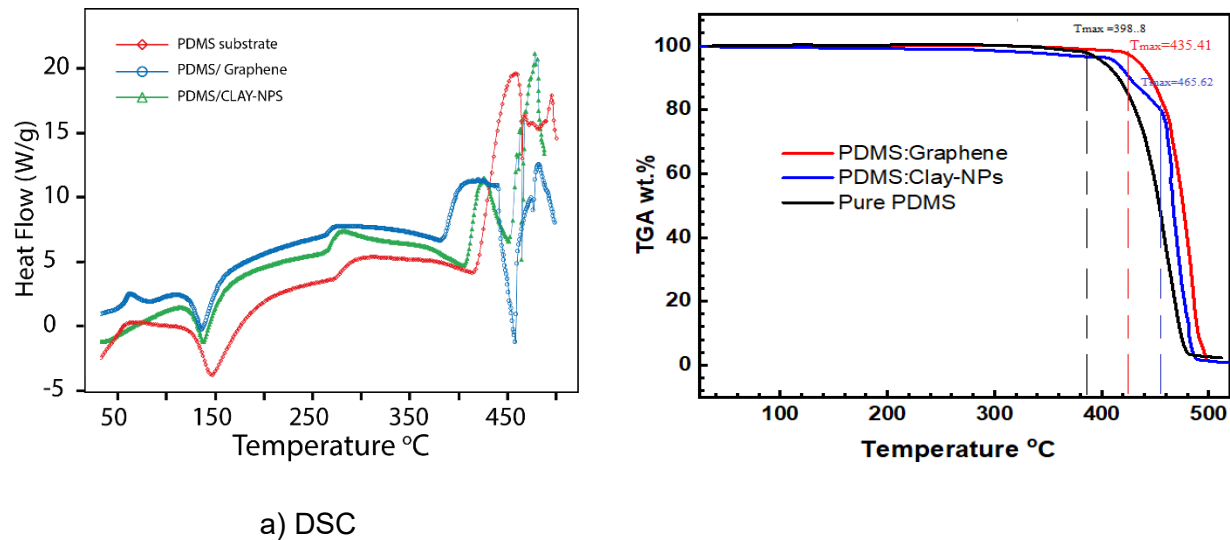
Figure 3-15 : DSC (a) and TGA (b) thermograms of PDMS, PDMS /Clay –NPs, and graphene-PDMS.

The DSC thermograms show comparable patterns for the investigated formulations except for a small deviation shown by pure PDMS around 450°C. All the formulations show four significant stages of thermal degradation. In the first stage, about 8.59% of weight loss found between 30 °C and 115 °C can be attributed to water molecules. In the second stage, a loss of 7% occurring between 115 °C and 160 °C. is attributed to the degradation of the SiO_2 is the main skeleton structure of PDMS polymer composition. The third degradation stage, between 160 °C. and 320 °C., indicates good thermal stability without exhibiting any chemical or physical changes[107].

In the fourth stage, located between 320 °C and 490°C, a weight loss of 22.36% was recorded and could be explained by the polymeric chain breakdown and the pyrolysis of the

composite structure. Based on the following thermal degradation reaction, water, carbon dioxide, light hydrocarbons such as methane, are byproducts, while clay acts as a cracking catalyst [108].

$$Si(CH_3)_2 + 4O_2 \rightarrow SiO_2 + 2CO_2 + 3H_2O \qquad (3\text{-}4)$$
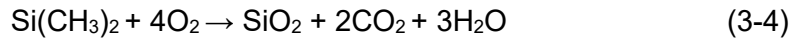
Additionally, the highest thermal stability was exhibited by PDMS-graphene and the lowest by pure PDMS. This could be caused by the interactions between PDMS and either clay or the nanoparticles, thereby reinforcing the crosslinks, reducing the intermolecular spacing, and increasing the degradation temperatures.

3.4.9 Measuring the performance of flexible antenna without bending.

Return Loss Characteristics

Figure 3.16 illustrates the capability of the fabricated composite to be used for a device such as an antenna, based on both the simulated and the measured data.

The simulations and measurements of the flexible antenna were recorded at two band frequencies between 1.9 GHz and 3.8 GHz with a frequency step size of 20 MHz [109]. The simulation results suggest that this flexible antenna and the transmission lines of that region made the fabricated material resonate at a frequency of 2.44 GHz.
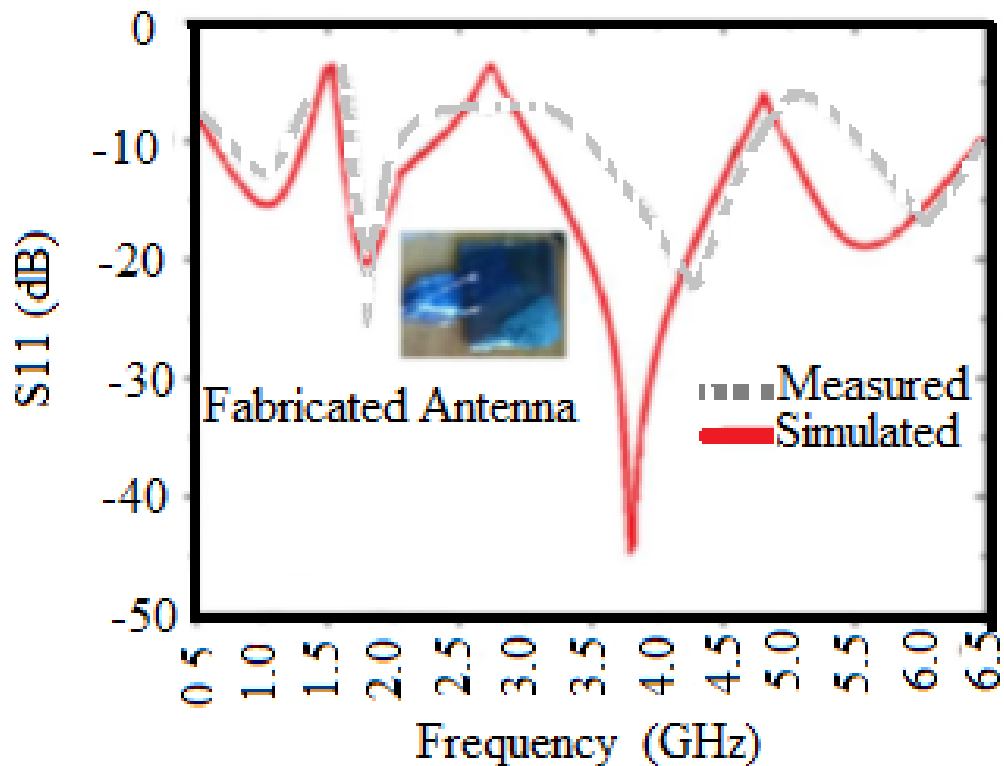
Figure 3-16: Return loss characteristics of the fabricated antenna.

3.5 Conclusion

In this experiment, polydimethylsiloxane and bentonite clay nanocomposites loaded with silver, copper, and graphene nanoparticles were successfully fabricated to create a stretchable and robust micro-strip antenna. Some characterization results were conducted with tensile and flexural tests, rheological and thermogravimetric analysis, UV-Vis analysis, electrochemical impedance spectroscopy, x-ray diffraction, scanning, transmission electron microscopy, dynamic viscosity analysis, and ion coupled plasma measurements of the associated loads of the nano additive. These tests show that these nanocomposites could be considered for microstrip antenna applications due to their electrical conductivity and mechanical flexibility. These composites may also be employed mainly for flexible RF devices in the military, sensor, and space industries. Additionally, the flexible composite has been used to fabricate an antenna device in the WLAN band area. The results of the measurements and the simulations show two frequencies at 1.9 and 3.8 GHz.

CHAPTER 4

FABRICATED WEARABLE AND FLEXIBLE CHIP MADE OF GALLIUM AND SILVER METALS COMPOSITES ASSEMBLED ON GRAPHENE INSIDE A PDMS MATRIX

Ameen Abdelrahman [a], Fouad Erchiqui [b], M. Nedil [c]

[a]Material Science Department / School of Engineering, Université Du Québec en Abitibi-Témiscamingue (UQAT), 445 Boulevard de l'Université, Rouyn-Noranda, QC, J9X 5E4, Canada

[b]Professeure- D'université | UQAT - Université Du Québec en Abitibi-Témiscamingue, 445 boul. de l'Université, Rouyn-Noranda, J9X 5E4, Canada

[c]Professeur Titulaire / Professor Directeur Du programme de la maîtrise en ingénierie École de génie / School of Engineering, Université Du Québec en Abitibi-Témiscamingue (UQAT), Campus de Val D'Or, 675, 1ère Avenue, Val D'Or, Québec, J9P 1Y3, Canada

Abstract:-

This work was done in view of creating a specific chip, that is wearable, flexible and which is a conductor, based on conventional physical methods like grafting and assembling metals (silver, copper, and gallium indium alloy) on graphene as a composite, following by immersion inside PDMS matrix. However, due to an incompatibility between liquid gallium and graphene sheets, a bridge of metallic nanoparticles ~~as~~ of silver and copper was used as a barieer to its different charges to maximize the interfacial interactions between amorphous carbon and liquid gallium. Different characterization methods such as EIS Impedance includes both resistance and reactance and CVT were used to evaluate the conductivity of the chip during the fabrication process. Moreover, the chip's thermal stability was evaluated by the differential scanning calorimetry (DSC), its mechanical properties determined by the tensile tests, and its morphology characterized by a combination of TEM IR and UV absorption techniques. The dielectric constant ($\acute{\varepsilon}$) of the composite was evaluated at a different range of frequencies as 3.73 which is higher than the value of PDMS which is 2.69.

Keywords:

PDMS, Tensile response, graphene, Ag, Cu nanoparticles, electrochemical impedance. DSC

4.1 INTRODUCTION.

Nowadays, flexible and wearable electronic devices are rapidly gaining ground around the world. It is found in many areas in the example of biosensing, human health monitoring, electronic communication and media devices. A variety of the integration and trials of liquid-phase technologies are used in the fabrication of these applications including spanning for smart packaging [110, 115] biosensing and macro chips [116] flexible fluidic antenna [117], renewable energy management [118], and printed electronics inks devices [119]. Central to this technology are high performance graphene which is an appealing material for electronics applications due to its unique properties, its high conductivity, flexibility, and mechanical stability. Recently, a wide variety of applications depending mostly on Graphene have been reported [120]. Many production routes exist for graphene; however, liquid-phase exfoliation is well-suited and cost efficient for electronic applications [121]. There are numerous advantages of using graphene in electronic applications, one of the most important being its stable and high-

concentration dispersion in suitable organic solvents. Although reduction of graphene-to-graphene oxide can meet this standard, the degradation might affect its efficiency, thus the motivation to use the pristine graphene during the preparation process. [122] The diffusion of pristine graphene demand adopts organic solvents, surfactants, or polymer stabilizers to reduce paring aggregation.

Therefore, a need for new composite materials in the fabrication of electronic and optical modules is pivotal [123]. Polydimethylsiloxane (PDMS) is an example of polymer used in such composite materials. In fact, PDMS is reported in the literature as used in most electronic technological applications. Its unique polymeric characteristics include stretchability, ease of handling and packing, transparency, non-toxicity, and low cost. [124]. Some applications making use of those features of PDMS include sensors, valves, detectors, filters, solid elastic lenses, and antenna substrate for microelectromechanical systems (MEMS) [125]. various literature studies had been carried out on the physical and chemical properties of PDMS, involving specific synthesis parameters like curing agent ratio, , curing temperature and curing times. In order to improve on the elastic modulus of PDMS, the use of reinforcements such as ceramics or fillers is needed, leading to more To suitable characteristics, such as surface energy compatibility, superior hydrophobicity [126]. A proper choice of those reinforcement and fillers is important, especially in terms of size and shapes, as well as their overall effect in the composites. In this regard, ZnO, Ag, and GO materials have been reported as appropriate candidates for biocompatible applications, and for their versatility in the fabrication of microstructures In fact, the concept "reinforcement" points out to the improvement of the stress-strain behavior, and the abrasion resistance, which can be achieved by either filling out or grafting nanomaterials inside the cross-sectional gaps of polymeric matrices. Some reported examples includes the grafting of carbon black on natural rubbers or metals oxides on polymers to improve their conductivity.   Numerous inorganic fillers have been used to reinforce the polymeric structure; some for examples include the nano metal oxides, SiO_2, Al$_2$O3, graphene, $CaCO_3$, fiber-glass, and carbon nanotubes [127,128], which offer special advantages such as appropriate size and shape, as well as the compatibility with the matrix. [129] During the reinforcement process, a special care has to be placed on both the miscibility and the homogeneous dispersal of the nanoparticles into the matrix [130]. Recent development in the field of nanotechnology are focused on the fabrication of ceramics – reinforced composites

owing to the positive physical and chemical effects of the ceramic materials on the final composites [131]. Similarly, silicates and carbon nanotubes (CNT) have been used as fillers for various polymeric materials with very promising results [132,134].

In the same manner, graphene is a potential sensing material for a flexible antenna; its special characteristics include its high Young's modulus, its ions charge mobility, and its piezoresistivity [135-137]. Significant efforts have been made in improving the conductivity of graphene-based material by either assembling or grafting a graphene membrane on a silicon substrate [138], depositing graphene thin layer on a silicon nitride substrate [139], or employing graphene as flakes coating into a silicon base [140]. Most of the common recent practices include the use of graphene-polymer composite [141-142], laser-scatter graphene foam [143], modal graphene on elastomer [144], and graphene rolling [145-147]. Furthermore, it has been suggested to work on a fluidic antenna, which has a great potential for wearable besides applications based on electric conductivity and flexibility Mercury has long been used in so many electronic devices, but it has a high toxicity as compared to eutectic Gallium-Indium (EGaIn), which is a liquid metal alloy at ambient temperature as well as a good conductor with appreciable wetting properties [148]. EGaIn used into a flexible substrate are found in unable and reconfigurable electronic applications, electromagnetic devices, and systems involving electrical probes [149], microfluidic channel electrodes [150], nanowire conductors [151], patch antennas [152], [153], as well as metamaterials and 3D electronics re-workable silicon [154].

In the same manner, graphene's unique characteristics and stable detection [155] which is known by its two-dimensional carbon structure, leads to special features applicable in electronics like the quantum dots effect [156] which helps understanding the Dirac fermions, the tunable bandgap based on channel width, and the localization spin at the zigzag edge state [157]. There are many conventional methods of the graphene growth in the example of the chemical vapor deposition (CVD) on a metal thin film such as Ni, Co, and Cu. Although CVD is an easier way to grow a large amount of graphene [158], it is mostly related to how to manage the disorder and the layers thickness of graphene. The scope of p−n heterojunction instruments with n-type 2D materials such as graphene and MoS2. GaTe also expounded high-interest levels anisotropy plane, electronic reflection, and optical properties. However, the forward movement of Ga silicone-based devices is quite challenging and requires special environmental conditions [159] Furthermore, 2D materials like graphene, and carbon nanotubes have a special

potential for that environmental stability, due to its excellent surface area to volume ratio. Herein we depict fluid metal eutectic, Ga–In "e-gain"; 75% Ga, 25% In by weight, m.p. =15.5 8C) [160]. Although the deposition of nanoparticles of metals like Au, Ag, Cu, and Ti is widely documented in the literature, it is considered as one of the conventional methods of electron-beam or thermal evaporation causing the damage of the deposited thin-layer of metals and organic materials, and the wall defection of the fabricated materials [161] [162].

There are numerous reported applications of the gallium-indium (Ga–In) alloys in different fields as biomimetic devices, biosensors [163], and communication, ̄, due to its unique metallic properties, as well as its compatibility with different polymeric substrates to form stretchable, wearable and robust conductors and sensors. Furthermore, other attractive properties of these materials include their low melting temperatures, low resistivity ($\approx 29 \times 10^{-6}$ Ω cm) [164], a low dynamic viscosity (≈ 2.4 mPa s) [165] which helps it to adapt and dilate to a different pattern during the process. Additionally, the existence of a thin layer of oxide at the surface of Ga–In alloy is the main cause of the induced high surface tension (≈ 0.6 Nm^{-1})–responsible for the formation of stable structures [166]. Recent applications based on distortion and deformable forming include tunable fluidic antennas, pressure sensors, elastomer materials conductors [167], 3D flexible conductors, (radio frequency (RF) sensor [168], and wearable tangible. Electrochemical techniques are some important methods to investigate the characteristics of materials related to its conductivity. Normally, liquid conductivity depends on molecular vibration and molecular motion which induces charge transfer; therefore, the measurement of the material conductivity is often made by electrochemical impedance spectroscopy (EIS) [169]. Different electrode systems have been adopted for measuring the impedence; Impedance we approach, different electrode system stander or reference, count, and working electrode with applying an alternative current (AC) to measure the effectiveness of the interface the resistance between the electrode and electrolyte substance [170]. In addition to impedance measurement acquire a relatively time with certain open voltage cycles [171] to performs the measurement [172, 173]. This paper explores and demonstrate the possibiliyy of impregnating PDMS with materials such as graphene, silver, copper, and gallium alloy to promote the physical and electrical properties of the composite to be applied as a flexible and stretchable chip .

4.2 MATERIALS AND METHODS.

4.2.1. Materials.

Gallium - Indium alloy, Graphene Nanopowders with a high purity (99%) and 300 mesh, as well as n-Hexane and Tetrahydrofuran (THF) both used as solvents were supplied by Sigma – Aldrich (Toronto, Canada). Most of the salts including copper sulfate and high purity silver nitrate (purity > 99%) were supplied by scientific Fisher (Toronto, Canada). Finally, Polydimethylsiloxane (PDMS) type Sylgard R 184, was supplied by Dow Coming Corporation (Toronto, Canada).

4.2.2 Methods.

The process is a three-step operation involving the compounding of PDMS and graphene, the preparation of an electrolyte solution enriched with graphene, and the molding of PDMS composite.

4.2.2.1 Compounding of PDMS and graphene.

It is achieved by dissolving graphene in n-hexane for several days, followed by blending with a PDMS solution while stirring for 5 hours.

4.2.2.2. Preparation of the electrolyte solution enriched with graphene.

A colloidal solution containing 0.5 M of AgNO3 and $CuSO_4$ was mixed with 3 ml solution containing 0.05 g   graphene, gallium indium alloy (75:25) and PDMS. In order to create oe phase between gallium and ygraphene, graphene was dissolved in hot water for several days, followed by an ultrasonic heat stirring with gallium for 1hour at 60 ºC; in the same manner an ultrasonic stirring overnight at ambient temperature led to a complete homogeneity.

4.2.2.3 Fabrication of PDMS composite.

The A̶ composite samples of PDMS reinforced with graphene nano particles (PDMS - G/NPs) w̶a̶s̶ were fabricated by mixing the two solutions, followed by stirring for 5 hrs. Then the final solution was molded by mixing with the curing agent at the ratio of w/w (1:10), while stirring for 20 min, and transferred into the degasser vacuum for 15 minutes for all the bubbles removal, prior to the heating on a hotplate at 70 ℃ for 45 min. The molding operation was followed by cooling at room temperature. The process is better illustrated in Figure (4 – 1).
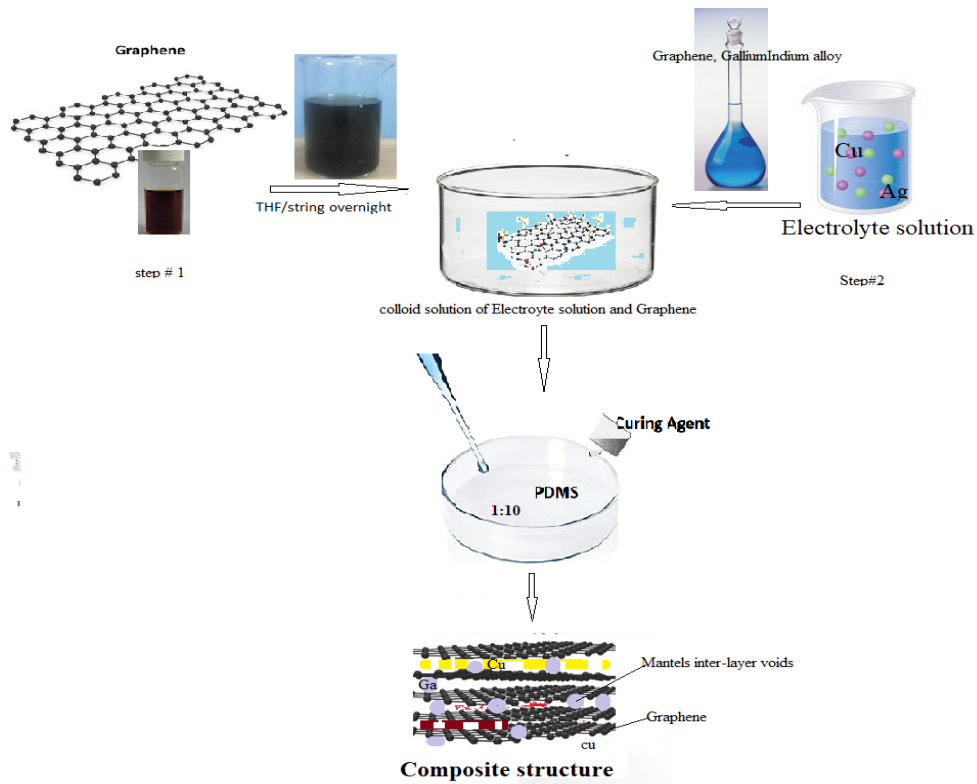
Figure 4-1: . Illustration of the PDMS composite fabrication process.

In that work, we detected the conductivity through impedance at frequencies 2.5 MHz to 1.5 kHz at open cycle volt (OCV =0.40) for deliberated the electrical properties of various conductivity composite and electrolyte solutions (composed of O.5M $CuSO_4$, Gallium/indium, and $AgNO_3$) as a liquid electrolyte and as grafting inside matrix composite of PDMS base.

4.2.3. Reactions mechanism

The first reaction consists in the grafting of graphene inside the PDMS material. It aims at creating a better adhesion at the interface through crosslinking. This is followed by the creation of more active sites inside the PDMS structure by engrafting metal nanoparticles like silver and copper. The system works by charge and ion transfer between graphene and the metals based on oxidation and reduction reaction.   The EGaIn junction (Cu–EGaIn), which inclusive of two interfaces—the metallic Cu–Cu interface, and the noncovalent PDMS /EGaIn interface—is also much modest than the Ag -connection, thus, creation of different sites of redox- chain reaction as follow,   (Cu^{+2}/ Cu graphene //graphene-Ag^-/Ag^+), and(Cu^{+2}/ Cu graphene //graphene-Ga^-/Ga^+). Which has, nominally, three interfaces: the covalent Ag–Ag interface, the van der Waals (//) interface between the two electrochemical forces (e.m.f) and third is graphene π-π   bonds, as resonance characteristic interface.

Assuming that EGaIn act correctly as a liquid, the energy E_r related to the attached EGaIn to graphene surfaces can be expressed using the Equation (3-1).

$$E_r = \gamma\left(1+\cos\theta_r\right)$$ (4-1)

EGaIn has smaller than its adhesion both of two substrates. Thus, it seeks to form metallic bonds with different specious silver and copper. Adhesion angle contact of Egalin, its makes it difficult to directly contact PMDS, so it makes abridge with other dissolved metals or graphene. Some studies worked on that phenomena Dickey et al. [174] confirm another reason for EGaIn is an oxide layer formed on its surface, thus it needed to more electron to facilities contact, to confirm that concept, gallium droplets coexistence with graphene layer partition inside PDMS matrix,

EDAX analysis is another technique used in identifying the main nano particles components such as sliver, copper, and gallium which had impregnated the composite structure. The results given in Figure (3-9) show some agreement with those from the **Ion coupled plasma (ICP)** analysis, which is a qualitative physical method of chemical analysis used for elements detection. It consists of a plasma torch (Model: Agilent Technologies, 5100) that simultaneously measures in a few minutes. the ionizing sample is injected into an argon plasma at about 6000K.   The prepared samples undergo wet mineralization or acid dissolution prior to the analysis.

This technique was carried out on (QuickTest QTS3) instrument in ETS, Canada. It is used for **Tensile Testing**, The 6 mm samples were clamped and pulled at a cross head speed of 60 mm/min until either failure or it reached 30% of its original length

The measurements were carried out in a Differential Scanning Calorimeter model Pyris 1 from Perkin Elmer. we used **Differential scanning calorimetry** (DSC), Model: Mettler Toledo, UQAM (Montreal, Ca). high heat capacity as well as, equipment provided with a heating rate around -60°C and +600°C under a controlled atmosphere (N_2 or air).by applying 0.25 mg of sample for twice scanning cycle 140uC to 270uC under the rate 10uC/minutes.

4.3. RESULTS AND DISCUSSION

4.3.1 Electrochemical characterization

4.3.1.1 Cyclic voltammetry (CV)

The main importance of conducting cyclic voltammetry (CV), is the detection of any reversible oxidation – reduction reaction inside the prepared solution. In this case, the composite samples were prepared from different homogenous solutions such as the graphene -PDMS, the electrolyte salts, and the composite solution. By setting up three cell electrodes (reference, working, and counter electrode) then applying voltage in the circuit between (relationship Current (I) and Volt (v)) The cyclic voltammetry of the prepared solutions is given in Figure (4 – 2). It shows a linear increase of the electrode potential with time in a cyclic manner following the

Ohm's law. This can be explained by the fact that dynamic potential has resulted into the chemical reactions and the charge transfers between different reactants
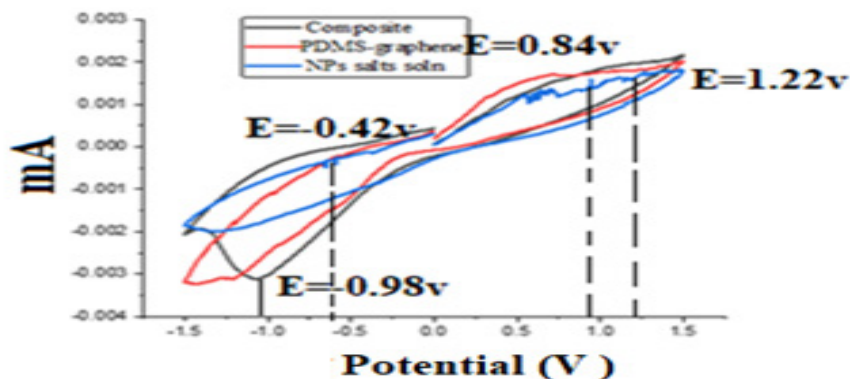
Figure 4-2 : Cyclic voltammetry (CV) of the prepared solutions.

The cyclic voltammetry was accomplished for potentials between 0.4 and 1.0 V as shown in Figure (4-2). Moreover, different peaks are shown as evidence for both reduction and oxidation processes. Such is the example of the peak found around −1.45 V, and varying in the opposite scanning (+1.45 V) which coincide with the electrolyte salt. Moreover, the sensibility of nanoparticles dissolved in the electrolyte solution is increased with increasing redox process, which means slightly shifting the oxidation potential peak from 1.8 to 0.6 on the one hand; on the other hand, that peak did not appear in the PDMS-Graphene solution. This illustrates that graphene conductivity is only dependable on BI-BI bonds' SP^2 resonance, thus, not creating enough active sites on its surface for reversible reactions as compared to the cases when ~~mixing~~ two components are mixed together to form the composite materials. In the later case, there are some peaks at (-1.1 V) which slightly shift at (+0.9V) and which can be explained by the loss of an electron by the composite and the formation of a ~~a~~ covalent bond with Ag $^+$ to become Ag^0.

4.3.1.2 EIS impedance measurements.

The conductivity of PDMS-composite, Nanoparticles electrolyte, and graphene -PDMS were measured by EIS which is a favorable used method, which is carried out by using a conductivity cell (HTCC, auto lab Bio-Logic Science Instruments) and EIS instrument(VMP-300, Bio-Logic) [63]. using multi-channel of Potentiostats sensor connected with a Frequency Analyzer (MPFA), operated by potentiostat -galvanostat united with eight channels, which used for electro-chemicals electrolytes and corrosive coating studies at (10V, 4A), applied of Sinusoidal voltage and different range of frequency from and a Nyquist plot software program to detection resistance of a material, then conductivity throughout equation $(\sigma = K/R)$ where, resistance (R) and specific resistance constant (K), which could count by the surface area electrode and length submerged in electrolyte or substance, we used three-electrode to complete circuit, reference electrode(glassy), stander (Pt)electrode and the counter electrode.
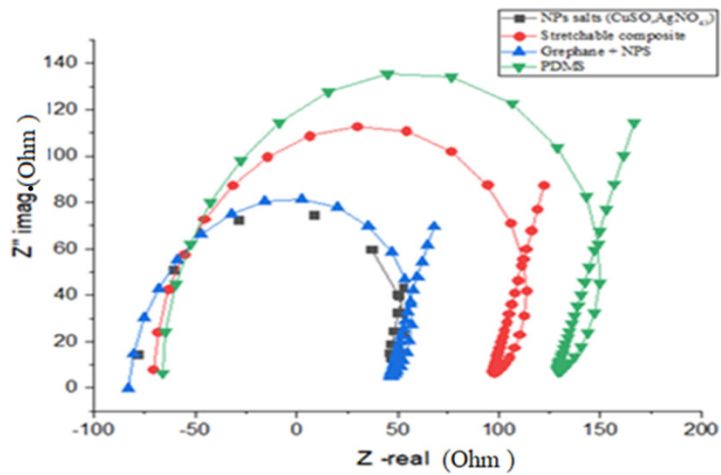
Figure 4-3 : Impedance diagram of various samples.

Fig (4-3) illustrates the resistivity of different prepared samples. It shows a reversible relationship between and resistance and conductivity (C=1/R), meaning that the conductivity decreases with an increase in the resistance. The measurements show that Cu_2SO_4 , $AgNO_3$, and Gallium alloy show the highest conductivity. In fact, due to their liquid and salt solutions, they offer an ease of mobility of the electrons as compared to the case of other components. In

the case of pure PDMS polymer, which is non-conductive polymer, the high value of the resistivity appears on the Nyquist plot. However, its conductivity increases with the addition of nano particles and graphene. Furthermore, treating graphene with either salt solutions or electrolytes increase its conductivity, however, its values remained below those of the electrolyte salt. In fact, graphene could be hindering the movement of ions in the solution. Fnally, the observed conductivity can be in summarized in the following order: Electrolyte salts >> Graphene-salt solution >> Ccomposite >> Pure PDMS.

4.3.2 Spectroscopic characterization.
4.3.2.1 The Fourier Transform Infra Red (FTIR) spectrometry.

This Raman microscope comprises an optical microscope Model: Renishaw, inVia Reflex (UQAM Montréal), dimension (x5, x20, and x50) connected to a Raman spectrometer, which its two lasers' sources (532 nm and 785 nm). The optical microscope is used to magnify and recognize the sample surface, mechanism of the Raman spectrometer is spread out light then, detected the irritation vibrations. Furthermore, it could obtain optimized Raman spectra of samples at resolution   2 µm.

The Raman spectroscopy was used to characterize the different samples of graphene/electrolyte salts (silver nitrate, copper sulfate, and gallium), electrolyte salts, and PDMS composite. The results summarized in Figure (4-4) show that the hybridized sp^2 carbon atoms' positions are stretched with a slight shifting from the electrolyte solution. The electronic configuration of graphene and the new metallic bonds between metals (M-M) and with graphene causes the disappearance of the graphene's double bond and the shifting of the spectrum.
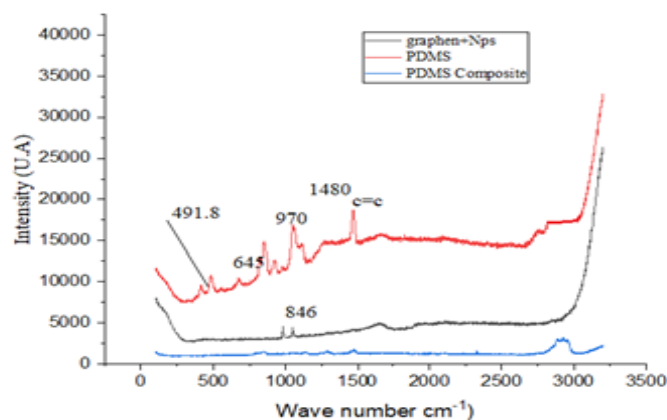
Figure 4-4 : Raman spectra of three different PDMS samples

spectrums peaks show outstanding at 109, 115,162, 176, 210, 270, and 285 cm^{-1} in good convention with previous assessment. 25, 26, 42 with a slight exception of two peaks for nanoparticles assembled on PDMS (Ag and Cu) appear at different slight peaks .this data agree with the previous literate reviewer[64].

4.3.2.2 The Ultraviolet (UV) Characterization.

The UV Characterization is carried out by Lambda 750 UV-vis-NIR spectrophotometer (UQAM, Montreal), from Perkin Elmer using blank sample distilled water as seen as Figure (4-5) demonstrated UV absorption spectra of comparing prepared samples composed of pure of PDMS, electrolyte salts solution –Graphene and composite PDMS. Figure (4-5) shows the comparative UV spectra of the investigated samples. There are specific peaks around 280–350 for the electrolyte salts (Ag, Cu, and gallium). which is slightly disappear on the spectrum of the PDMS composite. In the same manner, the matching peak with p–p* electronic transitions for the graphene resonance structure is also vanishes from the composite matrix. Various peaks are also revealed around the wavelengths of 350 and 280 nm in the electrolyte-graphene samples, and could respectively be attributed to the n–p* transition of Ag- Graphene or Cu –

Graphene . addition to other parts is related to metallic nanoparticles like silver and copper makes another bonded with amorphous carbon
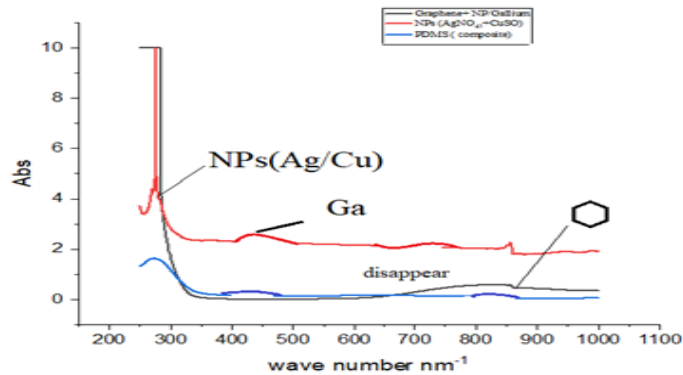
Figure 4-5: UV spectra of the prepared materials samples.

4.3.3 Surface morphology characterization

4.3.3.1 The Transmission Electron Microscopy (TEM) characterization.

The morphologies of PDMS and PDMS composites were investigated by scanning electron microscopy (SEM) carried out also (ETS, Canada) throughout the Zeiss Ultra plus (3 kV, 15 mA) instrument. The surface morphology which characterization is shown in Figure (4-6) shows that the surface morphology of PDMS is too smooth without flocculated and aggregated particles, as compared to Figure (4 -7 (a, b)) which is composed of the thin layer of graphene spread on the surface of PDMS; the added is submerged inside PDMS structure. Thus a good evidence for the reinforcement of the cross-section of structure; Furthermore, Figure (4- 7(a, b)) shows that graphene appears at the fold-up edge of the buckled surface. Fig. 4-7(b) shows graphene stacking which consists of different thin layers with a space area of 0.36 nm. The thickness of amorphous carbon film is roughly 15~20 nm based on previous knowledge, the thickness of graphene is changing randomly (slightly increase) by 2~3nm, as it could be deposited or aggregated of by many layers forming a thick layer of graphene nanotubes impregnated with dissolved metals like sliver and cupper

Figure (4-8a) further various nano suspended particles detached from the surface of liquid gallium. However, there are some films cut off into small fragments in the liquid but still in contact with each other. These fragments removed in a Cu-mesh tended to collapse .

4.3.3.2 The Scanning Electron Microscopy (SEM) And (TEM) analysis.

The newly fabricated composites have been characterized by SEM; ~~and~~ therefore, their cross-sectional morphology and their surface are shown in Figure (3-6)..the Moreover, Figure (3-7b) shows many ripped and shard pieces distributed on cross-sections of PDMS A comparison of the two figures shows smooth surface of PDMS without any depletion or aggregation, in the opposite of Figure (3-7a) which shows a complete change of the surface morphology of PDMS. This is an indication that many nano particles such as silver, gallium and copper fill out the space area of the PDMS matrix. Furthermore, it was noticed that whiskers are mostly arranged and expanded along the surface of PDMS as seen in Figure (3-8b). However, in the case of PDMS-NPS reinforced composites, an excellent dispersal of the nano composies is shown on the whole PDMS surface. This leads to the formation of the reinforcement matrix build-up that looks like tetrapod's arms oriented towards different directions, In the case of PDMS -NPS filled composite, the nanoscale particles are hardly dependable applicable structure . As shown in Figure (3-8b), a huge number of Ag nanoparticles are found in the vicinity of Cu nanoparticles; this ~~it~~ could be explained by the fact that electrostatic attractions result in the fornation of metallic bonds.
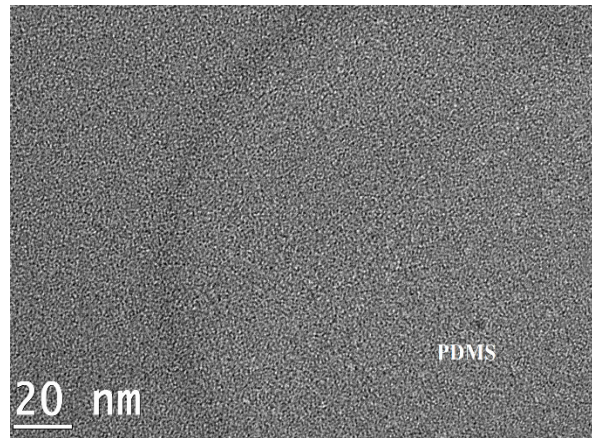
Figure 4-6 : Scanning electron micrograph of PDMS sample.
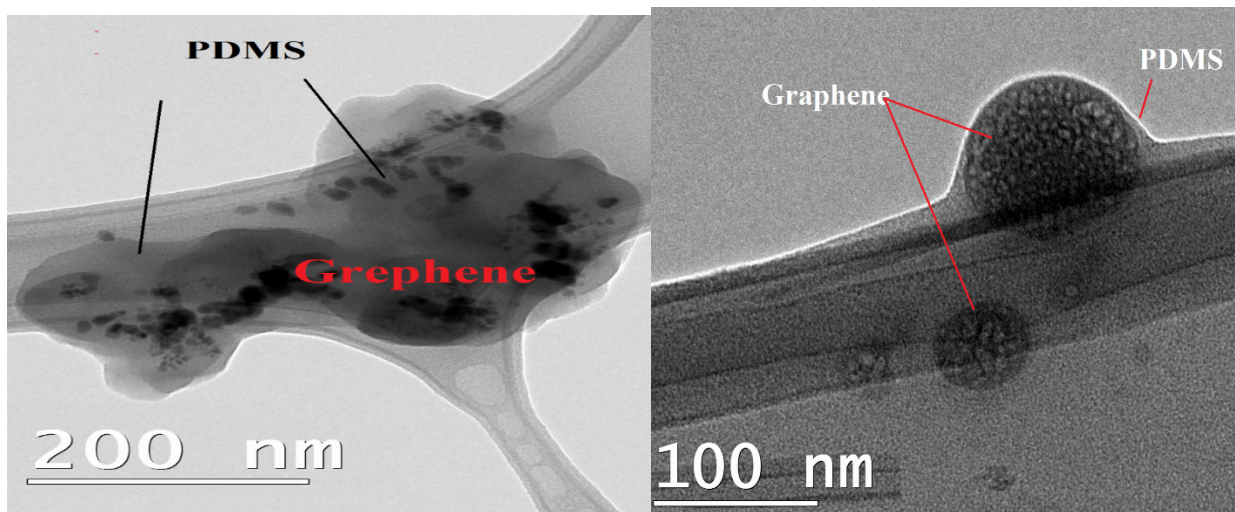
Figure 4-7: Transmission electron micrographs of PDMS –Graphene composite with

the magnification of 200 nm (a) and 100 nm (b) .
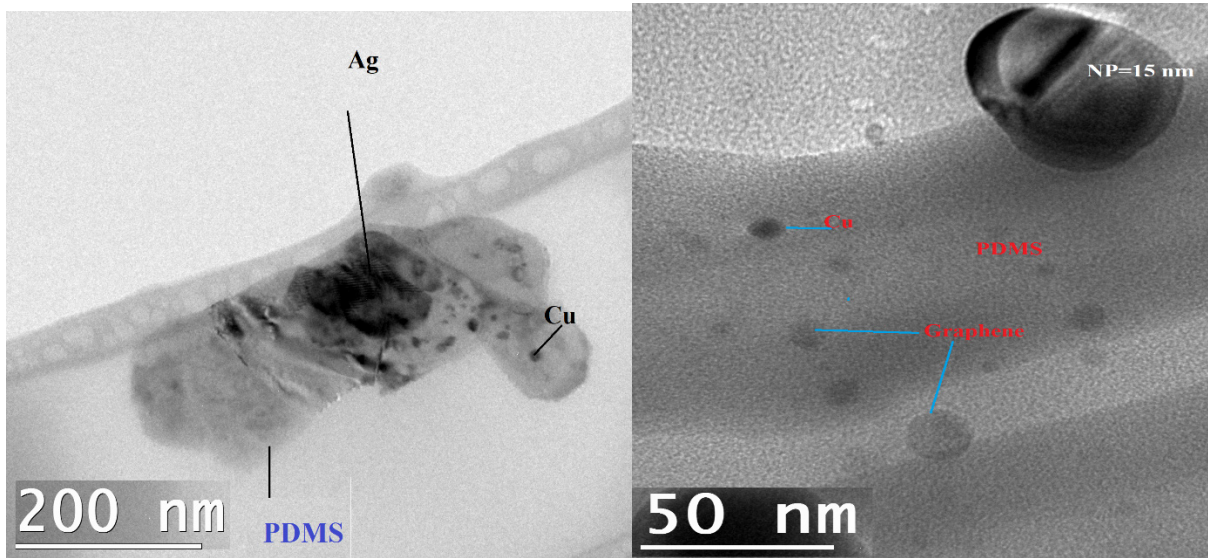
Figure **4-8**: Transmission electron micrographs of PDMS-nanoparticles (a), prepared composite (b) .

4.3.3.3 Energy-dispersive X-ray spectroscopy (EDAX) Characterization.

Figure (4-10) points out the nano metals like silver, copper, and gallium alloy, found in the sample and confirmed in the diagram below; all the data is confirmed by the EDAX analysis.
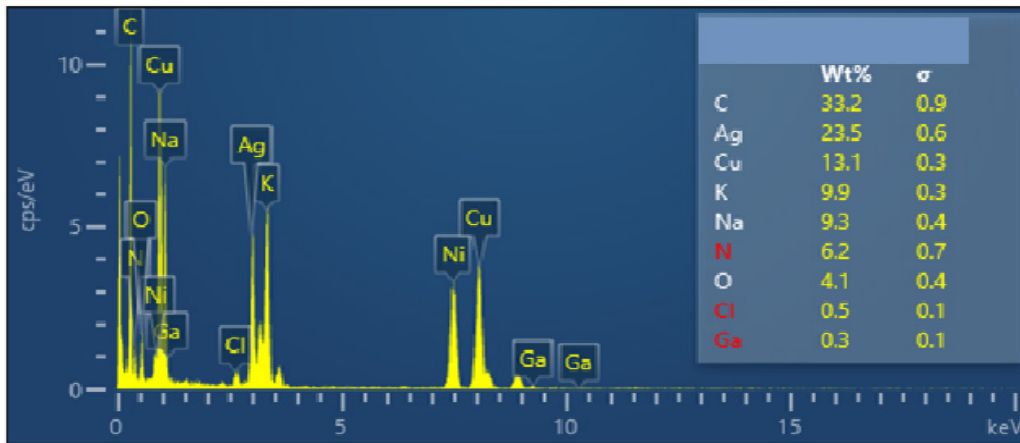
Figure 4.9 : EDAX measurements of the investigated samples
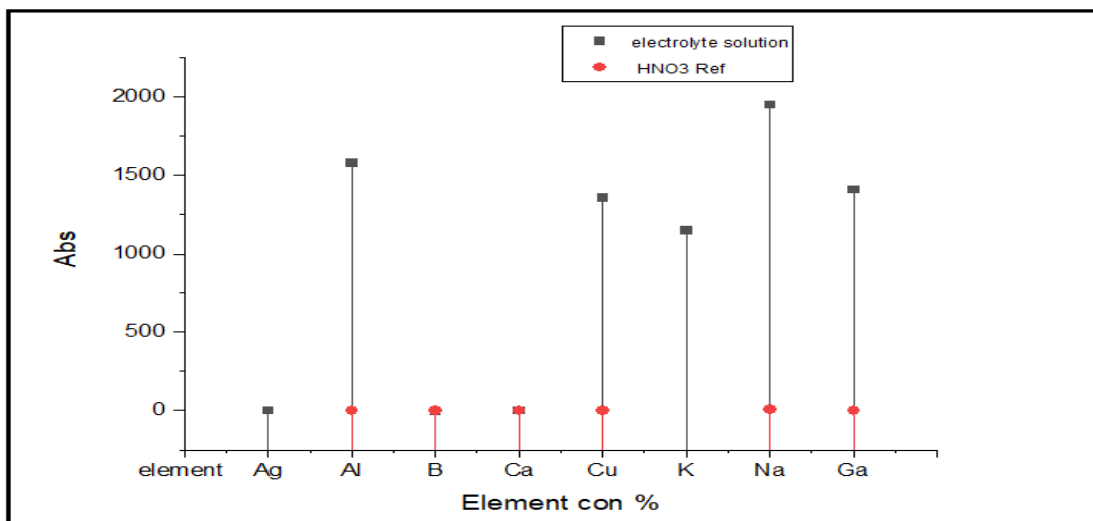
Figure 4-10 : ICP analysis of the composite matrix solution.

4.4 Physical characterization of the prepared composite samples.

4.4.1 Stress-strain analysis

.
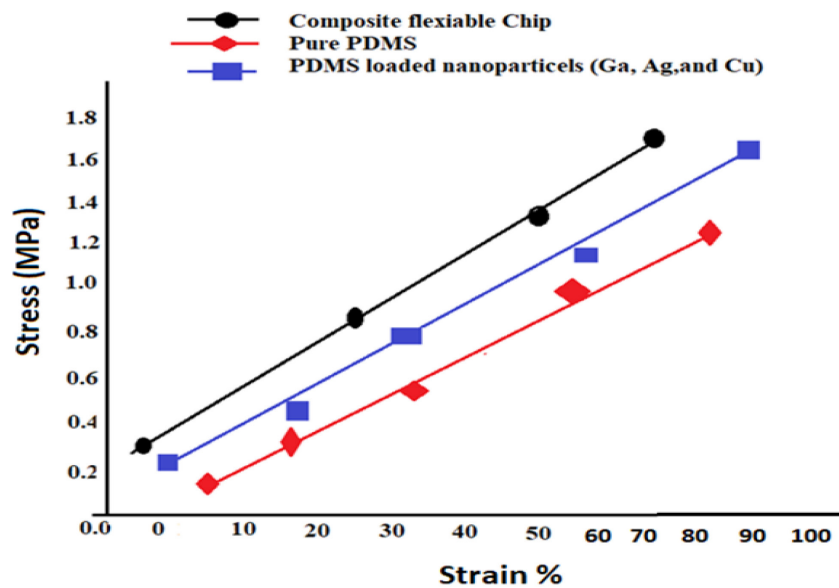
Figure 4-11: Tensile response of the fabricated composites of PDMS at applied stress

at 15% strain.

The mechanical properties are one of the main elements of the performance evaluation of new composites) especially with respect to their stretchability and flexibility. The tensile response experiment has been carried out on prepared composites to improve in the stiffness and reinforcement of synthesized PDMS, and PDMS -nanoparticles by applying stress-strain at 15% MPa . All the results are summarized in Figure (4-11). There is a direct correlation between applied strain and resulting stress for all prepared components, with the highest values found for PDMS /Graphene -NPS. This can be explained by the reinforcement of the 2D structure of by the graphene crosslinking with nano-particles like Ag and Cu. In conclusion, the inter-structural

64

attraction between Metals (silver, copper, and Gallium) and graphene   linkage requires a higher applied pressure to stretch.

4.3.4.2 The differential scanning calorimetry (DSC) measurements.

Figure (4-12) illustrates the differences between the investigated samples. Most polymeric elastomers compounds reveal glass transition temperatures (Tg) far below ambient temperature. Thus, it is considered a unique property of complexed branched polymeric chains which possess special abilities of elongating and stretching.

  Figure (4-12) shows that the elastic modulus of the polymer is slightly increases by grafting their nanoparticles like silver, copper, and graphene. A comparison of the glass transition temperature (Tg) for different investigated samples shows an increase as follows PDMS<< PDMS-graphene << PDMS -graphene –NPs. In fact, Tg increases with a decrease of either the fillers or the gaps inside PDMS polymer, thus, creating new attractive forces between NPS /PDMS/Graphene and new electrostatic attractive and repulsion forces between graphene carbon base throughout resonance of bi bond beside, NPS strong metallic bonds between NPS Ag-Ag or Cu-Cu. simply lead to deformable volume and more rigid parts Based on the Tg results curve, the sample's stiffness increases with the filler fraction. There is no change in heat flow (w/g) for Tg for pure PDMS elastomer sample, compared to the heat flow in the two other composite samples (PDMS-Graphene and PDMS -graphene /NPS).[175-177] Their values are respectively 0.13, 0.17 and 0.27.
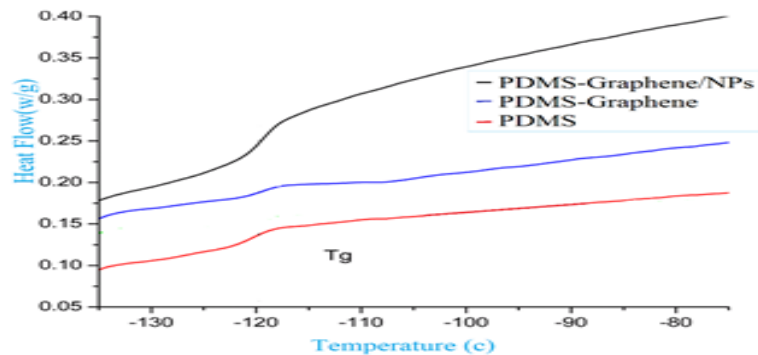
Figure 4-12 : DSC measurements for different PDMS based samples

4.3.4.3 Dielectric characterization

Figure (4-13) shows the variations of the dielectric constant of pure PDMS, PDMS-graphene, and PDMS-graphene nano composites. The results point out that there are more enhancements for electric characterize from 2.69, 3.21, and 3.73. The strong interface of the nano composites resulting from the ions mobility also has a predominant effect on their dielectric properties The increase in the interfacial area in polymer nanocomposites sets interfacial polarization which is based on the mobility of ions as a predominant physical effect for their dielectric performance [177-179]. Consequently, there are more similarities between the potential differences reported in Figure (4-13). The main generation of interfacial dipole moments that can occur, giving rise to significance.
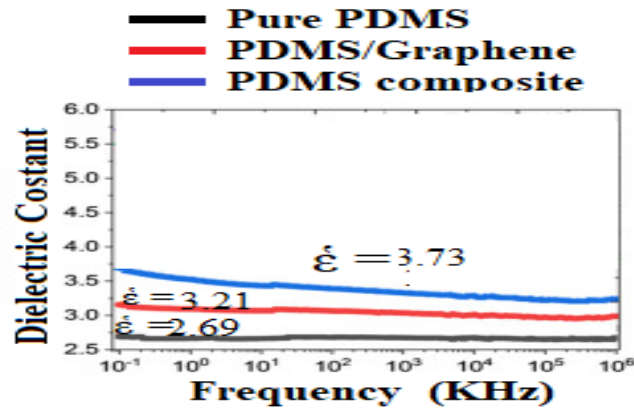
Figure 4-13 : Variations of the electric constants of the investigated formulations

4.5 Conclusion.

Moreover, using polymeric substrates like PDMS or styrene are conventional methods and works as a support material, being dielectric, flexible, and lightweight. On the other hand, there are effective materials, conductive nanomaterials, such as nanoparticles, graphene, and carbon nanotubes have been employed as flexible electronics and wearable devices.in our work, we depend specifically, on Graphene, due to it has been treated for fabricated many sensors moreover, its magnificent electrical and mechanical features and graphene-based nanomaterials have capable to created active sites with assembling nanoparticles like Ag, Cu, and gallium, because it has bi- bi bond which facilities move one charge and ions inside the structure .in that work we reached to created composite materials has unique characterize (thermal, conductivity and mechanicals) to apply on the flexible antenna next work.

This work has investigated the fabrication of wearable and flexible chip with gallium and silver metals composites assembled on graphene inside a PDMS matrix. It was found that it great achievement to print this is an important milestone as future applicable   antenna

CHAPTER 5

PREPARATION AND EVALUATION OF CONDUCTIVE POLYMERIC COMPOSITES FROM METAL ALLOYS AND GRAPHENE TO BE FUTURE FLEXIBLE ANTENNA DEVICE

Ameen Abdelrahman[1]* , Fouad Erchiqui [2] , Mourad Nedil[3]

[1] School of Engineering, Université du Québec en Abitibi-Témiscamingue,Canada

[2] Mechanical Engineering Department, Université du Québec en Abitibi-Témiscamingue, Canada

[3] Electric Engineering Department, Université du Québec en Abitibi-Témiscamingue, Canada *

abda02@uqat.ca

ABSTRACT

Every year hundreds of serious accidents and catrastrophies such as flooding and emolition occur in the mining sector. An effective communication is a way to possibly avoid those sad events or limit their consequnces. Such issue is addressed in this paper by the fabrication of a new durable, flexible and wearable chip that is highly efficient in sending and receiving communication signals at 2.4 GHZ band.   The process is based on doping a bunch of unique conductive metals (silver, copper, and gallium indium alloy) assembled on graphene, followed by its integration into Polydimethylsiloxane to be used in future antenna. Furthermore,

the physical, thermal, structural, and electric properties of the composite were evaluated using a variety of techniques such as the Electrochemical Impedance properties (EIS), the cyclic voltammetry (CV), the Differebtial Scanning calorimetry (DSC), as well as, the Transmission Electron Microscopy (TEM), and, the Scanning Electron Microscopy (SEM). Other spectroscopic techniques such as the Ultraviolet-visible (UV), inductively coupled plasma (ICP), and Energy-Dispersive X-ray (EDX) were applied to reinforce and elucidate the solid-state of ions inside fabricated antenna. On the other hand, throughout stress-strain for the stretchability of fabricated is expanded to 30% of its original length, It was found that the thermal stability was maintained until 485°C compared to pure PDMS substrate. Moreover, the electric conductivity of the composite ship was enhanced.

5.1 **INTRODUCTION**

There have been significant advances in the design and fabrication of antenna since the year 2000. This situation is normal as innovation is necessary for meeting the new market. These applications include biosensors used in huan health monitoring, and communication devices. Moreover, a variety of integration and trials of liquid-phase technologies are used in the process of fabrication of different electronic materials applications like smart packaging [180], biosensing and macro chips [181], flexible fluidic antenna [182], renewable energy management, and [183] printed electronics ink devices [184]. High-performance materials are indispensable to this technology. In this regard, graphene is an appealing material for the electronic field due to its unique properties, including a high conductivity, good flexibility, and mechanical stability. The literature contains a wide variety of applications based on graphene (the 2D, sp 2-bonded allocated carbon) [8]. Although there are many graphene production methods, liquid-phase exfoliation is a low-cost method that is well-suited for electronics [185-189], because graphene ~~has~~ possess some interesting features. In fact, graphene is made of a single atomic layer of graphite, it is an ~~a more~~ abundant mineral, and additionally, it is an allotrope carbon atom arranged in an hexagonal lattice structure. Graphene is formed with an has sp2 hybridization and its thickness is about 0.345 nm; furthermore, it has a high electron mobility that make it hundred times faster than silicon; while its electrical conductivity is 13x times higher than that of copper Graphene is used in various forms in the actual applications.

One method uses a stable and high-concentration dispersion in suitable organic solvents. Although reducing graphene to graphene oxide can meet this standard, degradation might affect the ions mobility in solution by the formation of a dielectric thin layer, which hinder charge transfer between atoms and motivates the use of pristine graphene during the preparation process. Thus, [190-192] the diffusion of pristine graphene demands the adaptation of organic solvents, surfactants, or polymer stabilizers to reduce the aggregation process [193].

Therefore, creating new composite materials composed of incompatible flexible materials (copper, gallium alloy, sliver, and graphene) in the fabrication of electronic antennas and optical modules is pivotal [194,195]. PDMS (sylgard 184), or polydimethylsiloxane, is known as an elastomer used in most electronic technological applications due to its unique polymeric characteristics like the stretchability, an ease of handling, , its structure, transparency, non-toxicity, and its low cost. Moreover, PDMS can reduce the time of elaboration or refinement of the electronic components [196,197]. The previously mentioned features of PDMS, has have been exploited in improving the design and fabrication of microelectronic components such as, sensors, valves, detectors, filters, solid elastic lenses, and antenna substrate for microelectromechanical systems (MEMS) [198]. On the other hand, there is significant literature dealing with the physico-chemical properties of PDMS, implied in specific process parameters such as curing agents, molding ratio, temperature and curing times, composite materials, among others [199-204]. In order to improve on the relatively low elastic modulus of PMDS, its been reinforced by other materials like the composites or ceramics, to improve on the desired characteristics, such as the surface energy, compatibility, modulus and superior hydrophobicity [205].

In order to improve on the elastic modulus of PDMS, an appropriate filler with specific characteristics such as size and shape must be selected and its overall effects on the material investigated. Based on the literature, ZnO, Ag, and GO materials are very appropriate candidates because of their biocompatible behavior. The materials used for antenna fabrication (such as graphene, and metals alloy immersed inside PDMS can also be suitable for applications for living tissue, especially for medical purposes, both for therapeutic and non-therapeutic applications; Moreover, they And are versatile in fabricating microstructures [206-209]. In addition, rigid particles or fibers should be incorporated to improve the properties of polymers. Refining the process could improve the material's stress-strain ability and its abrasion

resistance. This is achieved by filling out or grafting nanomaterials inside the gaps of the polymer matrix's cross-section. This could include grafting carbon black to natural rubber or metal oxides inside the polymer to achieve conductivity. Various inorganic filler have been used for reinforcing the polymeric structures. In fact, (it enhances the bonding between carbon chains inside the polymeric materials by filling the voids between the layers, and by reforming the chelating complexes with new bonds. Some examples include, nano metal oxides, SiO_2, Al_2O_3, Graphene, $CaCO_3$, fiber-glass, carbon nanotubes [210-216], which have certain characteristics like size, shape and compatibility with the main structure, and which are then good candidates to support the polymeric structures [217, 218]. One of the characteristics that should be considered is the miscibility and homogeneous dispersal of these nanoparticles as one phase that improves the electric conductivity efficiency of the fabricated composite by ions mobility [219]. Recently, nanotechnology has been very interested in developing methods of fabrication and reinforcement using ceramic composites owing to the material's physical and chemical properties [220-221]. Silicates and carbon nanotubes (CNT), used as fillers for various materials and polymeric compounds, have shown promising results [222-227].

Graphene is a potential sensing material for a flexible antenna due to some of its characteristics such as its high Young's modulus, its ions charge mobility, and its piezoresistivity [228-230]. Significant efforts were carried out to improve a graphene-based material and its conductivity by assembling or grafting a graphene membrane on a silicon substrate .. This has either involved depositing a thin layer of graphene onto a silicon nitride substrate [231, 232], or employing graphene as flakes to for coating well etched silicon base [233]. Lately, more applications have used graphene-polymer composite [234] laser-scattered graphene foam [235], modal graphene on elastomer [236-237], and graphene rolling [238]. Furthermore, it has been suggested that it may work in the fabrication of fluidic antenna, which has great potential for wearable devices besides their applications based on their electric conductivity and flexibility [239]. In the same manner, mercury was used in so many electronic devices. However, it is highly toxic compared to Gallium-Indium eutectic (E GaIn), a metal alloy that is liquid at ambient temperature. [240]. It is also possible to turn EGaIn into a flexible substrate used for tunable and reconfigurable electronic applications. This includes electromagnetic devices and systems involving electrical probes, microfluidic channel electrodes [241], nanowire conductors, patch

antennas [242], as well as metamaterials [243] and 3D electronics in re-workable silicon form [244]. Moreover, its unique characteristics and the stable detection of graphene [245], which is known by the two-dimensional carbon structure. Much of its astonishing electronic characteristics were also discovered including the quantum dots effect [246] which leads to the understanding of the Dirac fermions, tunable bandgap [247] based on the channel width, and the localization spin at the zigzag edge state [208]. Many conventional methods are associated with the graphene growth technique in the example of the, chemical vapor deposition (CVD) on a thin metal film such as Ni, Co, and Cu.

Although the CVD technique is an easier way to produce a large amount of growing graphene [249], it relates to managing the disorder and layer thickness of graphene. The scope of p−n heterojunction instruments with n-type 2D includes materials such as graphene and MoS$_2$ [250]. GaTe also expounded high-interested anisotropic planes, electronic reflection, and optical properties [251]. However, there is still challenges to tackle for the development and improvement of efficient Ga silicone-based devices which adhere to the environmental stability [252]. Furthermore, 2D materials like graphene and carbon nanotubes are specially fit for environmental stability because they possess an excellent surface area to volume ratio. Herein we depict a fluid metal eutectic, Ga–In "e-gain," 75% Ga, 25% by weight, m.p.=15.5 8C [213]. Although the deposition of metal nanoparticles ~~metals~~ like Au, Ag, Cu, and Ti is in widely published in the literature and is considered one of the conventional methods of electron-beam or thermal evaporation [254] , it causes damage to the thin layer of deposited metals and organic materials and reduces the efficiency of the fabricated materials [255].

Various advancements have actually been made in creating an outflow of gallium-indium (Ga–In) alloys in different fields of applications, especially in the area of biomimetic devices, biosensors, communication, and biocompatible devices. This is due to their metallic and conductive properties, their compatibility with the different polymeric substrates to form stretchable, wearable and robust conductors and sensors. Furthermore, the attractive quality of these materials, including their low melting temperatures, low resistivity ($\approx 29 \times 10^{-6}$ Ω cm), and a lower viscosity rate (≈ 2.4 mPa s) means that it can adapt and dilate to a different constellation during the process. Additionally, the existence of a thin layer of oxide on its exposed surface is the main cause of high surface tension induction (≈ 0.6 N m^{-1}), and formation of stable structures [256].

5.2 MATERIALS AND METHODS

5.2.1 **Materials**

Gallium indium alloy, graphene nanopowders (purity > 99%, 300 mesh), and— n-Hexane, THF were purchased from Sigma-Aldrich Co. Ltd (Toronto, Canada). Most of the salts (copper sulfate and silver nitrate, purity > 99%) were provided by Fisher Scientific ~~fisher~~. Polydimethylsiloxane (PDMS sylgard R 184) was purchased from Dow Corning Corporation, Canada.

5.2.2 Methods

The fabrication of a conductive, and flexible composite chip was done in the following steps: First the dispersion of the graphene nanopowder into the PDMS, which was done by immersing graphene Nanopowder in n-hexane for several days, followed by blending with 10 ml of polydimethylsiloxane (PDMS Sylgard R 184) using an overnight ultrasonic stirring to ensure complete homogeneity.

An electrolyte solution enriched with graphene/metals alloys was prepared with 10 ml of a 0.5M solution of silver nitrate, and copper sulfate salts solution mixed with 3 ml of another colloidal solution composed of (0.05 g graphene, gallium indium alloy (75:25), and PDMS. In order to integrate gallium metal alloys ~~gallium~~ and graphene as one phase, graphene nanopowder was dissolved in hot water at 80°C on ultra-sonic plates for 24 Hr.), then on the string at 60°C for one more hour till mixture is completely homogeneous. The third step, fabricated PDMS compositeis formed by mixing 5ml of PDMS graphene dispersion solution and 5ml of prepared electrolyte solution enriched graphene/metals alloys, stirring 3hrs, then the whole solution (10 ml) is molded by w/w (1:10) curing agent (cross-linker), mixed, stirring 20 minutes, then put inside a degasser vacuum for 15 minutes to remove all bubbles. Finally, the mold is heated on a hotplate at 70^{0}C for 45 minutes and left at room temperature to cool down to become ready for characterization and application.

In fact, the EIS or impedance of a material is related to the frequency range and is strongly connected to biological sensors or communication devices. DC voltage/current has been applied to gauge the conductivity of dielectric (i.e., low-conductivity) materials or gel-liquids due to resistivity effects by a few changes of ions concentration between interface resistance and

electrolysis of these liquids. The conductivity of solid-state materials is different from liquid conductivity measurements, and detection by DC approaches. Thus, the conductivity of materials is counted throughout the resistance and dimensions of a sample. However, the resistivity of solid material on the DC circuit needs a different electrode-material interface.

The conductivity of PDMS-composite, nanoparticles electrolyte, and graphene - PDMS was measured by EIS, a favorable and widely used method. It is carried out using a conductivity cell (HTCC, auto lab Bio-Logic Science Instruments) and an EIS instrument (VMP-300, Bio-Logic). Using a multi-channel sensor connected with a Frequency Analyzer (MPFA). The potentiostat - galvanostat was operated with eight channels for electro-chemicals electrolytes corrosive coating studies at (10V, 4A). The sinusoidal voltage was applied with different frequency ranges using the Nyquist plot software program to detect the resistance of a material followed by its conductivity based-on Equation (4-2)

$$(\sigma = K/R) \tag{5-1}$$

Where, the resistance (R) and the specific resistance constant (K), can be evaluated by the surface area of the electrodes and the length submerged into the electrolyte or the substance.

A three-electrodes system was used for the impedance measurements or to complete the EIS circuit. They are reference electrode (glassy), the stander (Pt) electrode, and the counter electrode. The conductivity was detected through impedance at frequencies between 2.5 MHz to and 1.5 kHz at open cycle volt (OCV) of 0.40 to derive the electrical properties of various conductive composites and electrolyte solutions (composed of 0.5M $CuSO_4$, gallium/indium, and AgNO UV characterization

The UV characterization is carried out by Lambda 750 UV-vis-NIR spectrophotometer (UQAM, Montreal) from Perkin Elmer using blank sample distilled water. The sample were prepared then had been tests procedure $_3$) both as a liquid electrolyte and as grafted inside the PDMS matrix composite.

This technique was carried out using a (Quick Test QTS3) instrument in ETS, Canada, for tensile detection testing; all fabricated samples were put on an elongation base of 6 mm. The expanded ratio is c.a. 30% of its original length. The sample is held on with clamps, and then the applied strain rate was carried out at 60mm/minute to avoid errors induced by sample

slippage from the clamps. The tensile stress of a specimen were calculated with an area of 206561 mm^2 at ambient temperature based on Equation (4-4).

$$S = F/A_0, \qquad (5\text{-}2)$$

Where F is the applied force and A_0 is the sample's cross-section area.

The measurement was carried out in a Differential Scanning Calorimeter (Perkin Elmer Pyris 1). The glass transition temperature (Tg) is one of the most important parameters of the polymer's physical properties. Tg of a (semi-crystalline materials) occurs in a range of temperatures that involves two phases of polymeric material (above Tg crystalline (rubbery) and below Tg is a liquid phase over which this glass transition occurs until the melting temperature (Tm) is reached. The differential scanning calorimetry (DSC) model: Mettler Toledo, UQAM (Montreal, Canada) was used in measuring the Tg values. The high heat capacity and equipment were provided with a heating rate around -60°C and +600°C under a controlled atmosphere (N$_2$ or air) by applying 0.25 mg of sample by scanning twice at 10 ℃/min between 140 ℃ and 270°C
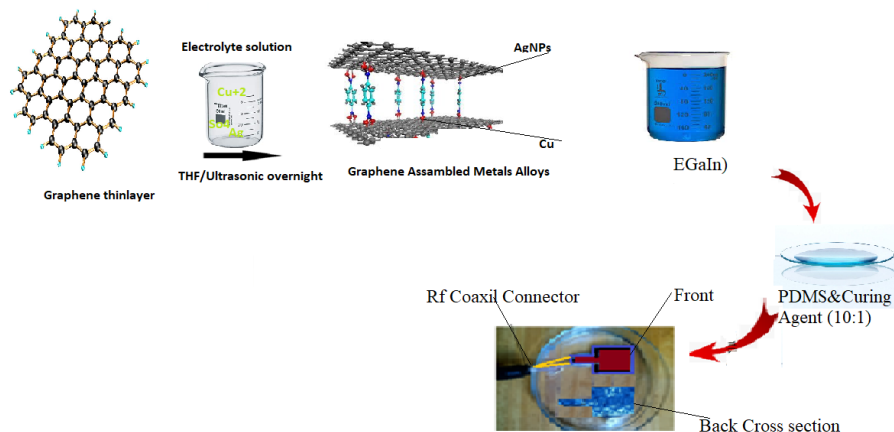
Figure 5-1: The pathway process of the PDMS composite

5.3 RESULTS AND DISCUSSIONs

Reaction mechanism

This part gives an explanation of the reaction mechanism during the process and it shows the importance of grafting graphene particles inside PDMS.

In fact, the grafting of graphene facilitates more adhesion and interfaces crosslink by converting PDMS to a conductive material. There was another attempt of creating more active site inside the PDMS structure by engrafting metal nanoparticles like silver and copper. Such operation led into a charge and ion transfer from graphene through metallic bonds basd on oxifdation and reduction reactions. The EGaIn junction (Cu–EGaIn) includes both a non covalent and a metallic Cu–Cu interface.

PDMS /E GaIn interface is also much modest than the Ag-connection. Thus, it creates different sites of redox-chain reaction as follows, (Cu^{+2}/ Cu graphene //graphene-Ag-/Ag^+), and (Cu^{+2}/ Cu graphene //graphene-Ga-/Ga^+) which has, nominally, three interfaces: the covalent Ag–Ag interface, the van der Waals interface between the two electrochemical force (e.m.f) and graphene π-π bonds, as a resonance characteristic interface. On the other hand, assuming that EGaIn act remains correctly as a liquid, the energy E r related to the attached EGaIn to graphene surfaces can be expressed using the following equation:

$$E = \gamma(1 + COS\ \theta)\qquad\qquad\qquad\qquad (5\text{-}3)$$

Another explanation for this electrochemical phenomenon, it could be returned to, the EGaIn adhesion surface tension force is lower than both of the two PDMS, and Graphene substrates. Thus, it seeks to form a metallic bond with different types of silver and copper. The adhesion angle contact of Egalin makes it difficult to contact PMDS directly, so it should be abridged with other dissolved metals or graphene.[257] on the other hand, Dickey et al. [258] confirm that E GaIn is an oxide layer formed on its surface. Thus, it needs more electrons to facilities contact to confirm that gallium droplets coexist with graphene layer partition inside the PDMS matrix. It is also related to metallic nanoparticles like silver and copper that make another bonded with amorphous carbon.

Electrochemical characterization

In order to study the behavior of the prepared solution, the cyclic voltammetry (CV) tests were conducted to describe the electrochemical reaction and detect the occurance of some reversible oxidation-reduction reactions_ inside the prepared solution. The composite was prepared from different homogenous solutions (graphene-PDMS, electrolyte salts, and a composite solution). By setting up three cell electrodes (reference, working, and counter electrode) then applying a voltage in the circuit it appreass that the potential of the electrode increases linearly with time. According to ohms law, the dynamic potential has resulted in a chemical reaction and charge transfer between different reactants.
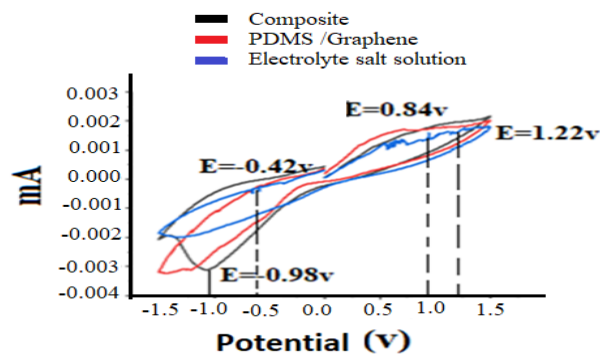
Figure 5-2: Cyclic voltammetry (CV) of the prepared solution

The cyclic voltammetry was accomplished for the potential between 0.4 and − 1.0 V. The results summarized in Figure (5-2) shows different potential (V) peaks, which is evidence for the occurance of various reduction and oxidation reactions inside the composite solution. Different active holes were created to transfer charges on the composite surface; such is the example of the peak found around −1.45V and varying in opposite scanning (+1.45 V) which coincides with the ions of the electrolyte salt solution. Moreover, the sensibility of the nanoparticles dissolved in the electrolyte solution increases with the strength of the redox process, which means a slight shift in the oxidation potential peak from 1.8 to 0.6. On the other hand, the peaks that did not appear in the PDMS-graphene solution illustrate that graphene is conductive only with π-π bond. It does not have enough active sites to create a reversible reaction on its surface. However, when mixing two components to form the composite, some peaks appear at (-1.1 V) which slightly shifted at (+0.9V), indicating the loss of an electron. As a result, the composite carries out a negative charge form a covalent bond with Ag^+ as it is reduced into Ag^0.

EIS Impedance measurements

The literature shows that the conductivity of a material is better measured by the impedance rather than by direct potentiometer .
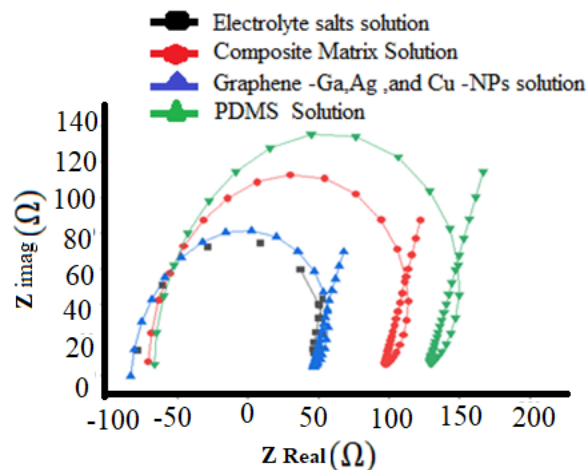
Figure   5-3 : EIS measurements for different investigated samples

Figure 5-3 illustrates the resistivity of various investigated materials. It confirms the existence of a reversible relationship C=1/R, meaning that the material's conductivity decreases with an increase in its resistance. According to Equation (4-3), the ionic conductivity of the prepared solution based on charge mobility inside the solution, and the ions mobility in the electrolyte salt solution, and graphene with suspended nanoparticles is higher than PDMS (dielectric).

$$\sigma = \frac{L}{RXS} \qquad\qquad (5\text{-}4)$$

Where electrolyte conductivity is (σ), (Ω) is the real electrolyte impedance, S (cm^2) is the electrode surface area, and L (cm) is the thickness of the working electrode.

In the first phase, dealing with the electrolyte salt solution (Cu_2SO_4, $AgNO_3$,) and the nanoparticles suspended solution (copper, silver, and gallium alloy), the measurements point out highly conductivity values compared to the others, due to different factors such as the ionic charge distribution, ions mobility, temperature, particle size, particle movement, and viscosity of the medium. In the case of pure PDMS or passive substrate for antenna device, the Nyquist plot curve indicates high values of resistivity and dielectricity of the polymer compared to the integrated PDMS with ceramic conductive metals, and graphene, the resistivity reduced and the conductivity of the polymer composite increased. Furthermore, when treating graphene with electrolyte salt solution or suspended metal nanoparticles, its conductivity gets better than that of both PDMS and the composite, since the solution is saturated with ionic charges. The cases of the matrix of PDMS, graphene, and the electrolytes, showed good results for them to be applicable as conductors' active part of the antenna. , which it will be applicable flexible and stretchable wearable composite and an acceptable conductor compared to the conductivity copper metals or electrolyte solution [259].

In summary, according to the EIS on the Nyquist plot ~~curve~~, the conductivity of the prepared materials is ordered as follows: Electrolyte salts >> graphene solution assembled with nanoparticles >> composite matrix >> pure PDMS.

Surface morphology characterization

Raman spectroscopy was used to characterize our different prepared samples of graphene/electrolyte salts (silver nitrate, copper sulfate, and gallium), electrolyte salts, and PDMS composite.

Raman microscope comprises an optical microscope model: Renishaw, inVia Reflex (UQAM Montreal), dimensions x5, x20, and x50 connected to a Raman spectrometer with two lasers sources (532 nm and 785 nm). The optical microscope is used to magnify and recognize the sample surface mechanism of the Raman spectrometer, spread out light, and detect the irritation vibrations. Furthermore, it could obtain optimized Raman spectra of samples at a resolution of 2 μm.

The Raman measurements are shown in Figure (4-4) as the variations of the intemsity with the wavelength. It shows that in a colloidal solution of graphene and electrolyte salts, the carbon atoms in the sp2 hybridized positions are stretched and slightly shifted, due to the electronic configuration of the graphene structure and the new metallic bond between M-M and M-graphene structure, which causes the disappearance of the resonance of double bonds of graphene and the shifting in the remaining spectra.
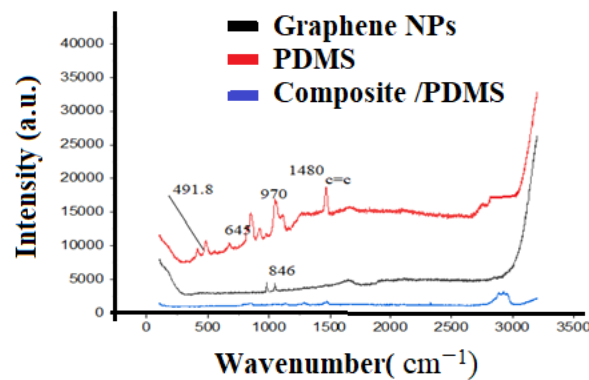
Figure 5-4 : Raman spectra of three different PDMS samples

The spectra show outstanding peaks at 109, 115,162, 176, 210, 270, and 285 cm^{-1} in good convention with previous assessment .25, 26, 42 with a slight exception of two peaks for nanoparticles assembled on PDMS (Ag and Cu) which appear at 128 and 145 cm^{-1}, respectively. These data are consistent with findings from existing literature [260-263].

.

The UV characterization results are shown in Figure (4-5), in the form of absorption spectra of the investigated samples of pure PDMS, electrolyte salts solution – graphene, and with PDMS composite. Figure (5-5) shows the appearance of a spectrum around the region of 280–350 for the electrolyte salts (Ag, Cu, and gallium), but slightly disappears in the PDMS composite. In the same manner, the matching p–p* electronic transitions for graphene resonance structure also vanishes inside the composite matrix. Various peaks are revealed around the wavelengths of 350 and 280 nm in the electrolyte and graphene samples respectively, and it could be attributed to the n–p* transition of Ag-graphene or Cu-graphene.
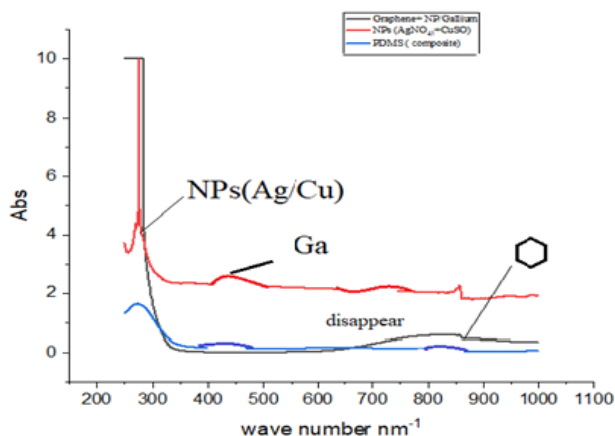
Figure 5.5: UV spectra of the investigated materials samples

The Energy Dispersive X-ray analysis (EDAX) is another technique used to illustrate the composite's main components, which are impregnated with nanoparticles of silver, copper and gallium. An analysis of the samples based on Figure (5-6) shows an agreement with the

analysis of Ion coupled plasma (ICP) analysis, a physical method of chemical analysis used to detect elements of the qualitative analysis. It consists of a plasma torch (model: Agilent Technologies, 5100) simultaneously measuring in a few minutes. The ionized sample is obtained by injection into an argon plasma with at a temperature around 6000K. The samples should be dissolved in acid (wet mineralization) prior to that injection. Figure (5-7) shows the elemental composition of a sample of a matrix consisting of different nano metals like silver, copper, and gallium alloy confirmed in the diagram below. All data is confirmed with EDAX analysis.
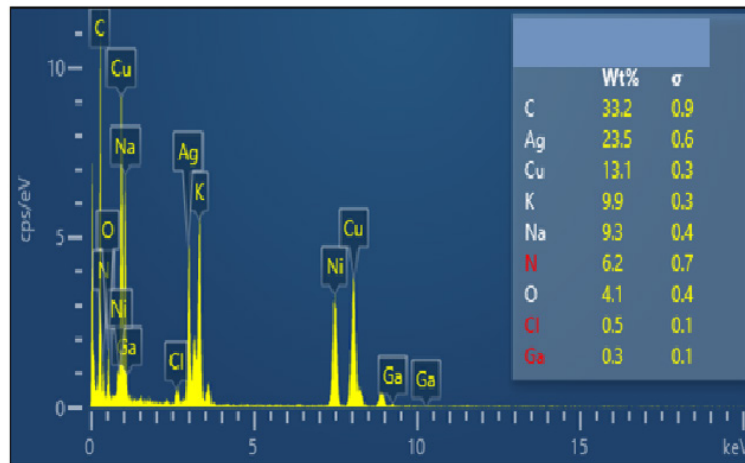
Figure 5-6 : EDAX measurements of the investigated prepared samples.
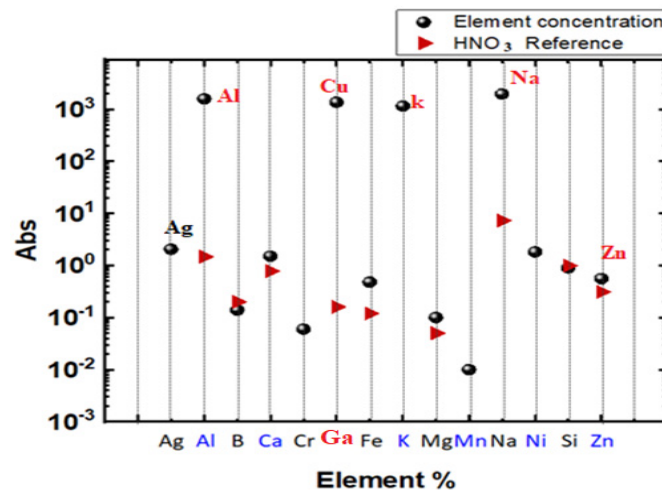
Figure 5-7 :ICP analysis of the composite matrix solution.

Study of the mechanical and thermal characteristics of the new composite

The stress-strain analysis
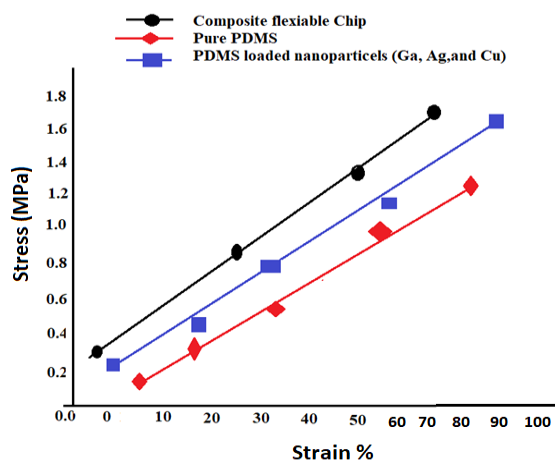
Figure   5- 8: The tensile response of the fabricated composites of PDMS at applied

stress at 15% strain

The stress-strain analyses are used to investigate some mechanical properties of the fabricated chip antenna' like the stiffness and flexibility. The values and measurements of the tensile tests of different fabricated samples are shown in Figure (4-8). The analysis is based on Equation (5-5).

$$E = \varepsilon/\sigma \qquad (5\text{-}5)$$

Where E is the Young's modulus, σ is the fracture stress, and ε the fracture strain.

The tensile experiment has been carried out on the prepared composites to improve on the stiffness and reinforcement of synthesized PDMS and PDMS nanoparticles based on an application of the stress-strain load at 15% MPa. [85-87]. According to the results shown in Figure (4-8), there is a direct proportion between the applied strain and stress of all prepared components, with a slight increase shown for the composite chip, PDMS/Graphene-NPS, and

pure PDMS. This can be explained by the fact that the second dimension of the graphene crosslink with Ag and Cu nanoparticles reinforced the composite structure. It can be concluded that the effect of inter-inter attraction between metals (silver, copper, and gallium) and graphene linkage requires a higher applied pressure or force to stretch [264].

The nano metals and PDMS were joined together in bearing the tensile load. No crack or cut was noticed in the samples with an increase of the stress rate compared to some deformation of the specimens of pure PDMS in the same conditons.

In addition to the metallic bonds, the σ-σ and n-π bonds which have the potential of effecting ~~on~~ or reinforcing the nanofillers on polymers crosslinking, the silicate groups of PDMS are the key factor for a larger Young's modulus based on the reports from previous authors [265].

DSC measurements

Figure (5-9) illustrates the DSC micrographs of various investigated PDMS-based materials at different rates. Most polymeric elastomers reveal a glass transition temperature (Tg) far below ambient temperature. Thus, it is considered that the unique properties of complicated branched polymer chains can be elongated and stretched due to the narrow molecular weight (NMWT) of polymeric chains during the synthesis as well as the segmental rotation between cross-linked networks. By comparing the transition temperature for PDMS, PDMS/Graphene, and PDMS-Graphene/NPS fillers, Tg increased in the following order: PDMS substrate << PDMS-graphene << PDMS-graphene-NPs, as shown in Figure (5-9). Tg increases with a decrease in the fillers or gaps inside the PDMS matrix. This can be possibly explained in two ways : Firstly, the new bond causes the net attractive force between the elements of NPS/PDMS/Graphene to be higher than bewteen the elements of Graphene/PDMS. Secondly, the electrostatic attraction and repulsion forces between graphene carbon bases throughout the π-π bond's resonance. NPs' strong metallic bonds between NPS and Ag-Ag or Cu-Cu lead to deformable volume and more rigid parts. Based on Tg results,[266]. The more the filler fraction increases, the stiffness increases linearly increase. There is no change in the heat flow (w/g) for Tg in the pure PDMS elastomer sample compared to the heat flow in two other composites

(PDMS-Graphene and PDMS-graphene/NPS). The values of the heat flow in these cases are respectively 0.13, 0.17, and 0.27
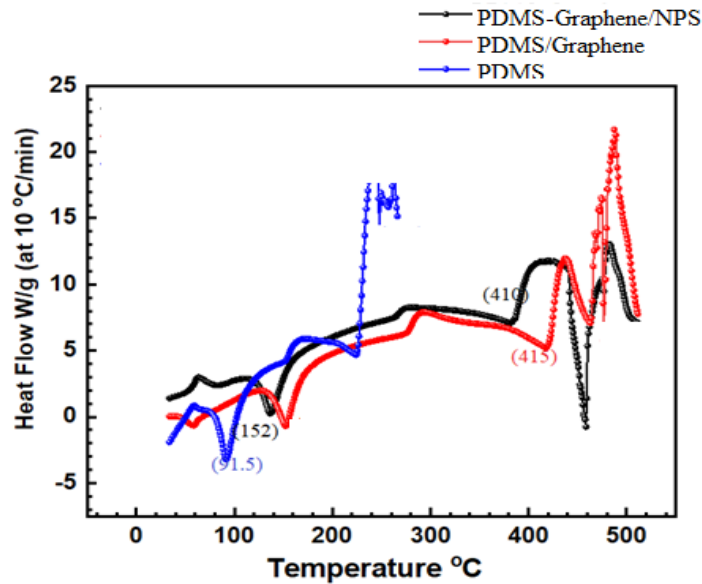
Figure 5-9: DSC measurements for different investigated PDMS-based materials.

5.4 CONCLUSIONS

This work has evaluated preparation and evaluation of conductive polymeric composites from metal alloys and graphene to be future flexible antenna device.Further work was done about the mechanical, thermal, and electrochemical of the prepared composites ~~devices~~ to evaluate their elementary properties (flexibility, stretchability, and robustness) prior to their application on antenna that can operate 2.4GHz broadband in the mining sector. Furthermore, the physical and mechanical properties of the fabricated antenna were studied using both different spectroscopic analysis techniques, and the evolution of the electrochemical reaction during its fabrication. It showed the importance of graphene as a working carrier or bridge which can create some active sites by assembling nanoparticles like Ag, Cu, and gallium, and which has a π-π bond that facilities the movement of charges and ions inside the structure.

CHAPTER 6

STUDYING AND EVALUATING THE PHYSICAL CHARACTERISTICS OF THE COMPOSITE SUBSTRATE CHIP AND ITS APPLICATIONS

Ameen Abdelrahman [a], Fouad Erchiqui [a], Mourad Nedil [b]

[a] Mechanical Engineering Department, Université du Québec en Abitibi-Témiscamingue, 445 Boulevard de l'Université, Rouyn-Noranda, QC, J9X 5E4, Canada

[b] Electerical Engineering Department, Université du Québec en Abitibi-Témiscamingue, Campus de Val d'Or: 675, 1ère Avenue, Val d'Or, Québec, J9P 1Y3, Canada

Abstract

This work shows the design and fabrication of a fluidic antenna based on dielectric PDMS substrate, its unique properties of conductivity, flexibility, robustness, and use as an antenna. An appropriate fluidic solution comprised of a polyethyleneimine (PEI) matrix assembled with nanoparticles of titatinum oxides and graphene were evaluated. The investigations the mechanical flexibility (stress), thermal properties (DSC), and IR spectroscopy have been carried out on fabricated PDMS substrates, and a dielectric was recorded at 2.67. In addition, (TEM), IR, UV, and Electrochemical Impedance (EIS) tests have been performed to evaluate the polyethyleneimine (PEI) matrix-like surface morphology. The measurement and simulation

outcomes show that the fabricated antenna operates at 1.8–2.6 GHz, which covers the WLAN band area.

Keywords

PDMS, tensile response, graphene, TiO_2 impedance, TGA, dielectric.

6.1 INTRODUCTION

At the beginning of the 1970s, it was possible to fabricate microsensors using bulk fluidic and silicon surface micromachining. In addition to replacing microelectronics, conventional processes used high-aspect-ratio structures and suspended layers techniques. These new techniques opened up the potential for biosensing applications technologies to integrate non-traditional (i.e., not silicon-based) materials. Thus, a new microelectromechanical system (MEMS) emerged.[267] The first iteration of fluidic channels in inkjet printer heads showed that tiny amounts of liquids could be handled in micromachined channels. A few years later, Terry et al. created a micro machined gas chromatograph in silicon[268].

Nanocomposite polymers have attracted a considerable deal of attention in recent years due to their remarkable mechanical and barrier properties, particularly compared to traditional micro and macroscale composites. They also usually have low filler content [269], for example, ceramic nanoparticles such as titania, alumina, silica,[270] carbon nanoparticles[271], graphite sheets, and 2D carbon nanotubes.[272] All the materials are used and reinforced with a carbon-black skeleton. Recently silica has been widely utilized for many applications. The main objective of nanoscale materials is to obtain materials with novel functions and enhance their overall characteristics. Among the various materials, Nano titanium plays a special role in a wide range of applications like biosensors, photo-catalytic cracking for the petrochemicals industry, and chelating complexes with alternative materials [273].   Several studies have been conducted on titanium dioxide's properties and its use as a reducing agent for degradation compounds in an aqueous solution based on its electronic configuration in D-orbitals [274], and, TiO2. It has been described in many scientific papers and is a widely used oxide in photocatalysis [275].

The elastomer matrix plays a vital role in controlling the dielectric constant, the dielectric breakdown strength, strain stress of silicone elastomers, and polydimethylsiloxane (PDMS). PDMS is one of the most widely used materials for dielectric elastomer actuators because of its good elasticity, reliability, and steady response speed [276]. In addition to the repeatability of actuation onto activation, it shows a lower tendency to age and experience Mullins (stress softening). PDMS increases actuation (at low strains) up to more than 4 million cycles without failure [277-280].

PDMS is an almost semi-crystalline silicone and non-entangled elastomer. It melts around -40°C, crystallizes at -90°C, and cools around -125°C. Previous studies have performed tests on PDMS's crystallization function and kinetic behavior based on DSC and TDG measurements (Dollase et al.) [281-283]. To our knowledge, in many conventional elastomeric materials, the combination of weak intermolecular forces, stretchability, and the high flexibility of PDMS chains lead to inferior mechanical and physical properties over the melting temperature area. This yields important challenges during the application process at room temperature. These challenges have been tacled in several studies conducted on PDMS by the use of various fillers [284-288].

Microfluidic devices were created from the microfabrication process, which used electronic dots, chips, and Micro Electro Mechanical Systems (MEMS). These devices are famous for their tiny features (sizes ranging from 1 to 100 μm) and high precision. Typically, most microfluidic devices are fabricated by a lithography process based on various molding techniques for applied to flexible silicone and elastomers, like PDMS (polydimethylsiloxane), polyacrylic rubber, and silicone rubber [289-293]. However, this material is compatible with aqueous solutions; moreover, it is non-toxic, inert and flexible, robust, optically transparent, and gas permeable. These properties make it more appropriate for biological and microscopic applications. In recent years, several studies and research efforts have been carried out to meet these needs, such as Surface Acoustic Wave (SAW) sensors [294], which are intuitive to surface contact radiofrequency-detection based fluidic or pitch antenna [295]. These studies led to a high degree of progress in the telecommunication and network sectors.

In this article, we describe the fabrication of a fluidic chip and its unique properties. It is comprised of a micro-fluidic solution (conductive) and dielectric PDMS substrate. It could

operate as an antenna device in the future. The fluidic or conductive is contained in a colloid solution of polyethyleneimine (PEI), titanium nanoparticles, and graphene. Various measurements and tests were performed on the chip during the fabrication process to identify and investigate future devices' efficiency and characteristics.

6.2 Materials and Methods

Dow Corning® Sylgard 184 and the curing agent (cross-linker) were purchased from Dow Corning Corporation Toronto, Canada. TiO_2 and graphene oxide were purchased from Sigma Aldrich, Canada.

6.2.1 MATERIALS CHARACTERIZATION

The Electrochemical characterization (EIS) of the materials was performed at NanoQam in Montreal, Canada. EIS is used to identify the fluidic liquid impedance. The instrument consists of an eight-channel battery, model: MTI Corporation, BST8-WA using rechargeable batteries at 0.002-1mA to and 5V. The data analysis was performed using the NOVA potentiostat software. The technique depends on the electrode setting (working, standard, and reference) at different frequencies.

The Ultraviolet-visible spectroscopy (UV-vis) was carried out using a Perkin Elmer, Lambda 750 spectrophotometer in the range of 200-1000 nm.

A Zeiss Evo 18 instrument was used to perform the transmission electron microscope (TEM) imaging analysis of the samples in NanQAM, Montreal, Canada.

The TDG measurement was done using a Thermogravimetric Analyzer (Q500), with the possible temperature variations up to 1000°C using inert N_2 gas.

In addition, mechanical (stress-strain) properties were characterized using an electronic tensile machine (JPL-2500 from Testing Instrument, ETS, Montreal, Canada) using an ASTM D882 standard for the tensile testing of thin layers of fabricated PDMS at room temperature.

The breakdown field strength of the PDMS was carried out using an AMS-10B2 high voltage amplifier (Matsusada Precision Inc., Montreal, Canada).

6.2.3 Preparation methods

6.2.3.1 Preparation of PDMS substrate

The PDMS prepolymer and curing agent were blended in 50 mL polyethylene cubes at a ratio of (10:1) by weight. It was placed in a vacuum and degassed for 5 to 15 minutes at room temperature to remove any bubbles. The PDMS was then coated in fabricated channel design (gum) fixed on the baking dish. It was finally transferred into a 75°C oven for curing during 45 minutes with the entry covered, and cooled down at room temperature. The same process was then repeated for the other PDMS substrates. Both sides of the two fabricated PDMS substrates were then joined. The two fabricated PDMS substrates were then placed inside the plasma reactor chamber as soon as it was set up. This procedure was performed according to reports from the existing literature. Thin PDMS slabs (~2mm) were also put inside the case. PDMS slides were degreased with acetone inside an ultrasonic bath, rinsed two times using IPA, and dried with nitrogen. Two PDMS substrates were joined together by placing them inside the oxygen plasma chamber (100 W for 2 minutes, 20 sc/cm O_2 flow rate, and 0.67 m bar); Then using a syringe, we injected the electrolyte solution inside the microfluidic channel.

6.2.3.2 Preparation of fluidic solution

Graphene oxide (GO) was generated by the chemical exfoliation method described by Hummers and Offerman[256-258]; then, 5 g of $KMnO_4$ was added to the suspension solution composed of 25 mL of 3% N concentration of H_2SO_4 and 3 g of graphite. An ultrasonic stirring was then performed for 4 hours. The mixture was treated by adding H_2O_2 (28 wt % in water) until all gasses had been released. The suspension solution was then intensively washed several times, once using a diluted hydrochloric acid (0.1 mol/dm^3). The filtrate was also washed using distilled water. Eventually, it was centrifuged and dried to get the GO. Graphene was obtained by reducing GO. This was done by adding 3 mL of NH_2OH (0.1 mol/dm^3) to 7 mL of a colloid solution of concentrated GO (0.5 mg/mL) followed by stirring for 20 minutes. In order to raise the solution's pH to 12, a few drops of concentrated NaOH (0.1 mol/dm^3) were added, ~~heated~~ the suspended solution was heated at 85 ºC for 1 hour, washed, and dried for characterization.

TiO_2/Graphene nanocomposites were synthesized using the hydrothermal method reported in previous studies . The proper amount of graphene/GO was scattered in a solution containing

1:1 deionized water and ethanol, and then an ultrasonic stirring was performed for 45 minutes. Subsequently, 25 mg of TiO$_2$ was mixed with a solution, stirred for 1 hour until the mixture ~~is~~ was fairly homogenous, and then 10 mL of this prepared solution was placed in a Teflon lined autoclave, sealed, and heated ~~to~~ at 120ºC for 3 hours. The final product was washed with distilled water and freeze-dried to avoid the agglomeration of the nanoparticles. Eventually, 0.5 mg of the prepared product was dissolved in 5 ml of PEI solution and stirred for 1 hour until complete spreading, and the homogenate matrix was achieved, as shown in Figure (6-1).
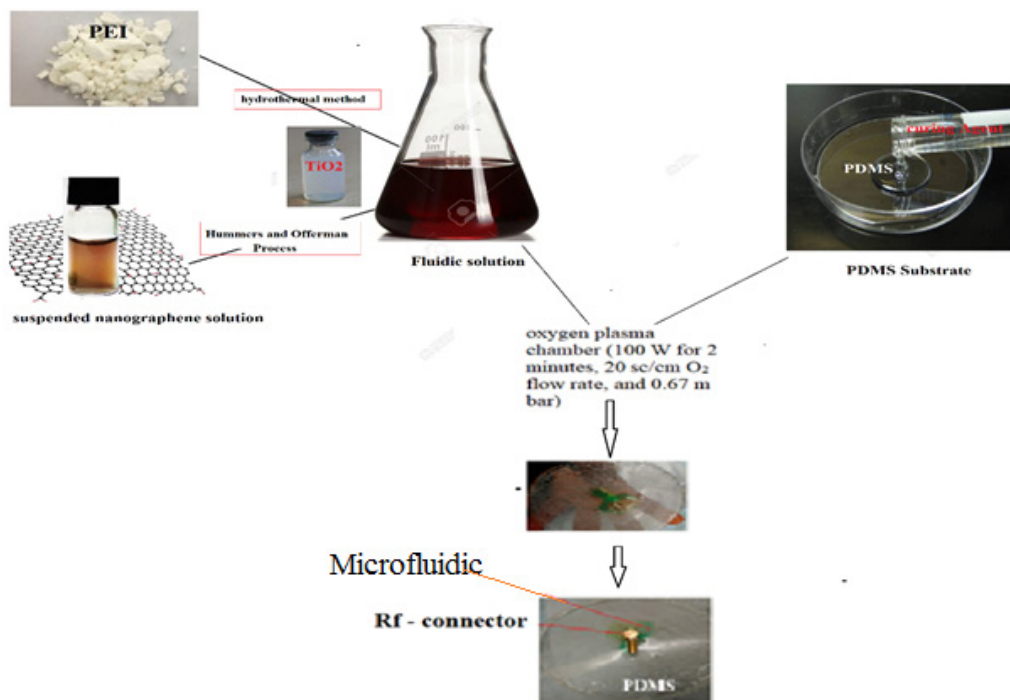
Figure 6-1 : The preparation method for a fluidic antenna device.

6.3 . Results and discussion

6.3.1 Fluidic liquid characterization

6.3.1.1Electrochemical characterization

Electrochemical Impedance Spectroscopy (EIS), is an excellent quantitative technique with widespread application in characterizing functionalized electrode surfaces and electrolyte

conductivity. Impedance is defined as an electric circuit element's capability to hold the current flow and, therefore, the reluctance force to electrical current in a circuit measured as resistance (Ω). The impedance of the electrolyte solution (Z) can be calculated according to Ohm's Law, given by Equation (6-1).

$$\mathbf{Z} = \frac{E(t)}{I(t)} \qquad (6\text{-}1)$$

Where E(t) is the applied potential I(t) resulting current, t is time, and I^o is the current oscillations' magnitude [259-261]. In order to obtain the ionic conductivity of two solutions (PEI and graphene /Ti-NPS/ PEI) at room temperature, optimize parameters like the operating frequencies range from 3 MHz to 1 kHz, an ~~and~~ open circuit potential (OCV) = 0.43 V must be respected using three electrodes (working, reference and counter electrodes) inside the prepared solution. The Nyquist diagram (a Cole-Cole plot) is used to study the electron transfer because it is an easy way to predict circuit elements. It includes plotting Z-imaginary as a function of Z-real, which usually appears as a semicircle, as shown in Figure (6-2), which provides a visual charge transfer dynamics at the electrochemical interface. This analysis is based on Equation (6-2),

$$Z = U / I = R + jX \qquad (6\text{-}2)$$

Where R = Re [Z] is the resistance and X = Im [Z] is the reactance, both expressed in Ohms units.

It is observed that the Nyquist diagrams varied incrementally with the successive modifications of the graphene/Ti/PEI solution as compared to PEI. It is due to the formation of an active layer of charge cloud on the graphene. In addition, the photoelectrochemical characteristics of titanium helped it to form a Ti-Ti metallic bond. These factors enhance the ion charge transfer, then increase the conductivity according to Equation (6-3).

$$\sigma = \frac{L}{RXS}. \qquad (6\text{-}3)$$

Where electrolyte conductivity is (σ), (Ω) is the real impedance of the electrolyte, S (cm^2) is the electrode surface area, and   L (cm) is the thickness of the working electrode. Finally, the conductivity of PEI composite is greater than the conductivity of pure PEI.
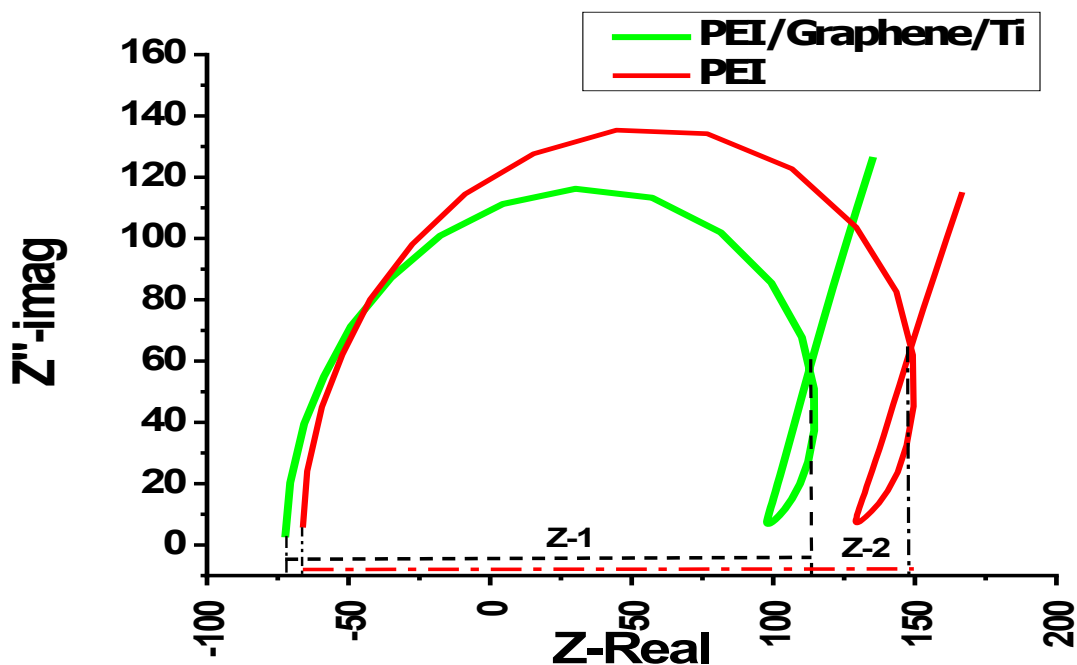
Figure 6-2 : Impedance measurement of a pure PEI and PEI /Graphene /Ti –NPs solutions.

6.3.1.2 IR Characterization

The chemical structure of PEI was detected with a Fourier transformation infrared spectroscopy (FITR) technique. The functional groups of PEI are shown in Figure (5-3). There are identical characteristic peaks for PEI at 3271 cm^{-1} (NH stretching), 2945–2833 cm^{-1} (CH stretching group), as well as, 1576 cm^{-1} (bending NH), 1465 cm^{-1} (CH bending), and 1350–980 cm^{-1} (–C–N stretching). There is another distinct peak at 1656 cm^{-1} for the –C=N bond.
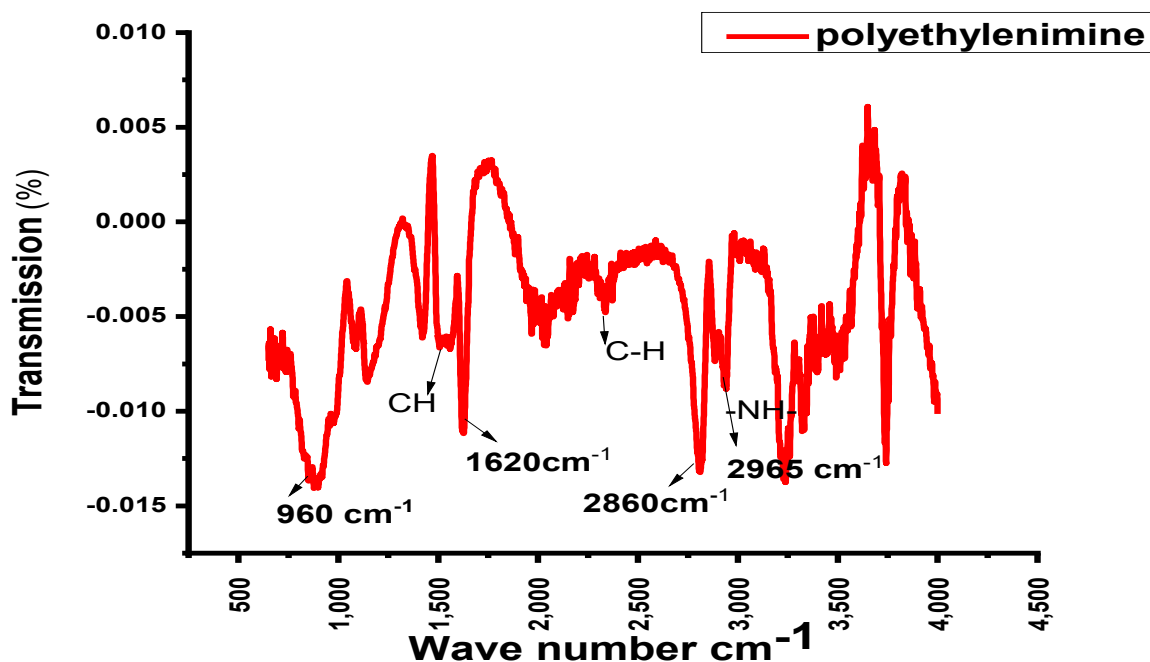
Figure 6-3: FT IR spectrum of polyethyleneimine.

6.3.1.3 UV analysis.

According to previous reports, PEI-TiO$_2$/Graphene NPS's zeta potentials shifted from +39.44 mV to +94.46 mV. TiO$_2$ nanoparticles are adapted between -56.61 mV and -119.34 mV. This indicates the dramatic adsorption and disappearance of TiO$_2$ nanoparticles inside the PEI matrix. Furthermore, the Ti peaks shifting from 267 nm to 285 nm are caused by UV-vis diffuse reflectance [296]. Additionally, the absorbance recorded in titanium and graphene causes relative ion interference between pairing electrons on NH and Ti –NPs. That means the PEI reveals a high affinity for Ti cations in an aqueous solution, which is also described in the literature [37].
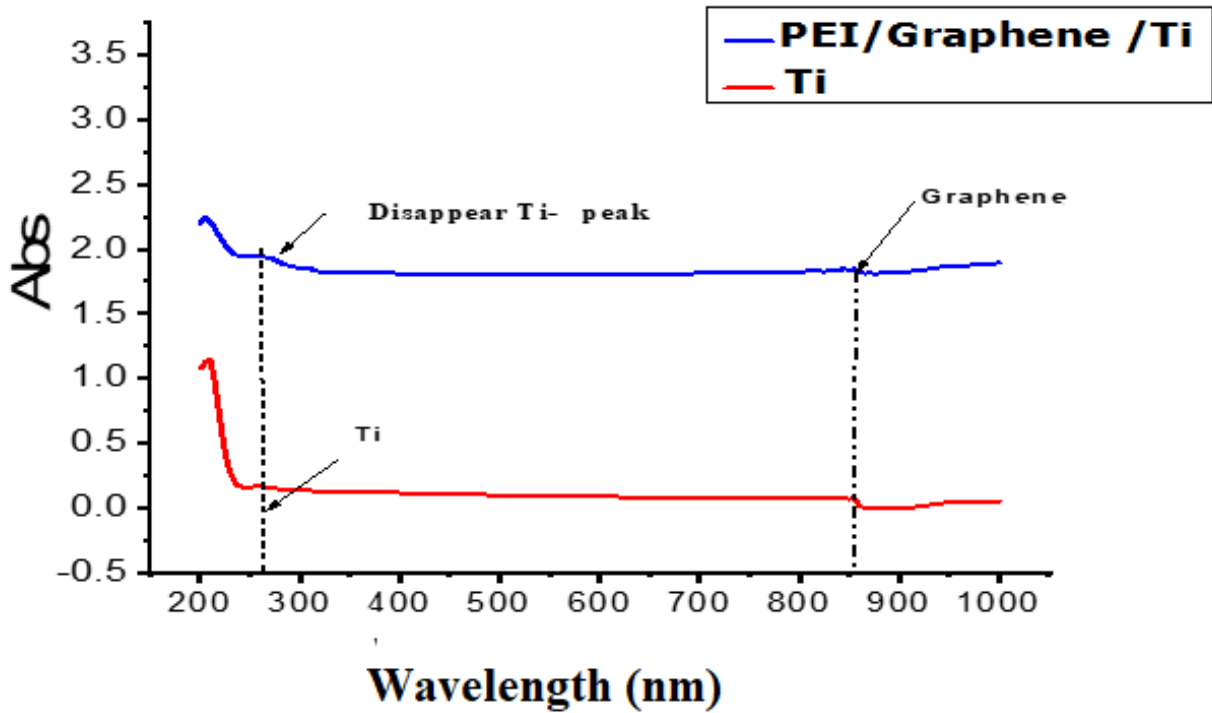
Figure 6-4: UV-Vis-NIR analysis of graphene/TiO$_2$/PEI, and TiO$_2$ solutions.

6.3.1.4 Morphological Analysis

It was common to observe that in terms of allocation, figure, and dimensions, the TiO$_2$ nanoparticles were far uniform because the tiny spherical Ti particles are around 20 - 25 nm, and in most cases, the nanoparticle composite leads to the aggregation and fluctuation.
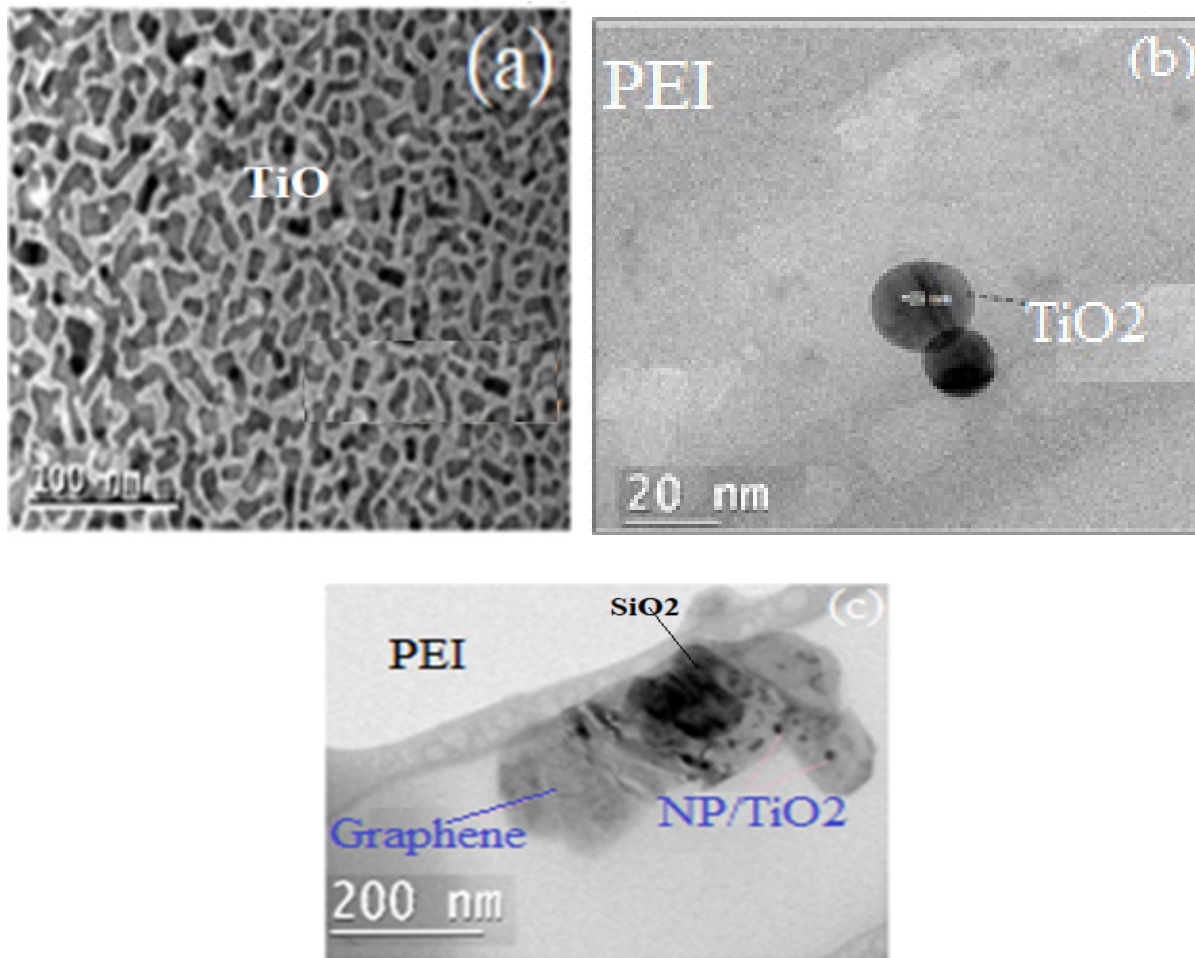
Figure 6-5 : TEM micrographs showing: a) TiO$_2$, b-c) Graphene /TiO$_2$ dispersion inside PEI solutions.

Figure (6-5a) points out Ti -NPs morphology, its existence, agglomerates, and the high volume of the spread of TiO$_2$ on the surface. Titanium oxide nanoparticles is a cubic structure which side is about 25 nm. Also, it is expected to have a more uniform spread in different areas on the image. It could be returning to the hydrothermal process treatment of the titanium oxide nanoparticles, which are wholly adhered and coherent to their surfaces. Figure (6-5b) shows the TEM micrographs of the colloid solution (PEI/Ti/Graphene). It is also possible to recognize some graphene spots which randomly spread on the TEM sheets. In addition, it has a unique size of

around 100 nm. We also found some flocculation and aggregation of graphene nanoparticles/PEI. The graphene carbon skeleton's nature may be more compatible with polyethyleneimine's carbon structure in solution.

6.3.2 Substrate Characterization

Figure (6-6) displays the PDMS dielectric substrate, which has been investigated using Fourier transform infrared spectroscopy. The IR spectra results are consistent with previous reports PDMS fingerprint spectra indicate some peaks at 860 and 795 cm^{-1} which are attributed to Si–CH$_3$ group and the stretching vibrations of (Si–C) bonds. In addition to the peaks appearing at 1400 and 1252 cm^{-1}, which are respectively assigned to symmetrical and asymmetrical distortion of CH$_3$ and Si–CH$_3$ groups. Two peaks were also observed at 1075 and 1015 cm^{-1}, which were associated with the Si–O–Si bonds stretching and bonds vibration. In the same manner, the bonds stretching of -CH$_2$ - and -CH$_3$ were assigned around the 2895–2950 cm^{-1} .
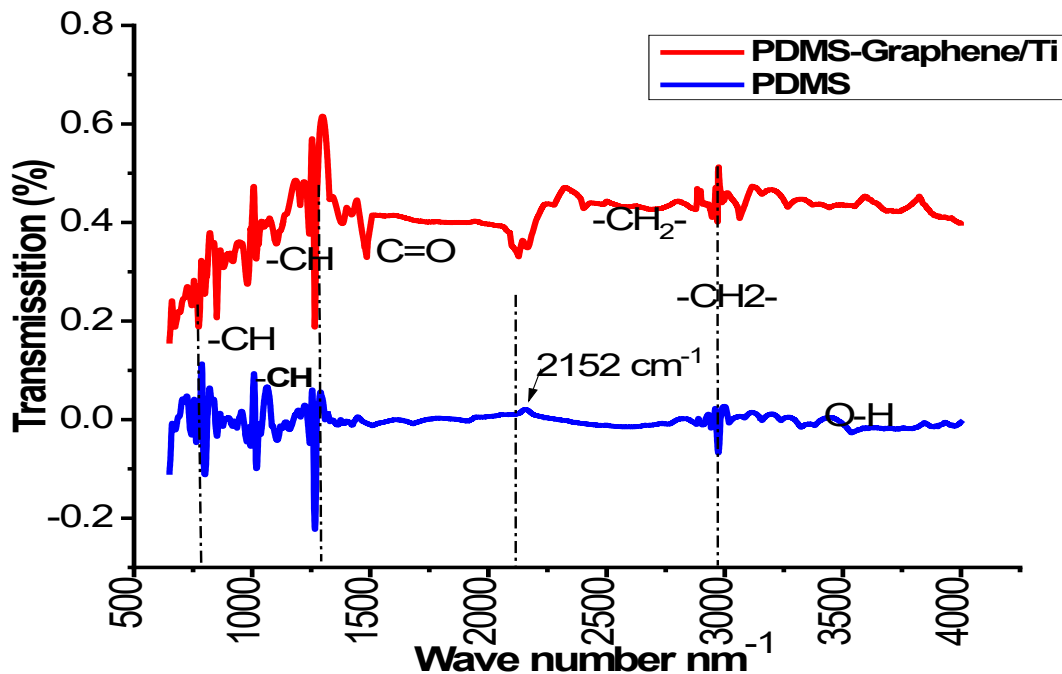
Figure 6- 6 : FT-IR spectra of PDMS and PDMS/graphene/Ti.

6.3.2.1 Dielectric measurements

Generally, when applying an electric field on an elastomer film, the dielectric constant is reduced along the thickness according to the electrostatic charges and it is elongated along the transverse direction under the compression force σ_z also known as Maxwell stress [297] which is calculated by Equation (5-4).

$$\sigma_z = \varepsilon_0 \varepsilon_r \left(\frac{V}{t}\right)^2$$

(6-4)

Where ε_r is the relative dielectric constant of the PDMS elastomer, and the dielectric constant is ε_0 of the air. **V** expresses the applied voltage, and **t** signifies the thickness of the elastomer. Figure (5-7) shows the variations of the dielectric constant and the dielectric loss of the PDMS substrate as a function of frequency. It can be found that the dielectric constant of the PDMS sample was a somewhat a constant recorded value at 2.67 compared to the improvement value of 4.98 of the dielectric constant of the PDMS/composite when the frequency was raised from 10 kHz to 10^{-6} kHz. There was no change in the dielectric loss of PDMS with the change in frequency.
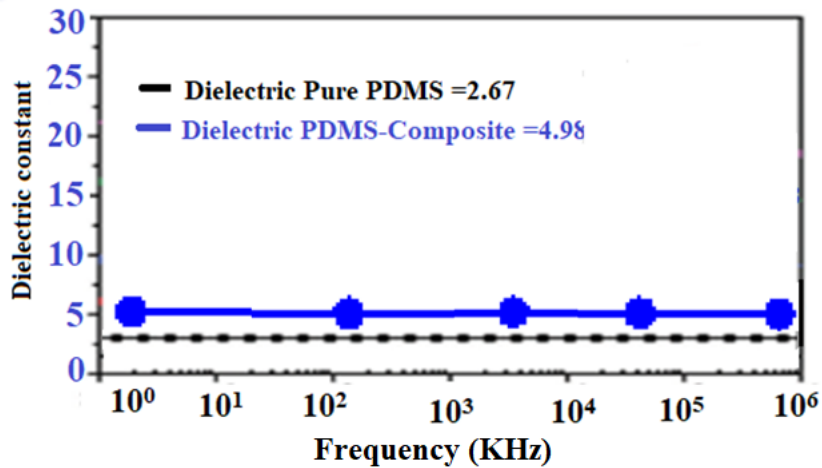
Figure 6-7 : Dielectric constant of the PDMS substrate film at 1 kHz.

6.3.2.2   DSC curves

Figure (5-8) shows the DSC curve carried out at different heating rates for the PDMS polymer. There are three highlighted clear peaks related to the glass transitions, crystallization, and melting. These results confirm the hypotheses made from the thermomechanical assumptions. The measurements show that the significant appearance of the glass transition temperature Tg of PDMS is around -120°C. The glass transition has transferred to a higher temperature in the PDMS sample. At a given heating rate, the addition of glass crystallization, the PDMS switches to a lower temperature. The melting temperature reduces with an increase in the silica (SIO_2) content, and the melting peak broadens in regards to minimizing temperatures. We can count the polymer's degree of crystallinity using the crystallization enthalpy divided by the sample percentage, ~~by~~ based on the formula

$X_c = \Delta H_c / \Delta H_{100\%}$, where $\Delta H_{100\%}$ is the enthalpy of fusion of PDMS, taken as 37.43 J/g [298] .

Moreover, the reaction curve dropped under the exothermic curve, which is directly proportional to the total crystallization rate. On the other hand, by raising the heating rate, the crystallization peak increased the PDMS structure's decomposition. In addition to the breakdown of some molecular bonds, some weak bonds between PDMS molecules eliminated water, a CO_2 molecule, a carbonyl group, and finally, some molecular decomposition took place.
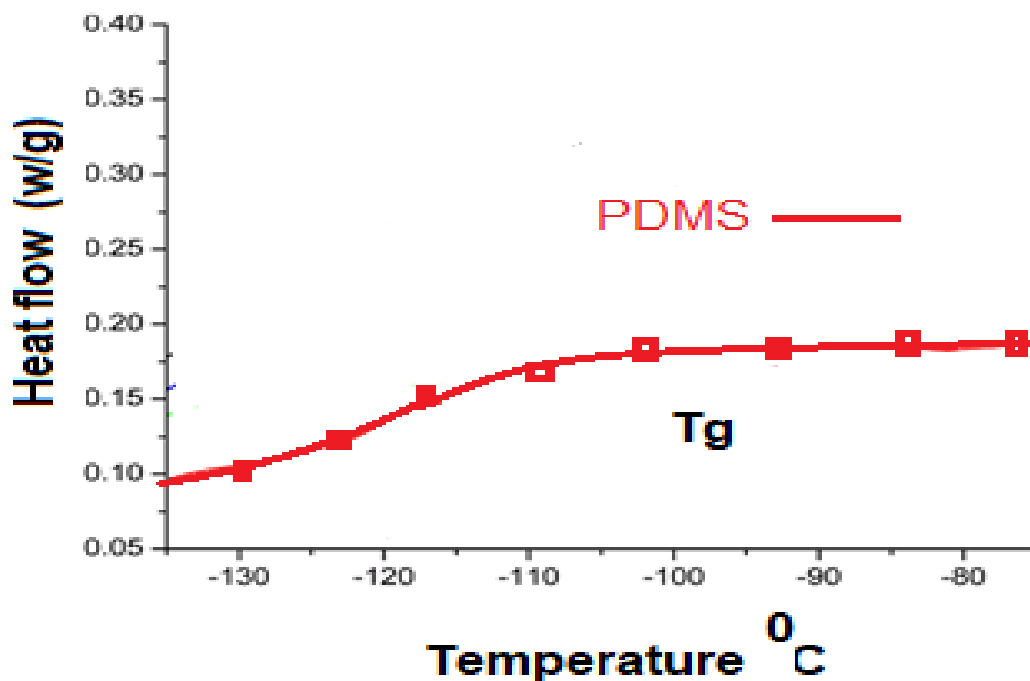
Figure 6-8: DSC thermograms of pure PDMS.

Figure (5-9) shows the tensile stress-strain curves of the pure PDMS tested in the form of thin layers at different applied pressures. Some mechanical properties such as shear strength and stretchability are also shown in Figure (5-9). It is noted that by increasing the applied stress, stretchability increases, which could lead to a softening of the PDMS structure and the formation of a passive charge ~~of~~ on its surface. PDMS films indicated the lowest Young's modulus and higher elongation at breaks at 15 MPa rather than layer PDMS films at the same value. That can be attributed to the stronger carbonyl group C=O in the PDMS structure, which act by reducing the PDMS molecules' crosslinking density. It has been reported that crosslinking between PDMS molecules depends on the hydrosilation, which occurs between the active pair of electrons in the carbonyl group and the other linear PDMS's carbon skeleton [42].
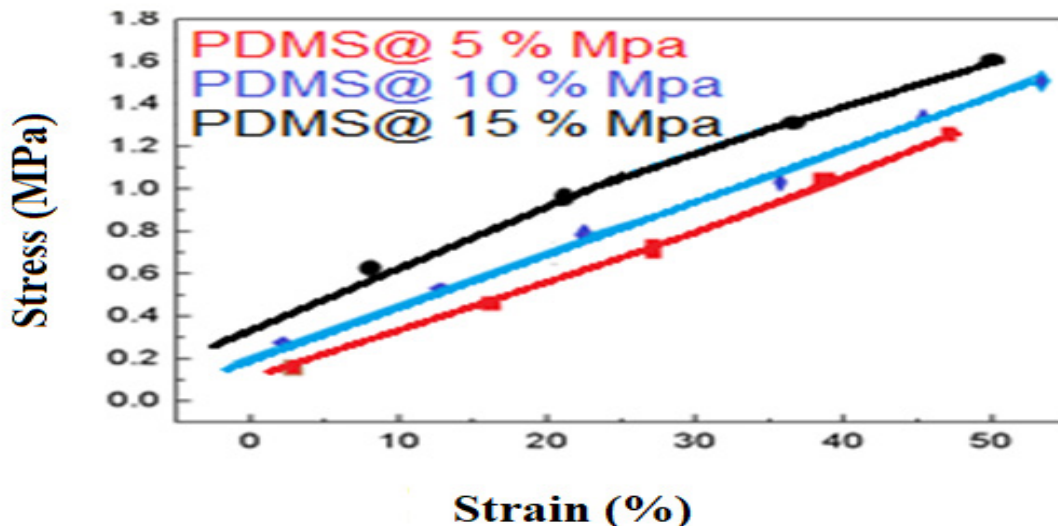
Figure 6.9: Tensile stress-strain curves of the pure PDMS

6.3.3 Measurement of the performance of fluidic antenna without bending**.**

The performance of the fabricated antenna was evaluated using a vector network analyzer (Model #5071 B) from Agilent Technologies, Polytechnique Montreal, Canada. Originally the network analyzer was slandered using the two-port Ecal module posture (Model #85092C) with applied range frequencies from 300 kHz to 10GHz, which supplies excellent accuracy.

Return Loss Characteristics

Simulated and Measured Results

The fluidic antenna's simulations and measurements had been investigated at frequencies from around 1.0 GHz to 3.0 GHz with a frequency step of 20 MHz. Figure (5-10) displays S11 plots that show good indicators. With some of the simulation results, this fluidic antenna resonates at a frequency of 2.44 GHz and reveals a -10 dB return loss bandwidth of 109.02 MHz
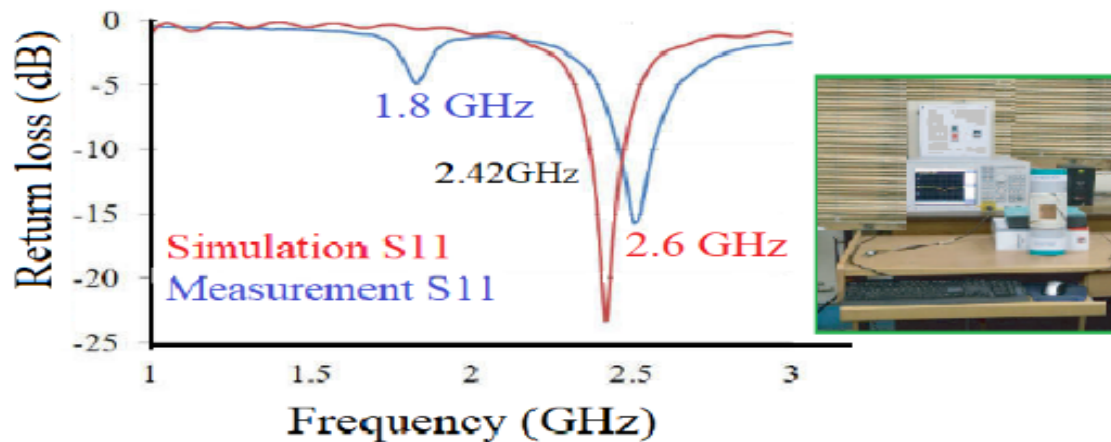
Figure 6-10 : Return loss characteristics of the fabricated antenna.

Gain, directivity, and efficiency of the fabricated antenna.

There are two parameters used in assessing the performance of an antenna. They are the directivity and the gain Directivity is a measurement of the radiation concentration in a direction while gain represents the power transmitted in the main beam.

Some simulations were carried out within a frequencies range of 1.0 GHz to 3.0 GHz, in order to obtain the fabricated antenna's parameters such as gain, directivity, and radiating efficiency. The equivalent gain of the antenna measured at the same frequency range is known as the gain-comparison method [299]. Figure (6-11) illustrates the simulated gain, experimental gain, and simulated directivity as a function of the applied frequency. Such characterization is based, on the standard detection formula. The values of the directivity of the fabricated antenna are calculated from the measurements of the radiation patterns. On the other hand, directivity can be extrapolated from the ratio between the power radiated in the direction of the strongest emission to the total power radiated by the antenna while gain is the ratio of the power radiated in the direction of the strongest emission to the total power accepted from the source. For this reason, the gain is basically the directivity multiplied by the efficiency of the antenna . In this regard, antennas applications with low directivity can generally function as good receivers while antennas with high directivity can be good transmitters.

"AntennaGain" is defined as the ratio of the radiation intensity in a given direction to the radiation intensity to be produced if the power accepted by the antenna were isotropically radiated. Usually this ratio is expressed in decibels with respect to an isotropic radiator (dBi). Gain is a unitless measure that combines an antenna's radiation efficiency displaystyle and directivity D through the following formula: **G=ηD** The radiation efficiency η of an antenna is the ratio of the total power radiated to the net power accepted by the transmitter antenna connected. G dBd =10.log 10 (G/1. [300-301]
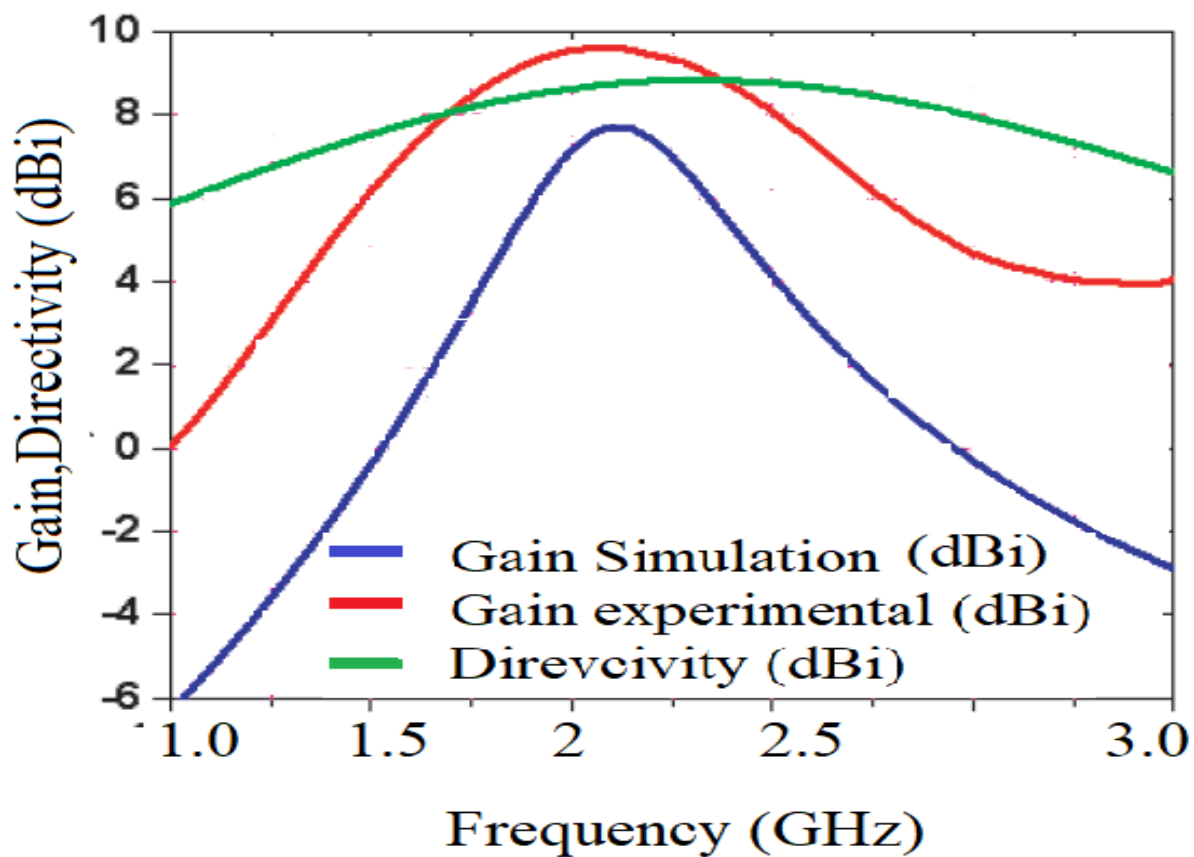
Figure 6-11: Gain and directivity plots for the fluidic antenna.

6.4 Conclusions

In recent years, a growing attention of the scientific researchers have been drawn to the

fabrication of dielectric elastomers   due to their unique characteristics such as flexibility, stretchability, ease of transport, mechanical resiliency, and low cost that make them auspicious materials for flash electromechanical applications in actuators, environmental sensing, and biomedical sensors. This paper introduces some novel composite strip materials to be be used in future applications. The device is composed of graphene immersed in Polyethyleneimine (PEI) matrix and assembled with Titanium oxide. That fluidic solution had been evaluated and characterized using different spectroscopic methods, then injected inside a microchannel of PDMS substrate to be evaluated. The gain, directivity, efficiency, and S11 measured at a broadband frequency of 2.44 GHz and 2.8 reveals a -10 dB return loss bandwidth of 109.02 GHz.

Conflicts of interest

There are no conflicts to declare.

Acknowledgments

CHAPTER 7

IN SITU- PREPARATION AND ESTIMATION OF THE PHYSICAL

CHARACTERIZATION OF NANOFLUIDIC SOLUTION AND ITS APPLICATION

Ameen Abdelrahmana, [a], Fouad Erchiqui[b], Mourd Nedil[c], Siaj Mohamed[d]

[a] Material Science Département/School of Engineering, Université du Québec en Abitibi-Témiscamingue (UQAT), 445 Boulevard de l'Université, Rouyn-Noranda, QC J9X

5E4, Canada

[b] Professeure-d'université, UQAT - Université du Québec en Abitibi-Témiscamingue, 445 boul. de l'Université, Rouyn-Noranda J9X 5E4, Canada

[c] Professeur Titulaire/Professor Directeur du programme de la maîtrise en ingénierie École de génie/School of Engineering, Université du Québec en Abitibi-Témiscamingue

(UQAT), Campus de Val d'Or, 675, 1ère Avenue, Val d'Or, QC J9P 1Y3, Canada

[d] Département of Chemistry, Université du Québec àMontréal (UQÀM)/NanoQÀM-CQMF, 2101 Jeanne-Mance street, Montreal, QC H2X 2J6, Canada

Abstract

In this work, the preparation and the physical evaluation of a series of miscible 0.2 M solutions in 50/50 volume ratios were addressed. A total of 5 solutions comprised of plain electrolyte/ graphene, plain electrolyte / graphene-ethylene Glycol, plain electrolyte/ graphene-poly-ethylene glycol, plain electrolyte/ graphene-glycerol, and plain electrolyte/ Graphene–Polyethylenimine was assembled with Ag, and copper metal nanoparticles. The physical properties were studied by electrochemical impedance spectroscopy, the solution conductivity calculations, the viscosity and flexibility measurements, as well as particle-size distribution analysis. Moreover, the surface morphology characterizations were done by transmission electron microscopy. A comparative

approach of the physical properties between the five solutions serves as a guide to select the most appropriate fluid applicable to the upcoming device.

Keywords**:** Electrolyte, electrical conductivity, graphene, Ag nanoparticles, electrochemical impedance.

7.1 INTRODUCTION

Nanomaterials and nanoparticles bound to organic or inorganic compounds in the form of nanowires are most often seen in sensing applications. In order to significantly magnify the device response, enhancing the physical properties such as the electrical conductivity and the impedance of a nanowire by associating complementary nanoparticles to form potent composites has been a common route for device engineering. Some materials can also react to light irradiation, which can be combined with nanomaterials for sensing purposes as well. Completely depending on the type of change induced by adduct material, an immediate effect will rise on charge and electron transfer efficiency. Also, by modifying the sensing surfaces with nanomaterials, some improvements in the electrochemical properties will result. Such improvements are low background current or higher signal-to-noise ratios.1 Many metallic nanoparticles, for example, silver (Ag), cobalt (Co), copper (Cu), iron (Fe), platinum (Pt), palladium (Pd), iridium (Ir), and nickel (Ni), either taken alone or in composites have also been embodied into biosensors.[302-205]. In the one hand, metal oxides and transition metals have been implemented in the fabrication of biosensor [306-309], -On the other hand, organic nanomaterials have also partaken in enhancing their electrochemical behaviors. Allotropes of carbon, such as carbon nanotubes (CNTs), graphene, carbon capsules, carbon powders, carbon nanowires, and carbon nanotube arrays are most frequently found in those applications.[310]. Many organic-inorganic hybrid nanomaterials such as graphene-Pt nanoparticle and Pt-nanoclusters planted with polypyrrole nanowires [311] have also been investigated as potential candidates for those applications.

A nanomaterial possesses an additional advantage of a considerable surface area to volume ratio. On this note, CNTs show a high loading capacity of biological or chemicals catalyst molecules capable of capturing target analyte signals, which is ideal for both identification and quantification purposes. Nanomaterial catalysts are one of the most-liked in terms of design and fabrication of applicable sensors and electrochemical detectors. This is mostly due to their

stability, conductivity, and sensitivity. In general, colloidal particle behavior does not allow adequate diffusion or sufficient homogeneity.[312-314] Nanomaterials also undergo numerous chemical reactions as soon as released into the vessel harboring reaction conditions in solution. Some of these nanomaterials, especially copper and silver nanoparticles (CuNPs and AgNPs respectively), carbon nanotubes (CNTs), and nanoscale cerium oxide, show many advantages. They provide an abrasion sphere during reaction times, that can be regarded positively, and they are also produced in many shapes and sizes. Different factors affect their applications such as the number of layers, thickness, length, and type of helicity. CNTs are known for their excellent surface area to weight ratios, that increase their electrical properties as shown by their high conductivity identifying as metals compared to other elements behaving more as semi-conductive. The CNTs' charge carrying capacity has been reported to reach a 1000 fold that of copper wires .[315] The literature contains many techniques used for the preparation of CNTs. They include amongst others, the chemical vapor deposition (CVD) ,[316-318] the electric arc discharge (EAD) ,[295] and the graphite electrode laser vaporization26 or laser extirpation (LA) Furthermore, CNTs have excellent commercial production value, trading high production costs for intensive labor. [319] However, a major challenge faced by the industry concerns the growth of CNTs of uniform lengths, without aggregation. Leading to reduced undesirable on specific binding of proteins or other molecules on the CNT walls. Despite the previously stated limitations, the electrochemical properties of different types of CNTs are excellent .[320]As mentioned above, nanoparticles of copper, palladium, cobalt, silver, platinum, and others have also been incorporated into various biosensors,[321-324]. In this regard, Baioni et al assembled 30 nm copper hex cyanoferrate nanoparticles by using the electrostatic deposition layer-by-layer (LBL) to deactivate fluorine-doped tin oxide electrodes. This technique has been produced by electroactive films capable of sensing hydrogen peroxide (H_2O_2) with remarkable detection limits, even in the presence of interfering ions. Conductive polymers are mainly organic compositions with a pi-orbital network responsible for electrons delocalization within the polymeric structure.[325-329] The modeling and synthesis process is based on methods that associate electronic and mechanical properties, thus improving the flexibility and conductivity of the produced polymer. Ideal polymers are well known for being thermally and environmentally stable, conditionally soluble, easily operated, and appreciably conductive. The electrical conductivity of polymers changes over several orders of magnitude depending on the applied potentials, pH, and environment. [330] The conducting polymers are usually linked to better

defined electroactive area or clearer electroactive area, when compared to other less efficient nano-scaled materials. In the same manner, conductive polymers have a remarkably ameliorated signal and performance in contrast to other classical materials used in biosensing, due to electroactive surface area exposure .[331] The electrochemical methods enable us to remove interferences resulting from other sample components. This is for example done, by picking out the specific amperometric response through electrode-solution interface detection. The sample color change or turbidity can be disregarded as interference, and can still be considered a homogeneous analysis.[332] Moreover, the electroanalytical processes require a small amount of sample and electrochemical analyte measurement and signal detection techniques trend towards inexpensive and portable handheld devices.

Numerous Nano electrodes have proved to be advantageous, especially in biological and industrial applications. In the biological sector for instance, applications have crossed single cell investigations, point-of-care clinical analysis, interconnected biosensor development, the invention of microchips [,333-335] and patterned electrodes[336, 337]. Overall, the nano electrode application discipline is a rapidly broadening its research area due to recurrent progress made in the area of material sciences, the cost-effectiveness, and the additional electrode fabrication methods integrating both electronic and biological components in the biosensor development. Many electrochemical techniques include handy screen-printed electrodes (SPEs) fabricated with graphite, gold, and silver ,[338-339] which can be mass-produced with high profitability.

The three-electrodes electrochemical cell setup is commonly used in electrochemical detection operations. Those electrodes are respectively the working electrode, the reference electrode, and the auxiliary electrode (usually a platinum wire). The working electrode is a strongly conductive material such as glassy carbon, gold, platinum, or mercury. In the three-electrodes setup, a charge flows through the electrolyte from the electroactive interface between the working electrode and the electrolyte solution to the auxiliary electrode. The reference electrode, ensures an accurate output of the tension at the electroactive site. Common reference electrodes are the reversible hydrogen electrode (RHE), silver/silver chloride electrode (Ag/AgCl), and the standard calomel electrode (SCE). All three electrodes must be distanced one from the other to avoid short-circuiting the cell. Generally, the electroanalytical techniques are used to gauge current, potential, or impedance. The techniques for these

measurements are respectively known as Potentiometry, Amperometry, voltammetry, and Coulometry.[340,344] Carbon-based electrodes are classified according to the carbon atoms hybridization comprising the electrode. Graphite for instance is highly oriented pyrolytic graphite (HOPG), adopting an sp2 hybridized orbital arrangement, whereas diamond structure is fabricated of sp3 hybridized carbon atoms. Glassy carbon is one of the widespread carbon materials for electrode applications. It complies conformably with the three sought-after characteristics of a good working electrode. In fact, it is chemically inert, its surface is easily renewed and it has a large stable potential range (ca. − 0.4 V to + 1.7 V (vs SHE)) .[345, 346] Consequently, carbon electrodes are easily coupled to work with organic redox molecules. The performances of electrode materials vary differently from noble metals to carbon or even conductive polymers for specific applications. Some metals like (platinum, gold, and silver) have excellent conductivity and superior kinetics with regard to electron transfer. Moreover, some of them like platinum and gold possess noticeable chemical stability and high inertness. Hence, gold contribution to microfabrication and immobilization in biological applications. Effective electrode material can be used dependably when potential stability domains are around − 0.1 and + 1.3 V (vs SHE) .[347] Although mercury is the most common electrode material in polarography, it has limited applications due to its inveterate toxicity.[348] Semiconductor electrode materials have gained some attention, for example, indium tin oxide (ITO), because they are cheaper than noble metals, transparent, and easily applicable. Furthermore, their potential stability domains are larger than that of gold (− 0.4 V to + 1.9 V vs (SHE)). However, ITO has a remarkably lower conductivity (104 S cm−1 vs 107 S cm−1), [349-350] and is unstable in an acidic medium . Based on electron transfer kinetics, ITO is slower than noble metals or and glassy carbon.[351,352].

One of the most applicable industrial polymers is polyethylene glycol (PEG) because it is a water-soluble neutral polyether (due to the polarity of the hydroxyl group). PEGs can be prepared with different molar masses. Interestingly, low molar mass PEGs are eco-friendly and non-hazard solvents with potential uses in industrial applications, especially in the biological field.[353,354] Due to PEG, aqueous biphasic systems (ABS) have been recognized as key tools for the extraction and purification of biomolecules.[355] UV/Vis spectroscopy is used for the characterization of metal nanoparticles suspended in plain electrolyte/ organic solutions, between wavelengths of 250 and 1000 nm, for investigating noble metals and graphene. In this

work, UV/Vis spectrophotometry scanned a series of prepared colloidal solutions made of a plain electrolyte solution made with graphene nano-tubes, silver nanoparticles, and gallium metal particles. The same electrolyte was also mixed with PEG, glycerol, and PEI. The size of Ag nanoparticles was estimated to be in the range of 15–20 nm depending on the solution composition. Ag NPs were also aggregated and their sizes did not remain in the nanoscale range due to particle enlarging following aggregation.

Various studies have worked on creating and characterizing metal nanoparticles for many applications in different areas of the field of life sciences, as well as the biological, industrial, and engineering sectors .66-69 Some strategies are used for the improvement of those fields like synthesis or fabrication to keep up with the demands from the different fields. They both optimize the size and shape of nanoparticles, which are important factors for potential applications [356] Besides, nanoparticles are highly unsteady because, they have high surface energy trending towards the conversion into bulk materials, as aggregated particles .[357-359] For this reason, metal nanoparticles must be prepared more stably by using many stabilizing agents like surfactants or emulsifiers [360], dendrimers, [361]Copolymers, [362] and gels Gels incorporated with nanoparticle metals have prospective applications in biomedicine, optics[363], Electronics, photonics [364], and catalysis [365]. These blends can be also conveniently characterized by different spectroscopic techniques like the transmission electron microscopy (TEM) [366] and the scanning electron microscopy (SEM). The Fourier transform infrared spectroscopy (FTIR) [367] and the ultraviolet-visible spectroscopy (UV/Vis) [368] have their characteristic advantages and disadvantages. In order to gain specific information for the single metal in composites, Khan et al. [369] assembled P(NIPAM-AA) gels by the microwave irradiation process. Some micro-reactors were used in situ for the synthesis of Ag NPs in the presence of glucose reducing agents [370], then confirming the incorporation of Ag NPs gel by acquiring the UV/Vis spectra at 429nm. On the other side, Metals are characterized by promising conventional EMI shielding material ascribable to their excellent electrical conductivity. For instance, metallic meshes are often used as a shielding material in smartphones protecting their electronic components from cellular transmitters and receivers. Though metals are highly-conductive, they suffer several drawbacks like corrosion, high density, rigidity, relatively high material and processing cost, and also limited tuning of shielding effectiveness (SE).[371-372].

The selective distribution of fillers including graphene filler in the polymer blends is quite easy. The case of fibrous fillers like carbon nanotube, carbon fiber, nanowire, which has a high aspect ratio (length/diameter), is quite difficult. In the literature, Ajayan et al. [373-376] have reported their use in the polymer matrix as it imparts a unique combination of electrical, thermal, and mechanical properties for conductive polymer composites.

7.2 EXPERIMENTAL

All chemicals (Copper (II) Sulfate (CuSO4), Aluminum Chloride hydrate ($AlCl_3$-$3H_2O$) and Sliver Nitrate 99 % ($AgNO_3$), Glycerol, Polyethylene Glycol (50v/50v) (PEG, MW = 2000), polyethyleneimine (PEI, average molecular weight of 750–1000 KDa (50% w/w aqueous solution) and graphene nanotubes used in the preparation were purchased from Sigma Aldrich at 99.9 % purity. Other organic solvents and polymers, stated below, were bought from Fisher Scientific, Toronto, Canada:

7.2.1 Preparation of the electrolyte solution

The electrolyte solution was prepared with 0.2 M of different salts (AgCl, $AlCl_3$, NaCl, and $CuSO_4$). Then 3-5 drops of acetic acid were added to keep the pH at around 4 and to prevent the precipitation of Ag. The prepared solutions were kept under stirring for 5 hrs.

7.2.2 Preparation of the colloidal composite solutions

A mass of 0.1 mg of nano graphene was dissolved in the 0.2 M electrolyte solution, followed by stirring for 24 h. The composite solutions were then prepared by adding organic compounds at a 50/50 volume ratio. Ethylene glycol, glycerol, polyethylene glycol, and polyethyleneimine were added to the electrolyte graphene solutions, then stirred overnight. Furthermore, 0.2 M of $AgNO_3$ was added to each solution while stirring for 8 additional hours, until the particles became homogeneously suspended.

7.2.3 polydispersity index (PDI) of polyethyleneimine

In that experiment we need to calculate (PDI) by retied compressed cycles of PEI synthesized nanoparticles are dispersed by using repeated centrifugation–redispersion cycle at 25,000rpm for at least 2 cycles (30 min each cycle). The supernatant thin layer from each centrifugation–

redispersion cycle were collected for determining the unbound PEI and a percentage of grafted PEI through the colloidal polymeric solution.

7.3 Materials characterization

Electrochemical characterization

The EIS, and CVT:

The EIS, and CVT experiments ~~was~~ were carried out in Nano- QAM, (Montreal, Canada); to detect the impedance.~~,~~ An 8 Channels Battery Analyzers model: MTI Corporation, BST8-WA was used. It ~~is~~ consists of an eight-channel with rechargeable batteries at 0.002 – 1mA up to 5V. It is operated by using Nova potentiostat software which provided the electrochemical impedance measurements, the OCV and the CVs impedance to detect the ionic conductivity using the EIS technique. The prepared solution was run at frequencies between 3 MHz ~~to~~ and 1 kHz and in an open circuit potential (OCV = 0.43 V) using three electrodes (working, standard, and reference). The surface area of the electrode is 15 mm at ambient temperature. The cyclic voltammetry measurements were conducted using a three-electrode, Ag/AgCl as a reference, platinum, and the counter electrode. The voltammetric analysis was reported with Princeton model: 263A potentiostat/galvanostat operated using a CV power software.

The dynamic viscosity:

The measurements of the **dynamic viscosity** of the prepared solutions were done using a Sine-wave vibro Viscometer SV-10. The viscosity detection was done by using an optimized electrical current to resonate both of sensor plates at a steady amplitude of less than 1 mm and at a frequency of 30 Hz. This viscometer is reliable up to viscosities between 0.3 and 10000 mPa·s at broad temperatures from 0 to 160 °C, with an accuracy of 1 %. The samples were added inside cubic cups at room temperature.

The Particle size analyzer:

The **Particle size~~r~~ analyzer** associated with Zetasizer Nano S90 (Malvern) from Nano-QAM, Montreal was used to measure the particles size in the liquid phase. The red laser (632.8cnm, 4 MW), used by the Zetasizer instrument at a receptor angle of 90 degrees was used to facilitates the detection of particles with diameters between 1nm and 5 microns.

The ICP Technique:

The ICP Technique is composed of the ionization of the prepared sample by injection into an argon plasma (Temperature around 6000 K). The samples have to be prepared by dissolution into acid (wet digestion) before analysis. The solution is then injected into the plasma as a fine aerosol, made by a pneumatic device (nebulizer). ICP analysis uses 2-5 % HNO_3 as a reference. All test has been carried out at Nano-QAM, Montreal.

The transmission electron microscope (TEM):

All analyses have been conducted by Transmission Electron Microscope H-9500, Which is a 100-300 VK TEM attached to an electron gun Panorama La B6 with high Diffraction Pattern. The specimen composed of Single crystal silicon (Si) and accelerating voltage range of 40 to 100KV; with a camera diffraction length: of 0.5m. The instrument has a magnification range of 18× to 450,000×; a resolution (objective lens) of 0.5nm/5.0Å (point), 0.34nm/3.4Å (line) The core-shell morphology of PEI-immobilized nanoparticles was distinguished by transmission electron microscopy (TEM; JEM-1400, JEOL, 100 kV). 15 µL of 500-fold diluted sample was deposited on a copper grid and stained with phosphotungstic acid (PTA, 2 wt.%). Then, a sample was dried under an ambient environment and inspected by TEM. TEM images were also used to determine the volume-average diameter of the core compartment (Dcv) and the number of particles per volume (Np), using the following Eq. (1) [377]

$$Np = \frac{Total\,volume\,of\,core\,polymer\,per\,volume}{volume\,of\,core\,compartment\,per\,particle} = \frac{mp/Pp}{n/6(Dcv)3} \qquad (7\text{-}1)$$

where mp is the total mass of polymerized monomer and ρp is the density of each core polymer assumed to be the density of the corresponding bulk polymer. [91,92] Some experiments have also been conducted at ETS, Montréal, Canada.

The UV-vis absorption analysis:

The UV-vis absorption analysis was carried out at the University of Québec in Montréal (Montréal, Canada), using a Perkin Elmer spectrophotometer, model Lambda 750 in the range

of 200–1000 nm. It is a double beam spectrometer that permits transmittance, absorbance, or reflectance detection for liquid or solid This spectrometer is operated by a temperature controller (Pelletier type) to keep the temperature constant during the analyzes.

7.4 Results and DiscussionS

Figure (7-1) explained that there are some wrinkles on the graphene nanotubes. They are induced by a reduction process that happens on the surface of graphene by both the Ag-NP and the hydroxyl groups of EG and PEG, thus turning the outer layer into a negative moiety. Ultimately, a charge flow is facilitated inside the composite solution.
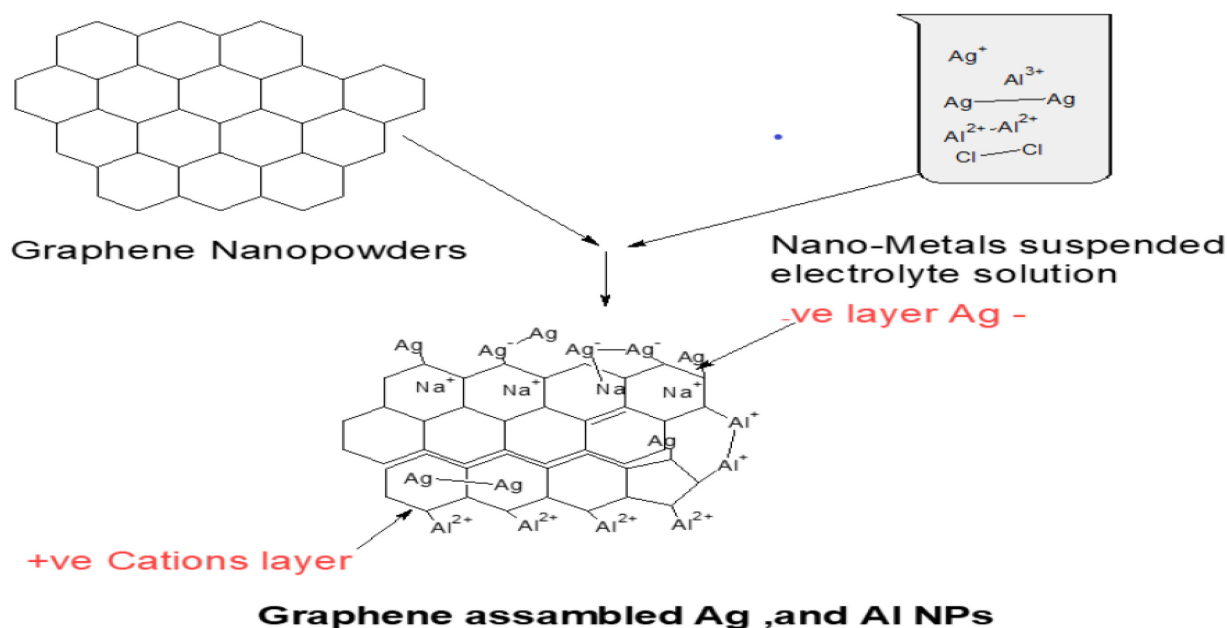
Figure 7-1: The reaction between graphene and the electrolyte solution

The importance of NPs in the electrolyte/organic solution is underlined by allowing fast electron transfer. Their small size and large surfaces lead to the formation of both Ag-Ag and Al–Al metallic bonds as well as an aggregation of the NPs.   These events are depicted in cyclic voltammetry figures below. An observation of these voltammograms marks a reversible redox reaction. On the other side of Ag-NPs (mean size 15 nm), self-assembled monolayers (SAMs) stabilize the particles by preventing aggregation within the slightly viscous solution. By doing so, they also prevent Ag-NPs from aggregation and encourage interactions with CNTs via p–p interactions to give a uniform dispersal of Ag-NPs on CNTs.

Electrochemical characterization

EIS analysis on the Nova potentiostats provided electrochemical impedance measurements,The open-circuit voltage (OCV), and the cyclic voltammogram (CVs).

The impedance results describe physicochemical properties such as conductivity and electron transfer rates and mass transfer kinetics at different frequencies.[378] Studies worked on impedimetric values are relatively common in electrochemical sensors, especially in medical applications. In this work we investigated the conductivity through impedance at frequencies ranging from 3 MHz to 1 kHz fixed at open circuit potential (OCV = 0.43 V) for the different 50v/50v modified miscible solutions plain electrolyte, electrolyte/graphene, EG/ electrolyte/ graphene, PEG/ electrolyte/ graphene, EG/ electrolyte/ graphene, glycerol/electrolyte/ graphene and PEI/electrolyte/ graphene. A three-electrode setup (working, reference, and counter electrodes).
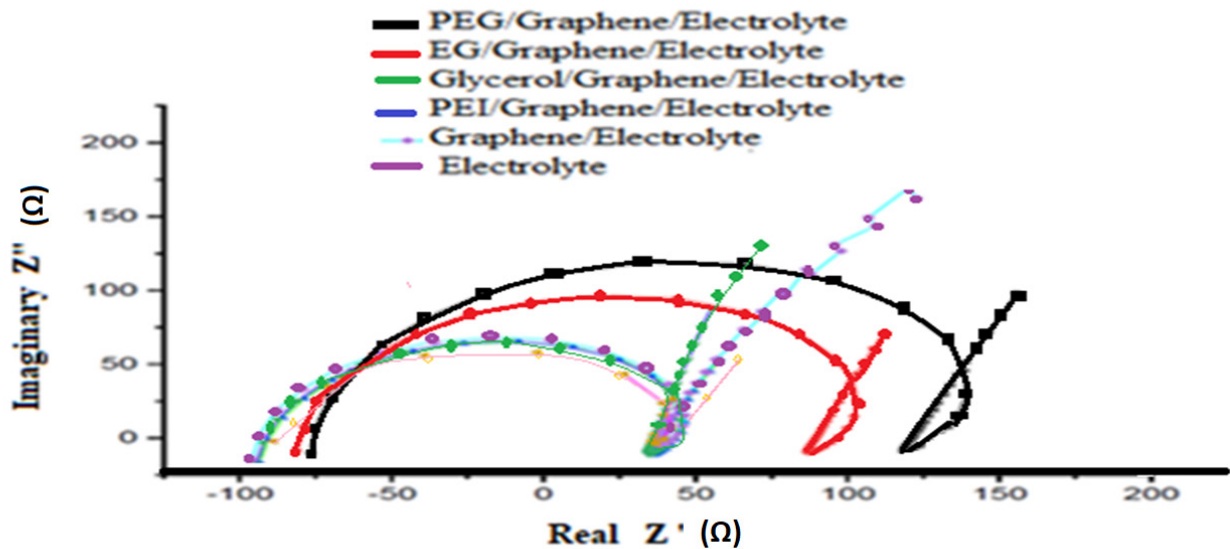
Figure 7-2: EIS results of plain electrolyte, electrolyte/graphene, EG/ electrolyte/ graphene, PEG/ electrolyte/ graphene, EG/ electrolyte/ graphene, glycerol/electrolyte/ graphene and PEI/electrolyte/ graphene.

Nyquist plots of the different solutions are depicted. In all cases, a similar semicircle is observed yet slightly increasing in real resistance as shown in fig.[6-2]. The observed trend goes as follows (electrolyte < electrolyte/ graphene < electrolyte/ graphene/ EG < electrolyte/ graphene/ PEG < electrolyte/ graphene/ glycerol< electrolyte / graphene/ PEI). Conductivity is inversely proportional to molar resistance. We also found another relationship between resistance and frequency. By decreasing resistance, an increase of the characteristic frequency was found in all solutions. The frequency ratio of the electrolyte solution sub-circuit was obtained via $1/ReCe$. Thus, by changing the electrolyte composition of nanomaterial consistency, the characteristic frequency of the electrolyte solutions would shift to bigger values. In other statements, if the electrolyte resistivity is high enough, the characteristic frequency would also be high. Therefore, the response of electrolyte solutions, which was shown as a small arc in the Nyquist plots, showed good conductivity within the plain electrolyte solution. On the other hand, as illustrated in Figure (7-2), in cases where EG and PEG were loaded by graphene Nanotubes, the real resistance spans from -70 to+110 and -75 to +150 ohms respectfully. This reflects that the

117

concavity of EG > PEG. Due to the viscosity parameters which are higher in PEG, obstruction of the movement of ions in solution increases resistance and suppresses the beneficial conductivity effects of graphene nanotubes.Looking into Z values for (PEI/ graphene, glycerol /graphene, and electrolyte/ graphene), high conductivity (low impedance) was noted.   The Z-value was roughly identical. Functional groups on the nitrogen atoms of PEI and the three hydroxyl groups in glycerol created a resonance complex that lead to higher conductivity. On the other hand, electrolyte/ graphene solution, also demonstrated high conductivity when compared, but less than the plain electrolyte. Our explanationconsiders graphene Nanotubes as semiconductors. When aggregated in solution, charge transfer capabilities might be affected, thus becoming less conductive than the plain electrolyte. We conclude that the conductivity arrangement in decreasing order is as plain electrolyte > electrolyte/ graphene > electrolyte/ PEI/ graphene > electrolyte/ glycerol/ graphene > electrolyte/ EG/ graphene > electrolyte/ PEG /graphene.

$$\sigma = \frac{L}{R \times S} \qquad (7-2)$$

Ionic conductivity tests were conducted at frequencies 3 MHz to 1 kHz at open circuit potential (OCV = 0.43 V) by using a working electrode surface area of 15 mm in diameter at ambient pressure and temperature. The ionic conductivity of solutions (σ) was calculated according to the equation above where (Ω) is the real impedance electrolyte, L (cm) is the thickness of the working electrode, and S (cm^2) is the electroactive surface area of the electrode.

Cyclic voltammetry (CV) of the fluidic solutions was conducted by a three-electrode electrochemical cell setup, we applied a changing bias between the counter and working electrodes whilst the reference electrode served as a reference for the applied bias. Cyclic voltammetry (CV) is a dynamic measurement technique where potential applied on the working electrode flows within a range while simultaneously monitoring the current on the working electrode. The range may be repeated in individual or numerous cycles before stopping. Cyclic voltammograms display the relationship between the current and the applied potential. This technique can illustrate a chemical reaction occurring between reactants, changes of energy in

species and relate these changes to the potential. All transformations are a result of electron transfers of species at the vicinity of the electroactive surface. The performance of the different miscible (organic/ salt solution), herein the plain electrolyte, electrolyte/ graphene nanotube, 50% electrolyte/ 50% ethylene glycol (EG) and graphene nanotube, 50% electrolyte/ 50% polyethylene glycol (PEG) and graphene nanotube, 0% electrolyte/ 50% poly ethylene imine (PEI) and graphene nanotube and 50% electrolyte/ 50% Glycerol and Graphene nanotube were evaluated by using cyclic voltammetry. Different scanning rates (10 to 100 Mv/s), using the three-electrode framework, involving carbon as the working electrode, Ag/AgCl reference electrode, and a platinum counter electrode.
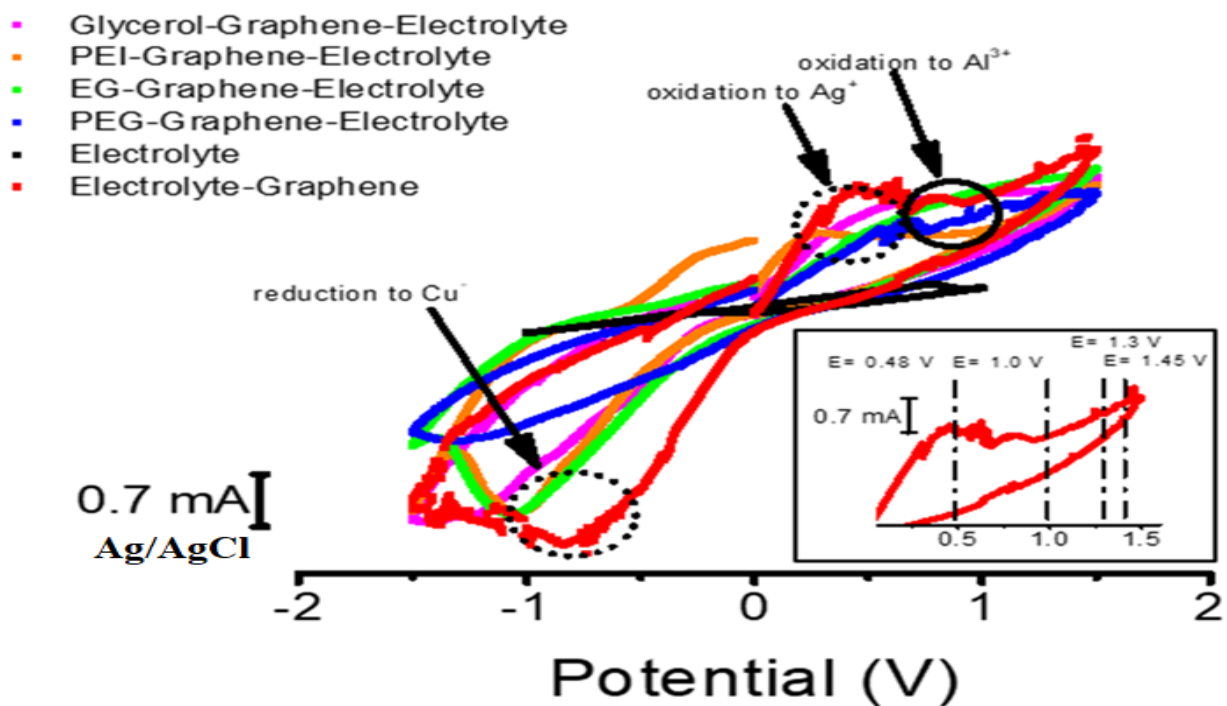
Figure 7-3 : Cyclic voltammetry (CV) of a) prepared solutions, b) plain electrolyte, c) PEG/ electrolyte –graphene, d) electrolyte –graphene, e) EG/ electrolyte – graphene, f) glycerol/ electrolyte – graphene.

Cyclic voltammetry was executed between potentials + 1.5 V to − 1.5 V. Many = reduction and oxidation peaks were observed in this scanned range. According to the results, the electrolyte salts sensitivity increased. This increase in sensitivity is seen as a shift in the redox potentials (Figure 7-E). The potential measurement in an electrochemical cell (E) can be predicted by the Nernst equation and the standard reduction potential of a specimen (E°) and the activities of the oxidized reduced forms of the analyte in solution. It is therefore also possible to derive the ratio of the activities of an analyte at a given potential. From the equation, *F* is Faraday's constant, a universal gas constant is *R*, number of electrons is n, and ambient temperature is *T*.   n the case of the EG/ graphene–electrolyte solution, there is

$$E = E° + \frac{RT}{nF} \ln \frac{(Ox)}{(Red)} = E° + 2.3025 \frac{RT}{nF} \, log \frac{(Ox)}{(Red)} \qquad (7-3)$$

Dynamic viscosity of the fluidic solution

Results for different fluids are seen in Figure 7-4. Dynamic viscosity (η) is a key tool for physically optimizing parameters for liquid-liquid equilibria andmass-charge transfer. Additionally, it is an important thermodynamic and kinetic value of reacting it is equal$v = η / ρ$ *Wherev is Kinematic viscosity,   ρ isfluid density and Dynamic viscosity ions is η.*

On the other side, we noticed T he densities (ρ) for studied polymer electrolyte solutions at room temperature is shown in a diagram below (4). By comparing densities of different prepared solutions: plain electrolyte, electrolyte-graphene-EG, electrolyte-graphene-PEG, electrolyte-graphene-PEI, and electrolyte-graphene-glycerol. We deduced that viscous fluids do not obstruct charge movement inside solutions, yet slightly decrease the flow rate and increase cohesiveness. Therefore, the solution gains stability at room temperature and remains continuously bound.[379-380]

$$\propto P = -\frac{1}{P}\left(\frac{dp}{dt}\right)\rho \qquad (7-4)$$

The relationship viscosity (ρ) and practical size r distribution are illustrated in the equation above. The particle sizes of dissolved particles are directly proportional with viscosity and inversely with conductivity, as evidenced in Figure [7.4]. Taken for example the plain electrolyte showing low real resistance (z –value), high charge transfer, in Figure [7-3], viscosity is lower.

Mass transport and the energy of reaction through this process have been investigated by Different studies worked on solvent reaction mediums that are dependent upon the viscosity factor of solvent. The ratio of the size of the hole to ion increases with an increase in the molar mass of the PEG of DES. Viscosity decreases with increased concentration (molar ratio) of the organic solvent solution, particle size distribution, and weakening of solute intermolecular interactions. The overall viscosities determined from the viscometer in decreasing order were PEI > GLYCEROL> PEG > EG > plain electrolyte.
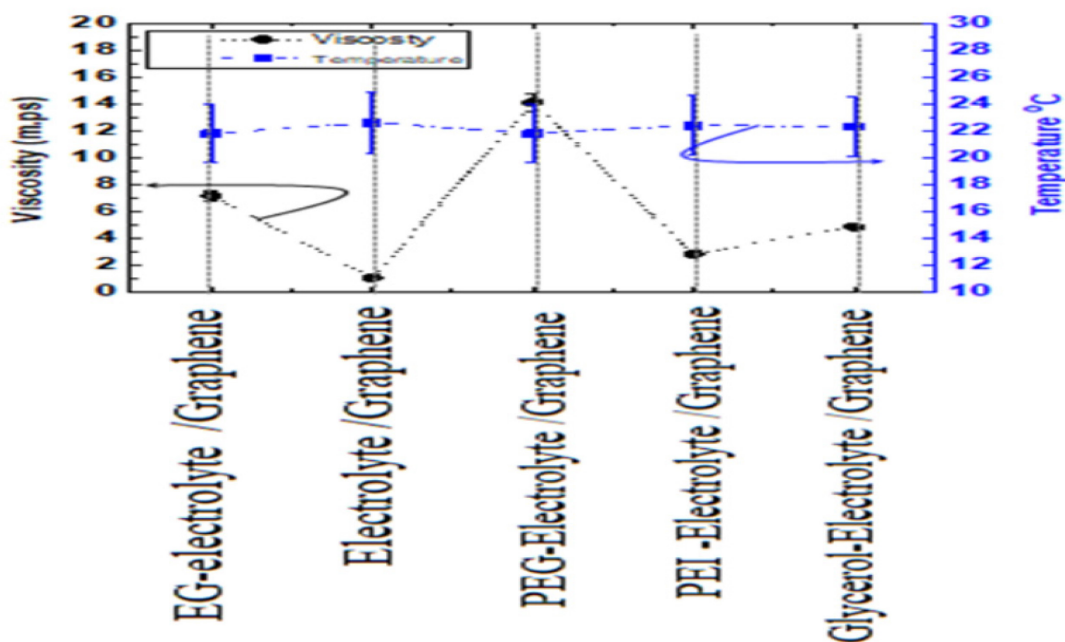
Figure 7-4:The viscosity of the miscible electrolyte solution

Raman spectroscopy of the fluidic solutions

A Technique used for investigating the liquid solution structure is Raman spectroscopy. It was used for the electronic characterization of graphene/ organic materials in prepared solution (Figure [7-5]. There are stacks of sp^2 hybridized carbon atoms associated with specific vibrations and the number of stacks might affect the electronic configuration of delocalized electrons in p-orbitals. Also, there are many wide bands of scattered light appearing on the

spectra for different material compositions, especially for carbon from graphene Nano Skelton at 1583 cm^{-1}. A broad peak located at 2715 cm^{-1} and a broad high peak located at 2700 cm^{-1} correspond to the 2D band. It is noticed that different peaks are not as intense and broad. This is a trait characteristic of amorphous carbon, provided by the light scattered from the carbon chain of polyethylene glycol or Ethylene glycol. On the other hand, the Raman spectrum of aqueous polyethylene glycol/ electrolyte is at different molten states which strongly appears in the spectrum through frequency shifts related to the helical splitting observed in the electrolyte solutions. Peaks may be subjected to change in presence of NP colloid in PEG. The particles' effect on bond stretching by forming metallic-organic or hydrogen bonds. By comparing spectra of EG, PEG, glycerol, PEI, and plain electrolyte solution, observations lead to believe that some of the solutions linked with NPS through polar functional groups (OH) in PEG, EG, and Glycerol. Thus, broad Hydroxyl group signals shifted softly and appear broad instead of sharp. In other cases, PEI marks its amino groups, which have a pair of electrons (electron-donating), to make a conjugated bond with NPs like Cu^{2+} and Al^{3+}. The methylene group's bending region is visible by two bands at 1475 and 1440 cm^{-l}. Between 800 and 900 cm^{-1}, as shown in Figure [6-5], considerable differences are noted in the band structure, another evidence for benzene ring resonance linked to the graphene structure. Raman peaks exist at 880, 840, and 805 cm^{-1}, due to methylene groups attached with ionic species (cations or anions), more prevalently in the plain electrolyte solution. In the lower frequency region, bands are observed at 520 and 551 cm^{-1}, with some residual scattering at 586 cm^{-1}.
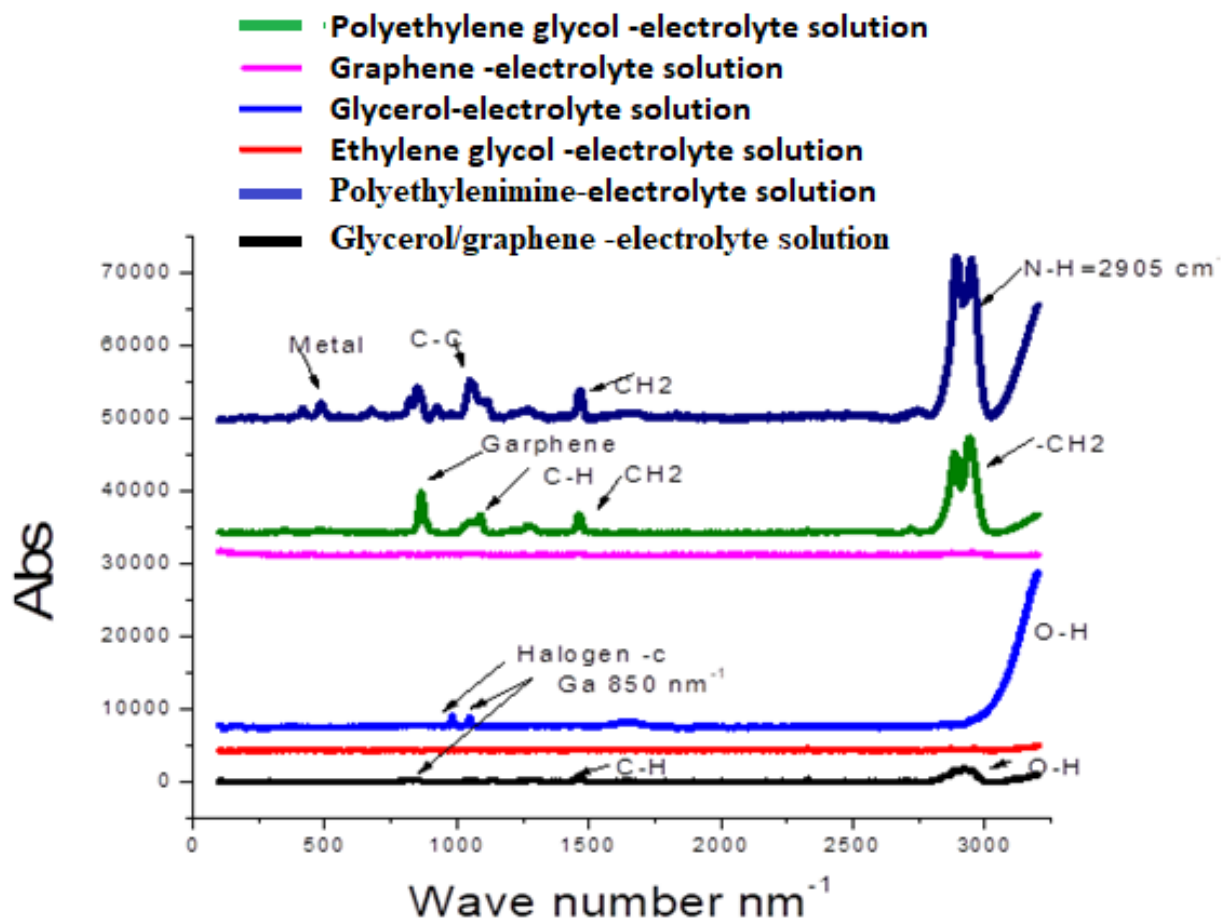
Figure 7-5: Annotated Raman spectra of the prepared solutions.

The scattering of PEI on the NPS (Ag–graphene) in solution leads to a marked change in the Raman spectrum. Noticeably, a decrease in intensity is observed for the bands corresponding to the formation complex (conductive polymer composites) which caused shielding, then shifted the amino($N-H_2$) bending peak closely. There are both asymmetric and symmetric stretching vibrations that, are carefully shifted upwards in PEI solution. PEI is one amino group carrying polymers. Through Raman spectrum of PEI/ electrolyte salts, Ag and Cu peaks disappear on IR spectrum Figure [7-5], Our explanation reasons that a pair of electrons on the donating nitrogen

atom on Aminos groups, conjugates and forms a complex with NPS (Ag and Cu), which has been confirmed by EDX and TEM analyses[381].

The particle size.it is considered one important method to judge on our physical properties prepared solution through charge transfer movement, carrying charge, depletion, and flocculated particles.
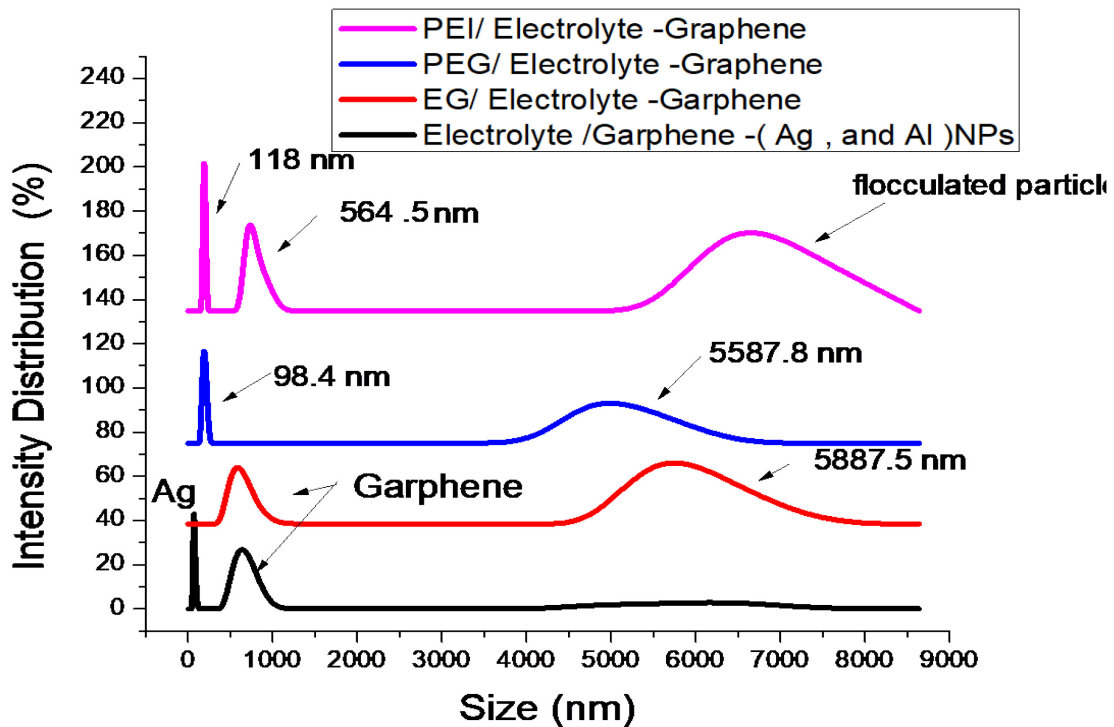
Figure 7- 6: Frequency size analysis of the prepared solution

Furthermore, Particle size analyzer is considered one of the important characterize techniques used to describe the physical distribution of particles in phase and stability of solution (inter-interaction) or intra –interaction molecules (van der Waals force) Also, it gave us surface charge of nanoparticles(Ag, Cu) colloid in solution .by forming a double layer (ions charge) from outers hare of NP charge and the solution, these ions pass through solution carrying charge. So if particles are too much size then it gets be depletion and aggregated then precipitated to become low efficiency in solution .through picture (6- 6) using modules used Malvern Instruments model NO. Zen 3600 Zeta sizer. GO-PEG-Cur aqua was diluted with DI

water and put in a zeta cell. Each spectrum was obtained using 25 scans. This analysis was repeated three times to detect Graphene and Ag NP in PEG, EG, Glycerol, and PEI solution. Glycerol and electrolyte solution were found withholding aggregated crystals of potentially salt crystalline flocculated graphene nanotubes and Rheology of organic composition. This results in detrimental charge transfer properties in our prepared solutions[382].

Inductively coupled plasma characterization.

This analysis had been done to qualitative the existence of Nano metals by using Inductively coupled plasma is a physical method of chemical analysis set aside confirmation of most of the elements simultaneously at a few minutes off preparation. Concerning Figure [6-7], it appears that sliver, Aluminum, and Copper are present in our prepared samples.We conduct that test to detect and measure qualities and quantify main elements inside prepared composite material besides its consider highly sensitive, its high degree of selectivity. Regarding figure [6-7], it was noticed many element spectra appear like Ag, Al, Cu, and Na, that is confirm dispersed metallic ions inside prepare solution and mobility of free ions inside the fluidic solution. All test has been carried out in Nano QAM ,Montreal,Canada
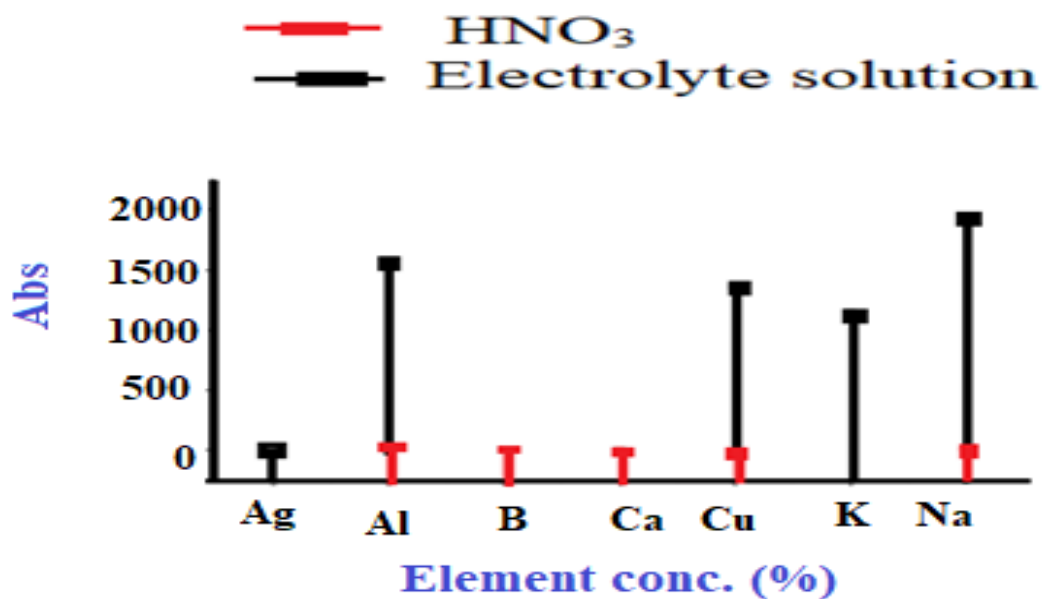
Figure 7-7: ICP for compositional analysis of the plain electrolyte solution.

Morphological study of fluidic solutions (TEM and EDX characterization).

Morphological and particle size studies hence, assert the existence and spread of Ag NPs (20-25 nm) was too small in the proximity of the larger PEI (25 nm) as depicted by the TEM results (Figure 7-8). By Correlating the results from the particles size distribution and TEM images (Figures 7-8a and 6-8b), it is clear that the small particle sizes can move freely without considerable restriction.
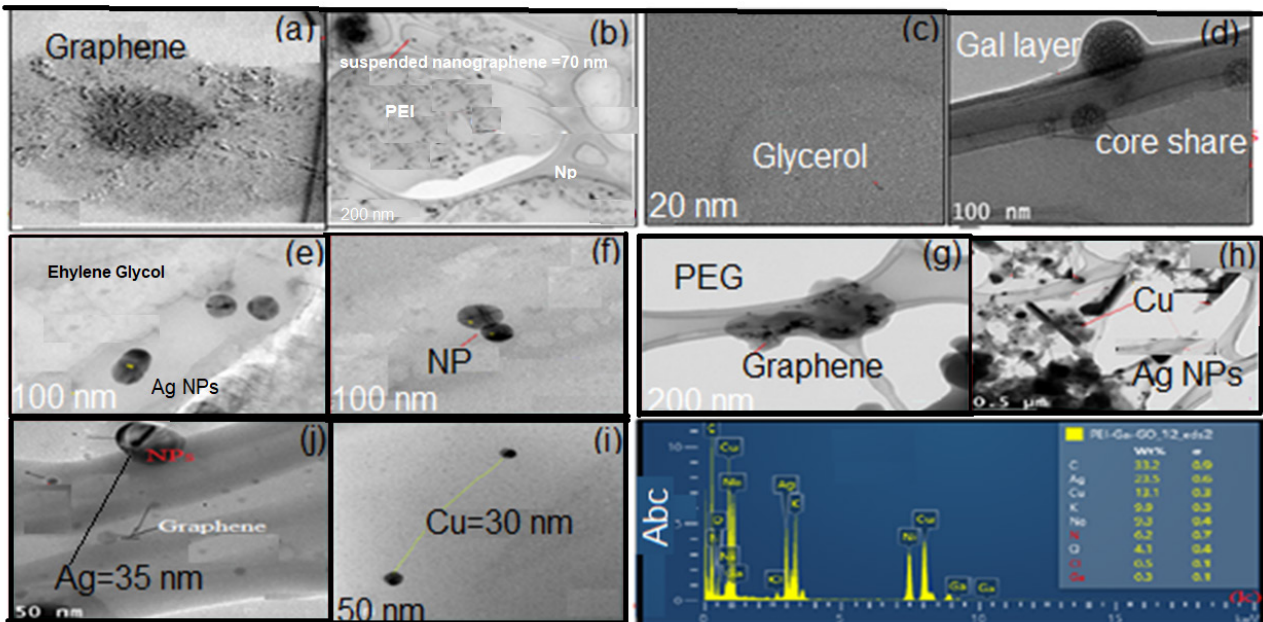
Figure 7-8 :TEM of different miscible solutions. (a-b) TEM of PEI Electrolyte–Graphene, (c-d) TEM Glycerol/ Electrolyte–Graphene, (e-f) TEM of EG/ Electrolyte–Graphene, (g-h) electrolyte –graphene/ PEG, (i-j) Electrolyte–Graphene, k) EDX of Electrolyte /Graphene–EG.

Furthermore, smaller particles have greater ease in charge transport due to the large surface area to volume ratio. Also, there is a significant distribution of nanoparticles in all the prepared solutions, apparently more abundant in PEG solution than PEI and glycerol solutions. This implies that the polarity of the hydroxyl groups of PEG easily attached graphene by hydrogen bonding as is shown in Figure (7-8). Although glycerol contains three hydroxyl groups, it seldom appears in the TEM images. The high viscosity of glycerol may have affected its interaction ability with nanoparticles (Ag, Cu, and graphene). This reasoning could appoint the flocculation and aggregation remarked in the DLS results Figure (6-7), and reinforced by the glycerol TEM (Figures 7-8(c –d). Supplementary evidence of metallic bonds among NPs of the same element (Ag-Ag) and (Cu-Cu) producing aggregated sediments is shown in (Figure 7-8). Graphene nanotubes are visible in all TEM photographs (Figure 6-8), despite shattering into fragments, due to small crystal masses of Cl–, Na$^+$, and K+. These salt were investigated by EDX (Figure

127

8-k).Although there were similarities in the structures of polyethylene (PEG) and Ethylene Glycol (EG) (Figures6- 8e and –h), there was homogeneity within the surface morphology of the two components. Small holes and flocculated spots, raised evidence of bond formation or active sites between hydroxyl groups and other metallic nanoparticles (Figures 7-8-e and f). TEM for glycerol/ electrolyte–graphene illustrated by (Figures 6-9-c and –d) portrayed many massive salt crystals deposited, covered by a jelly substance or layer of glycerol with some metallic NPs dispersion of different size ranges (15-35 nm). Regarding the electrolyte salt, solutions with Nano Graphene (Figures7-8 (i –h) illustrated the formation of graphene nanotubes inside the electrolyte solution containing 0.2 M of ($CuSO_4$, Ag Cl, $AgNO_3$, Na Cl, and $AlCl_3$) salts. Clustered inside those Nanotubes were large numbers of Nano-metals like copper, silver, and aluminum which have respectful sizes of 15, 25, and 20 nm. Sufficient proof of homogenously distributed metals and suspensions with relative bonds between them was found. There was a broken-down graphene nanotube, possibly issued by precipitations of some species. For example, Ag forming Ag Cl. As a remedy, Ph was decreased into a mildly acidic medium, favoring the soluble form of the salts and perhaps repacking the nanotubes (Figure 7-9). Figure 7- 9 displays M-M nanoparticles on the surface of graphene sheets, which set up two layers of different charges (resonance). The negative charge is carried by graphene and the positive charge is carried by the nanoparticles (Ag, Cu, and Al). Electrolyte–graphene/ PEI according to TEM of representations (Figures 7-8-(a) and – (b) depict the smooth morphology without any flocculationsnor aggregations of nanoparticles. The fine particles of Ag, Al, and Cu submerged inside the graphene sheets, confirmed by EDX (Figure 7-8k), seen are around (10-25 nm)). There is no depletion or massive crystals formed as observed in the previous figures. Our explanation, although organic solution has shear strength associated with its viscosity (carrying particle), it also obstructs the movement ions and causes deposition. Also, Figure (7-8)(I,j) show the images of Nanotubes graphene. It is possible to confirm that the graphene structure is formed by several thin layers arranged in stacks. Moreover, there is an oxidation process was happened for graphene slight changes appear in its surface morphology, with a rugged appearance with several lappets. This wrinkled or rugged portion might be explained by the oxidation process to elevated hydroxyl and with cations species in the solution created resonating electron inside carbon graphene structure depending on sp^2 hybridization of carbons (planar structure) to switch to sp^3 (tetrahedral structure). We could be mention another observation that the Graphene Oxide is formed on a layered structure might be associated with

material oxidation, since more degree of oxidation, most spaces are between the functionalized layers. Dikin et al (2007) investigated the same spotted during conducting a layered structure with several folding. [383-386]

UV Characterization

Characterize different prepared solutions by using Lambda 750 UV-vis-NIR spectrophotometer from Perkin Elmer, Nano-QAM, Montreal.it used to deionized water as blank sample Figure (6-9) represented   UV absorption spectra of comparing serious   0.2 M OF prepared solutions(electrolyte, electrolyte –graphene, PEG electrolyte –graphene, EG – electrolyte – graphene, PEI – electrolyte –graphene, and glycerol – electrolyte –graphene). Upon comparing the absorbance spectra of the prepared solutions, as can be seen in Figure (6-9), the absorption spectra of the electrolyte salts reveal strong absorption in the 280–300 region, matching with the p–p* transitions of the conjugated graphene nanotube rings. Many peaks appear in the region at wavelengths between 320 and 285 nm in the case of PEG/ electrolyte-graphene and electrolyte-graphene. Could be assigned to n–p* transition of Ag-Ag nanoparticles metals to Graphene molecules.[96]In contrast, the disappearance of that peak by using PEI, glycerol The importance of using Graphene in metallurgical applications is owed to high plasticity, low melting point, and relative stability with different material alloys (graphene–Ag, Graphene –Cu). Normal and derivative absorption spectra were recorded by   UV/vis in the following figure (7-9). In addition, we have seen different physical recorded peaks for metallic suspension on the fluidic solution, that is interpretation, mobility of free ion charge,[387] reversible redox reaction and miscibility of prepared solution without aggregation or any precipitation complex during the process. On the other hand, graphene works as an ionic bridge between both sides of the electrochemical cell of the reaction.
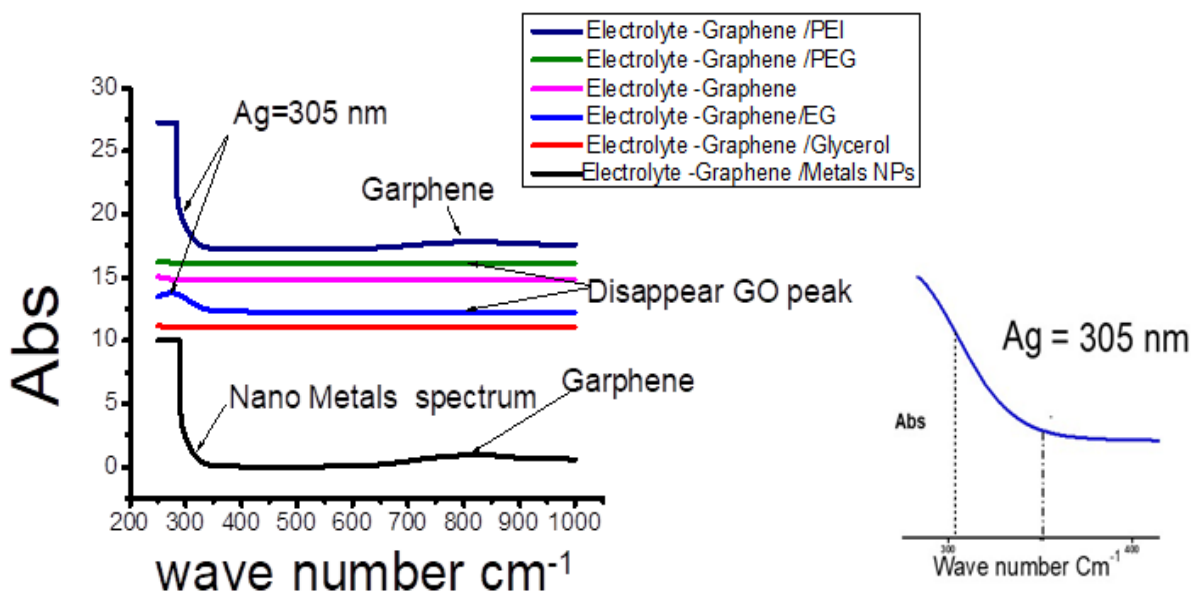
Figure 7-9 : Compilation of the absorption spectra of the different fluidic solutions.

7.5 Conclusion

Organic and inorganic nanocomposite materials play important roles in modern life. For example, nanoparticles or nanowires are mostly used in biological sensors to magnify their applications through nanowire electrical conductivity, electronic configuration, or modified way of nature. Nanoparticle complexes interact with matter. In the case of nanomaterials, they are usually employed for modifying the core or interface components.

Transducers are responsible to quantify the generated signal in the presence of the target object. Analytic measurements on the other hand, With a worldwide trend towards the effective use of electrolyte solutions in different fields like renewable energies, rechargeable battery technology, and biomedical sensors have especially steadily increased. Many researchers have stepped forward in developing electrolyte material by enhancing some improvements over salt concentrations in suitable salt solvent combinations. Contributing technical advantage lots of data of merit over alternative materials. Thus in this work, we have acquired fluidic solutions that will be applied in antenna fabrication. The highlighted properties are mainly conductivity, flexibility (viscosity-cohesiveness), non-toxic and compatible composition.

Author Contributions

Dr. Nedil is completely responsible for Conceptualization, Data curation, in addition to Investigation, Prof . Fouad is a Formal analysis data acquisition, Project administration supervision. DrSiaj is facilitated all, Resources, and Software in his lab. in UQAM, Montreal, Ameen is collaborated in the collection data ,conducting experiments , Validation, Visualization, Writing original drafts, Writing-review & editing with his advisors.

CHAPTER 8

INTEGRATED MATRIX INCORPORATING IMIDAZOLEGRAPHENE ASSAMBLED MATALLIC COPPERAND SILVER NANOPARTICALS TO BE A FLUIDIC ANTENNA DEVICE

Author(s): Ameen Abdelrahman[1], Fouad Erchiqui[2] and B M. Nedil[3]

[1]School of Engineering, Université du Québec en Abitibi-Témiscamingue (UQAT),445 Boulevard de l'Université Rouyn-Noranda (QC) J9X 5E4,   abda02@uqat.ca

[2,3] Professeure- d'université | UQAT - Université du Québec en Abitibi-Témiscamingue 445 boul. de l'Université Rouyn-Noranda J9X 5E4 819 762-0971

Abstract

In that work, we get to enhance the unique conductive of imidazole from (>1 × 10^{-5} S cm^{-1} to 1.2 × 10^{-4} S·cm^{-1} using Graphene and grafting Silver and copper Nano metals, which it worked as active sites and charge transfer based on Graphene barrier. Studying the Electrochemical behaviors and reaction mechanism using Cycle Voltammetry (CV) electrochemical technique. and it was reported multiple electrochemical reaction (redox) series between Imidazole and their complex .in order to justify the imidazole complex, We conduct various characterization likeElectrochemical impedance spectroscopy (EIS), Raman, Fourier-transform infrared spectroscopy (FTIR), Proton nuclear magnetic resonance ^{1}HNMR, and particle size analyzer has been performed to imidazole and their `composite mixture to evaluated the conductive solution to be ready in future work as an application for the fluidic antenna device

Keywords

Imidazole, graphene, copper–silver alloy, impedance, characterization

8.1 INTRODUCTION

Today, Nanocomposite materials consisted of metal nanoparticles, Silver, Copper Graphene, or organo-clays distributed into a polymer matrix reveal a significant absorbing property due to their unique physical and chemical properties. [388-389] For example, Epoxy/Metal composites were applied in microelectronic packaging for embedded capacitors, optical, fluidic antenna, and lead-free interconnecting materials. [390-395] As well, Nanostructured particles like nanowires, nanotubes, Nano rods, or nanofibers are playing an essential role in the manufacture of electronic devices and nanocomposites. Metal nanowires such as silver and copper nanowires (Ag or Cu NWs) were employed as conductive materials in many fabricated process.[376–386]Within the past decade, Metal−organic and Absorptive coordination polymers have been exhibited to be good conducting materials,[397-399] due to because their intrinsic structural features like , tunable porosity, highly crystalline nature , and tailorable functionality. The conductivity of polymeric materials strategy is involving the complicated preparation methods ,like encapsulating special nanomaterials into the pores of polymeric matrix to facile and enhance the performance proton conductors.[400-403]

Kitagawa and co-workers were worked on encapsulation of imidazole molecules into porous polymeric compounds using a composite some protonic conducting materials;[394]recently , considerable research attempt have been allocated to embedding the N-heterocyclic atoms (e.g.,Triazole, histamine ,and imidazole,) into the hole of various porous materials, like graphene ,clay and carbon nanotubes[404,405] or covalent organic structure,[399-401]and mesoporous organosilicons. [406]In order to get the objective and evolve high-performance conducting materials. Imidazole is a heterocyclic compound containing two donating N atoms, each N atom has a pair of electron which it capable of creating resonance of charge on imidazole molecule .Adding or Grafting Nano particles and Organic–inorganic to the composite materials will be enhanced and enrich whole physical and chemicals characteristic of liquid.[407-408]Moreover , The preparation methods of metals inorganic–organic composites matrix has also attracted much attention due to it may display

an excellent tunable physical properties, like electrical , mechanical and optical properties, as a result of cooperated properties of both organic polymers and inorganic metals.[409-411]

On the other side Researchers and Scientists are looking forward to developing sustainable and environmentally friendly materials resources.[412] Materials Engineers and specialized Researcher   have to followed up with various approaches to synthesize and enhance both proton and ion conductivity in the biomedical field, specifically in sensors, and fluidic antenna chips fabricated. Proton-conducting materials are of much interest for various uses in different applications such as fluidic antenna, energy conversion and storage applications, Biological and Environment sensors. Particularly , Anionic electrolyte combines performance, efficiency, stability, and be operated at different temperature ranges.[413]Protonic solution species is distinguished by a lower activation energy to convey through a liquid or solid-state crystal structures and associated interfaces due to the tiny ionic radius and lack of an electron cloud as compared another   conducting ionic species like   oxygen ions ($O2-$).[412]Moreover, the electrical characteristic for boundaries of nanostructured ionic conductors has attracted considerable attention by numerous scientists.[414,415]

 Park et al. fabricated Nanostructured yttrium-doped barium Zirconate ($BaZr0.9Y0.1O3$) and study its grain boundary of protonic conductivity. As well as, Proton conductors solutions are very appealing due to their higher efficiency and low activation energy, thus it encourages various of scientists to work on that point: for instance, Zhao et al.[416].Elleuch traveled over an oxalate co-precipitation process.[418]Richter utilized a solid-state reaction method.[417] Zhu et al. applied a wet chemical method.[419-420] Many Researchers are preferred the co-precipitation methods[421] in their experiments   to prepare the electrolyte protonic solution. The ionic liquid has unique properties and it can fulfill a cycle economics and environment protection due to its advantages inclusive of non-toxicity property and non-flammability, low vapor pressure, conductivity, high intensity of charge transfer, and good stability performance which is served electrochemical application.[422-424]Malavasi et al. mentioned that nanoscale material show important side effects in their reaction mechanism   because it has a short diffusion lengths and large density of molecule interfaces, Eventually it is consider a good evidence to justify the   effective nanomaterial commended and the grain boundary interfaces.[58, 59] Nobody denied the importance of Ionic liquids(IL) structural is playing an essential role in the electrochemical synthesis and reaction mechanism . There are many factories is also effect on

the ionic conductivity of solution ,like Temperature controlling limits, self-assembly, coordinated bonds , particles movement , viscosity, and associate functional properties. One of the main function is Self-assembly processes, it involve different types, cations, anions, and side-chains depend on the nature of base solution. Ionic liquids is also characterize by delocalized charge, which is responsible for intra-molecular interactions between molecules at less intensity. The organic and heterocyclic compounds' cations and anions of ionic liquids are mostly stabilized by resonance with highly delocalized charges.[425] Furthermore, their functional properties could be well-tuned, to be capable of creating an infinite number of different structural alteration with changing cations, anions, and substituents [426-427]

In that paper we reached to create a conductive solution, its specificionic conductivity equal 1.2 × 10^{-4} S·cm^{-1} .It   will be an active side of fabricated antenna device, addition to conduct several of analysis and characterization to evaluate the fabricated fluidic antenna such as[particle sizer analyzer, Proton Magnetic Resonance, and ICP coupled analysis] to assess fabricated fluidic liquid.

8.2 EXPERIMENTAL

8.2.1 Chemicals and Reagents

 Imidazole and organic solvents   were purchased from sigma –Aldrich (Toronto ,Canada) , Graphene Nano powders (purity > 99%, 300 mesh) was bought from sigma –Aldrich Co. Ltd. (Canada).Most of Nano metals   and other salts (copper oxide, sliver acetate , and sliver nitrate (purity > 99%,)) were   delivered by scientific fisher, Canada used ,n-Hexane, THF were purchased from sigma Aldrich, Canada.

8.2.2 Preparation Methods

8.2.2.1 Prepared electrolyte solution enriched graphene.

Electrolyte salt solution has been Prepared using 0.2 M of ($AgNO_3$, and Cu O) salts ,string ultrasonic for 45 minutes   , then   mixing with   5 ml of solution contains (0.05 g suspended graphene/assembled (Ag ,Cu Nano-metals).

8.2.2.2 Preparation of Silver/copper –Imidazole Complex

 Take 5 ml 0.2 M. of Silver acetate (Ag Ac) solution, then add 0.2 of Copper Oxide (Cu O), magnetic string for 30 minutes at ambient temperature, then mixed with (5mmol.)   Imidazole solution for stirring overnight.

8.2.2.3 Synthesis Colloid mixture imidazole/Graphene Metals nanoparticle.

In order to obtain fluidic solution, we mixed the same ratio of imidazole solution ($50_V/50_V$) with Graphene Metals Mixture, stirring for 3 Hrs.   (Completely homogeneity), as shown as in figure (8-1) then it will be ready to characterize and applicable.
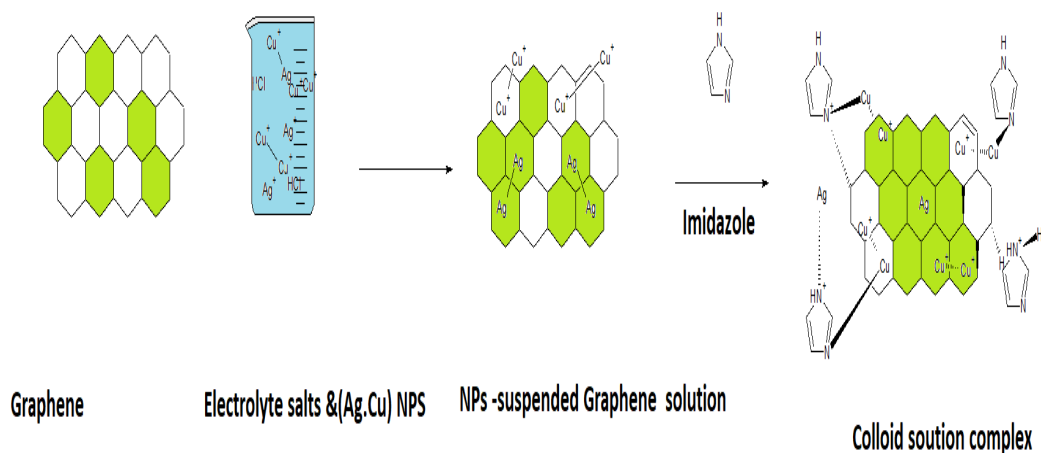
Figure 8-1 : Reaction pathway process of Fluidic Imidazole complex.

8.3 Instrumentation

   Ft-IR characterization,all analyses and characterizations are done using Spectrometer model Nicolet 6700/Smart FTTR at Nano QAM, Montreal Canada,and Attenuated Total Reflectance (ATR) which is used a Thermo- Fisher Scientific (diamond plate) as sampler carrier, operated by Omnic software. The absorption spectrum is covered a region between 650 - 4200 cm^{-1}.

Raman spectroscopyis usedto investigate the prepared imidazole, imidazole /Graphene and Imidazole, Imidazole/ Graphene /(Cu, Ag) NPs. Instrument Model: Renishaw, in Via Reflex: This Raman microscope includes an optical microscope (x5, x20 and x50) coupled to a Raman spectrometer with two sources of lasers (532 nm and 785 nm). Optical microscope is usually utilized to enlarge and detect the sample areas, spectrometer diffuses with a resolution of 2 μm.

Electrochemical characterization isone technique used to detect the potential of fluidic solution to be a good conductive .One of that technique is the Cyclic voltammetry (CV) ,which is consist of potentiostat-galvanostat including 8 channels optimized (10V, 4A). Model: Solartron Instruments, 1470/1255B Coupled with the 1255B frequency analyzers. It is characterized by high performance linked with versatile Corrware / Corrviewoperate software makes it easier to implement all of the electrochemical characterization methods. This equipment also allows to measure electrochemical impedances and potentiometric cyclic voltammetry. All analysis has been carried out at Nano QAM center, Montreal.

H^{1}NMR Characterization used for analysis imidazole solution is a Varian 600 MHz NMR spectrometer (Inova) located in Nano QAM Montreal, Canada.

Particle size distribution

All Characterization has been performed using Zetasizer Nano S90 (Malvern) device, modal Nano S90 analyzer at Nano-QAM, Montreal.

ICP coupled analysis is used for chemical analysis allowing to measure entire elements simultaneously inside mixture solution. Instrument is ionization chamber, Model: Agilent Technologies, 5100. It consists in ionizing the sample by injecting it into an argon plasma (temperature around 6000K.

8.4 RESULTS AND DISCUSSIONS

8.4.1 FT-IR spectra characterize

With regard to Figure [8-2] isillustratedthe specific spectrum for imidazole, imidazole/Graphene and their complex mixture (Graphene /Metals nanoparticles suspended in electrolyte and imidazole). Various spectrum had been recorded on figure such as the hydroxyl group (-OH-) absorbed region located at 3650 cm^{-1}. Moreover, two identical peaks which involved

asymmetrical stretching and bending vibrations restricted to C-C, C-O and C-H groups. The imidazole C-H symmetrical bending group was also reported at 2880 cm^{-1}. Methylene CH_2 group is observed at wavenumber of 1470 cm^{-1} ,as well as , C-O function group is manifested at 1360 cm^{-1} and 1284 cm^{-1}.different range of strong and week peak had been recorded at 950 cm$_{-1}$ to 840cm^{-1} ,it is specific for C-H aromatic hydrocarbon. Furthermore a peak for C-N group is appeared at 2180cm^{-1} . On the other hand, two or three sharp bonds arose at 700 – 900 cm^{-1}. These peaks are confirmed that the electrolyte salts halogenated attached with carbon atoms .Also, spectra of imidazole, and its colloidal are show in Figure[8-2]. There are many sharp: spectra at 475 cm^1 could be assigned to various Metals Element. Another peaks spectrum around at 2940 and 2839 cm^{-1} connected to the stretching of C–H and Aromatic –H bond back to structure imidazole. As wall as a strong sharp band appear at 1630 cm^{1}was allocated to the C=N bond fingerprint for imidazole compound. (Imidazolium ring) is observed spectra at 1631 cm^{-1}. Which agree with pervious literature.[428]
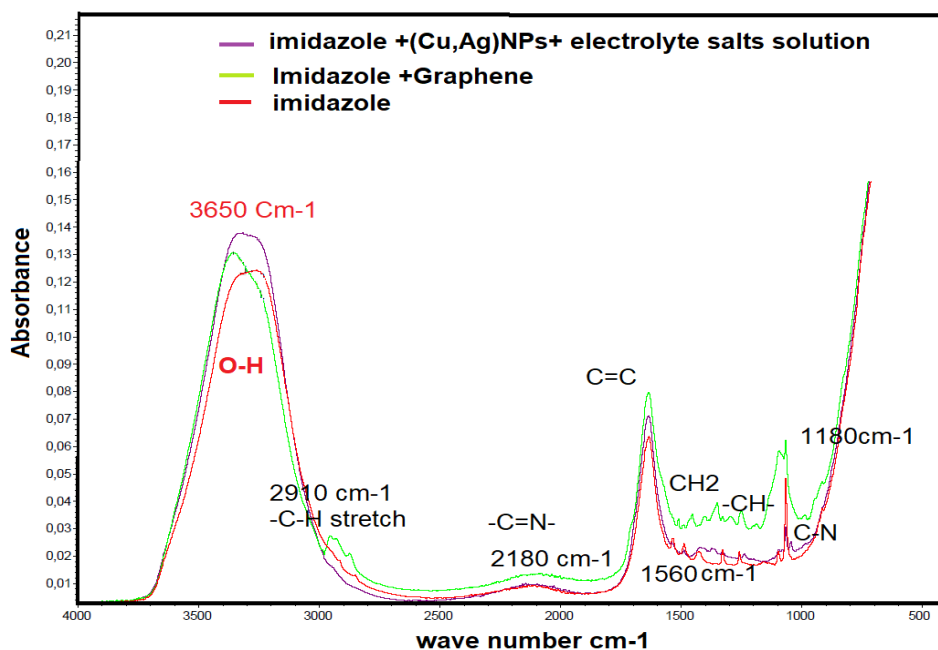
Figure 8-2 : Ft-IR spectra of different Fluidic Imidazole solutions

8.4.2 Raman spectroscopy analysis.

Figure [8-3] is explained the transmission spectrum intensity for imidazole samples related wave length. There are several a wide bands peaks of scattered light have been appeared on the spectra for different material compositions, specific at 1580 cm^{-1} that indicted for carbon skeleton of Graphene structure. Furthermore another broad peak located at 2710 cm^{-1}, and 2700 cm^{-1} correspond to the 2D band of Graphene, addition to report several peaks are not as intense and broad. On the other hand , existence of transmission intensity peaks inertly O-H at 3150 cm^{-1} .The intensity of some pecks is week and broad ,it might be effect of assembling Nano particles(Cu, and Ag) in side solution , it formed metallic bonds as well as hydrogen bonds.
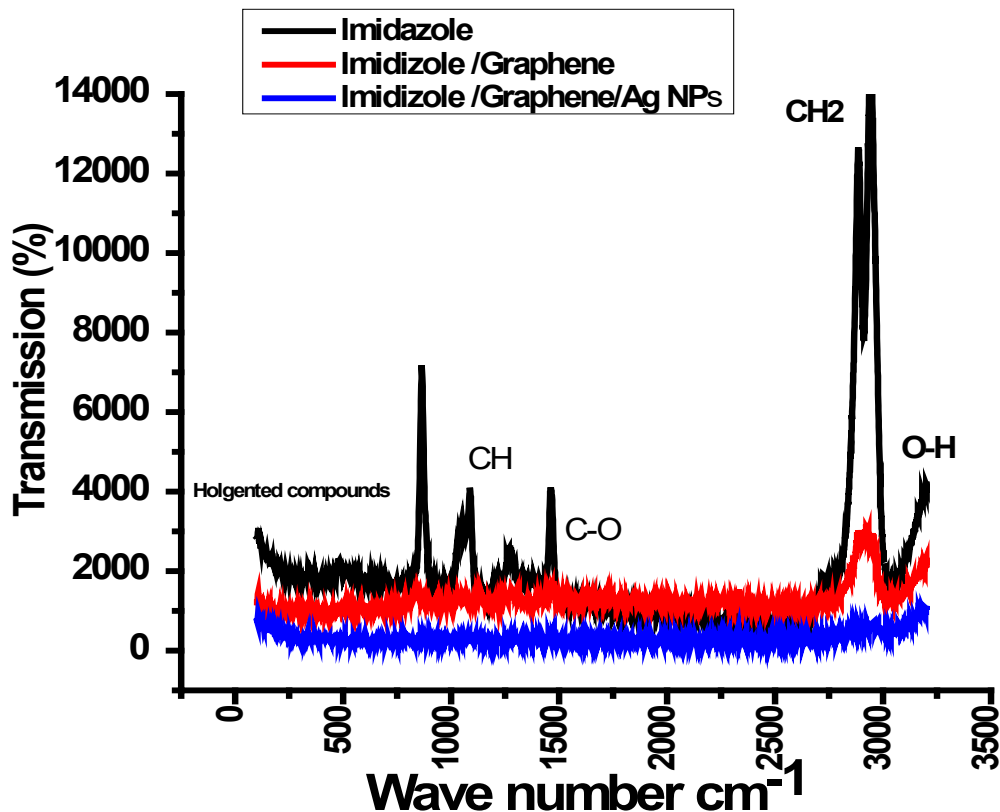
Figure 8-3: Raman spectroscopy of different fluidic imidazole solutions

In order to conduct that **voltammetry cyclic (CV)** measurement**.** We should use three electrode electrochemical framework, involving carbon as a working electrode, Ag/AgCl reference electrode, and a platinum counter electrode. Different scanning rates (10 to 100 mV/s) were carried out during process. Cyclic voltammograms diagram infigure [8-4] is display different redox electrochemical reaction for different specious related to change the current version with applied potential. Regarding to figure[7-4] ,There are several series electrochemical such as oxidizing and reduction inside the mixture of (imidazole , graphene and electrolyte salts) , due to oxidizing of Cu^{+2} to Cu^0 and reduction of Ag^0 to Ag in graphene bridge. Also , we noticed different E (potentials difference) -0.24,-0.47 ,0.44 ,and 1.24V in solution contain graphene and (Ag,and Cu) NPs in imidazole as shown as figure [8-4] . Several electrochemical reaction (Oxidizing and Reduction) take placed inside solution. It leads to created many active sites in graphene surface between Metal (M-M) an M-π Graphene. Also, it

point out there are various ions transfer between reactants, change of energy and eventually it describe the potential ionic conductivity of fluidic Imidazole.[429]
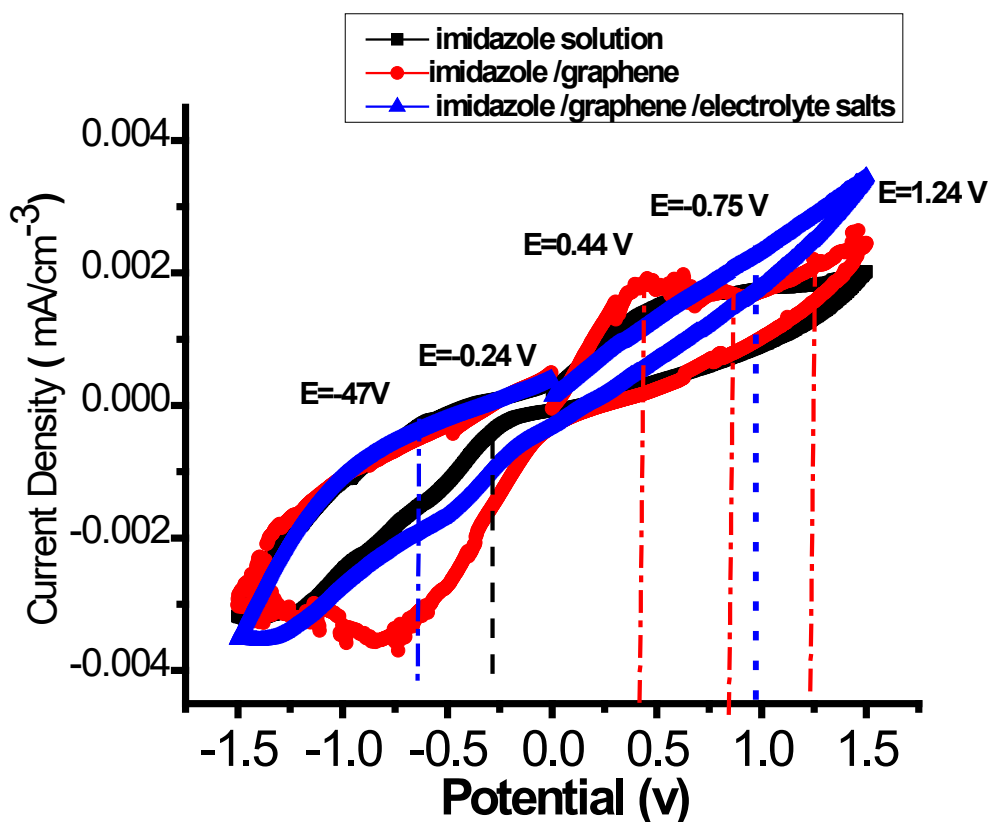
Figure 8-4: Cyclic voltammetry (CV) of a) imidazole solutions, b) Imidazole/Graphene

,c) Imidazole/Graphene/electrolyte, and Metals NPs

8.4.3 Impedance (EIS) Measurement

EIS characterize is another electrochemical technique has been used to detect the conductivity of imidazole solution. More over The impedance (EIS) results is one way to describe physicochemical properties of our prepared solution such as ion conductivity, ions and charge

transfer and electro chemicals reaction. As well as Masstransfer, and kineticsenergy varied with frequencies ranges. The instrument is composed of Novapotentiostast software, which is providedus electrochemical impedance measurements at open cyclic volt (OCV) and CVs. In this experiment, we reached to record the ionic conductivity of series different solution (imidazole/graphene ,Graphene /(Cu, Ag)NPs, and Imidazole /(Ag, Cu)NPs/Graphene) at applied frequencies from 3 MHz to 1 KHz and fixed at open circuit potential (OCV) = 0.42 V . We used three electrode setup (working, reference and counter electrodes) to do the characterization. The ionic conductivity of solutions (σ) were calculated according to the equation above where (Ω) is the real impedance electrolyte, L (cm) is the thickness of the working electrode, and S (cm^2) is the electroactive surface area of the electrode according to Equation.

$$\sigma = \frac{L}{R \times S}$$

(8-1)

Nyquist plots in figure [7-5] is delineated of the different prepared solutions .it represented the impedance plot (imidazole/graphene ,Graphene /(Cu, Ag)NPs, and Imidazole /(Ag, Cu)NPs/Graphene) measured at ambient temperature. With regard to figure [7-5], we noticed the ionic conductivity of solution is increased as Graphene/ (Cu, Ag)NPs>>Imidazole/ (Ag, Cu) NPs/Graphene >>imidazole/graphene. According to real resistance (Z') values 49Ω,100Ω, and 148Ω. By studying the individual curve for each prepped solution .incase mixture imidazole /NPs/Graphene, ionic conductivity is increase with the increase of the imidazole / graphene with metals nanoparticles (Ag, Cu). It could be related to the increase in the density of mobile charge carriers in solution. that due to two reason ,conjugation π-π bond (resonance) graphene particles and imidazole ,addition to redox of graphene to graphene oxide and imidazole has become has a pair free electron in solution .In case imidazole /Graphene solution ,although graphene is good conductor materials ,but a tiny viscosity of imidazole solution has a negative effect on mobility ions ,thus it coated the graphene particles with viscous outer shall, minimize inter-inter action force between particles ,eventually it leads to cause resistance of solution .
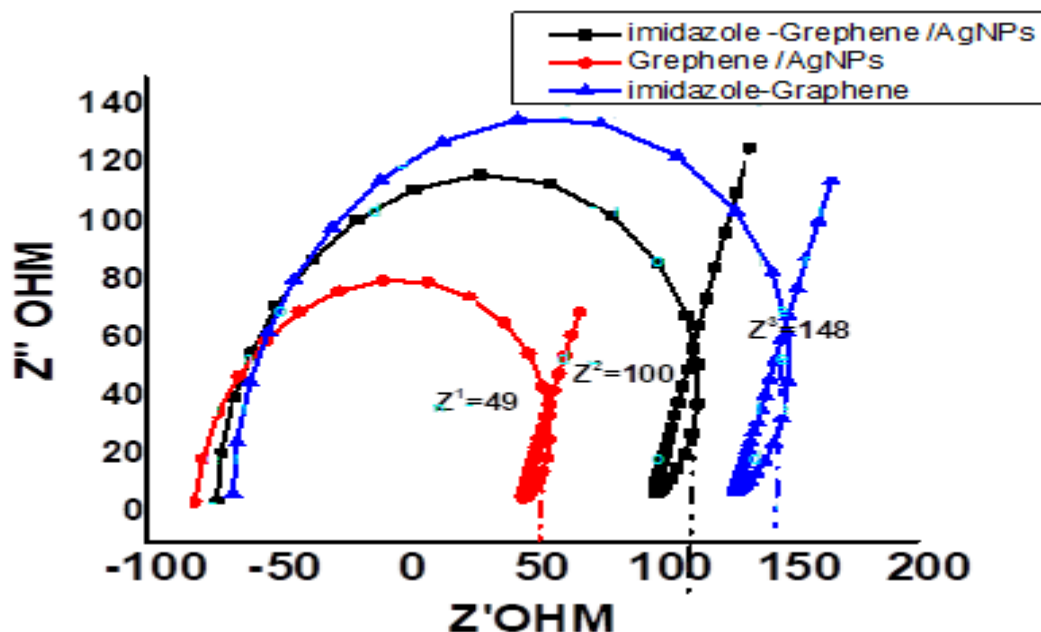
Figure 8-5 : impedance of Imidazole/Graphene /Ag NPs, Graphene /Ag NPs,

andImidazole/Graphene

8.4.4 H1 NMR Characterization.

With regarding to Figure [7-6] pointed out the H^1NMR characterize of serious solution composed from imidazole, imidazole /graphene and solution of imidazole/graphene /electrolyte salts using NMR spectrometer.The spectrum of the pure imidazole Figure[8-6] demonstrate a strong aliphatic and aromatic peaks ,addition to N–H resonance which is recorded at a high Frequency. Imidazole sharp peaks is reported at 7.49, 7.36, 4.82, and 5.25 ppm respectively. On the other side. Resonating peak has been observed at heterocycle region at higher frequency .it is finger print for imidazole cyclic ring. The importance of nitrogen atom in imidazole structure is contained a pair of electron, whichis ascribe "mobile motion " protons, whose dipolar- dipolar interactions were remarkably by the molecular motion lesson. As far N–H resonance behavior was orderly with proton transfer, withan intensity of the aromatic resonances indicated be reduced.

^{1}H NMR spectroscopy is also, one of the best instrument   allow us to go into directly the protons charge as the main responsible for ionic conductivity in that colloid solution. For imidazole heterocyclic compound, anisotropic conductivity has been adduced and assigned   to H-bonding direction in the crystalline material Throughout NMR spectra, we got excellent evidence based on sensitivity and high resolution, due to ^{1}H chemical shift is responsible for an indicative individual protons, especially in presence hydrogen bonds in structure . ^{1}H NMR chemical shifts is used to detected and be more sensitive to H-bonding and aromatic ring in the current effects, that analysis is built up on previously literature

Although Graphene is enhance the conductivity of solution ,due to rich electron clouds (π-π) but the viscosity of imidazole solution or imidazole content has a negative effect on the proton transfer inside solution that is also appear in figure [7-7]There is high peaks appear at 5 ppm it described Graphene structure in imidazole solution . Regarding Figure[8] is demonstrated   the assembling of nanoparticles metals (Sliver, and Copper) inside imidazole solution. Different peaks were appeared at different concentration 7.81, 7.17, 4.83, 369, 340, 2.77, and 1.22 ppm. That is lead to the local mobility of the grafted Copper and silver Metals in imidazole solution was highly promoted a protonated imidazole rings, forming N–H$^+$ charged groups.[430]

The proton transport rate between N–H$^+$ and –Ag or   redox among N–H+ groups and Cu^{+2} Furthermore ,it leads to protonic solution carrying ionic charger .On the other hand, figure [8-9] is illustrate the chemicals shift of HNMR for conductive mixture formed from imidazole, electrolyte solution and (Copper ,Silver) nanoparticles   .We noticed slightly shifted for some peaks in structure appear at 3.69,3.48,3.16,2.27,and 1.22 ppm . It is good evidence to assembling of Nano metals on graphene inside imidazole mixture, furthermore created new activate sites on structure, it makes it anionic solution enrich cloud charge.
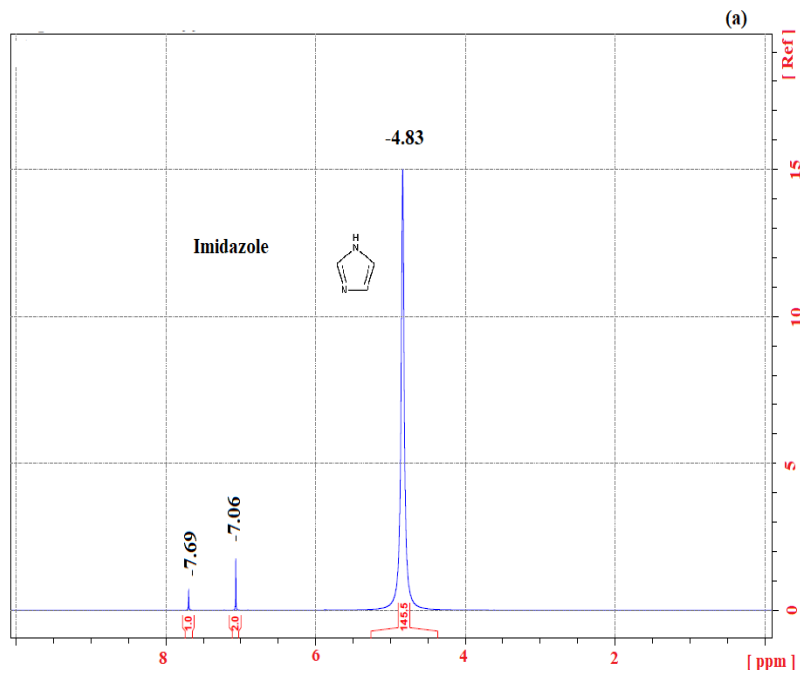
Figure 8-6: ^{1}**HNMR a) imidazole**
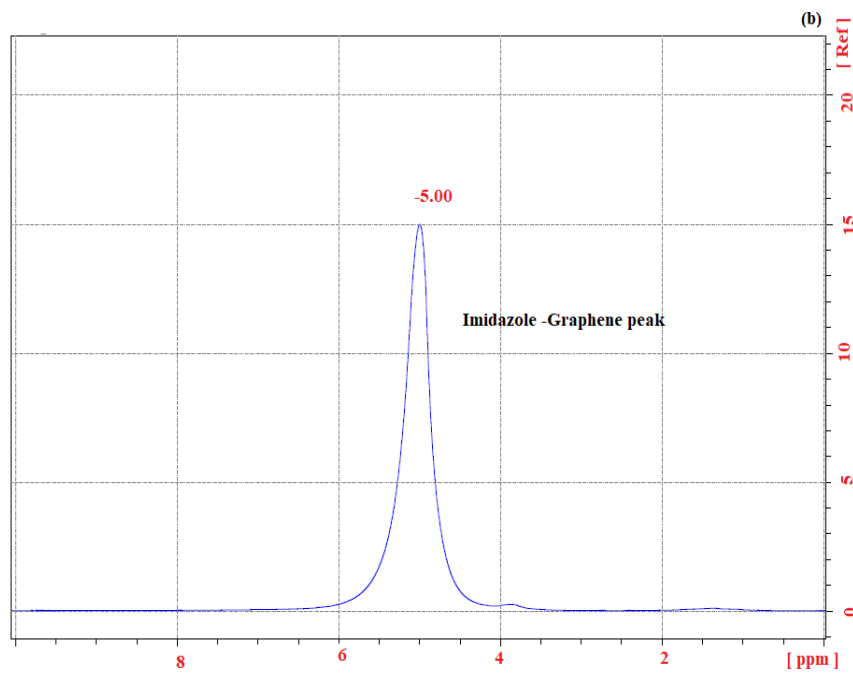
Figure 8-7: ^{1}HNMR b) Imidazole /Graphene Solution
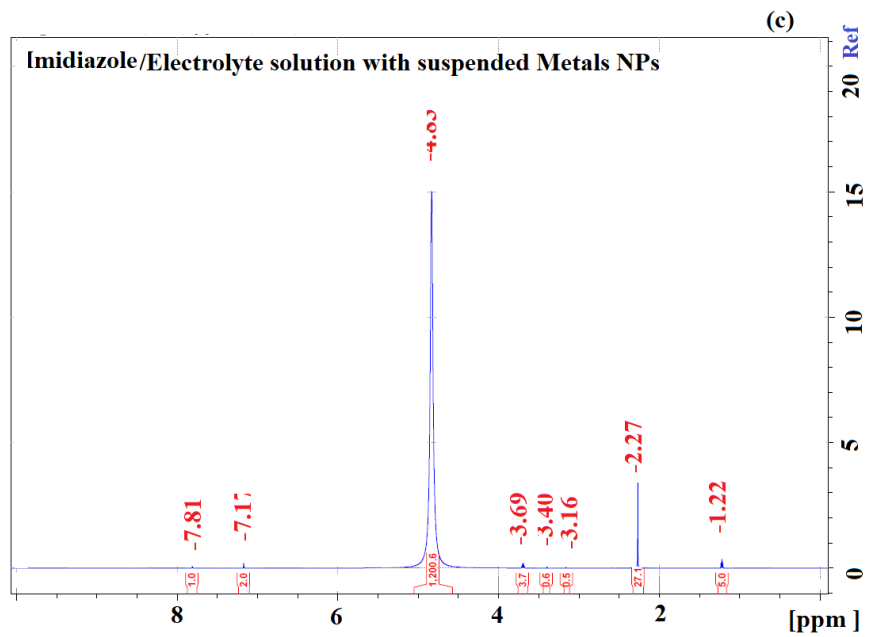
Figure 8-8: ^{1}HNMR solution contain Imidazole /Metals (Ag,Cu) NPs and Electrolyte
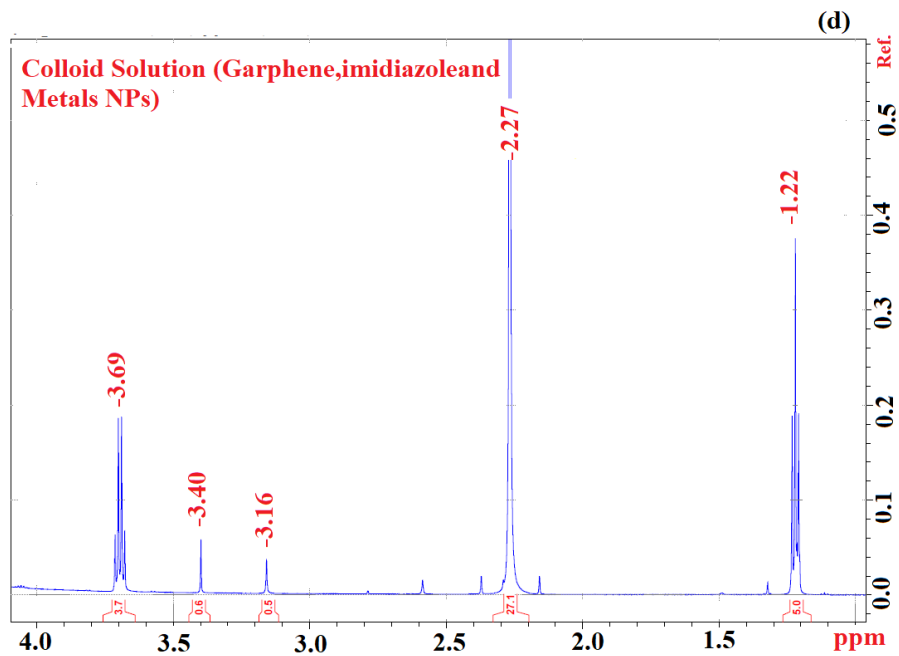
solution

Figure 8-9 : ^{1}HNMR Colloid solution (Graphene , Imidazole and suspended Metals

NPs)

8.4.4 particle size Analyzer
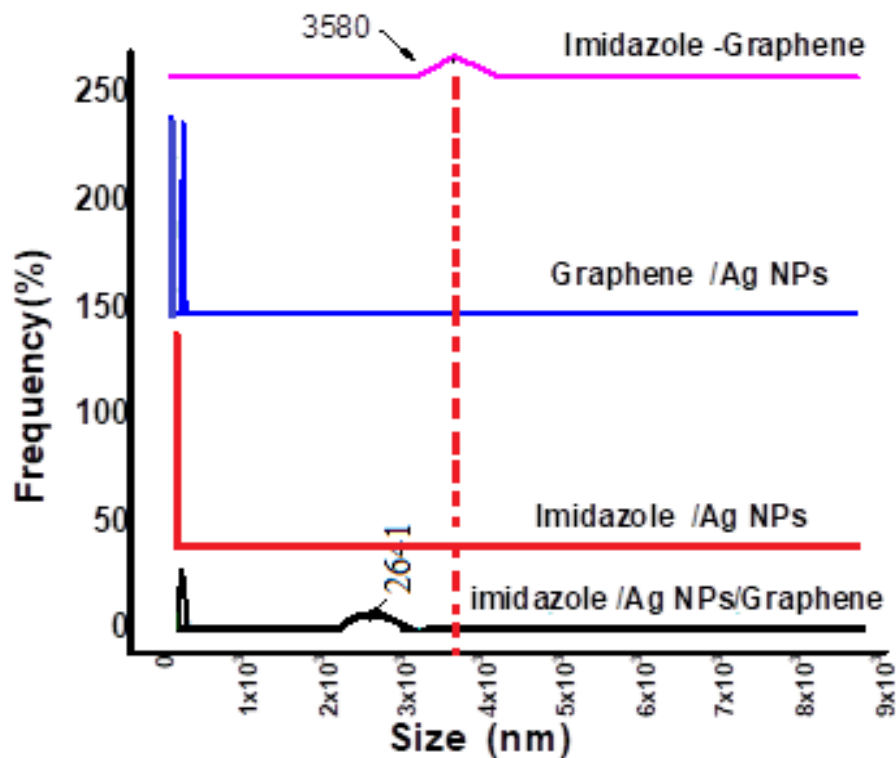
Figure 8-10: particle size analyzer of Fluidicprepared solution

Regard to Figure [8-10] is describethe particle size analyzer of prepared solution Imidazole /Graphene, Graphene Ag nanoparticles solution, imidazole /Ag, and theirmixture. The technique is used to measure and justify the suspended particle size in fluidic solution. It is associated with Red laser (632.8nm, 4 mW), and operateda Zetasizer instrument at 90 deg receptor angle, to make it easier the detection of particles around 1nm to 10 microns diameter. It is consider an important way to describe a physical properties of different prepared solution, throughout a charge transfer movement ,carrying charge ,depletion particle charge movement ,and flocculated particles.Moreover , Particle size analyzer is used also to characterize particles distribution inside colloid phase based on movement particle stability of solution (inter-interaction) or intra –interaction molecules (van der Waals force) .Graphene /imidazole in figure [8-10] ,the particles size is counted 3580 nm ,it is relative bigger comparing to nanoparticles metals (sliver ,and copper) /imidazole solution 103 nm . In other hand , we noticed the volume of particles is increased to 285 nm in(Ag, Cu) nanoparticles /Graphene solution in the same figure .It might be assembled of metals nanoparticles on surface of

148

graphene Referring figure [8-10] particles size is moderated, it recorded 2601 nm , that is indicator for coating of graphene/Metals NPs with imidazole shell , it might be effect on the motion of charge transfer inside solution, but the coordination bonds like metallic, and hydrogen bonds neutralized that effect .there are forming of some aggregated crystals inside solution caused by flocculated graphene and viscus rheology and shear rate   of imidazole organic composition ,then lead to change the size of suspended particles[431] .
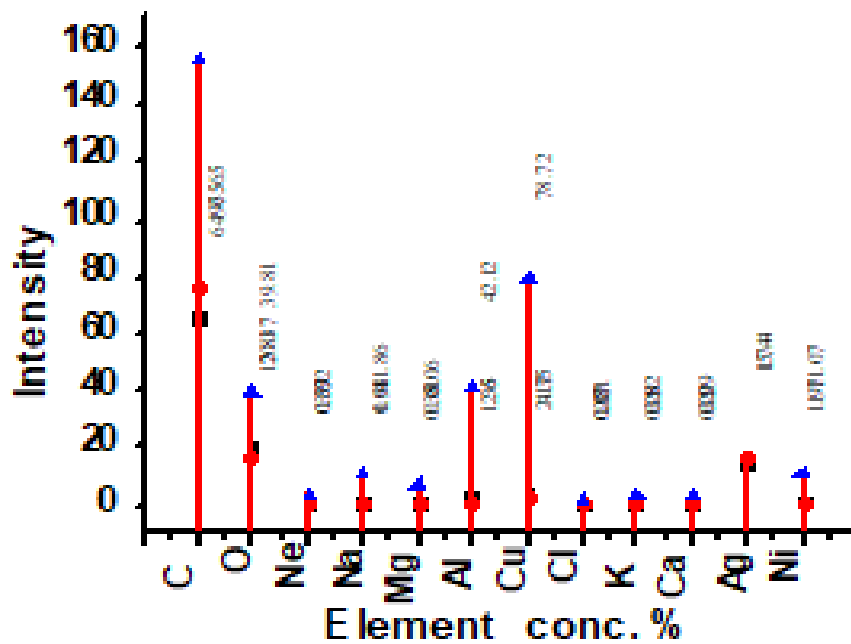
Figure 8-11: ICP for compositional analysis of the plain electrolyte solution.

8.4.4 ICP Coupled analysis

The plasma characterization is a physical method used for chemical analysis allowing to measure entire elements simultaneously insidesample. All Sampleswas prepared by dissolving in an acid (wet mineralization HNO_3, conc. 2-5 %)to be analyzed. Samples are injected into the plasma, then generated by a pneumatic device (nebulizer). All samples characterization is performed at Nano-QAM, Montreal. Canada.

With regard to Figure [8-11] isdemonstrated the main content of prepared samples at different concentrationmixture ,which is composed from suspended metals like Ag ,and Cu addition to

Al, and Na which are the main contain of electrolyte salts solution . Carbon peak intensity is recorded high value, it due to Graphene structure, and carbon skeleton of heterocyclic aromatic (Imidazole).

8.5 CONCLUSION

The main objective of that work, to obtain a Fluidic conductive solution to be used inside fluid antenna chip.We reached to improve the conductivity of imidazole from (>1 × 10^{-5} S cm^{-1} to 1.2 × 10^{-4} S·cm^{-1}) by using different additives (Graphene/electrolyte salt, and (Ag,Cu) NPs. The improvement of ionic conduction of imidazole is illustrated and evaluated using electrochemical impedance spectroscopy measurements, which is analytical technique to affirm the improvement of conductivity. Further, using electrochemical cycle voltammetry analysis to investigate the different electrochemical reaction inside liquid complex. Particle size analyzer is also confirmed imidazole mixture is compatible andhomogeneous withoutany particle deposition, aggregation as well, reforming Hydrogenbond (O–H....O and N–H... O) Between the imidazole molecules and others additives (Graphene and metals ions nanoparticles) in the solution which is based on, molecular rearrangements and surface energy variation. One of the main importance of hydrogen bonds thatis responsible for just enrich . It due to Nemours of reversible reaction and ions transfer (loses and gain) insidemixture. All in all, we got unique conductive solution non-toxic, biodegradable, could be used as a fluidic antennadevice.

150

GENERAL CONCLUSION

Finding a communication method similar to Intel for use in the mining industry specifically or in health and pharmacy in general is the major objective of this research.Due to their unique manufacturing requirements and the way these elements interact, these materials' features call for creativity in both development and manufacturing. Numerous flexible materials were created through research and analysis that function to receive or receive the signal at 2.4 KHz.In addition to using high-conductivity solutions, coarse solutions are also employed, and their properties are enhanced by the addition of non-metric materials including graphene, copper, and silver. Inside a specific variety of PDMS polymer are conductivity fuses. to perform the role of a microchannel fluidic antenna In order to end our investigation, this work includes more than 7 chapters that illustrate, analyze, discuss, and apply the findings.

We research the mechanisms underlying the reactions of conductive materials. One such substance is graphene, which exhibits dual characteristics and occasionally serves as an electron transfer catalyst in petrochemical reactions (oxidation and reduction). Ionic charge inside of a solution could be enhanced by an additional electron at work. In addition, we used a variety of produced nanometals with their application method and behavior being studied, such as titanium oxide and gallium indium. These metals affect the final product's physical and chemical qualities. In addition, we work with eco-materials like clay (bentonite) and embed it with nano metals, as well as research the chemical make-up of clay and its capacity to enrich the ionic charge in the mixture. Numerous experiments had been carried out to investigate the various properties of novel composite antennas, including mechanical shear stress, youngs moduli, and flexiblity, in addition to electrochemical properties like EIS (electrochemical impedance spectroscopy), cycle voulimeric, and additional pyhical properties like surface morphology, (TEM), (SCN), and EDAX, as well as micrfluid channel durability.Additionally, certain studies and experiments on the thermal characteristics of innovative fabrications, such as TGA and DSC, have been conducted.

Overall, we performed simulations and measurements using their calculations (return loss, gain, and directivity) for fluidic and composite chip microstrips, and the outcomes are excellent.

APPINDIX

➢ *Abdelrahman, A., Erchiqui, F., & Nedil, M. (2022). Fabricated wearable and flexible chip composed strain of gallium and silver metals composites assembled on graphene inside PDMS matrix. Journal of the Indian Chemical Society, 100345.https://doi.org/10.1016/j.jics.2022.100345*

➢ *Abdelrahman, A., Erchiqui, F., & Nedil, M. (2021). Preparation and Evaluation of Conductive Polymeric Composite from Metals Alloys and Graphene to Be Future Flexible Antenna Device. Advances in Materials Science, 21(4), 34-52.DOI: 10.2478/adms-2021-0023*

➢ *Fabricated and characterized a conductive polymeric composite constituted from Nano Metals Graphene assembled in polymeric Matrix J. Mater. Environ. Sci., 2021, Volume 12, Issue 11, Page 1472-1490*

➢ Abdelrahman, A., Erchiqui, F., Nedil, M., & Mohamed, S. (2022). In situ-preparation and estimation of the physical characterization of Nanofluidic solution and its application. *Proceedings of the Institution of Mechanical Engineers, Part N: Journal of Nanomaterials, Nanoengineering and Nanosystems*, 23977914221127527.

➢ Abdelrahman, A., Erchiqui, F., & Nedil, M. (2022). Studying and evaluation physical characteristic of composite substrate chip and, its application. *Results in Engineering*, *15*, 100533.

➢ Abdelrahman, A., Erchiqui, F., & Nedil, M. (2022). Improvement Physical Features Composite Comprise of Strain Nano-metals (Ag, Mn) Assembled on Graphene Suspended Inside PEG Matrix and Its Application. *Moroccan Journal of Chemistry*, *10*(3).

➢ Abdelrahman, A., Erchiqui, F., & Mourad, N. (2022). Enhancement the conductivity and flexibility of fabricated chip comprise from nano graphene metals assembled on polymeric PEI-PDMS matrix. *Engineering Solid Mechanics*, *10*(3), 215-226.

➢ Abdelrahman, A., Erchiqui, F., & Nedil, M. (2021). Preparation and evaluation of conductive polymeric composite from metals alloys and graphene to be future flexible antenna device. *Advances in Materials Science*, *21*(4), 34-52.

REFERENCES

1. Akyildiz, I. F., & Stuntebeck, E. P. (2006). Wireless underground sensor networks: Research challenges. Ad Hoc Networks, 4(6), 669-686.

2. Awolusi, I., Marks, E., & Hallowell, M. (2018). Wearable technology for personalized construction safety monitoring and trending: Review of applicable devices. Automation in construction, 85, 96-106.

3. Baggio, A., & Langendoen, K. (2008). Monte Carlo localization for mobile wireless sensor networks. Ad hoc networks, 6(5), 718-733.

4. Bhattacharjee, S., Roy, P., Ghosh, S., Misra, S., & Obaidat, M. S. (2012). Wireless sensor network-based fire detection, alarming, monitoring and prevention system for Bord-and-Pillar coal mines. Journal of Systems and Software, 85(3), 571-581.

5. Butlewski, M., Dahlke, G., Drzewiecka, M., & Pacholski, L. (2015). Fatigue of miners as a key factor in the work safety system. Procedia Manufacturing, 3, 4732-4739.

6. Chehri, A., Fortier, P., & Tardif, P. M. (2009). UWB-based sensor networks for localization in mining environments. Ad Hoc Networks, 7(5), 987-1000.

7. Chen, S., Xu, K., Zheng, X., Li, J., Fan, B., Yao, X., & Li, Z. (2020). Linear and nonlinear analyses of normal and fatigue heart rate variability signals for miners in high-altitude and cold areas. Computer Methods and Programs in Biomedicine, 196, 105667.

8. Chen, K., Wang, C., Chen, L., Niu, X., Zhang, Y., & Wan, J. (2020). Smart safety early warning system of coal mine production based on WSNs. Safety science, 124, 104609.

9. Cicioğlu, M., & Çalhan, A. (2019). Performance analysis of IEEE 802.15. 6 for underground disaster cases. Computer Standards & Interfaces, 66, 103364.

10. Golizadeh, H., Hon, C. K., Drogemuller, R., & Hosseini, M. R. (2018). Digital engineering potential in addressing causes of construction accidents. Automation in Construction, 95, 284-295.

11. Gyekye, S. A. (2003). Causal attributions of Ghanaian industrial workers for accident occurrence: Miners and non-miners perspective. Journal of Safety Research, 34(5), 533-538.

12. Hongqing, Z., Zeyang, S., Meiqun, Y., Zheng, L., & Jian, L. (2011). Theory study on nonlinear control of ventilation network airflow of mine. Procedia Engineering, 26, 615-622.

13. Keitel, A., Ringleb, M., Schwartges, I., Weik, U., Picker, O., Stockhorst, U., & Deinzer, R. (2011). Endocrine and psychological stress responses in a simulated emergency situation. Psychoneuroendocrinology, 36(1), 98-108.

14. Kennedy, G. A., & Bedford, M. D. (2014). Underground wireless networking: A performance evaluation of communication standards for tunnelling and mining. Tunnelling and underground space technology, 43, 157-170.

15. Kumari, S., & Om, H. (2016). Authentication protocol for wireless sensor networks applications like safety monitoring in coal mines. Computer Networks, 104, 137-154.

16. Li, J., Yang, L., Song, T., & Qi, R. (2019). Research on the effects of the high temperature and humidity environment on human comfort in coal mine emergency refuge system. Safety, 5(2), 28.

17. Li, C. T., Cheng, J. C., & Chen, K. (2020). Top 10 technologies for indoor positioning on construction sites. Automation in Construction, 118, 103309.

18. Li, Y., & Guldenmund, F. W. (2018). Safety management systems: A broad overview of the literature. Safety science, 103, 94-123.

19. Lu, X., & Davis, S. (2016). How sounds influence user safety decisions in a virtual construction simulator. Safety Science, 86, 184-194.

20. Mahdevari, S., Shahriar, K., & Esfahanipour, A. (2014). Human health and safety risks management in underground coal mines using fuzzy TOPSIS. Science of the Total Environment, 488, 85-99.

21. Milenković, A., Otto, C., & Jovanov, E. (2006). Wireless sensor networks for personal health monitoring: Issues and an implementation. Computer communications, 29(13-14), 2521-2533.

22. Moridi, M. A., Kawamura, Y., Sharifzadeh, M., Chanda, E. K., & Jang, H. (2014). An investigation of underground monitoring and communication system based on radio waves attenuation using ZigBee. Tunnelling and Underground Space Technology, 43, 362-369.

23. Adjiski, V., Despodov, Z., Mirakovski, D., & Serafimovski, D. (2019). System architecture to bring smart personal protective equipment wearables and sensors to transform safety at work in the underground mining industry. Rudarsko-geološko-naftni zbornik, 34(1), 37-44.

24. Ahn, C. R., Lee, S., Sun, C., Jebelli, H., Yang, K., & Choi, B. (2019). Wearable sensing technology applications in construction safety and health. Journal of Construction Engineering and Management, 145(11), 03119007.

25. Alam, A. A., Eyers, D., & Huang, Z. (2015, February). Helping secure robots in WSN environments by monitoring WSN software updates for intrusions. In 2015 6th International Conference on Automation, Robotics and Applications (ICARA) (pp. 223-229). IEEE.

26. Bauerle, T., Dugdale, Z., & Poplin, G. (2018). Mineworker fatigue: a review of what we know and future decisions. Mining engineering, 70(3), 33.

27. Antwi-Afari, M. F., Li, H., Wong, J. K. W., Oladinrin, O. T., Ge, J. X., Seo, J., & Wong, A. Y. L. (2019). Sensing and warning-based technology applications to improve occupational health and safety in the construction industry: A literature review. Engineering, Construction and Architectural Management, 26(8), 1534-1552.

28. Baek, J., Choi, Y., Lee, C., Suh, J., & Lee, S. (2017). BBUNS: Bluetooth beacon-based underground navigation system to support mine haulage operations. Minerals, 7(11), 228.

29. Bandyopadhyay, L. K., Chaulya, S. K., Mishra, P. K., Bandyopadhyay, L. K., Chaulya, S. K., & Mishra, P. K. (2010). Wireless information and safety system for mines. Wireless Communication in Underground Mines: RFID-Based Sensor Networking, 175-262.

30. Bandyopadhyay, L. K., Mishra, P. K., Kumar, S., Selvendran, D., & Chaulya, S. K. (2007). Studies on radio frequency propagation characteristics for underground coalmine communications.

31. Basu, S., Pramanik, S., Dey, S., Panigrahi, G., & Jana, D. K. (2019). Fire monitoring in coal mines using wireless underground sensor network and interval type-2 fuzzy logic controller. International Journal of Coal Science & Technology, 6, 274-285.

32. Blondeel, M., & Van de Graaf, T. (2018). Toward a global coal mining moratorium? A comparative analysis of coal mining policies in the USA, China, India and Australia. Climatic Change, 150(1-2), 89-101.

33. Bedford, M. D., Kennedy, G. A., & Foster, P. J. (2017). Radio transmission characteristics in tunnel environments. Mining Technology, 126(2), 77-87.

34. S. Nemat-Nasser, S. Nemat-Nasser, T. Plaisted, A. Starr, and A.V. Amirkhizi. Biomimetics:Biologically Inspired Technologies. CRC Press, 2005.

35. K.K. Wang, Y.L. Kang, P.G. Song, F. Xu, and X.H. Li. Preparation of sicp/a356 electronicpackagaing materials and its thixo-forging. Transactions of Nonferrous Metals Society of China, 20:s988–s992, 2010.

36. S.V. Nair, J.K. Tien, and R.C. Bates. Sic-reinforced aluminum metal matrix composites.International Metals Reviews, 30:275–290, 1985.

37. D. Cree and M. Pugh. Production and characterization of a three-dimensional cellularmetal-filled ceramic composite. Journal of Materials Processing Technology, 210:1905–1917,2010.

38. M.E. Smagorinski, P.G. Tsantrizos, S. Grenier, A. Cavasin, T. Brzezinski, and G. Kim. The properties and microstructure of al-based composites reinforced with ceramic particles. Material Science and Engineering, A244:86–90, 1998

39. K. Yoshida andH.Morigami. Thermal properties of diamond/copper compositematerial.Microelectronics Reliability, 44:303–308, 2004

40. J.A. Kerns, N.J. Colella, D.Makowiecki, and H.L. Davidson. Dymalloy: A composite substrate for high power density electronic components. Proceedings for SPIE - The International Society for Optical Engineering, pages 66–71, 1995.

41. H.L. Davidson, N.J. Colella, J.A. Kerns, and K. Makowiecki. Copper-diamond composite substrates for electronic components. Proceedings of 45th Electronic Components and Technology Conference, pages 538–541, 1995

42. W.B. Johnson and B. Sonuparlak. Diamond/al metal matrix composites formed by the pressureless metal infiltration process. Journal of Materials Research, 8:1169–1173, 1993

43. F.A. Khalid, O. Beffort, and U.E. Klotz. Microstructure and interfacial characteristics of aluminum-diamond compositematerials. Diamond and RelatedMaterials, 13:393–400, 2004

44. C. Zweben. Advanced composites and other advancedmaterials for electronic packaging thermal management. Proceedings of 2001 International Symposium on Advanced Packaging Materials, pages 360–365, 2001.

45. P. Yih and D.D.L. Chung. Copper-matrix molybdenum particle composites made from copper coated molybdenum powder. Journal of Electronic Materials, 24:841–851, 1995.

46. Y.M. Chen and J.M. Ting. Ultra high thermal conductivity polymer composites. Carbon,40:359–362, 2002.

47. G. Kalaprasad, P. Pradeep,G.Mathew, C. Pavithran, and S. Thomas. Thermal conductivityand thermal diffusivity analyses of low-density polyethylene composites reinforced with sisal, glass and intimately mixed sisal/glass fibres. Composites Science and Technology, 60:2967–2977, 2000.

48. J.M. Keith, J.A. King, M.G. Miller, and A.M. Tomson. Thermal conductivity of carbon fiber/liquid crystal polymer composite. Journal of Applied Polymer Science, 102:5456–5462,2006.

49. W.M. Alvino. Plastics for Electronics. McGraw-Hill, Inc., New York, New York, 1995

50. Y. Xu, D.D.L. Chung, and C. Mroz. Thermally conducting aluminum nitride polymermatrixcomposites. Composites: Part A, 32:1749–1757, 2001.

51. W.D. Callister Jr. Fundamentals ofMaterials Science and Engineering: An Integrated Approach.JohnWiley & Sons, Inc., Hoboken, NJ, second edition, 2005.

52. H. Ishida and S. Rimdusit. Very high thermal conductivity obtained by boron nitride-filledpolybenzoxazine. Thermochimica Acta, 320:177–186, 1998.

53. S.L. Shinde and J. Goela. High Thermal Conductivity Materials. Springer, 2006.

54. Y.M. Chiang, D.P. Birnie III, and D. Kingery. Physical Ceramics: principles for ceramic science and engineering. J.Wiley, New York, 1997.

55. K.Watari and S.L. Shinde. High thermal conductivitymaterials. Materials Research Society Bulletin, 26:440–444, 2001.

56. H. He, R. Fu, Y. Han, Y. Shen, and D.Wang. High thermal conductive si3n4 particle filler epoxy composites with a novel structure. Journal of Electronic Packaging, 129(49):469–472, 2007.

57. S.R. Kim, D.H. Kim, D.J. Kim, M.H. Kim, and J.M. Park. Study on thermal conductivity of polyetheretherketone/thermally conductive filler composites. solid State Phenomena, 124–126:1097–1082, 2007.

58. W.Y. Zhou, S.H. Qi, H.Z. Zhao, and N.L. Liu. Thermally conductive silicone rubber reinforced with boron nitride particle. Polymer Composites, 282:23–28, 2007.

59. A.R. Blythe. Electrical resistivity measurements of polymer materials. Polymer Testing,4:195–209, 1984.

60. H.G. Cho, U.Y. Lee, S.H. Kang, K.J. Lim, and I.H. Choi. Electrical property of polymer insulatorwith end-fitting design. Proceedings for IEEE International Symposium on Electrical Insulation, pages 296–299, 2004.

61. V. J. Lumelsky, M. S. Shur, and S. Wagner, "Sensitive skin," IEEE Sensors Journal, vol. 1, pp. 41-51, 2001.

62. G. H. Gelinck, H. E. A. Huitema, E. van Veenendaal, E. Cantatore, L. Schrijnemakers, J. B. P. H. van der Putten, et al., "Flexible active-matrix displays and shift registers based on solution-processed organic transistors," Nat Mater, vol. 3, pp. 106-110, 02//print 2004.

63. Akle BJ, Bennett MD, Leo DJ (2006) High-strain ionomeric-ionic liquid electroactive actuators.Sens Actuators A 126:173–181

64. S. Koulouridis, G. Kiziltas, Y. J. Zhou, D. J. Hansford, and J. L. Volakis, "Polymer-Ceramic Composites for Microwave Applications: Fabrication and Performance Assessment," *IEEE T. Microw. Theory,* vol. 54, pp. 4202-4208, Dec 2006.

65. S. p. P. Lacour, D. Chan, S. Wagner, T. Li, and Z. Suo, "Mechanisms of reversible stretchability of thin metal films on elastomeric substrates," *Applied Physics Letters,* vol. 88, p. 204103, 2006.

66. H. Tao, C. Bingham, A. Strikwerda, D. Pilon, D. Shrekenhamer, N. Landy*, et al.*, "Highly flexible wide angle of incidence terahertz metamaterial absorber: Design, fabrication, and characterization," *Physical Review B,* vol. 78, 2008.

67. D.-H. Kim and J. A. Rogers, "Stretchable Electronics: Materials Strategies and Devices," Advanced Materials, vol. 20, pp. 4887-4892, 2008.

68. Iijima, S., Helical microtubules of graphitic carbon. nature, 1991. 354(6348): p. 56-58.

69. Ebbesen, T., et al., Patterns in the bulk growth of carbon nanotubes. Chemical Physics Letters, 1993. 209(1): p. 83-90.

70. Dresselhaus, M., et al., Nanowires and nanotubes. Materials Science and Engineering: C, 2003. 23(1): p. 129-140

71.   A. Kiourti and J. L. Volakis, "Stretchable and flexible E-fiber wire antennas embedded in polymer," IEEE Antennas and Wireless Propagation Letters, vol. 13, pp. 1381-1384,   2014.

72. S. Shahid, M. Rizwan, M. A. B. Abbasi, H. Zahra, S. M. Abbas, and M. A. Tarar, "Textile antenna for body centric WiMAX and WLAN applications," in International Conference on Emerging Technologies (ICET), pp. 1–5, Islamabad, Pakistan, 2012.

73.   A. Rida, Y. Li, R. Vyas, and M. M. Tentzeris, "Conductive inkjet-printed antennas on   flexible low-cost paper-based substrates for RFID and WSN applications," IEEE Antennas and Propagation Magazine, vol. 51, no. 3, pp. 13–23, 2009.

74.   P. V. Nikitin, S. Lam, and K. V. S. Rao, "Low cost silver ink RFID tag antennas," in   IEEE International Symposium on Antennas and Propagation, vol. 2B, pp. 353–356,   Washington, DC, USA, 2005.

75.   S. Morris, A. R. Chandran, N. Timmons, and J. Morrison, "Design and performance of a   flexible and conformai PDMS dipole antenna for WBAN applications," in 46th European   Microwave Conference (EuMC), pp. 84–87, London, UK, 2016.

76.   R. B. V. B. Simorangkir, Y. Yang, L. Matekovits, and K. P. Esselle, "Dual-band dual- mode textile antenna on PDMS substrate for body-centric communications," IEEE Antennas and Wireless Propagation Letters, vol. 16, pp. 677–680, 2017.

77.   W. Zheyu, Z. Lanlin, Y. Bayram, and J. L. Volakis, "Embroidered conductive fibers on   polymer composite for conformal antennas," IEEE Transactions on Antennas and   Propagation, vol. 60, no. 9, pp. 4141–4147, 2012.

78.   Z. Lanlin, W. Zheyu, and J. L. Volakis, "Textile antennas and sensors for body-worn applications," IEEE Antennas and Wireless Propagation Letters, vol. 11, pp. 1690–1693,   2012.

79.   S. Amendola, E. Moradi, K. Koski et al., "Design and optimization of mm-size implantable and wearable on-body antennas for biomedical systems," in 8th European   Conference on Antennas and Propagation (EuCAP), pp. 520–524, The Hague,   Netherlands, 2014.

80.   K. Koski, E. Moradi, A. A. Babar et al., "Durability of embroidered antennas in wireless   body-centric healthcare applications," in 7th European Conference on Antennas and   Propagation (EuCAP), pp. 565–569, Gothenburg, Sweden, 2013.

81.   S. Shuai, A. Kiourti, R. Burkholder, and J. Volakis, "Broadband and flexible textile RFID tags for tires," in IEEE International Symposium on Antennas and Propagation, pp.   1507–1507, Memphis, TN, USA, 2014.

82.   E. Moradi, K. Koski, L. Ukkonen, Y. Rahmat-Samii, T. Bjorninen, and L. Sydanheimo, "Embroidered RFID tags in body-centric communication," in International Workshop on   Antenna Technology (iWAT), pp. 367–370, Karlsruhe, Germany, 2013.

83.   Kaufmann, T.; Verma, A.; Al-Sarawi, S.F.; Truong, V.-T.; Fumeaux, C. Comparison of   two planar elliptical ultra-wideband PPy conductive polymer antennas. In Proceedings of   the 2012 IEEE International Symposium on Antennas and Propagation, Chicago, IL,   USA, 8–14 July 2012; IEEE: Chicago, IL, USA, 2012; pp. 1-2.

84.   Tseghai, G.B.; Mengistie, D.A.; Malengier, B.; Fante, K.A.; Van Langenhove, L. PEDOT:PSS-Based Conductive Textiles and Their Applications. Sensors 2020, 20, 1881.

85.   Ghasemi, A.; Sousa, E.S. Spectrum sensing in cognitive radio networks: Requirements,   challenges and design trade-offs. IEEE Commun. Mag. 2008, 46, 32-39.

86.   Wojkiewicz, J.-L.; Alexander, P.; Bergheul, S.; Belkacem, B.; Lasri, T.; Zahir, H.; Kone,   L. Design fabrication and characterisation of polyaniline and multiwall carbon nanotubes   composites-based patch antenna. IET Microw. Antennas Propag. 2016, 10, 88–93.

87.   Shin, K.-Y.; Cho, S.; Jang, J. Graphene/Polyaniline/Poly(4-styrenesulfonate) Hybrid Film   with Uniform Surface Resistance and Its Flexible Dipole Tag Antenna Application. Small   2013, 9, 3792-3798.

88.   Lee, J.S.; Kim, M.; Oh, J.; Kim, J.; Cho, S.; Jun, J.; Jang, J. Platinum-decorated carbon   nanoparticle/polyaniline hybrid paste for flexible wideband dipole tag-antenna   application. J. Mater. Chem. A 2015, 3, 7029-7035.

89.	Mo, L.; Guo, Z.; Wang, Z.; Yang, L.; Fang, Y.; Xin, Z.; Li, X.; Chen, Y.; Cao, M.; Zhang, Q.; et al. Nano-Silver Ink of High Conductivity and Low Sintering Temperature for Paper Electronics. Nanoscale Res. Lett. 2019, 14, 197.

90.	Ankireddy, K.; Druffel, T.; Vunnam, S.; Filipič, G.; Dharmadasa, R.; Amos, D.A. Seed mediated copper nanoparticle synthesis for fabricating oxidation free interdigitated electrodes using intense pulse light sintering for flexible printed chemical sensors. J. Mater. Chem. C 2017, 5, 11128-11137.

91.	Guerchouche, K.; Herth, E.; Calvet, L.E.; Roland, N.; Loyez, C. Conductive polymer based antenna for wireless green sensors applications. Microelectron. Eng. 2017, 182, 46-52.

92.	Zare, Y.; Rhee, K.Y. Calculation of the Electrical Conductivity of Polymer Nanocomposites Assuming the Interphase Layer Surrounding Carbon Nanotubes. Polymers 2020, 12, 404.

93.	Hamouda, Z.; Wojkiewicz, J.-L.; Pud, A.A.; Kone, L.; Bergheul, S.; Lasri, T. Magnetodielectric Nanocomposite Polymer-Based Dual-Band Flexible Antenna for Wearable Applications. IEEE Trans. Antennas Propag. 2018, 66, 3271–3277.

94.	Ravindran, A.; Feng, C.; Huang, S.; Wang, Y.; Zhao, Z.; Yang, J. Effects of Graphene Nanoplatelet Size and Surface Area on the AC Electrical Conductivity and Dielectric Constant of Epoxy Nanocomposites. Polymers 2018, 10, 477.

95.	Elmobarak Elobaid, H.A.; Abdul Rahim, S.K.; Himdi, M.; Castel, X.; Abedian Kasgari, M. A Transparent and Flexible Polymer-Fabric Tissue UWB Antenna for Future Wireless Networks. Antennas Wirel. Propag. Lett. 2017, 16, 1333–1336.

96.	Scidà, A.; Haque, S.; Treossi, E.; Robinson, A.; Smerzi, S.; Ravesi, S.; Borini, S.; Palermo, V. Application of graphene-based flexible antennas in consumer electronic devices. Mater. Today 2018, 21, 223–230.

97.	Leng, T.; Huang, X.; Chang, K.; Chen, J.; Abdalla, M.A.; Hu, Z. Graphene Nanoflakes Printed Flexible Meandered-Line Dipole Antenna on Paper Substrate for Low-Cost RFID and Sensing Applications. Antennas Wirel. Propag. Lett. 2016, 15, 1565–1568.

98.	Zhou, X.; Leng, T.; Pan, K.; Abdalla, M.A.; Hu, Z. Graphene Printed Flexible and Conformal Array Antenna on Paper Substrate for 5.8 GHz Wireless Communications. In Proceedings of the 2020 14th European Conference on Antennas

and Propagation   (EuCAP), Copenhagen, Denmark, 15–20 March 2020; IEEE: Copenhagen, Denmark,   2020; pp. 1–4.

99.   Shin, K.-Y.; Hong, J.-Y.; Jang, J. Micropatterning of Graphene Sheets by Inkjet Printing   and Its Wideband Dipole-Antenna Application. Adv. Mater. 2011, 23, 2113–2118.

100.   Kopyt, P.; Salski, B.; Olszewska-Placha, M.; Janczak, D.; Sloma, M.; Kurkus, T.;   Jakubowska, M.; Gwarek, W. Graphene-Based Dipole Antenna for a UHF RFID Tag.   IEEE Trans. Antennas Propag. 2016, 64, 2862–2868.

101.   Dang, W.; Vinciguerra, V.; Lorenzelli, L.; Dahiya, R. Printable stretchable interconnects.   Flex. Print. Electron. 2017, 2, 013003.

102.   Song, L.; Myers, A.C.; Adams, J.J.; Zhu, Y. Stretchable and Reversibly Deformable   Radio Frequency Antennas Based on Silver Nanowires. ACS Appl. Mater. Interfaces   2014, 6, 4248–4253.

103.   Aïssa, B.; Nedil, M.; Habib, M.A.; Haddad, E.; Jamroz, W.; Therriault, D.; Coulibaly, Y.;   Rosei, F. Fluidic patch antenna based on liquid metal alloy/single-wall carbon-nanotubes   operating at the S-band frequency. Applied Physics Letters 103 (6), 06310,   http://dx.doi.org/10.1063/1.4817861.

104.   Guo, X.; Huang, Y.; Wu, C.; Mao, L.; Wang, Y.; Xie, Z.; Liu, C.; Zhang, Y. Flexible and   reversibly deformable radio-frequency antenna based on stretchable SWCNTs/PANI/Lycra conductive fabric. Smart Mater. Struct. 2017, 26, 105036.

105.   So, J.-H.; Thelen, J.; Qusba, A.; Hayes, G.J.; Lazzi, G.; Dickey, M.D. Reversibly   Deformable and Mechanically Tunable Fluidic Antennas. Adv. Funct. Mater. 2009, 19,   3632–3637.

106.   Park, M.; Im, J.; Shin, M.; Min, Y.; Park, J.; Cho, H.; Park, S.; Shim, M.-B.; Jeon, S.;   Chung, D.-Y.; et al. Highly stretchable electric circuits from a composite material of   silver nanoparticles and elastomeric fibres. Nat. Nanotech. 2012, 7, 803–809.

107.   Sebastian, M.T.; Jantunen, H.; Ubic, R. (Eds.) Microwave Materials and Applications; John Wiley & Sons: Chichester, UK; Hoboken, NJ, USA, 2017; ISBN 978-1-119-20852-5.

108.   Wong, W.S.; Salleo, A. (Eds.) Flexible Electronics: Materials and Applications; Electronic Materials: Science & Technology; Springer: New York, NY, USA, 2009;   ISBN 978-0-387-74362-2.

109.   Khan, S.; Lorenzelli, L.; Dahiya, R.S. Technologies for Printing Sensors and Electronics   Over Large Flexible Substrates: A Review. IEEE Sens. J. 2015, 15, 3164–3185.

110.   MacDonald, W.A.; Looney, M.K.; MacKerron, D.; Eveson, R.; Adam, R.; Hashimoto,   K.; Rakos, K. Latest advances in substrates for flexible electronics. J. Soc. Inf. Disp.   2007, 15, 1075.

111.   Subbaraman, H.; Pham, D.T.; Xu, X.; Chen, M.Y.; Hosseini, A.; Lu, X.; Chen, R.T.   Inkjet-Printed Two-Dimensional Phased-Array Antenna on a Flexible Substrate.   Antennas Wirel. Propag. Lett. 2013, 12, 170–173.

112.   Sanusi, O.M.; Ghaffar, F.A.; Shamim, A.; Vaseem, M.; Wang, Y.; Roy, L. Development   of a 2.45 GHz Antenna for Flexible Compact Radiation Dosimeter Tags. IEEE Trans.   Antennas Propag. 2019, 67, 5063–5072.

113.   Li, Z.; Sinha, S.K.; Treich, G.M.; Wang, Y.; Yang, Q.; Deshmukh, A.A.; Sotzing, G.A.;   Cao, Y. All-organic flexible fabric antenna for wearable electronics. J. Mater. Chem. C   2020, 8, 5662–5667.

114.   Hayes, G.J.; Ju-Hee, S.; Qusba, A.; Dickey, M.D.; Lazzi, G. Flexible Liquid Metal Alloy   (EGaIn) Microstrip Patch Antenna. IEEE Trans. Antennas Propag. 2012, 60, 2151–2156.

115.   Riheen, M.A.; Nguyen, T.T.; Saha, T.K.; Karacolak, T.; Sekhar, P.K. CPW fed Wideband   Bowtie Slot Antenna on PET substrate. Prog. Electromagn. Res. C 2020, 101, 147–158.

116.   Khaleel, H.R.; Al-Rizzo, H.M.; Abbosh, A.I. Design, Fabrication, and Testing of Flexible   Antennas. In Advancement in Microstrip Antennas with Recent Applications; Kishk, A.,   Ed.; InTech: London, UK, 2013; ISBN 978-953-51-1019-4.

117.   Bodö, P.; Sundgren, J.E. Titanium deposition onto ion-bombarded and plasma-treated   polydimethylsiloxane: Surface modification, interface and adhesion. Thin Solid Films   1986, 136, 147–159.

118.	Scarpello, M.L.; Kazani, I.; Hertleer, C.; Rogier, H.; Vande Ginste, D. Stability and Efficiency of Screen-Printed Wearable and Washable Antennas. Antennas Wirel. Propag. Lett. 2012, 11, 838–841.

119.	Rahman, M.A.; Hossain, M.F.; Riheen, M.A.; Sekhar, P.K. Early Brain Stroke Detection using Flexible Monopole Antenna. Prog. Electromagn. Res. C 2020, 99, 99–110.

120.	Mohamadzade, B.; Hashmi, R.M.; Simorangkir, R.B.V.B.; Gharaei, R.; Ur Rehman, S.; Abbasi, Q.H. Recent Advances in Fabrication Methods for Flexible Antennas in Wearable Devices: State of the Art. Sensors 2019, 19, 2312.

121.	Yang, L.; Rida, A.; Vyas, R.; Tentzeris, M.M. RFID Tag and RF Structures on a Paper Substrate Using Inkjet-Printing Technology. IEEE Trans. Microw. Theory Tech. 2007, 55, 2894–2901.

122.	Riheen, M.A.; Saha, T.K.; Sekhar, P.K. Inkjet Printing on PET Substrate. J. Electrochem. Soc. 2019, 166, B3036–B3039.

123.	Saha, T.K.; Knaus, T.N.; Khosla, A.; Sekhar, P.K. Investigation of Printing Properties on Paper Substrate. J. Electrochem. Soc. 2018, 165, B3163–B3167. [CrossRef].

124.	Raut, N.C.; Al-Shamery, K. Inkjet printing metals on flexible materials for plastic and paper electronics. J. Mater. Chem. C 2018, 6, 1618–1641.

125.	Romano, S., Brückner-Foit, A., Brandão, A., Gumpinger, J., Ghidini, T., & Beretta, S. (2018). Fatigue properties of AlSi10Mg obtained by additive manufacturing: Defect- based modelling and prediction of fatigue strength. Engineering Fracture Mechanics, 187, 165-189.

126.	Pinnola, F. P., Faghidian, S. A., Barretta, R., & de Sciarra, F. M. (2020). Variationally consistent dynamics of nonlocal gradient elastic beams. International Journal of Engineering Science, 149, 103220.

127.	Apuzzo, A., Barretta, R., Fabbrocino, F., Faghidian, S. A., Luciano, R., & Marotti De Sciarra, F. (2019). Axial and torsional free vibrations of elastic nano-beams by stress- driven two-phase elasticity. Journal of Applied and Computational Mechanics, 5(2), 402- 413.

128.   R. Barretta, M. Diaco, L. Feo, R. Luciano, F. Marotti de Sciarra, R. Penna, Stress-driven   integral elastic theory for torsion of nano-beams, Mech. Res. Commun. 87 (2018) 35-41.   Doi: 10.1016/j.mechrescom.2017.11.004.

129.   R. Barretta, M. Čanađija, R. Luciano, F. Marotti de Sciarra, Stress-driven modeling of   nonlocal thermoelastic behavior of nano-beams, Int. J. Eng. Sci. 126 (2018) 53-67. Doi: 10.1016/j.ijengsci.2018.02.012.

130.   A. Apuzzo, R. Barretta, R. Luciano, F. Marotti de Sciarra, R. Penna, Free vibrations of Bernoulli-Euler nano-beams by the stress-driven nonlocal integral model, Compos. Part   B. 123 (2017) 105-111. Doi: 10.1016/j.compositesb.2017.03.057.

131.   E. Mahmoudpour, S.H. Hosseini-Hashemi, S.A. Faghidian, Nonlinear vibration analysis   of FG nano-beams resting on elastic foundation in thermal environment using stress-   driven nonlocal integral model, Appl. Math. Modell. 57 (2018) 302-315. Doi: 10.1016/j.apm.2018.01.021.

132.   R. Barretta, S.A. Faghidian, R. Luciano, Longitudinal Vibrations of Nano-Rods by   Stress-Driven Integral Elasticity, Mech. Adv. Mater. Struct. (2018). Doi: 10.1080/15376494.2018.1432806.

133.   W. S. Hummers Jr. and R. E. Offeman, "Preparation of graphitic oxide," Journal of the   American Chemical Society, vol. 80, no. 6, p. 1339, 1958.

134.   Alamán, J., Alicante, R., Peña, J. I., & Sánchez-Somolinos, C , .Inkjet printing of functional materials for optical and photonic applications. Materials, . (2016)9(11), 910.

135.   Subramanian, Vivek, Jean MJ Fréchet, Paul C. Chang, Daniel C. Huang, Josephine B. Lee, Steven E. Molesa, Amanda R. Murphy, David R. Redinger, and Steven K. Volkman. "Progress toward development of all-printed RFID tags: materials, processes, and devices." Proceedings of the IEEE 93, no. 7 (2005): 1330-1338.

136.   Zhan, Yiqiang, Yongfeng Mei, and Lirong Zheng. "Materials capability and device performance in flexible electronics for the Internet of Things." Journal of Materials Chemistry C 2, no. 7 (2014): 1220-1232.

137.   Arias, A. C., S. E. Ready, R. Lujan, W. S. Wong, K. E. Paul, A. Salleo, M. L. Chabinyc et al. "All jet-printed polymer thin-film transistor active-matrix backplanes." Applied Physics Letters 85, no. 15 (2004): 3304-3306.Wang X.   , Lu X., Liu B, Chen D. ,Tong y, Shen G. Adv. Mater. (2014) 26 4763 .

138.   Tobjörk, D. and Österbacka, R., 2011. Paper electronics. Advanced materials, 23(17), pp.1935-1961..

139.   Ciesielski, Artur, and Paolo Samori. "Graphene via sonication assisted liquid-phase exfoliation." Chemical Society Reviews 43, no. 1 (2014): 381-398.

140.   Shaltout, Amr M., Nathaniel Kinsey, Jongbum Kim, Rohith Chandrasekar, Justus C. Ndukaife, Alexandra Boltasseva, and Vladimir M. Shalaev. "Development of optical metasurfaces: emerging concepts and new materials." Proceedings of the IEEE 104, no. 12 (2016): 2270-2287.

141.   Chujo, Yoshiki, and Kazuo Tanaka. "New polymeric materials based on element-blocks." Bulletin of the Chemical Society of Japan 88, no. 5 (2015): 633-643.

142.   Beadie, G., M. L. Sandrock, M. J. Wiggins, R. S. Lepkowicz, J. S. Shirk, M. Ponting, Y. Yang, T. Kazmierczak, A. Hiltner, and E. Baer. "Tunable polymer lens." Optics express 16, no. 16 (2008): 11847-11857..

143.   Santiago-Alvarado, A., Vazquez-Montiel, S., Gonzalez-Garcia, J., Iturbide-Jimenez, F., Cruz-Felix, A.S., Cruz-Martinez, V., Lopez-Lopez, E.A. and Castro-Gonzalez, G.,. Advances in the development of tunable lenses in Mexico. Photonics Letters of Poland,(2015) 7(1), pp.20-22.

144.   Park, J.S., Cabosky, R., Ye, Z. and Kim, I.I.. Investigating the mechanical and optical properties of thin PDMS film by flat-punched indentation. Optical Materials,(2018) 85, pp.153-161..

145.   Martinček, I., Turek, I. and Tarjányi, N., Effect of boundary on refractive index of PDMS. Optical Materials Express, 4(10),(2014) pp.1997-2005.

146.   Genzer, J. and Marmur, A., Biological and synthetic self-cleaning surfaces. MRS Bulletin, 33(8), (2008) pp.742-746.

147.   Zeng, H., Duan, G., Li, Y., Yang, S., Xu, X. and Cai, W.,. Blue Luminescence of ZnO nanoparticles based on non-equilibrium processes: defect origins and emission controls. Advanced Functional Materials, (2010) 20(4), pp.561-572.

148.   Devan, R.S., Patil, R.A., Lin, J.H. and Ma, Y.R., One-dimensional metal-oxide nanostructures: recent developments in synthesis, characterization, and applications. Advanced Functional Materials, 22(16),(2012) pp.3326-3370.

149.   Mishra, Y.K., Kaps, S., Schuchardt, A., Paulowicz, I., Jin, X., Gedamu, D., Wille, S., Lupan, O. and Adelung, R., Versatile fabrication of complex shaped metal oxide

nano-microstructures and their interconnected networks for multifunctional applications. KONA Powder and Particle Journal, 31,(2014) pp.92-110..

150.   Gorrasi, G., D'Ambrosio, S., Patimo, G. and Pantani, R., Hybrid clay-carbon nanotube/PET composites: Preparation, processing, and analysis of physical properties. Journal of Applied Polymer Science, (2014) 131(13)..

151.   Mannov, E., Schmutzler, H., Chandrasekaran, S., Viets, C., Buschhorn, S., Tölle, F., Mülhaupt, R. and Schulte, K., Improvement of compressive strength after impact in fibre reinforced polymer composites by matrix modification with thermally reduced graphene oxide. Composites science and technology, (2013) 87, pp.36-41.

152.   Raquez, J.M., Habibi, Y., Murariu, M. and Dubois, P., 2013. Polylactide (PLA)-based nanocomposites. Progress in Polymer Science, 38(10-11), pp.1504-1542.

153.   Abraham, Jiji, Sabu Thomas, and Soney C. George. "Micro and nano TiO2 reinforced natural rubber composites." Natural Rubber Materials (2013): 290-306.

154.   Petrović, Zoran S., and Richard Farris. "Structure-property relationship in fibers spun from poly (ethylene terephthalate) and liquid crystalline polymer blends. I. The effect of composition and processing on fiber morphology and properties." Journal of applied polymer science 58, no. 6 (1995): 1077-1085.

155.   Paul, Donald R., and Lioyd M. Robeson. "Polymer nanotechnology: nanocomposites." Polymer 49, no. 15 (2008): 3187-3204.

156.   Lachman, Noa, Erica Wiesel, Roberto Guzman de Villoria, Brian L. Wardle, and H. Daniel Wagner. "Interfacial load transfer in carbon nanotube/ceramic microfiber hybrid polymer composites." Composites science and technology 72, no. 12 (2012): 1416-1422.

157.   Pötschke, Petra, Beate Krause, Samuel T. Buschhorn, Ulf Köpke, Michael T. Müller, Tobias Villmow, and Karl Schulte. "Improvement of carbon nanotube dispersion in thermoplastic composites using a three roll mill at elevated temperatures." Composites science and technology 74 (2013): 78-84.

158.   Wichmann, Malte HG, Samuel T. Buschhorn, Lars Böger, Rainer Adelung, and Karl Schulte. "Direction sensitive bending sensors based on multi-wall carbon nanotube/epoxy nanocomposites." Nanotechnology 19, no. 47 (2008): 475503.

159.   Pavlidou, S., and C. D. Papaspyrides. "A review on polymer–layered silicate nanocomposites." Progress in polymer science 33, no. 12 (2008): 1119-1198.

160.   Breuer, Orna, and Uttandaraman Sundararaj. "Big returns from small fibers: a review of polymer/carbon nanotube composites." Polymer composites 25, no. 6 (2004): 630-645.

161.   Frank, Otakar, Georgia Tsoukleri, Ibtsam Riaz, Konstantinos Papagelis, John Parthenios, Andrea C. Ferrari, Andre K. Geim, Kostya S. Novoselov, and Costas Galiotis. "Development of a universal stress sensor for graphene and carbon fibres." Nature Communications 2, no. 1 (2011): 1-7.

162.   Tian, He, Yi Shu, Xue-Feng Wang, Mohammad Ali Mohammad, Zhi Bie, Qian-Yi Xie, Cheng Li, Wen-Tian Mi, Yi Yang, and Tian-Ling Ren. "A graphene-based resistive pressure sensor with record-high sensitivity in a wide pressure range." Scientific reports 5, no. 1 (2015): 1-6.

163.   Bae, Sang-Hoon, Youngbin Lee, Bhupendra K. Sharma, Hak-Joo Lee, Jae-Hyun Kim, and Jong-Hyun Ahn. "Graphene-based transparent strain sensor." Carbon 51 (2013): 236-242.

164.   Fu, Xue-Wen, Zhi-Min Liao, Jian-Xin Zhou, Yang-Bo Zhou, Han-Chun Wu, Rui Zhang, Guangyin Jing et al. "Strain dependent resistance in chemical vapor deposition grown graphene." Applied Physics Letters 99, no. 21 (2011): 213107..

165.   Wang, Yi, Rong Yang, Zhiwen Shi, Lianchang Zhang, Dongxia Shi, Enge Wang, and Guangyu Zhang. "Super-elastic graphene ripples for flexible strain sensors." ACS nano 5, no. 5 (2011): 3645-3650.

166.   Amjadi, Morteza, Ki-Uk Kyung, Inkyu Park, and Metin Sitti. "Stretchable, skin-mountable, and wearable strain sensors and their potential applications: a review." Advanced Functional Materials 26, no. 11 (2016): 1678-1698.

167.   R. C. Chiechi, E. A. Weiss, M. D. Dickey, and G. M. Whitesides, "Eutectic gallium-indium (EGaIn): A moldable liquid metal for electrical characterization of self-assembled monolayers," Angew. Chem. Int. Ed., vol. 47, no. 1, pp. 142–144, Dec. (2007).

168.   J. -H. So and M. D. Dickey, "Inherently aligned microfluidic electrodes composed of liquid metal," Lab Chip, vol. 11, no. 5, pp. 905–911, Jan. (2011).

169.   H. -J. Kim, C. Son, and B. Ziaie, "A multiaxial stretchable interconnect using liquid-alloy-filled elastomeric microchannels." Appl. Phys. Lett., vol. 92, no. 1, p. 011904, Jan. (2008).

170.   H. Hu, K. Shaikh, and C. Liu, Super flexible sensor skin using liquid metal as interconnect," in Proc. IEEE Sensors,(2007), pp. 815-817,.

171.   H. Yang, C. R. Lightner, and L. Dong, "Light-emitting coaxial nanofibers," ACS Nano, vol. 6, no. 1, pp. 622–628, Jan. (2012) .

172.   M. Jobs, K. Hjort, A. Rydberg, and Z. Wu, "A Tunable spherical cap microfluidic electrically small antenna", Small, vol. 9, no. 19, pp. 3230-3234, Apr. (2013).

173.   R. K. Kramer , C. Majidi , R. J. Wood , Adv. Funct. Mater. 2013 , 23 , 42 .

174.   K. S. Novoselov, A. K. Geim, S. V. Morozov, D. Jiang, Y. Zhang, S. V. Dubonos,I. V. Grigorieva, A."Electric field effect in atomically thin carbon films". Firsov, Science,306(2004)666-669.

175.   J. C. Meyer, A. K. Geim, M. I. Katsnelson, K. S. Novoselov, T. J. Booth and S. Roth, "The structure of suspended graphene sheets" .Nature 446(2007)60-63.

176.   K. S. Novoselov, D. Jiang, F. Schedin, T. J. Booth, V. V. Khotkevich, S. V. Morozov,and A. K. Geim, PANS 102(2005)10451-10453.

177.   K. S. Novoselov,1 Z. Jiang,2,3 Y. Zhang,2 S. V. Morozov,1 H. L. Stormer,2 U.Zeitler,4 J. C. Maan,4 G. S. Boebinger,3 P. Kim, A. K. Geim,Science, 315(2007)1379.

178.   S. D. Dalosto, and Z. H. Levine, J. Phys. Chem. C, 112 (2008)8196–8199.

179.   M. Fujita, K. Wakabayashi, K. Nakada and K. Kusakabe, "Peculiar Localized State at Zigzag Graphite Edge" J. Phys. Soc. Jpn. 65 (1996)1920-1923.

180.   K. Nakada, M. Fujita, G. Dresselhaus, and M. S. Dresselhaus," Edge state in graphene ribbons:

181.   Li X, Cai W, An J, Kim S, Nah J, Yang D, Piner R, Velamakanni A, Jung I, Tutuc E,Banerjee SK, Colombo L, and Ruoff   "Large-area synthesis of high-quality and uniform graphene films on copper foils. " RS, Science, 324(2009)1312-1314.

182.   Yang, S.; Wang, C.; Ataca, C.; Li, Y.; Chen, H.; Cai, H.; Suslu,A.; Grossman, J. C.; Jiang, C.; Liu, Q.; et al. 'Self-Driven Photodetectorand Ambipolar Transistor in Atomically Thin GaTe-MoS2 p-n vdWHeterostructure." ACS Appl. Mater. Interfaces (2016), 8, 2533−2539.

183.   Wang, F.; Wang, Z.; Xu, K.; Wang, F.; Wang, Q.; Huang, Y.;Yin, L.; He, J. Tunable GaTe-MoS 2 van Der Waals P−n Junctionswith Novel Optoelectronic Performance. Nano Lett. (2015), 15, 7558−7566.

184.   Huang, S.; Tatsumi, Y.; Ling, X.; Guo, H.; Wang, Z.; Watson,G.; Puretzky, A. A.; Geohegan, D. B.; Kong, J.; Li, J.; et al. "In-PlaneOptical Anisotropy of Layered Gallium Telluride". ACS Nano (2016),10, 8964−8972.

185.   Wen, Nan, Lu Zhang, Dawei Jiang, Zijian Wu, Bin Li, Caiying Sun, and Zhanhu Guo. "Emerging flexible sensors based on nanomaterials: recent status and applications." *Journal of Materials Chemistry A* 8, no. 48 (2020): 25499-25527.

186.   Shenoy, U. S.; Gupta, U.; Narang, D. S.; Late, D. J.; Waghmare,U. V.; Rao, C. N. R. Electronic Structure and Properties of LayeredGallium Telluride. Chem. Phys. Lett. (2016), 651, 148−154.

187.   Susoma, J.; Karvonen, L.; Säynätjoki, A.; Mehravar, S.;Norwood, R. A.; "Peyghambarian, N.; Kieu, K.; Lipsanen, H.;Riikonen, J. Second and Third Harmonic Generation in Few-LayerGallium Telluride Characterized by Multiphoton Microscopy". Appl.Phys. Lett. (2016), 108, 073103.

188.   Zhang, Lu, Dawei Jiang, Tianhe Dong, Rajib Das, Duo Pan, Caiying Sun, Zijian Wu, Qingbo Zhang, Chuntai Liu, and Zhanhu Guo. "Overview of ionogels in flexible electronics." *The Chemical Record* 20, no. 9 (2020): 948-967.

189.   Williams, R. H.; McEvoy, "A. J. Surface Properties of theGallium Monochalcogenides". Phys. Status Solidi (1972), 12, 277−286.

190.   Yan, Hai-liang, Yan-qiu Chen, Yong-qiang Deng, Li-long Zhang, Xiao Hong, Woon-ming Lau, Jun Mei, David Hui, Hui Yan, and Yu Liu. "Coaxial printing method for directly writing stretchable cable as a strain sensor." Applied Physics Letters 109, no. 8 (2016): 083502.

191.   Jiang, Dawei, Ying Wang, Bin Li, Caiying Sun, Zijian Wu, Hui Yan, Lixin Xing et al. "Flexible sandwich structural strain sensor based on silver nanowires decorated with self-healing substrate." *Macromolecular Materials and Engineering* 304, no. 7 (2019): 1900074.

192.   Yang, Zhenhua, Zijian Wu, Dawei Jiang, Renbo Wei, Xianmin Mai, Duo Pan, Sravanthi Vupputuri, Ling Weng, Nithesh Naik, and Zhanhu Guo. "Ultra-sensitive flexible sandwich structural strain sensors based on a silver nanowire supported PDMS/PVDF electrospun membrane substrate." *Journal of Materials Chemistry C* 9, no. 8 (2021): 2752-2762.

193. Dickey, Michael D., Ryan C. Chiechi, Ryan J. Larsen, Emily A. Weiss, David A. Weitz, and George M. Whitesides. "Eutectic gallium-indium (EGaIn): a liquid metal alloy for the formation of stable structures in microchannels at room temperature." *Advanced functional materials* 18, no. 7 (2008): 1097-1104.

194. G.C. Psarras Fundamentals of dielectric theories Dielectric Polymer Materials for High-Density Energy Storage, Elsevier (2018), pp. 11-57, 10.1016/b978-0-12-813215-9.00002-6

195. J.F. Capsal, J. Galineau, M.Q. Le, F. Domingues Dos Santos, P.J. Cottinet Enhanced electrostriction based on plasticized relaxor ferroelectric P(VDF-TrFE-CFE/CTFE) blends J. Polym. Sci. B Polym. Phys., 53 (2015), pp. 1368-1379, 10.1002/polb.23776

196. Wang, X., Lu, X., Liu, B., Chen, D., Tong, Y., & Shen, G. (2014). Flexible energy-storage devices: design consideration and recent progress. Advanced Materials, 26(28), 4763-4782.

197. Tobjörk, D., & Österbacka, R. (2011). Paper electronics. Advanced Materials, 23(17), 1935-1961.

198. Ranasingha, O. K., Luce, A., Strack, G., Hardie, C., Piro, Y., Haghzadeh, M., & Akyurtlu, A. (2020). Selective laser sintering of conductive patterns on a novel silver–barium strontium titanate composite material. Flexible and Printed Electronics, 5(4), 045007.

199. Weiss, N. O., Zhou, H., Liao, L., Liu, Y., Jiang, S., Huang, Y., & Duan, X. (2012). Graphene: an emerging electronic material. Advanced Materials, 24(43), 5782-5825.

200. Hernandez, Y., Nicolosi, V., Lotya, M., Blighe, F. M., Sun, Z., De, S., ... & Coleman, J. N. (2008). High-yield production of graphene by liquid-phase exfoliation of graphite. Nature Nanotechnology, 3(9), 563-568.

201. Torrisi, F., Hasan, T., Wu, W., Sun, Z., Lombardo, A., Kulmala, T. S., & Ferrari, A. C. (2012). Inkjet-printed graphene electronics. ACS Nano, 6(4), 2992-3006.

202. Gómez-Navarro, C., Weitz, R. T., Bittner, A. M., Scolari, M., Mews, A., Burghard, M., & Kern, K. (2007). Electronic transport properties of individual chemically reduced graphene oxide sheets. Nano Letters, 7(11), 3499-3503.

203.   Mao, S., Pu, H., & Chen, J. (2012). Graphene oxide and its reduction: modeling and experimental progress. RSC Advances, 2(7), 2643-2662.

204.   Ciesielski, A., & Samori, P. (2014). Graphene via sonication-assisted liquid-phase exfoliation. Chemical Society Reviews, 43(1), 381-398.

205.   Mayyas, M., Li, H., Kumar, P., Ghasemian, M. B., Yang, J., Wang, Y., & Kalantar-Zadeh, K. (2020). Liquid-Metal-Templated Synthesis of 2D Graphitic Materials at Room Temperature. Advanced Materials, 32(29), 2001997.

206.   Shaltout, A. M., Kinsey, N., Kim, J., Chandrasekar, R., Ndukaife, J. C., Boltasseva, A., & Shalaev, V. M. (2016). Development of optical metasurfaces: emerging concepts and new materials. Proceedings of the IEEE, 104(12), 2270-2287.

207.   Peng, Y., Liu, H., Xin, Y., & Zhang, J. (2021). Rheological conductor from liquid metal-polymer composites. Matter, 4(9), 3001-3014.

208.   Chujo, Y., & Tanaka, K. (2015). New polymeric materials based on element blocks. Bulletin of the Chemical Society of Japan, 88(5), 633-643.

209.   Beadie, G., Sandrock, M. L., Wiggins, M. J., Lepkowicz, R. S., Shirk, J. S., Ponting, M., & Baer, E. (2008). Tunable polymer lens. Optics Express, 16(16), 11847-11857.

210.   Santiago-Alvarado, A., Vazquez-Montiel, S., Gonzalez-Garcia, J., Iturbide-Jimenez, F., Cruz-Felix, A. S., Cruz-Martinez, V., & Castro-Gonzalez, G. (2015). Advances in the development of tunable lenses in Mexico. Photonics Letters of Poland, 7(1), 20-22.

211.   Judy, J. W. (2001). Microelectromechanical systems (MEMS): fabrication, design, and applications. Smart Materials and Structures, 10(6), 1115.

212.   Wang, Z., Volinsky, A. A., & Gallant, N. D. (2014). Crosslinking effect on polydimethylsiloxane elastic modulus measured by custom-built compression instrument. Journal of Applied Polymer Science, 131(22).

213.   Liu, M., Sun, J., & Chen, Q. (2009). Influences of heating temperature on mechanical properties of polydimethylsiloxane. Sensors and Actuators A: Physical, 151(1), 42-45.

214.   Prajzler, V., Nekvindova, P., Spirkova, J., & Novotny, M. (2017). The evaluation of the refractive indices of bulk and thick polydimethylsiloxane and polydimethyl-diphenylsiloxane elastomers by the prism coupling technique. Journal of Materials Science: Materials in Electronics, 28(11), 7951-7961.

215.   Martinček, I., Turek, I., & Tarjányi, N. (2014). Effect of boundary on refractive index of PDMS. Optical Materials Express, 4(10), 1997-2005.

216.   Zeng, H., Duan, G., Li, Y., Yang, S., Xu, X., & Cai, W. (2010). Blue Luminescence of ZnO nanoparticles based on non-equilibrium processes: defect origins and emission controls. Advanced Functional Materials, 20(4), 561-572.

217.   Devan, R. S., Patil, R. A., Lin, J. H., & Ma, Y. R. (2012). One-dimensional metal-oxide nanostructures: recent developments in synthesis, characterization, and applications. Advanced Functional Materials, 22(16), 3326-3370.

218.   Mishra, Y. K., Kaps, S., Schuchardt, A., Paulowicz, I., Jin, X., Gedamu, D., & Adelung, R. (2014). Versatile fabrication of complex shaped metal oxide nano-microstructures and their interconnected networks for multifunctional applications. KONA Powder and Particle Journal, 31, 92-110.

219.   Dai, L. (2013). Functionalization of graphene for efficient energy conversion and storage. Accounts of chemical research, *46*(1), 31-42.

220.   Pavlidou, S., & Papaspyrides, C. D. (2008). A review on polymer–layered silicate nanocomposites. Progress in Polymer Science, 33(12), 1119-1198.

221.   Breuer, O., & Sundararaj, U. (2004). Big returns from small fibers: a review of polymer/carbon nanotube composites. Polymer composites, 25(6), 630-645.

222.   Frank, O., Tsoukleri, G., Riaz, I., Papagelis, K., Parthenios, J., Ferrari, A. C., ... & Galiotis, C. (2011). Development of a universal stress sensor for graphene and carbon fibers. Nature Communications, 2(1), 1-7.

223.   Hempel, M., Nezich, D., Kong, J., & Hofmann, M. (2012). A novel class of strain gauges based on layered percolative films of 2D materials. Nano Letters, 12(11), 5714-5718.

224. Smith, A. D., Niklaus, F., Paussa, A., Vaziri, S., Fischer, A. C., Sterner, M., & Lemme, M. C. (2013). Electromechanical piezoresistive sensing in suspended graphene membranes. Nano Letters, 13(7), 3237-3242.

225. Zhu, Shou-En, et al. Graphene based piezoresistive pressure sensor. Applied Physics Letters 102.16 2013 161904..

226. Liu, H., Xin, Y., Bisoyi, H. K., Peng, Y., Zhang, J., & Li, Q. (2021). Stimuli-Driven Insulator–Conductor Transition in a Flexible Polymer Composite Enabled by Biphasic Liquid Metal. Advanced Materials, 2104634.

227. Yao, H. B., Ge, J., Wang, C. F., Wang, X., Hu, W., Zheng, Z. J., & Yu, S. H. (2013). A flexible and highly pressure-sensitive graphene–polyurethane sponge based on fractured microstructure design. Advanced Materials, 25(46), 6692-6698.

228. Bae, S. H., Kahya, O., Sharma, B. K., Kwon, J., Cho, H. J., Ozyilmaz, B., & Ahn, J. H. (2013). Graphene-P (VDF-TrFE) multilayer film for flexible applications. ACS Nano, 7(4), 3130-3138.

229. Fu, X. W., Liao, Z. M., Zhou, J. X., Zhou, Y. B., Wu, H. C., Zhang, R., ... & Yu, D. (2011). Strain dependent resistance in chemical vapor deposition grown graphene. Applied Physics Letters, 99(21), 213107.

230. Wang, Y., Yang, R., Shi, Z., Zhang, L., Shi, D., Wang, E., & Zhang, G. (2011). Super-elastic graphene ripples for flexible strain sensors. ACS Nano, 5(5), 3645-3650.

231. Amjadi, M., Kyung, K. U., Park, I., & Sitti, M. (2016). Stretchable, skin-mountable, and wearable strain sensors and their potential applications: a review. Advanced Functional Materials, 26(11), 1678-1698.

232. So, J. H., & Dickey, M. D. (2011). Inherently aligned microfluidic electrodes composed of liquid metal. Lab on a Chip, 11(5), 905-911.

233. Kim, H. J., Son, C., & Ziaie, B. (2008). A multiaxial stretchable interconnect using liquid-alloy-filled elastomeric microchannels. Applied Physics Letters, 92(1), 011904.

234. Hu, H., Shaikh, K., & Liu, C. (2007, October). Super flexible sensor skin using liquid metal as interconnect. In SENSORS, 2007 IEEE (pp. 815-817).

174

235.   Jobs, M., Hjort, K., Rydberg, A., & Wu, Z. (2013). A tunable spherical cap microfluidic electrically small antenna. Small, 9(19), 3230-3234.

236.   Liu, P., Yang, S., Wang, X., Yang, M., Song, J., & Dong, L. (2016). Directivity-reconfigurable wideband two-arm spiral antenna. IEEE Antennas and Wireless Propagation Letters, 16, 66-69.

237.   Yang, S., Liu, P., Yang, M., Wang, Q., Song, J., & Dong, L. (2016). From flexible and stretchable meta-atom to metamaterial: A wearable microwave meta-skin with tunable frequency selective and cloaking effects. Scientific Reports, 6(1), 1-8.

238.   Hernandez, G. A., Martinez, D., Ellis, C., Palmer, M., & Hamilton, M. C. (2013, May). Through Si vias using liquid metal conductors for re-workable 3D electronics. In 2013 IEEE 63rd Electronic Components and Technology Conference (pp. 1401-1406). IEEE.

239.   Kramer, R. K., Majidi, C., & Wood, R. J. (2013). Masked deposition of gallium-indium alloys for liquid-embedded elastomer conductors. Advanced Functional Materials, 23(42), 5292-5296.

240.   Kramer, R. K., Majidi, C., & Wood, R. J. (2013). Masked deposition of gallium-indium alloys for liquid-embedded elastomer conductors. Advanced Functional Materials, 23(42), 5292-5296.

241.   Novoselov, K. S., Jiang, D., Schedin, F., Booth, T. J., Khotkevich, V. V., Morozov, S. V., & Geim, A. K. (2005). Two-dimensional atomic crystals. Proceedings of the National Academy of Sciences, 102(30), 10451-10453.

242.   Han, M. Y., Özyilmaz, B., Zhang, Y., & Kim, P. (2007). Energy band-gap engineering of graphene nanoribbons. Physical Review Letters, 98(20), 206805.

243.   Nakada, K., Fujita, M., Dresselhaus, G., & Dresselhaus, M. S. (1996). Edge state in graphene ribbons: Nanometer size effect and edge shape dependence. Physical Review B, 54(24), 17954.

244.   van Gastel, R., N'Diaye, A. T., Wall, D., Coraux, J., Busse, C., Buckanie, N. M., ... & Poelsema, B. (2009). Selecting a single orientation for millimeter sized graphene sheets. Applied Physics Letters, 95(12), 121901.

245.   Li, X., Cai, W., An, J., Kim, S., Nah, J., Yang, D., & Ruoff, R. S. (2009). Large-area synthesis of high-quality and uniform graphene films on copper foils. Science, 324(5932), 1312-1314.

246.   Yang, S., Wang, C., Ataca, C., Li, Y., Chen, H., Cai, H., & Tongay, S. (2016). Self-driven photodetector and ambipolar transistor in atomically thin GaTe-MoS2 p–n vdW heterostructure. ACS Applied Materials & Interfaces, 8(4), 2533-2539.

247.   Wang, F., Wang, Z., Xu, K., Wang, F., Wang, Q., Huang, Y., & He, J. (2015). Tunable GaTe-MoS2 van der Waals p–n junctions with novel optoelectronic performance. Nano Letters, 15(11), 7558-7566.

248.   Huang, S., Tatsumi, Y., Ling, X., Guo, H., Wang, Z., Watson, G., & Dresselhaus, M. S. (2016). In-plane optical anisotropy of layered gallium telluride. ACS Nano, 10(9), 8964-8972.

249.   Shenoy, U. S., Gupta, U., Narang, D. S., Late, D. J., Waghmare, U. V., & Rao, C. N. R. (2016). Electronic structure and properties of layered gallium telluride. Chemical Physics Letters, 651, 148-154.

250.   Susoma, J., Karvonen, L., Säynätjoki, A., Mehravar, S., Norwood, R. A., Peyghambarian, N., ...& Riikonen, J. (2016). Second and third harmonic generation in few-layer gallium telluride characterized by multiphoton microscopy. Applied Physics Letters, 108(7), 073103.

251.   Yang, S., Cai, H., Chen, B., Ko, C., Özçelik, V. O., Ogletree, D. F., & Tongay, S. (2017). Environmental stability of 2D anisotropic tellurium containing nanomaterials: anisotropic to isotropic transition. Nanoscale, 9(34), 12288-12294.

252.   French, S. J., SAUNDERS, D. J., & INGLE, G. W. (2002). The system gallium-indium. The Journal of Physical Chemistry, 42(2), 265-274.

253.   Kim, T. W., Wang, G., Lee, H., & Lee, T. (2007). Statistical analysis of electronic properties of alkanethiols in metal–molecule–metal junctions. Nanotechnology, 18(31), 315204.

254.   Beebe, J. M., & Kushmerick, J. G. (2007). Nanoscale switch elements from self-assembled monolayers on silver. Applied Physics Letters, 90(8), 083117.

255.	Milani, F., Grave, C., Ferri, V., Samorì, P., & Rampi, M. A. (2007). Ultrathin π-conjugated polymer films for simple fabrication of large-area molecular junctions. ChemPhysChem, 8(4), 515-518.

256.	Dickey, M. D., Chiechi, R. C., Larsen, R. J., Weiss, E. A., Weitz, D. A., & Whitesides, G. M. (2008). Eutectic gallium-indium (EGaIn): a liquid metal alloy for the formation of stable structures in microchannels at room temperature. Advanced Functional Materials, 18(7), 1097-1104.

257.	Sargolzaeiaval, Y., Ramesh, V. P., Neumann, T. V., Miles, R., Dickey, M. D., & Öztürk, M. C. (2019). High thermal conductivity silicone elastomer doped with graphene nanoplatelets and eutectic gain liquid metal alloy. ECS Journal of Solid State Science and Technology, 8(6), P357.

258.	Dickey, M. D., Chiechi, R. C., Larsen, R. J., Weiss, E. A., Weitz, D. A., & Whitesides, G. M. (2008). Eutectic gallium-indium (EGaIn): a liquid metal alloy for the formation of stable structures in microchannels at room temperature. Advanced Functional Materials, 18(7), 1097-1104.

259.	Neumann, T. V., Kara, B., Sargolzaeiaval, Y., Im, S., Ma, J., Yang, J., ... & Dickey, M. D. (2021). Aerosol Spray Deposition of Liquid Metal and Elastomer Coatings for Rapid Processing of Stretchable Electronics. Micromachines, 12(2), 146.

260.	Saborio, M. G., Cai, S., Tang, J., Ghasemian, M. B., Mayyas, M., Han, J., & Kalantar-Zadeh, K. (2020). Liquid Metal Droplet and Graphene Co-Fillers for Electrically Conductive Flexible Composites. Small, 16(12), 1903753.

261.	Susoma, J., Lahtinen, J., Kim, M., Riikonen, J., & Lipsanen, H. (2017). Crystal quality of two-dimensional gallium telluride and gallium selenide using Raman fingerprint. AIP Advances, 7(1), 015014.

262.	Su, C., Zhao, X. (2021). A uniformly first-order accurate method for Klein-Gordon-Zakharov system in simultaneous high-plasma-frequency and subsonic limit regime. Journal of Computational Physics, *428*, 110064.

263.	Wang, T., Zhao, Q., Miao, Y., Ma, F., Xie, Y., & Jie, W. (2018). Lattice vibration of layered GaTe single crystals. Crystals, 8(2), 74.

264.   Al-Dhahebi, A. M., Gopinath, S. C. B., & Saheed, M. S. M. (2020). Graphene impregnated electrospun nanofiber sensing materials: A comprehensive overview on bridging laboratory set-up to industry. *Nano convergence*, *7*(1), 1-23

265.   Ramachandran, P., Naskar, K., & Nando, G. B. (2017). Exploring the effect of radiation crosslinking on the physico-mechanical, dynamic mechanical and dielectric properties of EOC–PDMS blends for cable insulation applications. Polymers for Advanced Technologies, 28(1), 80-93.

266.   Rimshin, V. I., Larionov, E. A., Erofeyev, V. T., & Kurbatov, V. L. (2014). Vibrocreep of concrete with a nonuniform stress state. Life Science Journal, 11(11), 278-280.

267.   Pei, A., Malho, J. M., Ruokolainen, J., Zhou, Q., & Berglund, L. A. (2011). Strong nanocomposite reinforcement effects in polyurethane elastomer with low volume fraction of cellulose nanocrystals. Macromolecules, 44(11), 4422-4427.

268.   M Gad-el-Hak , "Flow control: The future *J. Aircr.,* 38(3) 402-18. 2001.

269.   SC Terry, JH Jerman, JB Angell. A gas chromatographic air analyzer fabricated on a silicon wafer ,*IEEE transactions on electron devices* 26(12), 1880-6, (1979.

270.   O Gundogdu, M Roso, GC Stevens, u. Tüzün*Granul.* Nanoparticle structural organisation and scaffolding in organic media. *Matter*,10(2):123-32, 2008.

271.   J Breiner JM, JE Mark, Beaucage G. Dependence of silica particle sizes on network chain lengths, silica contents, and catalyst concentrations in in situ-reinforced polysiloxane elastomers . *J. Polym. Sci., Part B: Polym. Phys.***1,**37(13):1421-7,1999

272.   A. Rinaldi, T. Alessio , F. S . Maria "A flexible and highly sensitive pressure sensor based on a PDMS foam coated with graphene nanoplatelets." Sensors 16, no. 12: 2148, 2016

273.   N .Xia, Zhao, P. Zhao Y, Zhang J, Fu Integrated measurement of ultrasonic parameters for polymeric materials via full spectrum analysis *Polym. Test*, **70**:426-33,2018.

274.   H .Zhao, Y .Chen, Shao L, Xie M, Nie J, Qiu J, Zhao P, Ramezani H, Fu J, Airflow-Assisted 3D bioprinting of human heterogeneous micron spheroidal organoids with microfluidic Nozzle *Small*. **39**, 1802630,   2018 .

275.   L. Maffli, S .Rosset,.,Ghilardi, M., Carpi, F Shea, H. Ultrafast all-polymer electrically tunable silicone lenses *Adv. Funct. Mater.* 25(11), 1656-1665, 2015 .

276.   S .Rosset, M Niklaus, Dubois P, Shea HR. Large-stroke dielectric elastomer actuators with ion-implanted electrodes J *Microelectromech Syst*,18(6):1300-8, *2009.*

277.   T .Dollase, M .Wilhelm, Spiess HW, Yagen Y, Yerushalmi-Rozen R, Gottlieb M. Effect of interfaces on the crystallization behavior of PDMS   Interface *Sci.*, **(2),** 199-209, 2003.

278.   T .Dollase, HW .Spiess, Gottlieb M, Yerushalmi-Rozen R. Crystallization of PDMS: The effect of physical and chemical crosslinks *Europhysics Letters* . 60(3), 390, 2002 .

279.   Nguyen, NhuQuynh, Ting-Fang Chen, and Chieh-Tsung Lo. "Confined crystallization and chain conformational change in electrospun poly (ethylene oxide) nanofibers." Polymer Journal : 1-11, 2021 .

280.   Thostenson,T. Erik, LI. Chunyu Chou. Tsu-Wei . "Nanocomposites in context." Composites science and technology 65, no. 3-4: 491-516, 2005 .

281.   B. Samel,   M. KamruzzamanChowdhury , S. Göran   . "The fabrication of microfluidic structures by means of full-wafer adhesive bonding using a poly (dimethylsiloxane) catalyst." Journal of Micromechanics and Microengineering17 . 8: 1710, 2007 .

282.   J.C .McDonald,., Duffy, D.C., Anderson, J.R., Chiu, D.T., Wu, H.K., Schueller, O.J. Fabrication of microfluidic systems in poly (dimethylsiloxane) J. *Electrophor.***27**-40 , 2000.

283.   Whitesides, G. M. The origins and the future of microfluidics *nature,*, 442(7101), 368-373, 2006.

284.   Das-Gupta, D. K.,   J. S. Hornsby. "A non-destructive technique for the determination of spatial charge and polarization distributions in insulating polymers." Journal of Physics D: Applied Physics 23, no. 12 ,1485, 1990 .

285.   A Ruhanen, M Hanhikorpi, Bertuccelli F, Colonna A, Malik W, Ranasinghe D, López TS, Yan N, Tavilampi M. *sensor RFID* tag handbook. BRIDGE, IST-33546. (2005)

286.   A Lazauskas,.; J Baltrusaitis,.; Grigaliunas, V.; Jucius, D.; Guobien ¯ e, A.; Prosy˘cevas, I.; Narmontas, P. Plasma Chem. *Plasma Process*.   , **34**, 271–285, 2014.

287.   O. A. Biabangard   "Conductive Filler Modified Polymers for Structural Health Monitoring Applications." (2015).

288.   G Goncalves,., P. A Marques,.,Granadeiro, C. M., Nogueira, H. I., Singh, M. K., Gracio, Surface modification of graphene nanosheets with gold nanoparticles: the role of oxygen moieties at graphene surface on gold nucleation and growthJ. *Mater. Chem.,***(20),** 4796-4802, 2009.

289.   D.A. Van den Ende , P. De Almeida, V.Z. Sybrand . "Piezoelectric and mechanical properties of novel composites of PZT and a liquid crystalline thermosetting resin." Journal of materials science 42, 15, 6417-6425, 2007

290.   Lv, X. J., Fu, W. F., Chang, H. X., Zhang, H., Cheng, J. S., Zhang, G. J.,   Li, J. H*. Hydrogen evolution from water using semiconductor nanoparticle/graphene composite photocatalysts without noble metals   J. Mater. Chem.,***22(4),** 1539-1546, 2012

291.   J. Macdonald, J. Ross,   E. Barsoukov. "Impedance spectroscopy: theory, experiment, and applications." History 1, no. 8: 1-13, 2005.

292.   Barsoukov, Evgenij, and J. Ross Macdonald, eds. Impedance spectroscopy: theory, experiment, and applications. John Wiley & Sons, (2018).

293.   Weitz, Iris Sonia, Or Perlman, Haim Azhari, and Sarit Sara Sivan. "In vitro evaluation of copper release from MRI-visible, PLGA-based nanospheres." Journal of Materials Science 56, no. 1 718-730, 2021

294.   K Efimenko, WE Wallace, Genzer J. Surface modification of Sylgard-184 poly (dimethyl siloxane) networks by ultraviolet and ultraviolet/ozone treatment   J. Colloid *Interface Sci. .   ,***254** (2):306-15, 2002

295.   SK Jaganathan, A Balaji, Vellayappan MV, Subramanian AP, John AA, Asokan MK, Supriyanto E. Radiation-induced surface modification of polymers for biomaterial application . *J. Mater. Sci*, **50**(5),18,2007.

296.   Findlay, W. Paul, E. B. David   "Utilization of Fourier transform-Raman spectroscopy for the study of pharmaceutical crystal forms." Journal of pharmaceutical and biomedical analysis 16, 6, 921-930, (1998).

297.   M . Chang, W.   Zhenqing   "A numerical method characterising the electromechanical properties of particle reinforced composite based on statistics." Polymers 10,   4 (2018): 426.

298.   Office, Polymers Editorial. "Acknowledgement to Reviewers of Polymers in 2019." Polymers 12, no. 1 (2020).

299.   N.T Wagner, T.Sokoll,   O. Schimmer. "Robust low cost open-ended coaxial probe for dielectric spectroscopy in laboratory and in-situ applications." In Proc. CMM Conf.—Innovative FeuchtemessungForschung Praxis, pp. 1-11 (2011).

300.   S Sankaralingam, S. Dhar,B. Gupta, L. Osman L, *Procedia Eng.*, 64, 179-84. 2013

301.   Li, Jiahao, Qingxi Yang, Yuntao Song, Chao Yu, Shilin Chen, Hao Xu, and Dan Du. "RF wave propagation simulation for ICRF antenna in EAST." Journal of Nuclear Science and Technology (2021): 1-8.

302.   K Kerman,.; M Saito,.; E Tamiya,.; Yamamura, S.; Takamura, Y. "Nanomaterial-based electrochemical biosensors for medical applications." *Trends Anal. Chem.*, *27*, (2008) 585–592

303.   R.A.S Luz,.; R.M Iost,.; F.N. Crespilho, Nanomaterials for biosensors and implantable biodevices Springer-Verlag: Berlin, Germany, (2013); pp. 27–48,

304.   K.R.; Brown, A.P Fox,; M.J Natan, Morphology-dependent electrochemistry of cytochrome c at Au colloid-modified SnO2 electrodes *J. Am. Chem. Soc. 118*,(1996), 1154–1157

305.   M.M ,Maye,.; Y Lou,; C.J.Zhong, "Core− shell gold nanoparticle assembly as novel electrocatalyst of CO oxidation.*Langmuir 16*, (2000). 7520–7523.

306.   Y Xiao,; Patolsky, F.; E Katz,.; Hainfeld, J.F.; Willner, I. Plugging into enzymes": Nanowiring of redox enzymes by a gold nanoparticle." *Science*, *299*,(2003), 1877–1881

307.   J Chen,.; J Tang,.; H Ju,. A gold nanoparticles/sol-gel composite architecture for encapsulation of immunoconjugate for reagentless electrochemical immunoassay. *Biomaterials 27*,(2006), 2313–2321.

308.   J Njagi,.; S Andreescu, table enzyme biosensors based on chemically synthesized Au–polypyrrolenanocomposites. *Biosens. Bioelectron.*, *23*, (2007), 168–175

309.   M Haruta,.; M Daté, "Advances in the catalysis of Au nanoparticles.". *Appl. Catal. A*, *222*,(2001),427–437.

310.   Xu, Q.; Zhao, Y.; Xu, J.Z.; Zhu, J.J. Preparation of functionalized copper nanoparticles and fabrication of a glucose sensor."   *Sens. Actuat. B Chem*., *114*, (2006), 379–386.

311.   J Shen, L Dudik,.; Liu, C.C. "An iridium nanoparticles dispersed carbon-based thick film electrochemical biosensor and its application for a single-use, disposable glucose biosensor.An. *Sens. Actuat. B Chem*., *125*, (2007), 106–113.

312.   G Lai,.; Yan F.; J Wu,.; Leng, C.; Ju, H. "Ultrasensitive multiplexed immunoassay with electrochemical stripping analysis of silver nanoparticles catalytically deposited by gold nanoparticles and enzymatic reaction.". *Anal. Chem.*, *83*, ,(2011),2726–2732.

313.   S Guo, D Wen,Zhai, Y.; Dong, S.; Wang, E. One-dimensional CdS nanostructures: synthesis, properties, and applications.. *ACS Nano*, *4*,(2010) 959–3968.

314.   Mubeen, S.; Zhang, T.; Yoo, B.; Deshusses, M.A.; Myung, N. Palladium nanoparticles decorated single-walled carbon nanotube hydrogen sensor. *J. Phys. Chem. C*, *111*, ,(2007) 6321–6327.

315.   S Shahrokhian, M Ghalkhani.; Adeli, M.; Amini, M.K. "Multi-walled carbon nanotubes with immobilised cobalt nanoparticle for modification of glassy carbon electrode: Application to sensitive voltammetric determination of thioridazine." *Biosens. Bioelectron. 24*, (2009)3235–3241.

316.   A Kaushik,.; R Khan,.; P.R Solanki,.; Pandey, P.; Alam, J.; Ahmad, S.; Malhotra, B.D. Iron oxide nanoparticles–chitosan composite based glucose biosensor *Biosens. Bioelectron.*, *24*, ,(2008) 676–683.

317.   A Kaushik,; Khan, R; Solanki, P.R.; Pandey, P.; Alam, J.; Ahmad, S.; Malhotra, B.D "Iron oxide nanoparticles–chitosan composite based glucose biosensor   Biosens. Bioelectron., 24, ,(2008), 676–683.

318.   Ping, J.; Ru, S.; Fan, K.; Wu, J.; Ying, Y. "Copper oxide nanoparticles and ionic liquid modified carbon electrode for the non-enzymatic electrochemical sensing of hydrogen peroxide.". Microchim. Acta, 171,(2010),117–123.

319.   M.S.   Johal, 1st ed.; Multifunctional polymer   CRC Press by Taylor and Francis Group: Boca Raton, FL, USA, (2011).

320.   N. Moghimi,   K. T. Leung. "FePt alloy nanoparticles for biosensing: enhancement of vitamin C sensor performance and selectivity by nanoalloys." J. Phys. Chem. C, 85,   12 (2013): 5974-5980

321.   Q.; Xu, Zhao, Y.; Xu, J.Z.; Zhu, J.J. "Preparation of functionalized copper nanoparticles and fabrication of a glucose sensor."   *Actuat. B Chem.*, *114*,(2006) 379–386.

322.   Overbeek, J. Th. Colloids, a fascinating subject: Introductory lecture.   Royal Society of Chemistry: London, UK, (1982).

323.   M.H.. Fulekar, Nanotechnology: importance and applications International Pvt Ltd.: New Delhi, India, (2010).

324.   M.S Bell,; K.B.K Teo,Lacerda, R.G.; Milne, W.I.; Hash, D.B. Carbon nanotubes by plasma-enhanced chemical vapor deposition." Pure Appl. Chem., 78,(2006) 1117–1125.

325.   H.Zhu, A. Cao, X, Li, X., Xu, C., Mao, Z., Ruan, D, Wu, D. Hydrogen adsorption in bundles of well-aligned carbon nanotubes at room temperature. Applied surface science, 178(1-4), (2001), 50-55.

326.   C Journet,.; W.K Maser,.; Bernier, P.; Loiseau, A.; de laChapelle, M.L.; Lefrant, S.; Deniard, P.; Lee, R.; Fischer, J.E. Large-scale production of single-walled carbon nanotubes by the electric-arc technique *Nature*, *388*, ,(1997),756–758.

327.   A Thess,.; R Lee,.; Nikolaev, P.; Dai, H.J.; Petit, P.; Robert, C.H.; Xu, C.H.; Lee, Y.H.; Kim, S.G.; Rinzler, A.G.; *et al*. ongjie Dai, Pierre Petit, Jerome Robert, ChunhuiXu et al. "Crystallineropes of metalliccarbon nanotubes. *Science*, *273*, (1996) 483–487.

328.   H. Hu, B. Zhao, M.E.C Itkis, R.C Haddon,   Nitric acid purification of single-walled carbon nanotubes. J. Phys. Chem. B , 107(50), (2003),13838-13842.

329.   A.J.S.; Ahammad, J.-J.; Lee ,A. Rahman, Electrochemical sensors based on carbon nanotubes. *Sensors*, *9*, ,(2009) 2289–2319.

330.   A.P Baioni,; M Vidotti,.; Fiorito, P.A.; Córdoba de Torresi, S.I. Copper hexacyanoferrate nanoparticles modified electrodes *J. Electroanal. Chem*, *622*, (2008) 219–224 .

331.   Z Li,.; X Wang.; Wen, G.; Shuang, S.; Dong, C.; Paau, M.C.; Choi, M.M Application of hydrophobic palladium nanoparticles for the development of electrochemical glucose biosensor." . *Biosens. Bioelectron. 26*, (2011)4619–4623.

332.   A Salimi,.; R Hallaj,.; Soltanian, S. Fabrication of a Sensitive Cholesterol Biosensor Based on Cobalt-oxide Nanostructures Electrodeposited onto Glassy Carbon Electrode.". *Electroanal 21*, ,(2009)2693–2700.

333.   C.Y Liu,; Hu, J.M. "Fabrication of a Sensitive Cholesterol Biosensor Based on Cobalt-oxide Nanostructures Electrodeposited onto Glassy Carbon Electrode." *Biosens. Bioelectron.*, *24*, 2149–2154.(2009).

334.   F. Okumu, M. Mangaka   "Electrochemical Characterization of Silver-Platinum Various Ratio Bimetallic Nanoparticles Modified Electrodes." Nano Res.,(2016)   44, pp. 114-125.

335.   F.L Stoddard, C. Balko, E. William   H. R. Khan, W. Link, aA. Sarker. "Screening techniques and sources of resistance to abiotic stresses in cool-season food legumes." Euphytica 147, 1 (2006): 167-186.

336.   A Guiseppi-Elie,; Wallace, G.G.; Matsue, T. Skotheim, T.A., Elsenbaumer, R., Reynolds, J.R., Eds.; Marcel Dekker: "Handbook of conducting polymers New York, NY, USA, (1998), pp. 963–991,

337.   A .Murat,   A. SezaiSarac. "Electrochemical impedance spectroscopic study of polythiophenes on carbon materials." PolymPlastTechnolEng . 50, 11 (2011), 1130-1148.

338.   E.W Paul,; A.J Ricco,; Wrighton, M.S. Resistance of polyaniline films as a function of electrochemical potential and the fabrication of polyaniline-based microelectronic devices." *J. Phys. Chem.*, *89*, (1985) 1441–1447.

339.   T Ahuja,.; D Kumar, "Recent progress in the development of nanostructured conducting polymers/nanocomposites for sensor applications. *Sens. Actuat. B Chem.*, *136*, (2009) 275–286.

340.   N.J Ronkainen,; Halsall, H.B.; Heineman, W.R. "Electrochemical biosensors.*Chem. Soc. Rev.*, *39*, (2010) 1747–1763.

341.   J.I.; Yeh, Shi, H. *WIREsNanoelectrodes for biological measurements. Nanomed. Nanobiotechnol. 2*, (2010) 176–188.

342.   Njagi, J.; Chernov, M.M.; Leiter, J.C.; Andreescu, S. Amperometric detection of dopamine in vivo with an enzyme based carbon fiber microbiosensor*Anal. Chem. 82*, (2010), 989–996

343.   N Sato,.; , H.. Okuma "Development of single-wall carbon nanotubes modified screen-printed electrode using a ferrocene-modified cationic surfactant for amperometric glucose biosensor applications *Sens. Actuat. B Chem. 129, (*2008),188–194.

344.   Y Wan,; W Deng,.; Su, Y.; Zhu, X.; Peng, C.; Hu, H.; Peng, H.; Song, S.; Fan, C Carbon nanotube-based ultrasensitive multiplexing electrochemical immunosensor for cancer biomarkers." *Biosens. Bioelectron., 30*, (2011). 93–99.

345.   Z Taleat,; C Cristea,.; Marrazza, G.; Mazloum-Ardakani, M.; Săndulescu, R. Electrochemical immunoassay based on aptamer–protein interaction and functionalized polymer for cancer biomarker detection." *J. Electroanal. Chem. 717–718*, (2014) 119–124

346.   I Ojeda,.; Moreno-Guzmán, M.; González-Cortés, A.; Yáñez-Sedeño, P.; Pingarrón, J.M.. Electrochemical magnetic immunosensors for the determination of ceruloplasmin." *Electroanal*, 25, (2013)2166–2174.

347.   B Garcinuño,.; Ojeda, I.; Moreno-Guzmán, M.; González-Cortés, A.; Yáñez-Sedeño, P.; Pingarrón, Amperometricimmunosensor for the determination of ceruloplasmin in human serum and urine based on covalent binding to carbon nanotubes-modified screen-printed electrodes J.M.. Talanta, 118, (2014) 61–67.

348.   J. D Benck,.; Pinaud, B. A.; Gorlin, Y.; Jaramillo, T. F. Neutral, and Basic Electrolyte. PLoS One, 9, .(2014) e107942

349.   D.Braun, "Recycling of PVC." Prog. Polym. Sci. 27, 10 (2002): 2171-2195.

350.   J. D Benck,; Pinaud, B. A.; Gorlin, Y.; Jaramillo, T. F. Substrate selection for fundamental studies of electrocatalysts and photoelectrodes: inert potential windows in acidic Neutral, and Basic Electrolyte. PLoS One, 9, .(2014).e107942

351.   M. Mizuhashi, Electrical properties of vacuum-deposited indium oxide and indium tin oxide films, Thin Solid Films 70, (1980).91−100.

352.   H. Qiang, W. Chen, W. Shutong ,X. Gang. "Anomalous Hall effect and magnetic properties of FexPt100-x alloys with strong spin-orbit interaction." *Int. J. Appl. Phys.* 122,. 3 (2017): 033901.

353.   M. B Rooney, Coomber, D. C.; Bond, A. M.. Achievement of near-reversible behavior for the [Fe (CN) 6] 3-/4-redox couple using cyclic voltammetry at glassy carbon, gold, and platinum macrodisk electrodes in the absence of added supporting electrolyte. Anal. Chem., 72, ,(2000) 3486−3491.

354.   J Stotter,.; Show, Y.; Wang, S.; Swain, G. "Comparison of the electrical, optical, and electrochemical properties of diamond and indium tin oxide thin-film electrodes.. Chem. Mater., 17. (2005), 4880−4888.

355.   W.R.Gombotz, G. Wang, A. Thomas .S. Allan. "Protein adsorption to poly (ethylene oxide) surfaces." Journal of biomedical materials research 25, 12 (1991): 1547-1562.

356.   Stith, M. Sandra, l. Ting Liu, D. Christopher, M.McPherson, "Risk factors in child maltreatment: A meta-analytic review of the literature." *Aggress Violent Behav*14, 1 (2009): 13-29.

357.   A. Carlson, "Factors influencing the use of aqueous two-phase partition for protein purification." *Sep SciTechnol .* 23, 8-9 (1988): 785-817.

358.   J Han, M Wang,.; Hu, Y.; Zhou, C.; Guo, R "Conducting polymer-noble metal nanoparticle hybrids: Synthesis mechanism application Prog. Polym. Sci. 70, (2017) 52–91,

359.   Z. U. Khan, H.; Khan, A.; Chen, Y. M.; Shah, N. S.; Muhammad, N.; Khan, A. U.; Tahir, K.; Khan, F. U.; Murtaza, B.; Hassan, S. U.. J. Photochem. Photobiol. 173, , (2017) 150–164

360.   Zalipsky, Samuel, and J. Milton Harris. "Introduction to chemistry and biological applications of poly (ethylene glycol)." (1997): 1-13.

361.   J Prakash,.; Pivin, J.; Swart, H. Noble Metal Nanoparticles Embedding into Polymeric Materials: From Fundamentals to Applications Adv.   Colloid. Interface Sci., 226, (2015) 187–202

362.   Farooqi, Z. H.; Khan, S. R.; Hussain, T.; Begum, R.; Ejaz, K.; Majeed, S.; Ajmal, M.; Kanwal, F.; Siddiq, M. Korean Facile synthesis of silver nanoparticles in a cross-linked polymeric system by in situ reduction method for catalytic reduction of 4-nitroaniline. Environmental technology, J. Chem. Eng., 31, (2014) 1674–1680.

363.   Gorelikov, I.; Field, L. M.; Kumacheva, E. Hybrid MicrogelsPhotoresponsive in the Near-Infrared Spectral Range. J. Am. Chem. Soc., 126, (2004)15938–15939.

364.   Z. H Farooqi,.; Khalid, R.; Begum, R.; Farooq, U.; Wu, Q.; Wu, W.;Ajmal, M.; Irfan, A.; Naseem, K. Environ. Technol. (2018)

365.   An, L Liz-Marz_. M.; Lado-Touri~no, I,   Reduction and Stabilization of Silver Nanoparticles in Ethanol by Nonionic Surfactants Langmuir. 12, (1996) 3585–3589.

366.   Niu, Y.; Crooks, R. M. Preparation of Dendrimer-Encapsulated Metal Nanoparticles Using Organic Solvents. Chem. Mater., 15, (2003),3463–3467.

367.   T Sakai, P Alexandridis. Engineering of Silver Nanoparticle Fabricated Poly(N-isopropylacrylamide-co-acrylic acid) Microgels for Rapid Catalytic Reduction of Nitrobenzene . Langmuir., 20, (2004)8426–8430.

368.   Farooqi, Z. H.; Naseem, K.; Ijaz, A. Engineering of Silver Nanoparticle Fabricated Poly(N-isopropylacrylamide-co-acrylic acid) Microgels for Rapid Catalytic Reduction of Nitrobenzene J. Polym. Eng. 36, (2016) 87–96,

369.   R Begum,.; Naseem, K.; Farooqi, Z. H.. J. Review of Responsive Hybrid Microgels Fabricated with Silver Nanoparticles: Synthesis, Classification, Characterization, and Applications Sol-Gel Sci. Technol. 77, (2016), 497–515.

370.   Wu, W.; Shen, J.; Banerjee, P.; Zhou, S. Chitosan-based ResponsiveHybridNanogels for Integration of Optical pH-sensing, Tumor Cell Imaging and Controlled Drug Delivery Biomaterials., 31, (2010).8371–8381

371.   W Wu,; Zhou, T.; Shen, J.; Zhou, S. Optical Detection of Glucose by CdS Quantum Dots Immobilized in Smart Microgels. Chem. Commun., (2009) 4390–4392.

372.   Thomas, V.; Namdeo, M.; Murali Mohan, Y.; Bajpai, S.; Bajpai, M. J Review on Polymer, Hydrogel and Microgel Metal Nanocomposites: A Facile Nanotechnological Approach . Macromol. Sci. A45, (2007)107–119.

373.   S Xu,; Zhang, J.; Paquet, C.; Lin, Y.; Kumacheva, E. From Hybrid Microgels to Photonic Crystals. Adv. Funct. Mater. 13, (2003) 468– 472.

374.   F Naseer,:Ajmal, M.; Bibi, F.; Farooqi, Z. H.; Siddiq, Copper and cobalt nanoparticles containing poly (acrylic acid-co-acrylamide) hydrogel composites for rapid reduction of 4-nitrophenol and fast removal of malachite green from aqueous medium M. Polym. Compos. (2017)

375.   Z. H Farooqi, A Ijaz,; R Begum,.; Naseem, K.; Usman, M.; Ajmal, M.; Saeed, U. Synthesis and Characterization of Inorganic–organic Polymer Microgels for Catalytic Reduction of 4-Nitroaniline in Aqueous Medium Polym. Compos., 39, (2016)645–653.

376.   Y Lu,.; Mei, Y.; Ballauff, M.; Drechsler, M Thermosensitive Core¡- shell Particles as Carrier Systems for Metallic Nanoparticles ,J. Phys. Chem. B., 110, (2006), 3930–3937.

377.   L.-Q Yang,; Hao, M.-M.; Wang, H.-Y.; Zhang, Y. Amphiphilic Polymer-Ag Composite Microgels with Tunable Catalytic Activity and Selectivity , Colloid Polym. Sci., 293, (2015)2405–2417.

378.   J. T Zhang,; Wei, G.; Keller, T. F.; Gallagher, H.; St€otzel, C.; M€uller, F. A.; Gottschaldt, M.; Schubert, U. S.; Jandt, K. D. Responsive Hybrid Polymeric/Metallic Nanoparticles for Catalytic Applications , Macromol. Mater. Eng. 295, (2010). 1049–1057

379.   Ravindren, R., Mondal, S., Nath, K., & Das, N. C. Investigation of electrical conductivity and electromagnetic interference shielding effectiveness of preferentially distributed conductive filler in highly flexible polymer blends nanocomposites. Composites Part A: Applied Science and Manufacturing, 118, (2019). 75-89

380.   Ho, Kin Man, Wei Ying Li, Cheng Hao Lee, Chun Ho Yam, Robert G. Gilbert, and Pei Li. "Mechanistic study of the formation of amphiphilic core–shell particles by grafting methyl methacrylate from polyethylenimine through emulsion polymerization." Polymer 51, no. 15 (2010): 3512-3519.

381.   Lewis, Christina L., Caelli C. Craig, and Andre G. Senecal. "Mass and density measurements of live and dead gram-negative and gram-positive bacterial populations." Applied and environmental microbiology 80, no. 12 (2014): 3622-3631.

382.   Lewis, Christina L., Caelli C. Craig, and Andre G. Senecal. "Mass and density measurements of live and dead gram-negative and gram-positive bacterial populations." Applied and environmental microbiology 80, no. 12 (2014): 3622-3631.

383.   Kim, Sujin, Byung Ho Shin, Chungmo Yang, SoohyunJeong, Jung Hee Shim, Min Hee Park, Young Bin Choy, Chan YeongHeo, and Kangwon Lee. "Development of poly (HEMA-Am) polymer hydrogel filler for soft tissue reconstruction by facile polymerization." Polymers 10, no. 7 (2018): 772.

384.   Khan, A.; El-Toni, A. M.; Alrokayan, S.; Alsalhi, M.; Alhoshan, M.;Aldwayyan, A. S. Microwave-Assisted Synthesis of Silver Nanoparticles Using Poly-N-Isopropylacrylamide/Acrylic Acid Microgel Particles, Colloids Suf., A., 377, (2011), 356–360.

385.   D.A DIKIN, "Preparation and characterization of graphene oxide paper ., Nature, 448, . (2007) pp 457-460

386.   Yagci, Y., Sangermano, M.,Rizza, G. (2008). Synthesis and characterization of gold− epoxy nanocomposites by visible light photoinduced electron transfer and cationic polymerization processes. Macromolecules, 41(20): 7268-7270.

387.   Mauro, M., Acocella, M. R., Corcione, C. E., Maffezzoli, A Guerra, G. (2014). Catalytic activity of graphite-based nanofillers on cure reaction of epoxy resins. Polymer, 55(22) : 5612-5615.

388.   Greco, A., Corcione, C. E., &Maffezzoli, A. (2016). Effect of multi-scale diffusion on the permeability behavior of intercalated nanocomposites. Journal of Membrane Science, 505: 92-99.

389.   Lee, H. H., Chou, K. S., Shih, Z. W. (2005). Effect of nano-sized silver particles on the resistivity of polymeric conductive adhesives. International Journal of Adhesion and Adhesives, 25(5): 437-441.

390.   Jiang, H., Moon, K. S., Li, Y Wong, C. P. (2006). Surface functionalized silver nanoparticles for ultrahigh conductive polymer composites. Chemistry of Materials, 18(13): 2969-2973.

391.   Lu, J., Moon, K. S., Wong, C. P. (2008). Silver/polymer nanocomposite as a high-k polymer matrix for dielectric composites with improved dielectric performance. Journal of Materials Chemistry, 18(40): 4821-4826.

392.   Liu, K., Liu, L., Luo, Y.,Jia, D. (2012). One-step synthesis of metal nanoparticle decorated graphene by liquid phase exfoliation. Journal of Materials Chemistry, 22(38): 20342-20352.

393.   Ghosh, K., &Maiti, S. N. (1996). Mechanical properties of silver-powder-filled polypropylene composites. Journal of AppliedPolymer Science, 60(3) : 323-331.

394.   Otari, S. V., Pawar, S. H., Patel, S. K., Singh, R. K., Kim, S. Y., Lee, J. H , Lee, J. K. (2017). Canna edulis leaf extract-mediated preparation of stabilized silver nanoparticles: characterization, antimicrobial activity, and toxicity studies. Journal of microbiology and biotechnology, 27(4): 731-738.

395.   Bureekaew, S., Horike, S., Higuchi, M., Mizuno, M., Kawamura, T., Tanaka, D., Kitagawa, S. (2011). One-dimensional imidazole aggregate in aluminium porous coordination polymers with high proton conductivity. In Materials For Sustainable Energy: A Collection of Peer-Reviewed Research and Review Articles from Nature Publishing Group (pp. 232-237).

396.   Ye, Y., Guo, W., Wang, L., Li, Z., Song, Z., Chen, J Chen, B. (2017). Straightforward loading of imidazole molecules into metal–organic framework for high proton conduction. Journal of the American Chemical Society, 139(44): 15604-15607.

397.   Zhang, F. M., Dong, L. Z., Qin, J. S., Guan, W., Liu, J., Li, S. L., Zhou, H. C. (2017). Effect of imidazole arrangements on proton-conductivity in metal–organic frameworks. Journal of the American Chemical Society, 139(17): 6183-6189.

398.   Liu, S., Yue, Z., & Liu, Y. (2015). Incorporation of imidazole within the metal–organic framework UiO-67 for enhanced anhydrous proton conductivity. Dalton Transactions, 44(29): 12976-12980.

399.   Lo, T. H., Nguyen, M. V., & Tu, T. N. (2017). An anchoring strategy leads to enhanced proton conductivity in a new metal–organic framework. InorganicChemistryFrontiers, 4(9) :1509-1516.

400.   D. Umeyama, S. Horike, M. Inukai, Y. Hijikata, S. Kitagawa, Transfer. Angew. Chem., (2011)Int. Ed) **123**, 49:11910-11913

401.   A .Jankowska , A .Zalewska, A .Skalska, A. Ostrowski S. Kowalak(2017) Chem. Commun. **53.**16 :2475-2478

402.   Ye, Y., Zhang, L., Peng, Q., Wang, G. E., Shen, Y., Li, Z.Xiang, S. (2015). High anhydrous proton conductivity of imidazole-loaded mesoporous polyimides over a wide range from subzero to moderate temperature. Journal of the American Chemical Society, 137(2):913-918.

403.   Wu, L., Yang, Y., Ye, Y., Yu, Z., Song, Z., Chen, S, Xiang, S. (2018). Loading Acid–Base Pairs into Periodic Mesoporous Organosilica for High Anhydrous Proton Conductivity over a Wide Operating Temperature Window. ACS Applied Energy Materials, 1(9), 5068-5074.

404.   Wu, Y., Wu, C., Yu, F., Xu, T., & Fu, Y. (2008). Free-standing anion-exchange PEO–SiO2 hybrid membranes. Journal of Membrane Science, 307(1) : 28-36.

405.   Miyoshi, S., Akao, Y., Kuwata, N., Kawamura, J., Oyama, Y., Yagi, T., Yamaguchi, S. (2014). Low-temperature protonic conduction based on surface protonics: an example of nanostructured yttria-doped zirconia. Chemistry of Materials, 26(18), 5194-5200.

406.   Hojo, H., Mizoguchi, T., Ohta, H., Findlay, S. D., Shibata, N., Yamamoto, T., &Ikuhara, Y. (2010). Atomic structure of a CeO2 grain boundary: the role of oxygen vacancies. Nano letters, 10(11) : 4668-4672.

407.   Bretado, M. E., Lozano, M. G., Martínez, V. C., Ortiz, A. L., Zaragoza, M. M., Lara, R. H., Medina, C. M. (2019). Synthesis, characterization and photocatalytic evaluation of potassium hexatitanate (K2Ti6O13) fibers. International Journal of HydrogenEnergy, 44(24) :12470-12476.

408.   Zhao, Y., Xu, Z., Xia, C., Li, Y. (2013). Oxide ion and proton conduction in doped ceria–carbonate composite materials. International Journal of HydrogenEnergy, 38(3) : 1553-1559.

409.   Elleuch, A., Sahraoui, M., Boussetta, A., Halouani, K., Li, Y. (2014). 2-D numerical modeling and experimental investigation of electrochemical mechanisms coupled with heat and mass transfer in a planar direct carbon fuel cell. Journal of Power Sources, 248: 44-57.

410.   Richter, J., Holtappels, P., Graule, T., Nakamura, T., Gauckler, L. J. (2009). Materials design for perovskite SOFC cathodes. MonatsheftefürChemie-Chemical Monthly, 140(9):985-999.

411.   Zhu, B., Yang, X. T., Xu, J., Zhu, Z. G., Ji, S. J., Sun, M. T., Sun, J. C. (2003). Innovative low temperature SOFCs and advanced materials. Journal of Power Sources, 118(1-2):47-53.

412.   Gao, Zhan, J.Huang, Z. Mao, C. Wang ,Zhixiang Liu. (2010) J. Hydrog**35**. 2**:**731-737

413.   Huang, J., Gao, Z., Mao, Z. (2010). Effects of salt composition on the electrical properties of samaria-doped ceria/carbonate composite electrolytes for low-temperature SOFCs. International journal of hydrogen energy, 35(9):4270-4275.

414.   Raza, R., Wang, X., Ma, Y., Liu, X., Zhu, B. (2010). Improved ceria–carbonate composite electrolytes. International Journal of Hydrogen Energy, 35(7): 2684-2688.

415.   Kuo, P. L., Tsao, C. H., Hsu, C. H., Chen, S. T., Hsu, H. M. (2016). A new strategy for preparing oligomeric ionic liquid gel polymer electrolytes for high-performance and nonflammable lithium ion batteries. Journal of Membrane Science, 499:462-469.

416.   Liu, C., Qiu, S., Du, P., Zhao, H., Wang, L. (2018). An ionic liquid–graphene oxide hybrid nanomaterial: synthesis and anticorrosive applications. Nanoscale, 10(17) : 8115-8124.

417.   Li, L., Yang, X., Li, J., Xu, Y. (2018). A novel and shortcut method to prepare ionic liquid gel polymer electrolyte membranes for lithium-ion battery. Ionics, 24(3): 735-741.

418.   M. Lorenzo, C. AJ. Fisher, M. Saiful Islam.(2010) J,.ChemSoc Rev.**39**,11: 4370-4387

419.   D. Kobayashi, K. Fujita, N. Nakamura ,H. Ohno ,(2015)Applied microbiology and biotechnology**99**, 4 :1647-1653

420.   A. S. M. C. Rodrigues, M. A. A. Rocha, H. F. D. Almeida, C. M. S. S. Neves, J. A. Lopesda-Silva, M. G. Freire, J. A. P. Coutinho , L. M. N. B. F. J. (2015) Phys. ChemB 119.28 :8781-8792

421.   M. Wang, X. Pan, J. Chen ,S. Dai   Sci. China Chem.58(12):1884-1890(2015)

422.   Tao, R., Simon, S. L. (2015). Rheology of imidazolium-based ionic liquids with aromatic functionality. The Journal of Physical Chemistry B, 119(35):11953-11959.

423.   Castner Jr, E. W., Wishart, J. F.,Shirota, H. (2007). Intermolecular dynamics, interactions, and solvation in ionic liquids. Accounts of chemical research, 40(11): 1217-1227.

424.   Greaves, T. L., Drummond, C. J. (2008). Protic ionic liquids: properties and applications. Chemical reviews, 108(1): 206-237.

425.   Lin, C. W., Huang, Y. F., Kannan, A. M. (2007). Semi-interpenetrating network based on cross-linked poly (vinyl alcohol) and poly (styrene sulfonic acid-co-maleic anhydride) as proton exchange fuel cell membranes. Journal of Power Sources, 164(2): 449-456.

426.   M . Nagai,., K. Kobayashi,   Y. Nakajima. TrAC Trends in Analytical Chemistry**27**.7 604-611(2008)

427.   Kawada, A., McGhie, A. R., Labes, M. M. (1970). Protonic conductivity in imidazole single crystal. The Journal of Chemical Physics, 52(6): 3121-3125.

428.   Hasegawa, N., et al., Nylon 6/Na–montmorillonite nanocomposites prepared by compounding Nylon 6 with Na–montmorillonite slurry. Polymer, 2003. 44(10): p. 2933-2937.

429.   Bondeson, D. and K. Oksman, Polylactic acid/cellulose whisker nanocomposites modified by polyvinyl alcohol. Composites Part A: Applied Science and Manufacturing, 2007. 38(12): p. 2486-2492.

430.   Helbert, W., J. Cavaille, and A. Dufresne, Thermoplastic nanocomposites filled with wheat straw cellulose whiskers. Part I: processing and mechanical behavior. Polymer composites, 1996. 17(4): p. 604-611.

431.   Iwamoto, S., et al., Mechanical properties of polypropylene composites reinforced by surface-coated microfibrillated cellulose. Composites Part A: Applied Science and Manufacturing, 2014. 59: p. 26-29.